
27 April 2007 | $10
Science
AAAS

Antimicrobial Peptides

Antimicrobial peptides are important members of the host defense system. They have a broad ability to kill microbes. Antimicrobial peptides and proteins form an important means of host defense in eukaryotes. Large antimicrobial proteins (>100 a.a.), are often lytic, nutrient-binding proteins or specifically target microbial macromolecules. Small antimicrobial peptides act by disrupting the structure or function of microbial cell membranes. A multitude of antimicrobial peptides have been found in the epithelial layers, phagocytes and body fluids of multicellular animals including man. Beside their role as endogenous antibiotics, antimicrobial peptides have functions in inflammation, wound repair and regulation of the adaptive immune system. Cell Sciences offers the following associated products.

Description	Applications
Alpha-Defensin 1-3, human, ELISA	IA
Alpha-Defensin 1-3, human, mAb D21	F FC IA P W
Alpha-Defensin 1-3, mAb D21, biotinylated	F FC IA P W
Alpha-Defensin 1-3, natural, human	FS
BPI, human, ELISA	IA
BPI, human, mAb 3F9	IA
BPI, human, mAb 4E3	B FC IA
BPI, human, mAb 4H5	IA
BPI, human, pAb	IA IP
Calprotectin, human, ELISA	IA
Calprotectin, human, mAb 27E10	F FC IA IP P W
CHIPS (C-terminus), mAb JCC1	B F FC IA P W
CHIPS (N-terminus), mAb JNC1	B F FC IA P W
CHIPS, purified	
CRISP-3, human, pAb	IA P W
Elafin/SKALP, human, ELISA	IA
Elafin/SKALP, human, mAb TRAB2F	IA P W
Elafin/SKALP, human, mAb TRAB2O	IA P W
Elafin/SKALP, human, pAb	IA P W
Elafin/SKALP(57aa), recombinant, human	
Elastase, human, ELISA	IA
Elastase, human, mAb 265-3K1	IA W
Elastase, human, pAb	IA
Galectin-3, human, mAb B2C10	F FC FS IA P W
Galectin-3, mouse, mAb B2C10	F FC FS IA P W
HNP 1-3, human, ELISA	IA
HNP 1-3, human, mAb D21	F FC IA P W
HNP 1-3, human, mAb D21, Biotin	F FC IA P W
HNP 1-3, purified, natural, human	FS
Lactoferricin, bovine, mAb 5F12.1.2	IA W
Lf, C-lobe, bovine, mAb a-bC-lobe	IA W
Lactoferrin, bovine, pAb	IA IP W
Lactoferrin, human, ELISA	IA
Lactoferrin, human, mAb 265-1K1	F IA W
Lactoferrin, human, pAb	IA IP W
LBP, multi-species, ELISA	IA
LBP, multi-species, mAb 6G3	FS IA IP
LBP, human, ELISA	IA
LBP, human, mAb 1C7	FS IA IP
LBP, human, mAb 6G3	FS IA IP
LBP, human, pAb	IA IP W
LBP peptide (a.a. 86-99), human	
LBP, recombinant human	
Plasma with low LBP level, human	
LBP, mouse, ELISA	IA
LBP, mouse, mAb M330-19	B IA W
LBP, mouse, mAb M392-2	IA W
LBP, mouse, mAb RR433-8	B IA W
LBP, recombinant mouse	
LL-37, human, ELISA	IA
LL37/CAP18, human, mAb 1-1C12	W
LL37/CAP18, human, mAb 3D11	P
LL37 peptide, human	
Lysozyme, human, pAb	IA IP W
Mannose Receptor, human, mAb 15-2	F FC FS IA IP W
Mannose Receptor, mouse, mAb MR5D3	F FC IP W
Mannose Receptor, human, mAb 15-2, Biotin	F FC IA W
MPO, human, ELISA	IA
MPO, human, mAb 266-6K1	F IA W
MPO, human, mAb 266-6K1, Biotinylated	F IA W
MPO, human, mAb 266-6K1, FITC	F IA W
MPO, mouse, ELISA	IA
MPO, mouse, mAb 8F4	F FC IA
MPO, mouse, mAb 8F4, biotinylated	F FC IA
MPO, mouse, mAb 8F4, FITC	F FC IA
MPO, rat, mAb 2D4	F FC IA IF
MPO, rat, mAb 2D4, biotinylated	F FC IA IF
MPO, rat, mAb 2D4, FITC	F FC IA IF
MRP-8/MRP-14, human, ELISA	IA
MRP-8/MRP-14, human, mAb 27E10	F FC IA IP P W
Neutroph Defensin 5, rabbit, mAb R3	F FC IA P W
Neutroph. Lipocalin, human, mAb 697	IA IF
nGAL, Lipocalin, human, mAb 697	IA IF
Polymyxin B, mAb 45	IA W
Proteinase 3 (PR3), human, mAb PR3G-2	F FC IA W
Proteinase 3 (PR3), human, mAb WGM2	B F FC IA P W
S100A8/A9, human, mAb 27E10	F FC IA IP P W
S100A8/S100A9, human, ELISA	IA
SLPI, human, ELISA	IA
SLPI, human, mAb 31	F IA IP P W
SLPI, human, mAb 31, Biotin	F IA P W
SLPI, human, pAb	IA IP W
TfR1, CD71, human, mAb 3B8 2A1	F FC IA IP W
TfR1, CD71, human, mAb 66-IG10	F FC IP

Applications Key

B: Inhibition of biological activity **F:** Frozen Sections **FC:** Flow cytometry **FS:** Functional Studies **IA:** Immunoassay
IF: Immunofluorescence **IP:** Immunoprecipitation **P:** Paraffin sections **W:** Western blot

480 Neponset Street, Building 12A, Canton, MA 02021 • TEL (781) 828-0610 • EMAIL info@cellsciences.com
CALL TOLL FREE (888) 769-1246 • FAX (781) 828-0542 • VISIT www.cellsciences.com

you've got **better** things to do...

better consistency

better purification

better results

Volume 316, Issue 5824

COVER

Microscopic marine plants (*Chaetoceros*, a chain-forming diatom) are consumed by zooplankton animals (*Neogloboquadrina*, a foraminifera, lower inset; tail of *Neocalanus* copepod, upper inset). Marine plankton food webs can affect climate by regulating the removal of carbon dioxide in surface waters and transporting this carbon to the deep sea via sinking particles. See page 567.

Photos: Mary Silver

DEPARTMENTS

EDITORIAL

NEWS OF THE WEEK

NEWS FOCUS

532

LETTERS

BOOKS ET AL.

544

POLICY FORUM

EDUCATION FORUM

PERSPECTIVES

CONTENTS continued >>

Science

SCIENCE EXPRESS

www.sciencexpress.org

REVIEW

BREVIA

RESEARCH ARTICLES

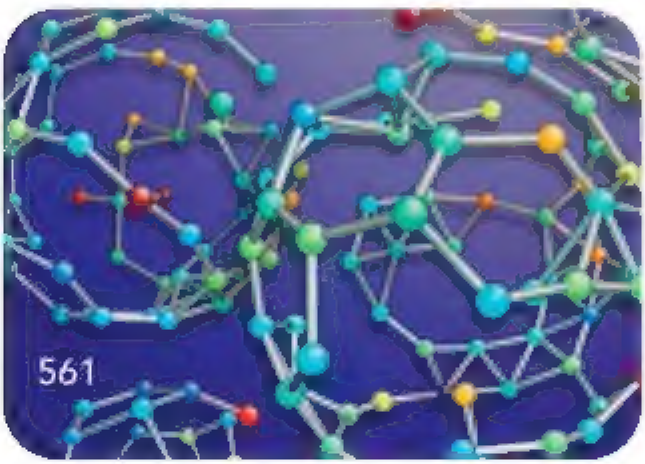

561

REPORTS

CONTENTS continued >>

585

REPORTS *CONTINUED*

597

AAAS

ADVANCING SCIENCE, SERVING SOCIETY

SCIENCE (ISSN 0036-8075) is published weekly on Friday, except the last week in December, by the American Association for the Advancement of Science, 1200 New York Avenue, NW, Washington, DC 20005. [illegible] Printed in the U.S.A.

Change of address: [illegible] Postmaster: Send change of address to AAAS, P.O. Box 96178, Washington, DC 20090–6178. Single-copy sales: [illegible] Authorization to photocopy [illegible] The identification code for Science is 0036-8075. Science is indexed in the Reader's Guide to Periodical Literature and in several specialized indexes.

CONTENTS continued >>

SCIENCE NOW

www.sciencenow.org DAILY NEWS COVERAGE

Ancient Rainforest Rises Again
A 300-million-year-old jungle found in Illinois coal mine may give clues to major extinction.

Hopes Dim for Perfect Lens
Plans to develop necessary "left-handed" materials for visible light run afoul of causality.

No Fountain of Youth for Fibrotic Cells
Aging lung tissue may explain some cases of mysterious lung disease.

Research exchanges with India

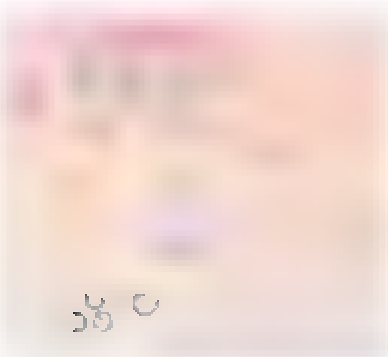

Resolving inflammation

SCIENCE'S STKE

www.stke.org SIGNAL TRANSDUCTION KNOWLEDGE ENVIRONMENT

EDITORIAL GUIDE: Focus Issue—Keeping the Immune Response in Check
J. F. Foley, E. M. Adler, N. R. Gough
Switching off the immune response is as important as switching it on.

PERSPECTIVE: Professional and Part-Time Chemokine Decoys in the Resolution of Inflammation
C. Hansell and R. Nibbs
Chemokine receptors that mediate the cellular infiltration that causes inflammation can change hats and help to bring about resolution.

PERSPECTIVE: Striking Back at the Activator—How IκB Kinase Terminates Antigen Receptor Responses
M. Hinz and C. Scheidereit
The scaffold involved in activating NF-κB also plays a role in terminating the immune response.

PERSPECTIVE: Regulation of Interferon Production by RIG-I and LGP2—A Lesson in Self-Control
D. Vitour and E. F. Meurs
Interactions in cis and trans control the activity of CARD-domain proteins involved in regulating immune responses.

PERSPECTIVE: CARD-Bcl10-Malt1 Signalosomes: Missing Link to NF-κB
E. Wegener and D. Krappmann
Signaling complexes using different CARD scaffolds, as well as Bcl10 and Malt1, link receptors in various cells to NF-κB.

SCIENCE CAREERS

www.sciencecareers.org CAREER RESOURCES FOR SCIENTISTS

GLOBAL: Special Feature—Research Opportunities in India—An Upward Trajectory
A. Kotok
Science Careers reviews the current and future state of scientific exchanges with India.

MISCINET: Educated Woman, Postdoc Edition—Baby Steps
M. P. DeWhyse
Micella hasn't made any concrete decisions, but she has taken baby steps to make life more tolerable.

ASIA: India—A New Knowledge Hot Spot
P. Bagla
India is fast becoming a place where people from around the world go to do scientific research.

EUROPE: U.K.-India Initiative Aims to Renew Old Ties
A. [illegible]
Research opportunities in India are limited for U.K. citizens, but new initiatives are making up for lost time.

US: American Tales in India
A. Fazekas
American researchers who have lived and worked in India say that the benefits outweigh the many challenges.

GRANTSNET: Guide to Financing Research Exchanges With India
A. Kotok
Scientists seeking funds for research in India can look to international and bilateral sources.

CREDIT (SCIENCE CAREERS): PALLAVA BAGLA

Separate individual or institutional subscriptions to these products may be required for full-text access.

EDITED BY STELLA HURTLEY AND PHIL SZUROMI

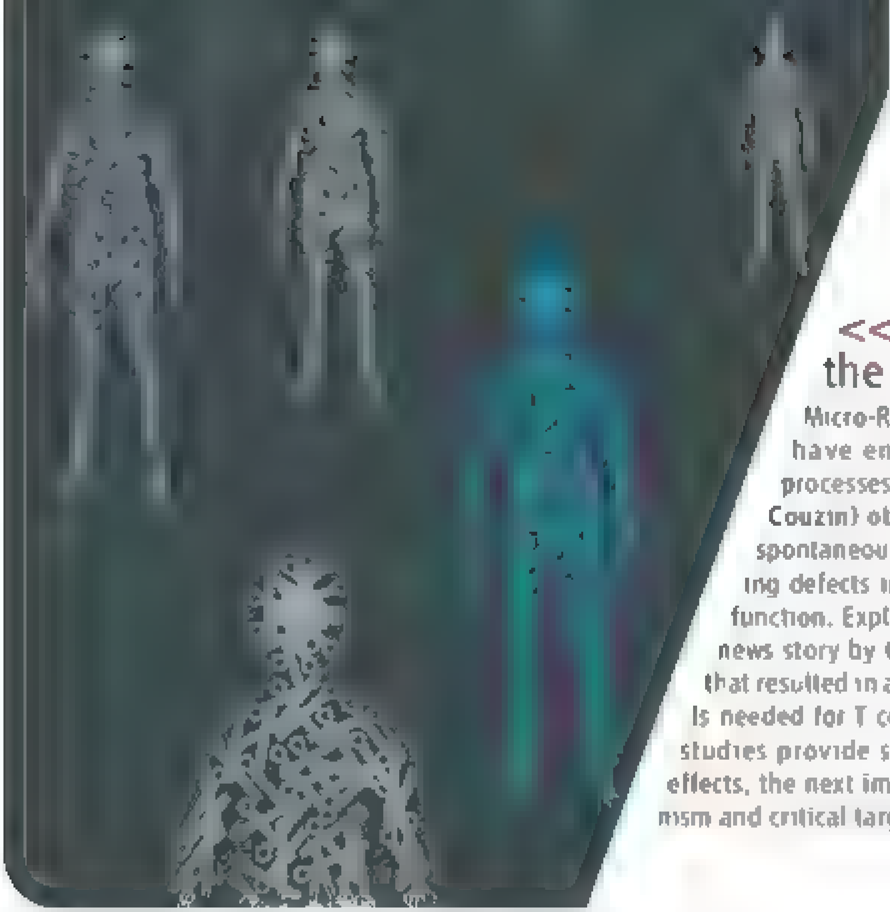

<< Micromanaging the Immune System

Micro-RNAs (miRNAs) are abundant small RNA species that have emerged as key regulators in many biological processes. **Rodriguez *et al.*** (p. 608, see the news story by **Couzin**) observed that mice deficient in miRNA-155 develop spontaneous inflammation of the lungs and have accompanying defects in antigen presentation, as well as T cell and B cell function. Exploring the same miRNA, **Thai *et al.*** (p. 604, see the news story by **Couzin**) observed a similar T and B cell deficiency that resulted in a suboptimal response of the germinal center, which is needed for T cell–mediated antibody production. Although both studies provide some evidence for how this miRNA mediates its effects, the next important step will be to identify the precise mechanism and critical target genes involved.

Solving Nanoscale Structure

For many materials, if you can grow sufficiently large, high-quality crystals, there are many tools for determining the crystal structure, and in some cases the process can be fully automatic. However, for materials that have structural features that are inherently nanoscale (such as cages in zeolites) or that may not be fully crystalline, the solution of the phase problem is more daunting. **Billinge and Levin** (p. 561) review recent progress in this area and note the benefits of greater integration of data through complex modeling from a wide of range of direct and indirect methods that probe both bulk and local details.

Disappearing in the Twilight Zone

Most of the organic carbon produced in the sunlit upper layer of the ocean is recycled (remineralized) as dead organisms sink to greater depths but there is considerable uncertainty about how efficient this remineralization process is in the ocean's "twilight zone" (depths between the bottom of the euphotic zone and about 1000 meters). **Buesseler *et al.*** (p. 567, see the cover) have used neutrally buoyant sediment traps that can sample sinking particles more faithfully than traps moored in fixed spots that are subject to strong cross flow from ocean currents. The transfer efficiency of sinking particulate organic matter differed by more than a factor of 2 between the two sites examined; this difference is poorly represented in present biogeochemical models.

CREDITS (TOP TO BOTTOM): TOGETHER DESIGN/LONDON UK; MITSUKO HAYASHI

Life Without Dynamin

Dynamin 1 is a neuron-specific guanosine triphosphatase involved in the endocytic recycling of synaptic vesicle membranes. **Ferguson *et al.*** (p. 570, see the Perspective by **Robinson**) created genetically engineered mice lacking dynamin 1 and found, surprisingly, that they maintained functional synapses and had limited postnatal viability. However, the synapses of these dynamin 1 knockouts contained branched, tubular plasma membrane invaginations capped by clathrin-coated pits, consistent with dynamin 1's proposed role in clathrin-coated vesicle scission. Also, after strong stimulation, synaptic vesicle endocytosis was severely impaired but could resume efficiently upon stimulus termination. This finding reveals the existence of a dynamin 1–independent mechanism that can support limited synaptic vesicle endocytosis.

Mimicking Hydrogenase

Hydrogenase enzymes rely on the cooperation of two metal centers in their active sites (either iron, or iron and nickel) to break down H_2 into protons and electrons. In contrast, effective synthetic H_2 cleavage catalysts tend to be monometallic, and the mechanisms underlying hydrogenase efficiency remain only loosely understood. **Ogo *et al.*** (p. 585, see the Perspective by **Rauchfuss**) have enhanced the mechanistic picture by synthesizing an active site model, consisting of ruthenium and nickel centers, that replicates the enzyme's essential feature of heterolytically cleaving H_2 in water at room temperature. The reaction liberates a proton and leaves behind a paramagnetic hydride-bridged Ni-Ru complex, the structure of which the authors confirmed using neutron diffraction.

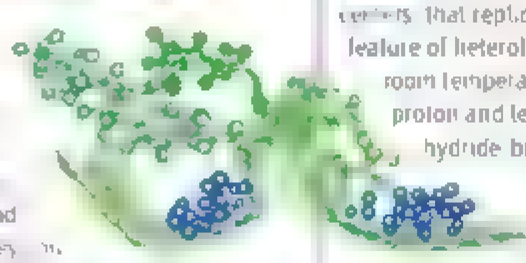

Sudden Death of Entanglement

Quantum information processing relies on the constituent parts, the qubits, forming entangled states and remaining coherent. The quantum features of many systems decay uniformly as the result of decoherence, which arises from the unavoidable coupling to the environment, and much effort has been directed to extend the coherence time of these qubits. However, **Almeida *et al.*** (p. 579, see the Perspective by **Eberly and Yu**) show that under particular circumstances where there is even only a partial loss of coherence of each qubit, entanglement can be suddenly and completely lost.

Continued on page 513

Continued from page 511

These results should mark an important consideration in the design and operation of future quantum information networks.

The Heart of Stress Responses

Two myosin heavy chain (MHC) genes are expressed in opposing manners in the mouse heart: βMHC is expressed embryonically, whereas αMHC is up-regulated postnatally. Cardiac stress shifts this ratio toward βMHC with negative effects on cardiac function, and previous work has identified microRNAs (miRNAs) as possible regulators of cardiac growth and function. **Van Rooij *et al.*** (p. 575; published online 22 March) now show that miR-208, which is encoded by an intron of the *αMHC* gene, is a cardiac-specific regulator of βMHC expression in response to stress and hypothyroidism in the heart. Deletion of the coding region of miR-208 resulted in inhibition of βMHC expression and a reduced stress response in the heart. Thus, miR-208 may act through thyroid signaling to regulate βMHC expression, possibly by repressing expression of the thyroid receptor co-regulator THRAP1.

Volcanic Release of Buried Greenhouse Gases

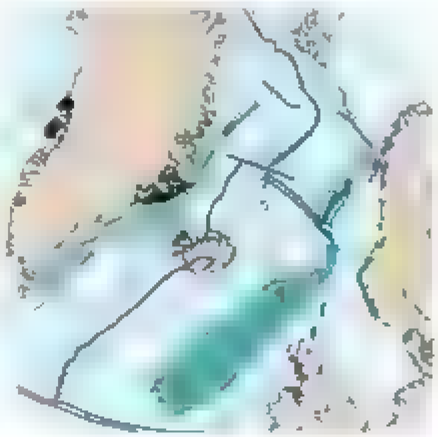

The Paleocene-Eocene thermal maximum (PETM) about 55 million years ago was marked by a rapid emission of greenhouse gases (either CO_2 or methane) during a period of a few thousand years that increased global temperatures by 5° to 10°C. However, the trigger for this sudden event has been uncertain. **Storey *et al.*** (p. 587; see the news story by **Kerr**) date a volcanic layer that overlies the marine sections marking the PETM and a volcanic ash at the top of a massive volcanic sequence in Greenland and Europe that likely erupted within about 300,000 years, marking the beginning of the opening of the Northern Atlantic Ocean. The dates are identical within error, implying that timing of the PETM overlaps that of the volcanic sequence. Massive intrusion of basalt into carbonaceous sediments may have released methane or CO_2 to the atmosphere, perhaps explaining at least some of the causes of the PETM.

Selfish Genes, Pushy Genotypes

In the past few years, transgenic mosquitoes have been developed with significantly lower ability to transmit dengue and malaria based on the action of single "effector" transgenes. These genotypes are exciting, but they are of little practical use without a gene-drive mechanism to force them to high frequencies in natural populations of the pathogen-vectoring mosquito species. **Chen *et al.*** (p. 597, published online 29 March; see the 30 March news story by **Enserink**) provide one potential drive mechanism that is expected to be very efficient at quickly increasing the frequency of nonvectoring genotypes. They engineered a maternal-effect selfish drive element in *Drosophila* by using RNA interference against essential, maternally supplied RNAs and rescue by a zygotically expressed gene. This modification, which provides the capacity to move to fixation after introduction in only about 10 generations, may provide a route by which wild insect populations can be replaced with insects unable to transmit disease.

Modeling Human Leukemia in Mice

Mouse models have been a mainstay of leukemia research for two decades and have provided many important insights into the physiological roles of genes that cause or suppress the disease. One limitation of these models, however, is that the leukemias typically originate from mouse rather than human hematopoietic cells, thereby precluding analysis of the human cell types that initiate the disease. **Barabe *et al.*** (p. 600) have created a new mouse model in which acute myeloid and lymphoid leukemias arise from primitive human hematopoietic cells expressing an *MLL* (*mixed lineage leukemia*) fusion oncogene. The leukemias in these mice show many features of the human diseases. The authors identified the leukemia-initiating cell and studied its evolution during disease progression.

CREDIT: STOREY ET AL.

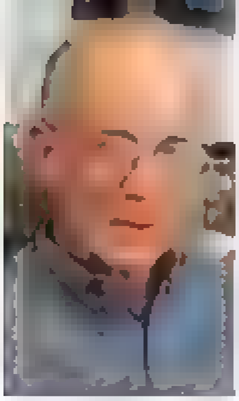

Donald Kennedy is the Editor-in-Chief of *Science*

The Biofuels Conundrum

THIS STORY BEGINS WITH GOOD NEWS, FOLLOWED BY A PROBLEM. MANY GOVERNMENTS around the world, and even some states within the United States, are finding ways to reduce greenhouse gas emissions. A major step is the almost completed buyout of the giant Texas electric utility TXU by an improbable concatenation of big investors, environmental organizations, and bankers. This promising deal would kill 8 of 11 projected coal-fired power plants and require the others to meet environmental performance standards. That's like a 15th seed making the final four or Watford winning the FA Cup. Meanwhile, there is hopeful talk in Silicon Valley about "clean tech," and "biofuels" is the new entrepreneurial mantra there. But the problem is that cutting carbon emissions with biofuels, like so many [illegible] attractive [illegible] most proposals turn out to carry external costs.

Let's start with the explosive growth of a corn ethanol industry in the tallgrass prairies of America's West. This boom for those rural economies succeeds a long history of dual-purpose farm legislation, in which production objectives are mixed with rural welfare goals. Refineries now number well over 100 with more being added rapidly, as farmers expand cultivation into lands formerly set aside for conservation and drop soybeans to make room for corn. Even if corn could yield 30% of the equivalent energy of gasoline (the goal set by the Secretary of Energy), that would create a whole array of collateral distortions. One would be its environmental impact in the United States. Another would be distortion of the price structure of an important grain commodity that is traded in world markets and used in livestock production. Will that make maize or meat more affordable to poor countries that must import it, or to the poor people who need to buy it? Not likely.

Ethanol derived from sugar cane is better: Growing the plant is energetically less costly, and extraction and fermentation are more efficient. That's what must have interested President Bush during his "Chavez shadow tour" of South America in March. Of course, U.S. companies would love to import this valuable product, which now accounts for a quarter of the ground-transportation fuel in Brazil. Despite such hopes, some senators supporting alcohol-from-corn have helped lay a heavy U.S. protective tariff on Brazilian alcohol derived from sugar. If we got rid of that, it would reduce total carbon emissions, though only if Brazil could expand its production substantially. Is there some deal in progress? Alas, nothing's up.

Sugar alcohol is better than corn alcohol, but palm oil is even better in your tank (though not in your martini). Its relatively high energy efficiency per unit volume makes it a good biodiesel fuel. Trucks can run entirely on palm oil, although it is usually mixed with conventional fossil fuels. A large-scale effort is under way to convert lands in Indonesia to palm oil plantation agriculture, with plans to double current production in a few years. But again, the effort has a downside. Not only will the needed rainforest destruction (by burning) partly cancel any energy advantage supplied by the palm oil, but the conversion will also threaten orangutans and other endangered species.

The best course is to abandon this cluttered arena and invest seriously in a direct approach. As Chris Somerville pointed out in this space,* the conversion of cellulosic biomass (corn stover, wood chips) has a far higher potential for fuel production than any of the above biofuels. The challenge is biochemical. Plant lignins occlude the cellulose cell walls; they must be removed, and then the enzymology of cellulose conversion needs to be worked out. The technology is complex.† No commercial reactor has yet been built, though six are funded. Some hope has been raised by new commitments, like the $500 million joint project between British Petroleum and the Universities of California and Illinois. Nevertheless, as Somerville notes, the sobering reality is that what the U.S. government spends on all of plant physiology is only one-hundredth of the research budget of the National Institutes of Health. That's far too little for a venture this important.

–Donald Kennedy

10.1126/science.1142978

*C. Somerville, *Science* **312**, 1277 (2006). †R. F. Service, *Science* **315**, 1488 (2007).

CREDIT: JUPITER IMAGES

EDITED BY GILBERT CHIN AND JAKE YESTON

MATERIALS SCIENCE

Reducing Together

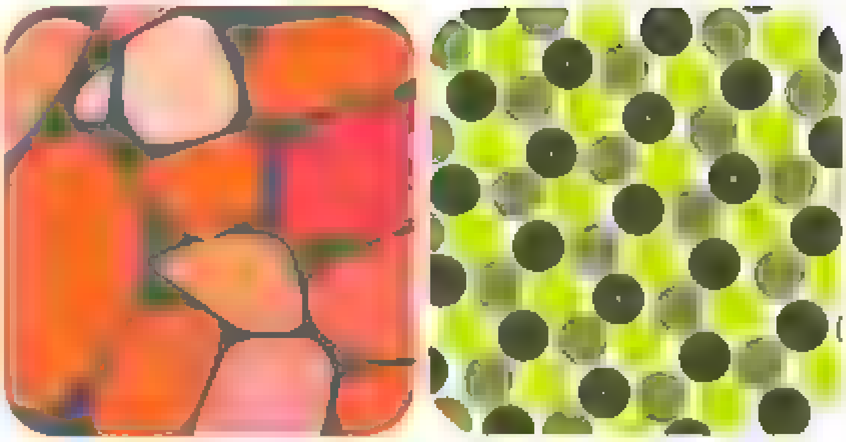

Reduction of an amorphous particle (left) to a ternary alloy (right)

Lanthanide intermetallics, which display the large magnetic anisotropies needed for high-field permanent magnets, are usually synthesized by reaction-diffusion processes that require the removal of components previously introduced to accelerate these transformations. For example, the synthesis of the ternary material $Nd_2Fe_{14}B$ with CaH_2 necessitates the removal of the calcium ions. Kim *et al.* report the aqueous synthesis of this intermetallic by sodium borohydride reduction of the metallic chlorides to form an easily isolable amorphous nanoparticulate product, which they characterized by electron microscopy and a range of diffraction techniques. The authors argue that electrostatic coupling of the Nd(III) ion with an initially formed Fe-B alloy helps to overcome the high reduction potential of the lanthanide ion to the corresponding metal. Heating of the product converts these soft magnets into a ferromagnetic material with higher coercivity. — PDS

J. Am. Chem. Soc. **129**, 10.1021/ja0706347 (2007).

BIOTECHNOLOGY

Improving the Balance Sheet

Plants incorporate (fix) CO_2 into hexoses (sugars) by coupling it to the five-carbon compound ribulose 1,5-bisphosphate in a reaction that is catalyzed by the enzyme rubisco. Unfortunately, a competitive and apparently unavoidable reaction, which is also catalyzed by rubisco (see Tcherkez *et al.* for more on this abominably perplexing phenomenon), uses O_2 as a substrate and generates one molecule each of glyoxylate and glycerate (instead of two equivalents of glycerate). Glyoxylate is then converted—via subsequent reactions in the peroxisome and mitochondrion—into glycerate, but in doing so one-quarter of the already fixed carbon atoms are lost as CO_2, with the concomitant debiting of already fixed nitrogen atoms in the form of ammonia. Increasing the local concentration of CO_2 relative to O_2 is an evolutionary achievement found in C_4 plants (such as corn), and efforts to introduce a CO_2-concentrating module into C_3 plants (such as rice) have been pursued.

Kebeish *et al.* describe a means of reducing the material cost of carbon atom recovery from glyoxylate. They have engineered the targeting of three bacterial enzymes to the chloroplast in *Arabidopsis*. The result is that when two molecules of glyoxylate are converted into one of glycerate, the CO_2 that is liberated is not lost, but is recaptured by rubisco; the consequences are a decrease in photorespiration, an increase in photosynthesis, and more biomass (leaves and roots) produced. — GJC

Proc. Natl. Acad. Sci. U.S.A. **103**, 7246 (2006); *Nat. Biotechnol.* **25**, 10.1038/nbt1299 (2007).

GENETICS

Are We Close Yet?

Large-scale genome-based surveys that look for correlations of phenotype with genotype typically examine large numbers of individuals. The results often depend on assumptions, which may not always withstand close scrutiny, about the underlying structure of the populations from which these individuals are drawn. Building on analysis of variance tests that assess whether the observed variation between populations is significant and on cluster analytic methods, Nievergelt *et al.* introduce the generalized analysis of molecular variance (GAMOVA). This approach extends a previous technique known as the analysis of molecular variance by creating a genetic background distance matrix and applying it to a multivariate regression analysis to test hypotheses about population structure. Several large human data sets (Centre d'Etude du Polymorphisme–Human Genome Diversity Project, Howells's craniometric characters, and HapMap) were reanalyzed with GAMOVA in order to demonstrate its potential for detecting population-level structure even among individuals in regions of low population differentiation. — LMZ

Genetic relations across 51 populations.

PLoS Genet. **3**, e51 (2007).

CHEMISTRY

Heptacoordinate Mercury

Although diffraction techniques have offered detailed pictures of atomic arrangements in solids, determining the corresponding structures in solution, where most reactions occur, is hindered by rapid fluctuations in the coordination environment. The solvation shell structure of aqueous mercuric ions is of interest on account of the metal's toxicity, but has proven to be an especially elusive target because of the absence of strong characteristic features in the visible absorption spectrum. Inferences from the solid state have favored a distorted octahedral, or hexacoordinate, arrangement of water molecules around the central Hg(II) ion.

Chillemi *et al.* present experimental and theoretical evidence implicating the presence of an extra water molecule in the shell, giving rise to an unusual seven-coordinate arrangement. Primary support for this claim emerges from x-ray

CREDITS (TOP TO BOTTOM): KIM ET AL., J. AM. CHEM. SOC. 129, 10.1021/JA0706347 (2007); NIEVERGELT ET AL., PLOS GENET. 3, E51 (2007)

absorption near-edge spectra, which are not consistent with an octahedral shell. Quantum chemical calculations and accompanying molecular dynamics simulations paint a picture of a flexible seven-membered shell that persists for several nanoseconds, while occasionally accepting or expelling water to create much shorter lived six- and eight-coordinate environments. — JSY

J. Am. Chem. Soc. **129**, 10.1021/ja066943z (2007).

CELL BIOLOGY

A Ribbon-Cutting Ceremony

The Golgi complex is a collection of stacked and interconnected membranes found in a juxtanuclear position in most nucleated animal cells. During cell division the Golgi complex fragments, presumably to allow for the partitioning of Golgi membranes to both daughter cells, and a protein referred to as BARS (brefeldin A–ADP ribosylated substrate, also known as CtBP1-S) is important in this process. The BARS protein acts to disconnect Golgi stacks from one another, and this fissional step has been shown to be required for successful mitosis. How then can some cells ... without BARS? Colanzi *et al.* addressed this issue by examining Golgi characteristics in a variety of cell types. They found that fibroblasts from mice genetically deficient in BARS did not possess an interconnected Golgi ribbon, and that BARS activity was not required for the completion of mitosis. On the other hand, in normal fibroblasts, where Golgi stacks were robustly linked, BARS-mediated scission was essential. — SMH

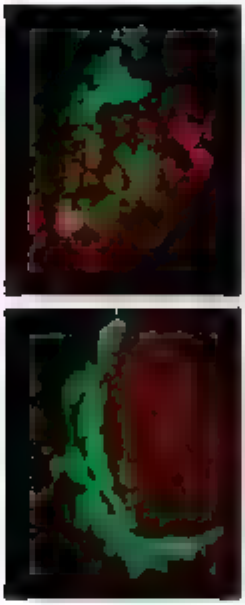

Intact (bottom) and severed (top) Golgi ribbons.

EMBO J. **26**, 10.1038/sj.emboj.7601686 (2007).

IMMUNOLOGY

Alleviating Allergies

The aberrant activation of T helper 2 $CD4^+$ lymphocytes can result in damaging allergic responses, and hence a great deal of effort has been directed toward understanding the mechanisms that normally regulate these cells. Grohmann *et al.* show that a soluble form of the glucocorticoid-inducible tumor necrosis factor receptor (GITR) cross-regulates allergic responses ... ligand. This causes plasmacytoid dendritic cells (pDCs) to produce indoleamine 2,3-dioxygenase (IDO), which mediates strong immunoregulatory effects through the catabolism of tryptophan. Administration of the synthetic glucocorticoid dexamethasone reduced symptoms of allergic responses in mice, including airway inflammation, and this effect depended on GITR-induced IDO, suggesting that this pathway may promote some actions of corticosteroids. In another study, Xanthou *et al.* observed that the regulatory cytokine osteopontin is expressed in the lungs of asthma patients and can directly affect allergic airway inflammation in mice, again via the activities of pDCs. In this system, however, allergic responses were promoted by osteopontin during the primary phase of antigen challenge, whereas ... inflammatory influence ... secondary challenge. The two mediators identified in these studies—GITR-induced IDO and osteopontin—may offer targets for the treatment of asthma. — SJS

Nat. Med. **13**, 10.1038/nm1563; 10.1038/nm1565 (2007).

APPLIED PHYSICS

An Electrical Spin on Magnetism

Magnetic ferroelectrics (multiferroics) are materials that can respond to ... electric and magnetic fields. It is common ... curves that take advantage of the large response to an applied magnetic field of the electronic state of a material with ... magnetic ... In contrast, the inverse effect, control of the magnetic structure by an applied electric field, is comparatively rare. Because of the prospect of faster switching times in smaller ... devices, there is much interest in developing such electrically controlled magnetic materials.

Recent theoretical work suggested that a key property to look for in such a material is spin chirality. It was proposed that materials in which the magnetic moments of the individual atoms form a spiral structure should also exhibit an electrical response. Yamasaki *et al.* go some way toward putting that theory into practice by showing that the spin helicity in ... perovskite $TbMnO_3$ can be electrically switched from rotating clockwise to counterclockwise by application of an electric poling field as the material is cooled through the helical spin transition temperature. Probing by neutron scattering revealed that the handedness of the chiral spin structure is controlled by the polarity of the poling field. — ISO

Phys. Rev. Lett. **98**, 147204 (2007).

Dr. Edison Liu is Pushing Science to the Highest Level at Singapore's Cancer Syndicate and Genome Institute

Q&A

With breast cancer as your special area of interest, what is your research focusing on right now?

We are focusing on the systems biology of cancer. Transcription factors such as the estrogen receptor and p53 are central to the development of breast cancer. With genomic technologies, we can map the exact control mechanisms of these factors and potentially direct precise changes using special drugs. We are hoping to make targeted therapeutics a reality.

What drew you to relocate after so many years in the U.S. and your success at the National Cancer Institute (USA)?

I was intrigued by the offer to create a research institute that integrates genomics with computational sciences, biology and medicine. I knew this required not only excellent funding, but also administrative freedom and the ability to craft a new research culture. All of this was built into Singapore's scientific environment. Then there was Singapore's vision of making science and technology a real cornerstone of its economy, and research a part of its social culture. The opportunity to do good for a society through one's daily work was too good to pass up.

Do you enjoy everyday life in Singapore?

Yes, very much. It is a lively, changing environment that is truly multicultural. The efficiency and rationality of the government is legendary, but the real joy has been in participating in the buzz of change. Singapore is a very cosmopolitan metropolis, an example of what we will all need to become. As natural resources become depleted in this world and there are no more habitable territories to colonize, we must all emulate Singaporeans in how we manage our precious natural and human resources. This requires thoughtful leadership and for all of us to be intelligent stewards of our environment.

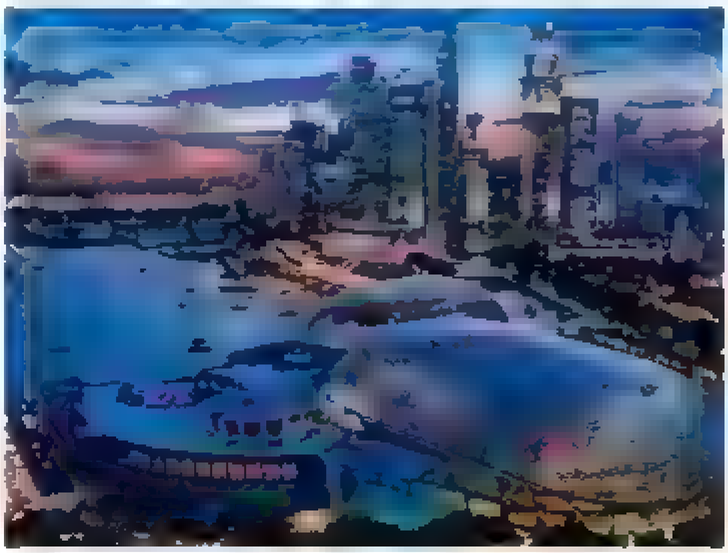

Tell us about the Singapore Cancer Syndicate.

The cancer syndicate is a funding agency that arose from my conversations with Sydney Brenner (Chairman of the Biomedical Research Council, A*STAR, Singapore) and Philip Yeo (former Chairman of A*STAR, now Senior Adviser on Science and Technology to the Minister for Trade and Industry, Singapore). They asked my opinion of what Singapore needed to solidify its beachhead in cancer research. I told them that the greatest challenge was to enhance translational research capabilities and to encourage organized cooperation among Singaporean

researchers. Knowing precisely what the challenges are for translational research from my experience at the National Cancer Institute (USA), I proposed a funding agency that supports physical and talent infrastructure, uses "just-in-time" funding to encourage progressive results and continuous quality improvement, and demands the building of research consortia. This was a significant break from the standard funding mechanisms, but it worked. This syndicate template is being used in other fields now, such as stem cell biology and bio-imaging.

And how about your work as director of the Genome Institute of Singapore?

It has been one of the most rewarding experiences of my life. We started from scratch with only three members and now have over 260 full-time staff. Following examples in Singaporean history, we were able to create something good out of nothing. My time is devoted to recruiting and mentoring scientists, to helping my colleagues here push their science to the highest level, to maintaining a culture of excellence, cooperation and collegiality, and to enhancing the reach of research and science into the fabric of a society.

Tell us about some of the exciting work at the Genome Institute. Are there recent breakthroughs?

Over the past few years, our Genome Biology and Technology group, headed by Yijun Ruan and Chialin Wei, has developed several novel cloning technologies that allow for remarkable speed and precision in identifying all the transcripts in a cell system and all the binding sites of any transcription factor. This breakthrough technology has enabled us to explore fundamental control mechanisms, especially in cancer (p53, myc, and estrogen receptor) and stem cells (Oct4, Sox2, Sal4, Nanog).

Biopolis, Singapore's biomedical sciences hub

How does the Genome Institute fit into Biopolis, Singapore's biomedical hub?

Biopolis is a 210,000 square meter biomedical research complex comprised of nine buildings. It houses six research institutes and more than 2,000 scientists. Built at a total cost of more than S$500 million (approx. US$328 million), Biopolis has state-of-the-art facilities for biomedical research. The Genome Institute of Singapore is one of the research institutes, and it is housed in its own building.

What makes Biopolis a unique home base for research?

The concept is that Biopolis is a place where scientists can work, live and play. With its superb scientific facilities, plus restaurants, cafes and bistros, shops, gyms and access to public transportation, Biopolis provides a complete environment in which research can be conducted with minimal external stress. The co-location of private sector R&D labs also allows for close interaction and collaboration and synergizes well with the public research institutes.

Who are some of the other scientists working in Singapore that you particularly admire?

There are too many to count. However, special mention should be given to the remarkable scientists working in the Genome Institute of Singapore. Yijun Ruan and Chialin Wei, who head our Genome Technologies group, have developed very novel ways to clone and sequence cDNA libraries to achieve up to 300-fold efficiency from standard approaches. Huck Hui Ng from our Stem Cell and Developmental Biology group has done a superb job of mapping the precise control nodes of the master switches of embryonic stem cell differentiation. Qiang Yu, who came with me from the National Cancer Institute (USA), has identified a novel compound that disrupts an epigenetic pathway to kill cancer cells.

What does Singapore's ability to attract high-profile scientists from around the globe mean for your work?

It means we have more friends to play with and that the impact of our work will be even greater. It also means that Singapore will achieve international status as a locus for scientific research much faster than one can imagine.

The Lancet Asia Medical Forum

Healthcare Information & Management Systems Society (HIMSS)

27th International Epilepsy Congress

AIGS World Glaucoma Congress

18th WONCA World Conference Genomics & Family Medicine

American Association of Cancer Research (AACR) Conference on Translational Cancer Medicine

World Healthcare Congress Asia

For more information, contact Singapore Exhibition & Convention Bureau

www.sciencemag.org

Science

1200 New York Avenue, NW
Washington, DC 20005
Editorial: 202-326-6550, FAX 202-289-7562
News: 202-326-6581, FAX 202-371-9227

Bateman House, 82-88 Hills Road
Cambridge, UK CB2 1LQ
+44 (0) 1223 326500, FAX +44 (0) 1223 326501

Subscription Services For change of address, missing issues, new orders and renewals, and payment questions: 866-434-AAAS (2227) or 202-326-6417, FAX 202-842-1065. Mailing addresses: AAAS, P.O. Box 96178, Washington, DC 20090-6178 or AAAS Member Services, 1200 New York Avenue, NW, Washington, DC 20005

Institutional Site Licenses please call 202-326-6755 for any questions or information

Reprints: Author Inquiries 800-635-7181
Commercial Inquiries 803-359-4578

Permissions 202-326-7074, FAX 202-682-0816

Member Benefits Bookstore: AAAS/BarnesandNoble.com bookstore www.aaas.org/bn; Car purchase discount: Subaru VIP Program 202-326-6417; Credit Card: MBNA 800-847-7378; Car Rentals: Hertz 800-654-2200 CDP#343457, Dollar 800-800-4000 #AA1115; AAAS Travels: Betchart Expeditions 800-252-4910; Life Insurance: Seabury & Smith 800-424-9883; Other Benefits: AAAS Member Services 202-326-6417 or www.aaasmember.org.

science_editors@aaas.org	(for general editorial queries)
[illegible]	(for queries about letters)
[illegible]	(for returning manuscript reviews)
science_bookrevs@aaas.org	(for book review queries)

Published by the American Association for the Advancement of Science (AAAS), *Science* serves its readers as a forum for the presentation and discussion of important issues related to the advancement of science, including the presentation of minority or conflicting points of view, rather than by publishing only material on which a consensus has been reached. Accordingly, all articles published in *Science*—including editorials, news and comment, and book reviews—are signed and reflect the individual views of the authors and not official points of view adopted by the AAAS or the institutions with which the authors are affiliated.

AAAS was founded in 1848 and incorporated in 1874. Its mission is to advance science and innovation throughout the world for the benefit of all people. The goals of the association are to: foster communication among scientists, engineers and the public; enhance international cooperation in science and its applications; promote the responsible conduct and use of science and technology; foster education in science and technology for everyone; enhance the science and technology workforce and infrastructure; increase public understanding and appreciation of science and technology; and strengthen support for the science and technology enterprise.

Information for Authors

See pages 120 and 121 of the 5 January 2007 issue or access www.[illegible]

[illegible] **Donald Kennedy**
[illegible] **Monica M. Bradford**
[illegible]
R. Brooks Hanson, Barbara R. Jasny, Katrina L. Kelner
Colin Norman

Editorial [illegible] Elizabeth Sandler [illegible] Sylvia Kihara [illegible]

News [illegible] Robert [illegible]

Production director James Landry; **senior manager** Wendy K. Shank; **assistant manager** Rebecca Doshi; **senior specialists** Jay Covert, Chris Redwood; **specialist** Steve Forrester; **Prepress director** David M. Tompkins; **manager** Marcus Spiegler; **specialist** Jessie Mudjitaba

Art director Kelly Buckheit Krause; **associate art director** Aaron Morales; **illustrators** Chris Bickel, Katharine Sutliff; **senior art associates** Holly Bishop, Laura Creveling, Preston Huey; **associates** Nayomi Kevitiyagala, Jessica Newfield; **photo editor** Leslie Blizard

Science International

Europe (science@science-int.co.uk) [illegible] Caroline Ash (Geneva: +41 (0) 222 346 3106), Stella M. Hurtley, Ian S. Osborne, Stephen J. Simpson, Peter Stern; **associate editor** Joanne Baker; **editorial support** Alice Whaley, Deborah Dennison; **administrative support** Janet Clements, Jill White; [illegible] John Travis; [illegible] Daniel Clery; **correspondent** Gretchen Vogel (Berlin: +49 (0) 30 2809 3902, FAX +49 (0) 30 2809 8365); **contributing correspondents** Michael Balter (Paris), Martin Enserink (Amsterdam and Paris), John Bohannon (Vienna); **intern** Krista Zala

Asia Japan Office: Asca Corporation, Eiko Ishioka, Fusako Tamura, 1-8-13, Hirano-cho, Chuo-ku, Osaka-shi, Osaka, 541-0046 Japan; +81 (0) 6 6202 6272, FAX +81 (0) 6 6202 6271; asca@os.gulf.or.jp; **Asia news editor** Richard Stone +66 2 662 5818 (rstone@aaas.org); **contributing correspondents** Dennis Normile (Japan: +81 (0) 3 3391 0630, FAX 81 (0) 3 5936 3531; dnormile@gol.com); Hao Xin (China: + 86 (0) 10 6307 4439 or 6307 3676, FAX +86 (0) 10 6307 4358; [illegible]); Pallava Bagla (South Asia: +91 (0) 11 2271 [illegible])

Africa Robert Koenig (contributing correspondent, rob.koenig@gmail.com)

Executive Publisher **Alan I. Leshner**
Publisher **Beth Rosner**

Fulfillment & Membership Services (membership@aaas.org) **director** Marlene Zendell; **manager** Waylon Butler; **systems specialist** Andrew Vargo; **customer service supervisor** Pat Butler; **specialists** Laurie Baker, Tamara Alfson, Karena Smith, Vicki Linton, Latoya Casteel; **circulation associate** Christopher Refice; **data entry supervisor** Cynthia Johnson; **specialists** Tomeka Diggs, Tarrika Hill, Erin Layne

Business Operations and Administration director Deborah Rivera-Wienhold; **business manager** Randy Yi; **senior business analyst** Lisa Donovan; **business analyst** Jessica Tierney; **financial analysts** Michael LoBue, Farida Yeasmin; **rights and permissions: administrator** Emilie David; **associate** Elizabeth Sandler; **marketing director** John Meyers; **marketing managers** Darryl Walter, Allison Pritchard; **marketing associates** Julianne Wielga, Mary Ellen Crowley, Catherine Featherston, [illegible]; **international marketing manager** Wendy Sturley; **marketing executive** Jennifer Reeves; [illegible] **services executive** Linda Rusk; **Japan sales** Jason Hannaford; **site license sales director** Tom Ryan; **sales and customer service** [illegible]; **electronic media manager** Lizabeth Harman; **project manager** Trista Snyder; **assistant manager** Lisa Stanford; **production associates** Michele Johnston, [illegible]

[illegible]

Product [illegible] **Midwest** Rick Bongiovanni: 330-405-7080, FAX 330-405-7081 • **West Coast/W. Canada** Teola Young: 650-964-2266 • **East Coast/E. Canada** Christopher Breslin: 443-512-0330, FAX 443-512-0331 • **UK/Europe/Asia** Julie Skeet: +44 (0) 1223-326-524, FAX +44 (0) 1223-325-532 • **Japan** Mashy Yoshikawa: +81 (0) 33235 5961, FAX +81 (0) 33235 5852 • **traffic manager** Carol Maddox; **sales coordinator** Dejandra Simms

Commercial Editor Sean Sanders: 202-326-6430

Classified [illegible] **US/recruitment sales manager** Ian King: 202-326-6528, FAX 202-289-6742; **US/Industry** Darrell Bryant: 202-326-6533; [illegible] Daryl Anderson: 202-326-6543; **Northeast** Allison Millar: 202-326-6572; **Southeast** Fernando Junco: 202-326-6740; **West** Katie Putney: 202-326-6577; **sales coordinators** Erika Bryant, Rohan Edmonson, Shirley Young; **international: sales manager** Tracy Holmes: +44 (0) 1223-326525, FAX +44 (0) 1223-326532; **sales** Christina Harrison, Svitlana Barnes; **sales assistant** Louise Moore; **Japan** Jason Hannaford: +81 (0) 52 757 5360, FAX +81 (0) 52 757 5361; **advertising production operations manager** Deborah Tompkins; **associates** Christine Hall, Amy Hardcastle; **publications assistants** Robert Buck, Mary Lagnaoui

AAAS Board of Directors retiring president, chair John P. Holdren; **president** [illegible]; **president-elect** [illegible]; **treasurer** David E. Shaw; **chief executive officer** Alan I. Leshner; **board** John E. Dowling, Lynn W. Enquist, Susan M. Fitzpatrick, Alice Gast, Linda P. B. Katehi, Cherry A. Murray, Thomas D. Pollard, Kathryn D. Sullivan

ADVANCING SCIENCE, SERVING SOCIETY

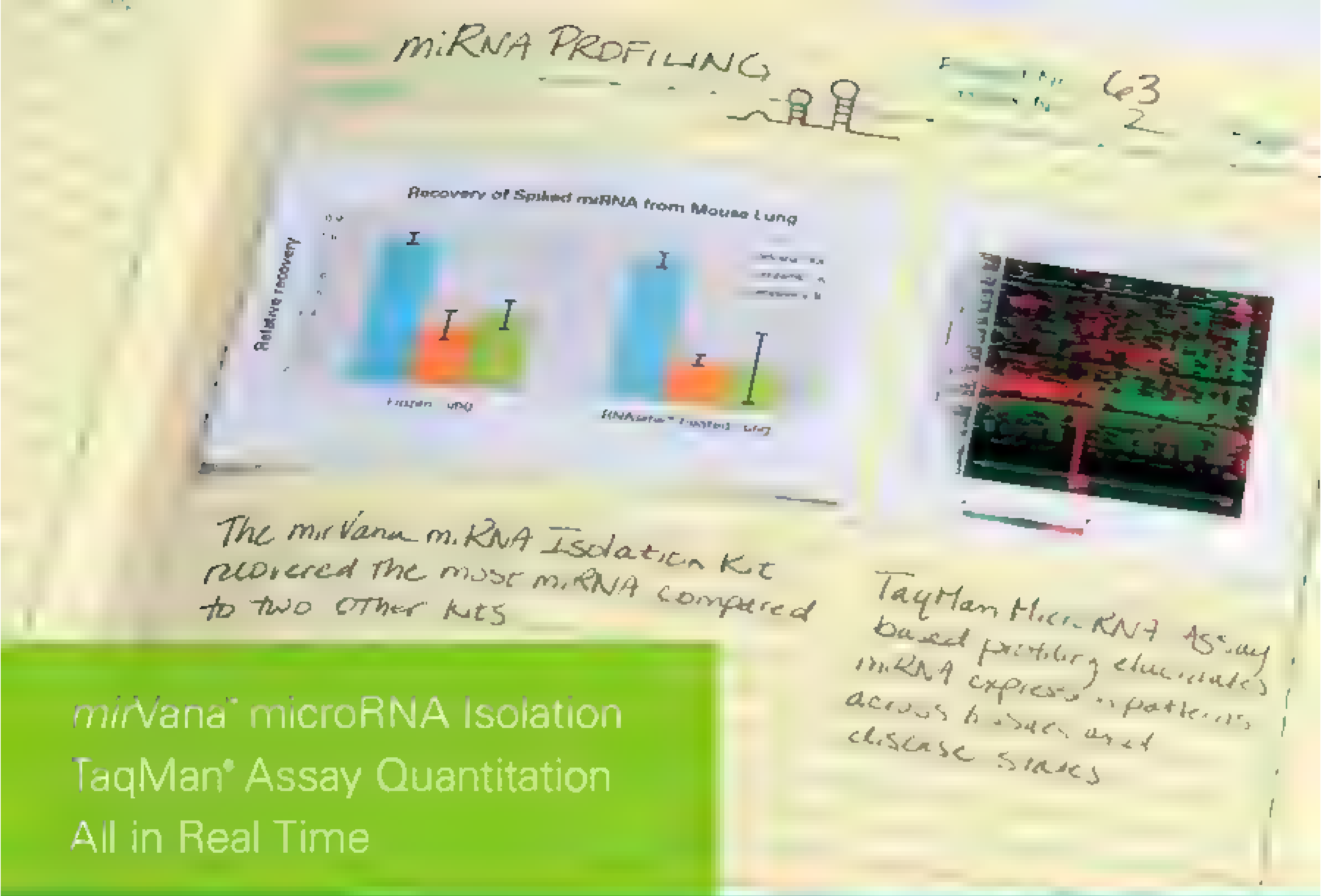

miRNA PROFILING
Recovery of Spiked miRNA from Mouse Lung
Relative recovery
The mirVana miRNA Isolation Kit recovered the most miRNA compared to two other kits
TaqMan MicroRNA Assay based profiling elucidates miRNA expression patterns across tissues and disease states

EDITED BY CONSTANCE HOLDEN

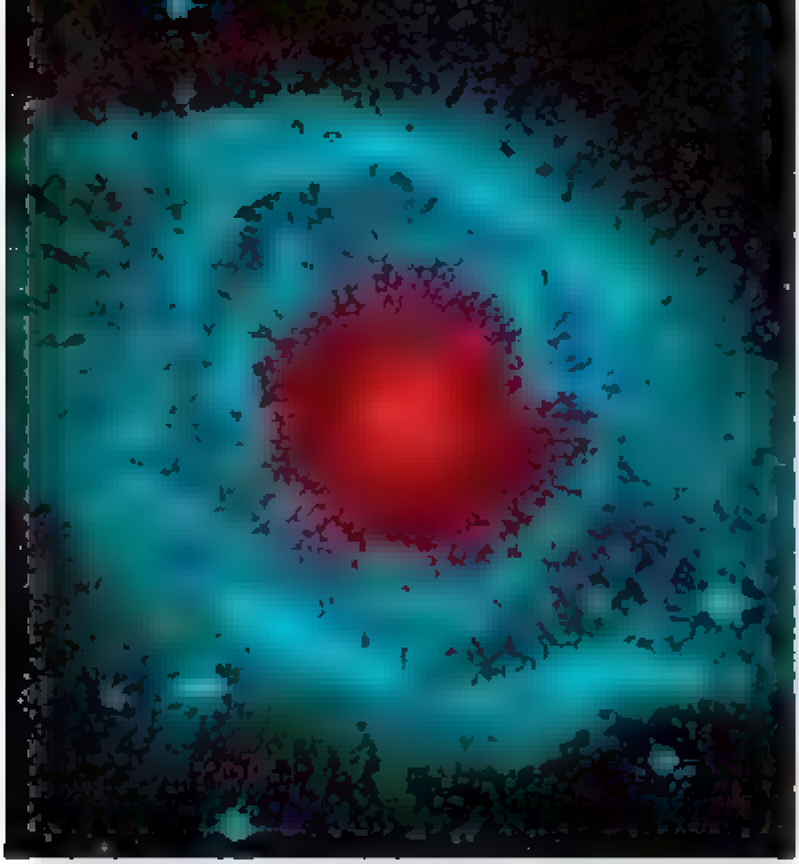

Astro Tool Kit

Whether [illegible] reams of data files or manually clean[illegible] charge-coupled device images of galaxies, astronomers face their share of drudgery. The National Virtual Observatory (NVO) aims to make those tasks less burdensome by pointing space researchers to tools, databases, and other useful sites. Run by scientists from around the United States, the portal is part of an international network of astronomy resources. It includes a master list of cosmic catalogs, image archives, and other information caches. If you've already nabbed an exposure of the night sky, another feature will unwarp it to remove telescope distortion and [illegible] the image to celestial objects. For more [illegible] as a tool for analyzing and comparing spectra, check the related VO Web Services [illegible]

Algorithmically Yours

[illegible] controversial [illegible] Wildlife Service (FWS).

This [illegible] National Science Foundation are creating [illegible] and even [illegible] whether a comment [illegible] relevant [illegible]

[illegible] Shulman of the University of Pittsburgh in Pennsylvania. [illegible] Administration [illegible] emotionally charged [illegible] out what the agency wants to hear about most science and economics. FWS [illegible] to make a final decision.

Modern Life Bad for Boys?

A study this month reported a slight but steady decline in the ratio of boys to girls born in both the United States and Japan since 1970.

Normally, 105 boys are born for every 100 girls. Epidemiologists Devra Lee Davis and colleagues at the University of Pittsburgh, Pennsylvania, report [illegible] between 1970 and 2002 [illegible] 135,000 [illegible]

Many [illegible] say. For example, researchers at the University of Ottawa, Canada, reported in 2005 that [illegible] First Nation [illegible] about 10 [illegible] 199[illegible] [illegible]

The decline [illegible] Davis [illegible] Harvard [illegible] Marc Weisskopf says [illegible] are clear.

THE RABBIT AND THE CUCKOO

[illegible] Wildlife Conservation Society (WCS) [illegible] with a [illegible] Sumatran [illegible] National Park [illegible] 7 years ago. "You don't expect [illegible] WCS [illegible] since 199[illegible]

Meanwhile, the team [illegible] by scientists [illegible] Perhaps more importantly [illegible] they have [illegible] the forest [illegible]

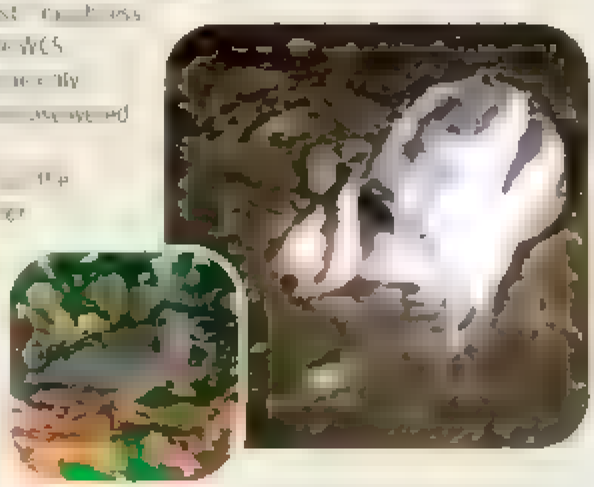

An Unspeakable Campus Tragedy

A candlelight vigil at Virginia Tech on 17 April.

BLACKSBURG, VIRGINIA—Two days after a student gunman killed 32 people and himself here at Virginia Polytechnic Institute and State University, the Drillfield [illegible] campus was eerily quiet. Instead of hundreds of students [illegible] tossing Frisbees, a few dozen people [illegible] solemnly around a makeshift memorial. Among those killed in the massacre were a popular professor and eight students in the Department of Civil and Environmental Engineering (CEE). The Department of Engineering Science and Mechanics (ESM) lost two esteemed faculty members and their home building, Norris Hall, where most of the victims died, will be closed indefinitely. Last week, the faculty of [illegible] departments [illegible] emergency meetings [illegible] trying to [illegible].

[illegible] lives lost on 16 April and offers condolences to the survivors. Staff writer Greg Miller provides these remembrances of some of the victims.

LIVIU LIBRESCU

A Romanian-born aerospace engineer, Librescu, 76, survived the Holocaust as a child and emigrated to Israel in the 1970s. He joined the ESM department at Virginia Tech in 1985. Librescu studied how the inherent flexibility in structures such as airplane wings and helicopter rotor blades affects their aerodynamic properties, says Walter Silva, an aerospace engineer at NASA's Langley Research Center in Norfolk, Virginia. "He's very well known in the [illegible], and he had some reason to be arrogant, but he was actually very humble," Silva says.

Students [illegible] Librescu as a father figure. A former [illegible] longtime [illegible] Ohseop Song of Chungnam National University in Daejeon, South Korea, says that Librescu always [illegible] from [illegible] conferences with presents for [illegible] graduate students, treating them as if they were his own grandchildren.

According to many reports, Librescu threw his body against the door of his classroom, giving his students time to flee as the gunman tried to force his way in. One note left at the Drillfield memorial reads, "Librescu: My hero. Goodbye, Professor."

KEVIN GRANATA

Granata, 46, an ESM faculty member, was a rising star in biomechanics whose research bridged the gap between engineering and medical sciences. "Kevin had a very keen mind for evaluating movement disorders," says Mark Abel, an orthopedic surgeon at the University of Virginia in Charlottesville who [illegible] with Granata, aimed at designing better [illegible] for children with cerebral palsy.

Granata was also a valued mentor. "He taught me how to be an engineering professor," says Sara Wilson, a mechanical engineer at the University of Kansas in Lawrence who trained with Granata as a postdoc. "He was passionate about his research and worked really hard, but he also reserved time for his family."

Granata's office was on the third floor of Norris Hall, one floor above where the shootings took place. Hearing the noise below, Granata went to see what he could [illegible] but only after [illegible] 20 students from a nearby classroom into the safety of his office, according to a report in the *Washington Post*. "Kevin was a tough guy," says Abel. "He's not the kind of guy to hear a bunch of commotion and crawl under a desk."

G. V. LOGANATHAN

Colleagues uniformly describe Loganathan, 51, as one of the nicest people they'd ever met. Born in India, Loganathan [illegible] the United States for graduate school and joined the CEE department at Virginia Tech in 1982. He was an expert in water resources management.

[illegible] and collegial, Loganathan had a gift for teaching. Among many other accolades, he won one of three university-wide [illegible] Awards for Excellence in Teaching last year. Loganathan seemed to [illegible] and [illegible] with his [illegible] and says his colleagues knew how to push his good students hard without [illegible].

Loganathan was teaching [illegible] Advanced Hydrology course in Norris Hall when the gunman [illegible] him and many students.

THE STUDENTS

"It was clear from the beginning that Jeremy Herbstritt was enthusiastic about science," says CEE professor Panayiotis Diplas, who was his adviser. At an open house for prospective graduate students last year, Herbstritt stretched his scheduled 15-minute [illegible] with Diplas into a 40-minute discussion of potential research projects. "He was a person with tremendous energy," Diplas says.

Herbstritt was one of seven CEE graduate students from Loganathan's class who died, along with Brian Bluhm, Daniel O'Neil, Juan Ortiz, Waleed Shaalan, Matthew Gwaltney, and Partahi Lumbantoruan. The other two victims in that class were Julia Pryde, a graduate student in biological systems engineering, and Jarrett Lane, a civil engineering major.

Six other undergraduates majoring in science or engineering were killed in the rampage.

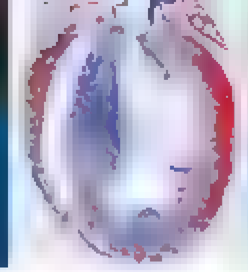

STEM CELLS

Stem Cell President Quits After Acrimonious Meeting

Zach Hall was so rattled by a recent meeting at the California Institute for Regenerative Medicine (CIRM)—the $3 billion stem cell institute set up by statewide referendum in 2004—that he decided to quit as president earlier than he had planned. Hall cited the "contentious" nature of the meeting as well as his disappointment over likely delays in disbursing money for construction of new research facilities that scientists say are crucially needed.

CIRM has scheduled a special teleconference meeting of its board for 2 May to respond to Hall's 30 April departure and the conflict over how to proceed with a $222 million construction program.

Both issues arose from a 13 April meeting of CIRM's facilities working group, at which patient advocates balked at the idea of having a Request for Applications (RFA) ready by June for the so-called large facilities grant program. The members of the group wanted more time to consult experts on technical issues and sound out the public on what and where facilities are needed.

Neuroscientist Hall, CIRM's founding president, had earlier intended despite planned prostate surgery in May to stay through the 5 June meeting of the Independent Citizens' Oversight Committee (ICOC). But, he wrote the board, "the exceedingly contentious and occasionally personal tone of the ... meeting suggests that it is in both my best interest and that of the Institute for me to step down at this time."

The state's universities see construction of new research facilities as an essential part of the grand plan for CIRM. At a 10 April ICOC meeting, members representing research institutions expressed the need to move speedily. ICOC Chair Robert Klein observed that costs are rising—and at a 10% inflation rate, a 1-year delay would cost $60 million. The panel decided in a straw vote not to lose more time by conducting a "survey of institutional plans" to gain more information on which to base the RFA. Hall confidently predicted that the RFA—covering $150 million for a handful of big construction grants and $72 million for $5 million to $10 million grants—would be ready by July at the latest.

Hall was taken aback by the very different reception he got at the facilities group meeting 3 days later. That group is made up of disease advocates who are also members of ICOC as well as California real estate specialists; for conflict-of-interest reasons, it contains no researchers or university officials.

Arguing that they were ill-prepared to gauge the need for facilities in the state, members of the working group lobbied for more time for assessment. "If we don't, we're going to be in a situation where we're backing the Brinks truck up to a couple of really well-established institutions that have access to a ton of wealth," warned AIDS patient advocate Jeff Sheehy. Diabetes patient advocate Marcy Feit said the public has to be consulted. "I don't care if we have to meet with a hundred people or a million people. ... That's our responsibility."

Burned out. Zach Hall, facing surgery, is leaving CIRM this month.

Judging by the meeting transcript, the atmosphere got a bit tense. Hall seemed perplexed, saying that he faced a "dilemma" because "there is a real split between what this ... working group is saying, and what was said at the ICOC meeting by ... those representing the scientific community." The facilities group ended up voting unanimously for public hearings. There is a "cultural difference" between the disease advocates and scientists "who understand the urgency" of the program, Hall concluded.

Such a difference was evident in comments by Joan Samuelson, who represents the Parkinson's Action Network. "I've been hearing from lots of people ... who say, 'Don't throw a lot of money at facilities,'" said Samuelson. She added that it's private companies, not universities, that come up with cures. Sheehy later told *Science*, "I'm stunned. ... I feel betrayed" by Hall's attempt to dismiss the arguments of the disease advocates. At this point, he says, the working group has "no evidence basis from which to proceed."

CIRM's board faces a full agenda at next week's meeting: whether to go ahead with hearings on the facilities program, and whom to appoint as interim head of CIRM. Also needed is a new head for the facilities committee, whose chair, California developer Albert "Rusty" Dobbs, resigned abruptly without explanation after the 13 April meeting.

But there's light at the end of the tunnel. The presidential search is moving ahead apace. The search committee will be interviewing a half-dozen top contenders in May, with final candidates to be considered at the June ICOC meeting. CIRM also faces its final hurdle in the lawsuits that have stymied its efforts to raise money. The California Supreme Court is expected shortly to turn down a final appeal from groups that have been trying to get CIRM declared unconstitutional, in which case money from bond sales may start rolling in as early as this summer.

—CONSTANCE HOLDEN

CREDIT: HOWARD LIPIN/ZUMA PRESS/NEWSCOM

Pipsqueak. Large igneous provinces can boast a million times the lava produced by [illegible] not to scale).

GEOCHEMISTRY

Humongous Eruptions Linked to Dramatic Environmental Changes

Researchers looking for the cause of big catastrophic changes on planet Earth have fingered a new one: so-called flood basalt eruptions, or large igneous provinces (LIPs) eruptions. These are no Mount St. Helenses or even Krakataus, which cooled the planet a degree or so and painted pretty sunsets for a couple of years. No, a single LIP eruption can spew 100 times the magma of anything seen in historical times. The 1000 such eruptions that can follow the first could build a lava pile of millions of cubic kilometers. Such massive volcanic activity seems to have dramatically altered the atmosphere and oceans for hundreds of thousands of years 94 million years ago and again 56 million years ago, according to two new studies.

The newly strengthened link between mega-eruptions and major environmental events comes in studies that draw on a single geologic record containing two signatures: that of a LIP eruption and another of geologically abrupt environmental change. On page 587, geochronologist Michael Storey of Roskilde University in Denmark and colleagues use precise rock dating to tie the outpourings of a LIP—whose remains now span the North Atlantic from Greenland to Great Britain—to the sudden 5°C warming 56 million years ago known as the Paleocene-Eocene thermal maximum, or PETM (*Science*, 19 November 1999, p. 1465).

Scientists have long thought that the great burst of greenhouse gas—carbon dioxide or methane—that marked the beginning of the PETM must be linked to the 5 million to 10 million cubic kilometers of erupted North Atlantic magma, if only because they happened at about the same time. But having to date the two events in different records using different techniques made the case less than convincing. So Storey and his colleagues dated more rocks from the LIP using the argon-argon technique based on the radioactive decay of potassium-40. Combined with previously published data, the dating places one of the largest surges of magma of the past quarter-billion years at 56.1 ± 0.5 million years ago.

The team also applied argon-argon dating to volcanic ash buried in marine sediments southwest of Great Britain that also contain a record of the PETM. That ash layer had been linked to a LIP ash deposit in East Greenland with a similar age, but the researchers beat down the uncertainty by making a total of 50 age measurements on the two ashes. Using additional published dating of the sediment between the ash layer and the start of the PETM, Storey and his colleagues put the beginning of the PETM at 55.6 million years ago.

The new dating thus places the most dramatic warming of its kind just within the uncertainty of the beginning of one of the largest volcanic outpourings ever. "I think that the dating is quite good," says Paul Renne of the Berkeley Geochronology Center in California. It "certainly provides strong linkage between the PETM and the [LIP]."

Another study has strengthened the linkage between massive volcanism in the Caribbean and an abrupt transformation of the oceans 94 million years ago, known as oceanic anoxic event 2 (OAE 2). OAEs were a half-dozen episodes in the warm mid-Cretaceous period 120 million to 80 million years ago when ocean sediments accumulated with so much organic matter that the sediments turned black. Something shifted ocean conditions to produce these "black shale" sediments, perhaps by eliminating oxygen from the deep sea. The leading candidate for a trigger is large volcanic eruptions.

OAE 2, the archetypal OAE event, had been linked to the massive Caribbean LIP through dating, but geochemist Junichiro Kuroda of the Institute for Research on Earth Evolution in Yokosuka, Japan, and colleagues took a different approach. They harked back to the search in the 1980s for markers of a large impact buried along with the remains of dinosaurs and other life snuffed out 65 million years ago. Instead of the element iridium brought in by an impacting asteroid, they looked in sediments for lead, a potential marker of a rock's source. They traced lead's isotopic composition across the onset of OAE 2 at an outcrop in Italy.

In a few centimeters of sediment leading up to the start of OAE 2 and beyond, the relative proportion of lead-208 dropped precipitously, they found. "The way it moves is difficult to explain without a volcano" contributing its distinctive mix of lead isotopes, says geochemist Catherine Chauvel of the University of Grenoble, France. In addition, the new lead-isotope composition bears a particular resemblance to that of the Caribbean LIP.

So, rare and extraordinary volcanic eruptions coincide in time with rare and exceptional environmental changes, strongly linking eruptive cause to environmental effect. However, that link isn't yet clarifying just how LIPs wreak their havoc. For that, researchers will need more timing on more of the cascading effects of humongous eruptions.

—RICHARD A. KERR

CREDIT: ALAN ROBOCK

LUNAR SCIENCE

Congress Restores Funds for NASA Robotic Landers

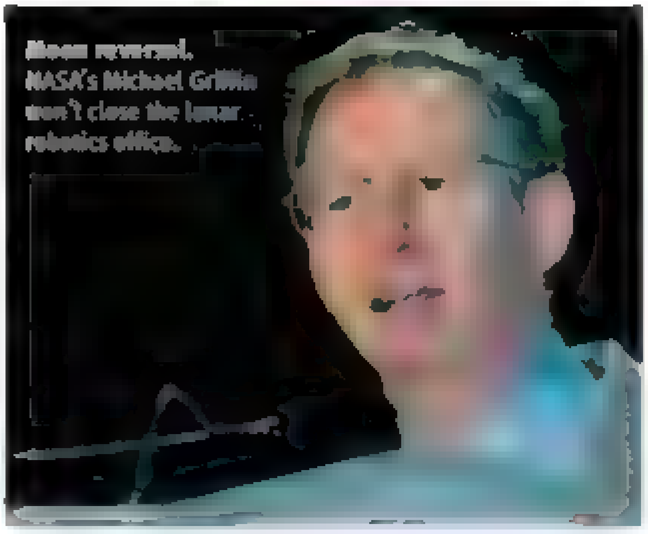

Moon reversal. NASA's Michael Griffin won't close the lunar robotics office.

Angry U.S. lawmakers have come to the rescue of NASA's robotic lunar lander program. NASA chief Michael Griffin had pledged to shut down the program to save money, but after strong pressure from both House and Senate members, the space agency has granted it a reprieve. The reversal, although welcomed by lunar researchers, puts more pressure on Griffin to pare other missions or win additional funding from Congress.

In a 10 April letter, the chairs of NASA's two spending panels, Senator Barbara Mikulski (D–MD) and Representative Alan Mollohan (D–WV), ordered Griffin to restore $20 million to operate the lunar robotics office based at Marshall Space Flight Center in Huntsville, Alabama. The letter is a response to the agency's 2007 operating plan detailing how it intends to spend its $16.2 billion budget, approved in February; the plan must pass muster with Congress. As late as 12 April, Griffin was insisting that there is no need for robots beyond the Lunar Reconnaissance Orbiter planned for launch next year. But on 19 April, a NASA spokesperson said that "right now there are no plans to close" the lunar robotics office.

The about-face has more to do with jobs than lunar data. Faced with a $700 million shortfall in NASA's exploration program, Griffin decided this winter that the landers—the details of which have not yet been defined—were a luxury he could not afford (*Science*, 16 March, p. 1482). That decision upset Alabama Republican Senator Richard Shelby, who spearheaded the effort to keep open the Marshall office, with its 32 employees. In an 18 April speech, according to *The Huntsville Times*, the senator noted that he was "counting the days ... 1 year and eight-and-a-half months—[until] we have a new [NASA] administrator." Two days earlier, Griffin had reminded an Alabama delegation visiting Washington about Marshall's central role in the human exploration effort, which aims to return astronauts to the moon by 2020.

NASA's operating plan for the fiscal year that ends on 30 September also reflects the rising costs of several science missions. NASA will spend $63 million more in 2007 than it initially planned to keep the launch date for its Mars Science Laboratory from slipping beyond 2009. It will add $17 million to ensure a November launch of the Gamma Ray Observatory and $37 million above what it had anticipated so that the Kepler mission to find extrasolar planets can take off by the end of 2008.

Those increased costs, combined with completing the space station and building a new launcher, are forcing NASA to find ways to save money. Although the proposed elimination of the lunar robotics program didn't fly with key legislators, NASA's larger budget problems aren't going away. Last week, several Democratic lawmakers urged the White House to meet with congressional leaders to find a way out of the morass. But so far, that call for a space summit has elicited no response.

—ANDREW LAWLER

EXOPLANETS

Habitable, But Not Much Like Home

For the first time, astronomers have found an Earth-like planet that could be habitable. Like an oasis in space, the rocky world, possibly covered with oceans, orbits a puny red dwarf star just over 20 light-years away in the constellation Libra. "On the treasure map of the universe, one would be tempted to mark this planet with an X," says team member Xavier Delfosse of Grenoble University in France.

Most of the 200-plus exoplanets found to date are massive balls of gas similar to Jupiter. Only two have been found weighing less than eight times the mass of Earth. One of these is too cold, the other too hot for liquid water to exist on its surface. But the new planet, found by Stéphane Udry of Geneva Observatory in Switzerland and his colleagues, orbits right in the habitable zone of its mother star, Gliese 581, where temperatures are between 0° and 40°C.

Being a cool red dwarf, Gliese 581's habitable zone is close-in. The planet is a mere 10.7 million kilometers from the star—one-fourteenth the distance of Earth from the sun—and completes an orbit every 13 days. Two years ago, the team found a more massive planet in an even closer orbit around the same star. And in the new data, taken by the European Southern Observatory's 3.6-meter telescope at La Silla in Chile, they also uncovered a third planet in a wider 84-day orbit. The results have been submitted to *Astronomy & Astrophysics*.

Tiny periodic wobbles of the star indicate that the mass of the new planet could be as small as five times that of Earth, strongly suggesting a ball of rock, not gas. Udry concedes that the true mass might be larger, depending on the angle between the orbit and our line of sight. But he says, the mass cannot be much larger or the planetary system would be unstable.

The new discovery is "wonderful news," says Geoffrey Marcy of the University of California, Berkeley, whose team has found more than half of all exoplanets so far. But planet hunter William Cochran of the University of Texas, Austin, says, "It remains to be seen how habitable this planet actually is." Cochran points out that the planet may always keep one face toward its mother star. Moreover, some theorists think that because of the way they form, planets close to red dwarfs may accumulate little water.

Although it could in principle harbor liquid water, anyone visiting this cosmic oasis would find it very different from Earth. Says Udry: "The Holy Grail would of course be a planet with the mass of the Earth orbiting a star like the sun, in a 365-day orbit. But we have to go step by step."

—GOVERT SCHILLING

Govert Schilling is an astronomy writer in Amersfoort, the Netherlands.

CREDIT: 23RD NATIONAL SPACE SYMPOSIUM

BIODEFENSE

Proposed Biosecurity Review Plan Endorses Self-Regulation

A federal advisory group has come up with a long-awaited blueprint for how the U.S. government should oversee biological research known as "dual use," or experiments that could potentially be used by bioterrorists to cause harm. The voluntary plan would let scientists themselves decide whether their project raises concerns, which would then trigger a higher-level review—a process some critics think is woefully inadequate.

Many microbiologists like the idea of self-regulation. But even supporters are frustrated by the lack of details provided by the 25-member National Science Advisory Board for Biosecurity (NSABB) after 2 years of work. Meanwhile, a few universities have begun reviewing all genetic engineering experiments for dual use, an approach that some say is inevitable.

The report follows the explosion of federal biodefense research in response to the 2001 anthrax attacks. A 2004 National Research Council (NRC) report warned that stringent regulations could impede legitimate research and called for a self-governing system of oversight. That panel described seven types of "experiments of concern" that would automatically be reviewed, such as enhancing the virulence of a pathogen, but left it to a new federal advisory committee—NSABB—to develop guidance.

NSABB, chaired by microbiologist Dennis Kasper of Harvard Medical School in Boston, has now done that. In a 50-page draft report released last week, it says scientists should report annually whether their research is potentially "dual use of concern," perhaps starting with a check box on their grant proposal. A committee, perhaps an expanded version of the institutional biosafety committees (IBCs) that now oversee genetic engineering experiments, would then review the flagged projects.

Although the microbiology community is generally pleased with the plan, it is not entirely clear how it might work, Ronald Atlas of the University of Louisville in Kentucky says it is "somewhat schizophrenic" that the report calls for a voluntary system yet suggests that funding agencies make compliance a condition of funding. Nor does the report tackle synthetic biology directly, he says, leaving it unclear whether an experiment 5 years ago that built a poliovirus from scratch would even be covered. Also left undecided is whether the rules should cover fields outside the life sciences, such as chemical engineering.

Richard Ebright of Rutgers University in Piscataway, New Jersey, is much harsher. He lambastes the committee's recommendation that even if an experiment fits into one of the NRC report's seven categories, an investigator could decide that the work isn't risky enough to be "of concern." These subjective criteria "preclude meaningful oversight," Ebright says. Ebright and others, such as Alan Pearson of the Center for Arms Control and Non-Proliferation in Washington, D.C., also say the guidelines should be mandatory and should cover privately funded research.

The report will now go to an interagency committee, which will seek public comment and likely ask NSABB to hone the guidelines. But some universities are going ahead on their own. At Duke University in Durham, North Carolina, and two other schools participating in a regional biodefense center, IBCs are already screening all genetic engineering projects for biosecurity risks, on the grounds that scientists don't have the expertise or objectivity to decide, says Megan Davidson of Duke.

–JOCELYN KAISER

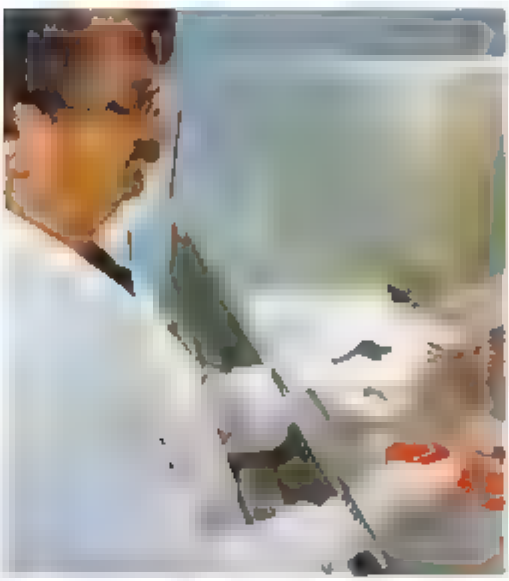

CREDIT: JAMES GATHANY/CDC

Screen test. Proposed guidelines would have investigators decide whether their research could be useful to bioterrorists.

Think Tiny, Kremlin Says

With $1 billion in new announced government financing at its disposal, one of Russia's leading centers of scientific research, the Kurchatov Institute, will manage Russian nanotech research and development. The $1.1 billion nanotech windfall, announced last week, is an enormous sum for science in Russia, where the average researcher is slated to earn only $1000 per month by 2010. The first 3 years of investment, aimed to outfit a dozen or so research centers with laboratory equipment, will be followed by a second stage to run through 2015.

"This will help Russia emerge on the international stage in nanotechnology, where it had been in a state of decay," says Mihail Roco of the U.S. National Science Foundation.

–BRYON MACWILLIAMS AND JOHN SIMPSON

Think Big, Report Suggests

The U.S. government needs to do a better job of putting into strategic context its plans for new nuclear weapons, says a panel convened by the American Association for the Advancement of Science, which publishes *Science*. The main points of a new report by the panel were disclosed in February (*Science*, 9 March, p. 1348) but the final version includes new emphasis on the "international implications" of the nascent Reliable Replacement Warhead (RRW) effort to make bombs that don't need to be tested. C. Bruce Tarter, panel chair and former director of Lawrence Livermore National Laboratory, says that the White House must explain "what are nuclear weapons for ... [and] how many do we need." The chair of the House spending panel that controls nuclear weapons, Peter Visclosky (D–IN), is an RRW skeptic and has called for such big picture answers.

–ELI KINTISCH

Indian Rockets Prove Lucrative

NEW DELHI—India entered the fiercely competitive commercial space market with a bang on 23 April with the launch of an Italian astronomy satellite. The Indian Space Research Organisation (ISRO) is muscling in on a multibillion-dollar business that has been the exclusive domain of rocket efforts in Europe, China, Russia, and the United States. ISRO is trumpeting its cost advantage: It charged Italy about $11 million, a competitive price given the launch location close to the equator. Italy's AGILE craft will study among other things, gamma ray bursts and dark matter. ISRO chair G. Madhavan Nair called AGILE's launch a "historic moment."

–PALLAVA BAGLA

GENETICS

Erasing MicroRNAs Reveals Their Powerful Punch

For more than 2 decades, biologists have illuminated the roles of genes by deleting them in mice and studying these "knockout" animals, which lack the proteins encoded by the targeted genes. Now, scientists say they're beginning to uncover an entirely new layer of gene regulation by using the same strategy to erase portions of genes that make snippets of RNA. Just as knockouts of traditional protein-coding genes yielded a treasure trove of knowledge about how different genes govern health and disease, this next generation of knockouts could fill in the gaps that remain.

In a flurry of papers, four independent groups have for the first time deleted mouse genes for microRNAs, RNA molecules that can modulate gene behavior. Each time, the rodents were profoundly affected, with some animals dropping dead of heart trouble and others suffering crippling immune defects.

Since their discovery more than a decade ago, microRNAs have electrified biologists. Geneticists estimate that the human body employs at least 500 during development and adult life. But it wasn't clear, especially in mammals, how important individual microRNAs were, because some evidence suggested that these gene-regulators had backups. In worms, for example, erasing a particular microRNA by deleting the relevant stretch of DNA occasionally had a dramatic effect but more often didn't appear to do much.

"I think there was a fear that nothing could be found" by deleting microRNA genes in mammals one at a time, says David Corry, an immunologist at Baylor College of Medicine in Houston, Texas. As it turns out, the opposite is true. "There's a lot more that the microRNAs are doing that we didn't appreciate until now," says Frank Slack, a developmental biologist at Yale University who studies microRNAs in worms.

Two of the groups that produced the mammalian microRNA knockouts deleted the same sequence for miR-155 and describe the effects on the mouse immune system on pages 604 and 608. One team was led by Allan Bradley at the Wellcome Trust Sanger Institute and Martin Turner of the Babraham Institute, both in Cambridge, U.K., and the other by Klaus Rajewsky of Harvard Medical School in Boston. The other teams, one whose results were published online by *Science* on 22 March (www.sciencemag.org/cgi/content/abstract/1138089) and one whose work appears in the 20 April issue of *Cell*, eliminated different microRNAs and documented defects in mouse hearts.

The two groups that deleted miR-155 found that the rodents' T cells, B cells, and dendritic cells did not function properly, leaving the animals immunodeficient. The mutation also cut down the number of B cells in the gut, where the cells help fight infection, and triggered structural changes in the airways of the lungs, akin to what happens in asthma.

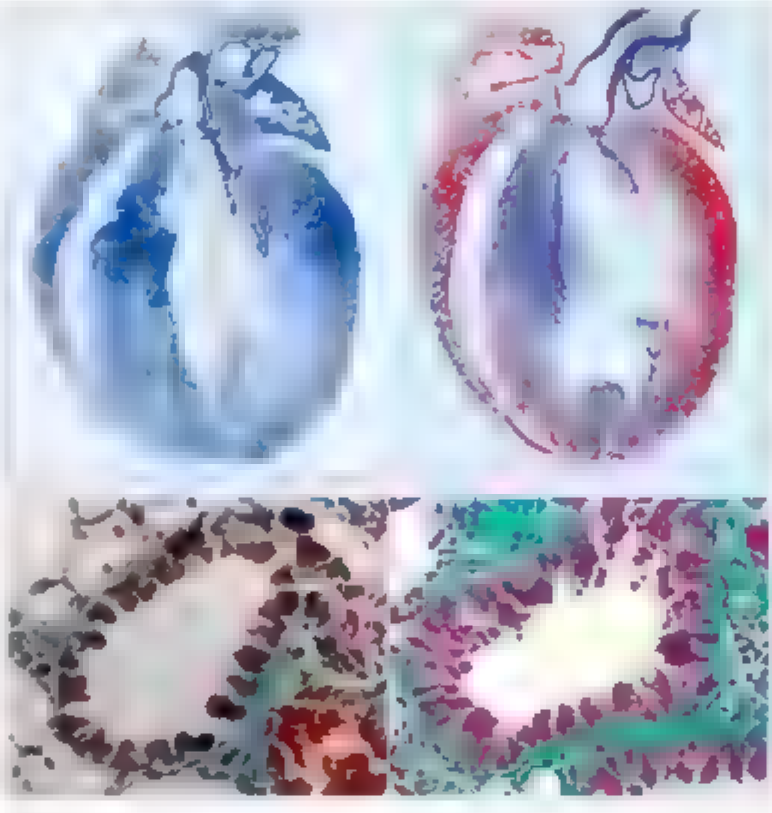

Missing molecules. Compared to a normal mouse heart (*top, left*), one from a mouse with a deleted microRNA (*top, right*) overexpresses a skeletal muscle gene (in red), among other defects. Erasing a different microRNA increased collagen deposits (green) in mouse lungs (*above, right*) compared to a normal organ (*above, left*).

Still, left alone in a relatively sterile lab, mice lacking miR-155 survived easily. But when vaccinated against a strain of salmonella, the animals failed to develop protection against the bacterium—as quickly became apparent when most who were exposed to it died within a month. "The animals were no longer able to generate immunity," says Turner, an immunologist.

Biologists typically see a specific defect when they knock out a protein-coding gene, but eliminating a microRNA may pack a bigger a punch, because many are thought to control multiple genes. In the case of miR-155, "you get much broader brush strokes … [and] very diverse immunological perturbations," says Corry.

There's a flip side to the promiscuity of microRNAs. A single gene may be the target of many microRNAs. That led some biologists to speculate that built-in redundancy would limit the effects caused by deleting individual microRNAs. In the *Cell* study, in which miR-1-2 was deleted, the microRNA actually has an identical twin that's encoded by a gene on another chromosome. "We thought that we'd have to delete both of them to see any abnormality in the animal," says Deepak Srivastava of the University of California, San Francisco, who led the work. But half of his group's mice died young of holes in the heart. Others later died suddenly, prompting Srivastava and his colleagues to look for, and find, heart rhythm disturbances.

The heart problems discovered by Eric Olson of the University of Texas Southwestern Medical Center in Dallas and his colleagues, which are also described on page 575, were more subtle. They erased the microRNA miR-208 and at first thought the mice were normal. Only after they subjected the animals to cardiac stress, by mimicking atherosclerosis and blocking thyroid signaling, did they observe that the animals' hearts reacted inappropriately to such strain.

The four teams that knocked out the various microRNAs still don't know all the gene targets of each molecule. The findings, says Turner, "really do leave open a lot more questions, perhaps, than there are answers."

One is whether these and other microRNAs help explain inherited defects and diseases for which genes have been elusive. Ailments from cancer to Alzheimer's disease, says Carlo Croce of Ohio State University in Columbus, who is studying microRNAs in malignancies, may "have a microRNA component." It's one that scientists are beginning to hunt for in earnest.

–JENNIFER COUZIN

CREDITS: TOP TO BOTTOM: EVA VAN ROOIJ ET AL., SCIENCE; MADHURI V. WARREN

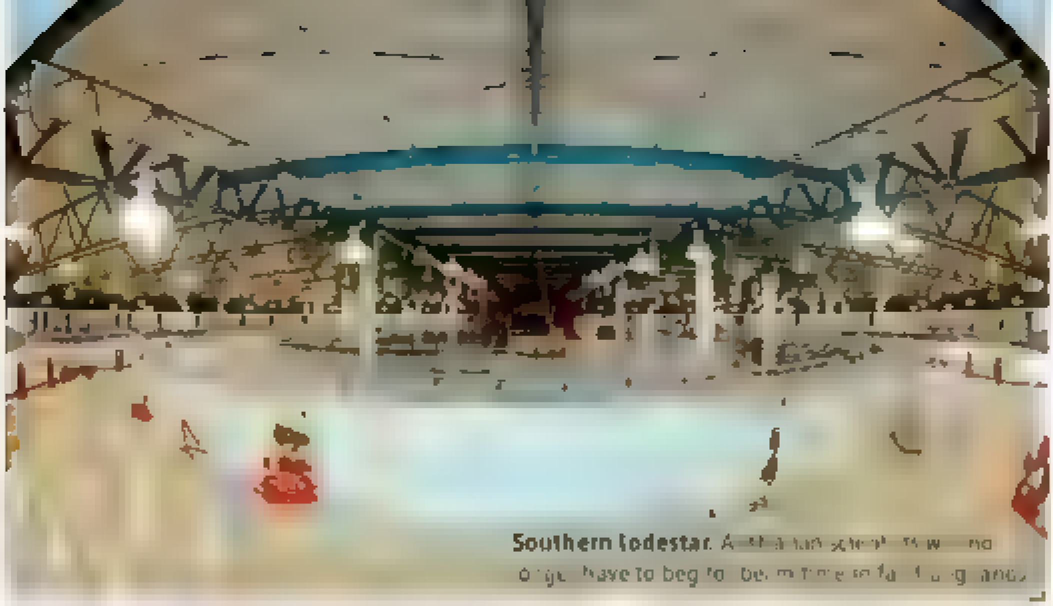

Southern lodestar. Australian scientists will no longer have to beg for beam time in faraway lands.

BIG FACILITIES

Researchers Get in Synch Down Under

MELBOURNE, AUSTRALIA—When his protein crystals melted en route to Japan last June, Jose Varghese bemoaned the loss of "months of work." Varghese, a protein crystallographer who directs the structural biology program at CSIRO, Australia's national science agency, had planned to use Japan's Photon Factory to study the structure of human β amyloid, a protein implicated in Alzheimer's disease. Now he no longer has to worry about project-wrecking long-distance journeys. Starting this summer, he will be able to carry out the same studies without leaving the continent.

Last week, the state of Victoria unveiled the \$170 million Australian Synchrotron, the nation's first. "We've always been the poor neighbor who can't come to the party," says Dean Morris, a physicist who has directed the machine's construction and fine-tuning. But with a synchrotron of their own—and the only one on this side of the Southern Hemisphere—set to come on-line in July, Morris says, "Australia will be a destination for researchers from around the world."

Australia is pinning much of its hopes for blossoming into a science powerhouse on what is essentially a gigantic souped-up microscope. By accelerating electrons to nearly the speed of light and bending their path within a 200-meter-long magnetic racetrack, the synchrotron produces pencil-width beams of photons a million times more intense than sunlight. The Australian Synchrotron will not be the most powerful in the world; that title belongs to the SPring-8 synchrotron in Hyogo, Japan. But its design allows for a wide range of applications, from nanotechnology and cell biology to forensic sciences. Because of this versatility, the synchrotron "has attracted more support across the whole spectrum of national science than any other project in Australia's research history," says John Brumby, Australia's minister for innovation.

At full capacity, the synchrotron is expected to host as many as 1200 scientists a year, up to a third of whom will be from abroad. (Four of 13 planned beamlines will be available by summer.) The dream, Morris says, "is to put Australia on the scientific map for big international collaborations." He says that many here were chagrined that Australia was not invited to join the ITER fusion reactor now being built in Cadarache, France. "We have the expertise to take part in these sorts of projects, but without any world-class research facilities of our own, we're not considered as being in the same league." The new synchrotron is half of the solution, Morris says. The other half is a new research reactor near Sydney—a replacement for an older facility—that provides neutron beams for materials science experiments.

Earning respect isn't the only aim. The synchrotron should also boost homegrown products. Casting the high beams on wool, for instance, will reveal the fine structure of fibers and enable scientists to tinker with textile properties. And the country's mining establishment will benefit from a future beamline dedicated to minerals research. The facility "will transform the technical nature of many Australian industries," predicts synchrotron director Robert Lamb.

Lamb and others hope the new machine will help squelch one export: scientific talent. By opening major science facilities, Australian universities hope to entice top expatriate scientists to come back home. "These tools ... will enable Australia to compete effectively with researchers in the strongest Northern Hemisphere countries," says Robert Robinson, head of the Bragg Institute in Sydney. The Australian Synchrotron puts out its first call for project proposals next month.

—JOHN BOHANNON

Things Looking Up

To keep up with other spacefaring nations, the United Kingdom needs its own space agency, the Royal Society said this week in a submission to a government consultation aiming to draw up a space strategy for the years 2007–10. With government spending spread across nine departments and funding agencies, Britain's space effort lacks focus, the society says, making it particularly hard for the U.K. to speak with one voice when negotiating bilateral projects apart from the multinational programs of the European Space Agency.

A new national agency would replace the British National Space Centre, which now plays a coordinating role but has a staff of just 45 and no budget of its own. The U.K. spent just over \$400 million on space research and missions in the 2005–06 fiscal year and provides only 7% of the budget of the European Space Agency. France and Germany give 25% and 20%, respectively. "It can be difficult at times to get agreements for international missions," says space scientist Andrew Coates of University College London. "A more effective voice would be extremely welcome." But it's not all about perception. "We should be fighting for more money for space," Coates says. "Our ambitions go far beyond what we can currently do."

—DANIEL CLERY

Lights Out, Please

Astronomers upped the ante in their efforts to fight light pollution with an international conference last week that drew up a declaration on a "right to observe the stars" and promoted the idea of specially protected dark sky reserves. "There is lots of protection for different environments. Now there is a movement to look at the night sky in the same way," says Graham Bryant of the British Astronomical Association.

A UNESCO-sponsored meeting, Starlight 2007, brought astronomers together with tourism, environment, and culture experts on the Spanish island of La Palma, whose dark night skies have been protected by law since 1988. "By mixing up the various communities everyone wins," says David Crawford, head of the International Dark-Sky Association. Cipriano Marin of UNESCO suggests that tourism authorities in astronomy hot spots such as La Palma and Hawaii could develop trip packages that exploit each locale as a "clean-sky destination."

—DANIEL CLERY

CREDITS (TOP TO BOTTOM): DANIEL MENDELBAUM/STATE OF VICTORIA; PHOTOS.COM

Killing Whales For Science?

A storm is brewing over plans to expand Japan's scientific whaling program

Humpback populations are rebounding ... them for research purposes.

WHEN LOUIS HERMAN, PROFESSOR EMERITUS at the University of Hawaii, Manoa, sets out to study humpback whales in Hawaii, the goal is to see the animals as individuals. His team identifies whales genetically, with small skin samples taken with a retractable dart, and physically, with photos of their tail flukes. Whale by whale, he and other marine biologists around the world are building a picture of a population rebounding from the overhunting of the last century. At the same time, however, another kind of study is planned for Antarctic humpbacks. Japanese researchers plan to kill 50 annually in an effort they claim will help explain ecosystem dynamics in the Southern Ocean. It would be the first time in 33 years that humpbacks have been killed for science.

Japan's intention to expand their scientific whaling, which has been condemned by many Western scientists, will be discussed at what all expect to be a fiery meeting next month in Anchorage, Alaska, when some 200 whale researchers gather for the Scientific Committee meeting of the International Whaling Commission (IWC). It will be followed by the commission's full-court meeting, which is expected to be equally rancorous.*

"There are going to be some fireworks," predicts Doug DeMaster, a marine mammal biologist, director of the Alaska Fisheries Science Center in Seattle, Washington, and deputy commissioner of the U.S. delegation. The roster is peppered with contentious topics, including aboriginal subsistence whaling and whales as bycatch, but none is as explosive as scientific whaling.

Even before the delegates have gathered, tempers are flaring over Japan's [illegible] of Antarctic minke whales (in 2005, it upped its annual take from 440 to 935) and its plans to kill 50 humpback and 50 fin whales each year. "If Japan wants to resume commercial whaling, it should just come out and say that's what it's doing," fumes marine biologist Nick Gales of the Australian Antarctic Division in Kingston, Tasmania, who is a member of IWC's Scientific Committee (IWC-SC). "But to do this in the name of science is simply not defensible."

Scientists at the Government of Japan's Fisheries Agency, which oversees the hunts, contend that their project is indeed scientific. "We are attempting to build an ecosystem model of the Antarctic's Southern Ocean," explains Joji Morishita, director for the agency's international negotiations. "And to do that, we need to include data from the humpback and fin whales since their biomass now equals that of the minke whales. We need to know their numbers, what they eat, how much, when and where, and whether they are outcompeting other whale species."

The issue highlights the sharply differing perspectives of wildlife conservation and resource management. Humpbacks, for example, were nearly hunted to extinction in the 20th century and now serve as the poster child for many conservation organizations; most Western nations consider them, as well as the fin whales, to still be endangered. But Morishita takes a different view. "It's dangerous to make the humpback a special animal that cannot be used," he says. "What's wrong with using an abundant species while we still protect the endangered ones?"

Some fear that the tension may ultimately break the fragile convention itself. The 73-member voluntary organization is virtually divided between pro- and anti-whaling nations and suffers from unhappy memories of previous meetings marred by insults and physical attacks. IWC, many say, is sinking like a harpooned humpback (although at least six new countries will join this year as each side cultivates new members). Scientific whaling "has polarized the [IWC's] Scientific Committee,"

* 59th Annual Meeting of the International Whaling Commission, 4–31 May, Anchorage, Alaska.

says Scott Baker, a conservation geneticist at Oregon State University's (OSU's) Marine Mammal Institute in Newport. "We're asked to review Japan's proposals, to treat them as science when they are not. And that is objectionable."

In the beginning

Scientific whaling was not the original purpose behind IWC, which serves as the decision-making body for the International Convention for the Regulation of Whaling (ICRW). Rather, it was set up in 1948 for the interests of commercial whaling. At the time various nations, including the United States, were concerned that many species of the great whale were being overhunted. According to ICRW's charter, it was organized "to provide for the proper conservation of whale stocks and thus make possible the orderly development of the whaling industry." The convention also sanctioned scientific whaling under the four sentences of Article VIII, which allows members to catch whales for scientific purposes. Countries doing so are charged with regulating their own hunts, with no catch limits or oversight from member nations.

Article VIII was drafted by Norwegian whaling expert and first chair of IWC, Birger Bergersen, now deceased. "It's clear that in his mind he was thinking that the number of whales a country could take for science was less than 10; he didn't intend for hundreds to be killed for this purpose," says Lars Walloe, a physiological biologist at the University of Oslo, Norway, who has written about Bergersen and heads the Norwegian delegation to the Scientific Committee. "He had in mind, for instance, the possibility of finding a new animal and thus needing to take some in order to describe them scientifically."

In 1982, with many populations plummeting to near-extinction levels, IWC enacted a moratorium on commercial whaling, which took effect in 1986, and its focus shifted to conservation. "The moratorium is probably one of the greatest conservation success stories of the 20th century," says Phillip Clapham, a marine biologist with the Alaska Fisheries Science Center in Seattle. "Many species of whales that were really hammered are now making remarkable comebacks," including some populations of humpback and fin whales. But some blue, right whale, and bowhead populations remain worrisomely low, he adds.

Not every IWC nation joined the moratorium. Member nations can lodge formal objections to the body's decisions, which it has no authority to enforce. Norway objected and has continued commercial hunting of minke whales, which are smaller (8 meters in length) baleen whales thought to number in the hundreds of thousands. Last year, Norway unilaterally upped its annual quota from 745 to 1052. Japan settled on a different tack, withdrawing its formal objection but launching scientific whaling programs in the Southern Ocean and North Pacific under Article VIII. In the past 5 years, Iceland has also started both scientific and commercial whaling programs targeting minke and fin whales, although its take is only a fraction of Japan's (see table, below).

Although many whale researchers decry Iceland's decision, they are even more alarmed by the ever-increasing scale of Japan's scientific program and the fact that Japan kills whales within IWC's Southern Ocean Whale Sanctuary. Under the scientific whaling program launched in 1987 (called JARPA, for Japan's Whale Research Program under Special Permit in the Antarctic), the Japanese have killed an estimated 6500 minke whales there; that compares to about 2100 whales killed worldwide under Article VIII by all nations combined between 1952 and 1986.

Recent Total Whale Catches by Country

	Norway Commercial	Iceland Commercial & scientific	Japan Scientific	Russian Federation Subsistence	U.S. Subsistence	Denmark (Greenland) Subsistence
2001	552		598	113	75	158
2002	634	—	684	134	50	164
2003	647	37	704	131	41	209
2004	544	25	755	112	43	204
2005	639	39	1243	126	68	193
2006 *	546	37	1320	140	39	197
Total *	**3562**	**138**	**5304**	**756**	**316**	**1125**

* 2006 data incomplete.

Japan began its second scientific whaling operation (JARPN) in the North Pacific in 1994, where it targets minke, Bryde's, sei, and sperm whales. According to Article VIII, the meat from these hunts should be used, and despite low demand, it is available in Japanese markets. Some is now stewed in ketchup at schools for lunches, and some can be found in restaurants and for sale online, says Naoko Funahashi, a conservationist with the International Fund for Animal Welfare in Tokyo.

In 2005, at the 57th IWC meeting in Ulsan, South Korea, Japan stunned IWC SC with its announcement that it was beginning a new operation (JARPA II), which would include taking humpback and fin whales in the Southern Ocean Sanctuary. So far, it has harpooned 12 fin whales and intends to begin killing humpbacks in 2007–08.

Science under scrutiny

Under the convention, the Scientific Committee is required to review scientific whaling proposals, and many researchers are sharply critical of the results of JARPA I.

"The science and data are very poor," says Clapham, echoing a complaint voiced by many other IWC SC members. "It's outrageous to call this science; it's a complete charade," charges Daniel Pauly, director of the Fisheries Centre at the University of British Columbia in Vancouver.

The committee produced a consensus review of the 18-year JARPA I study last December, but the document includes few areas of agreement. On minke whale abundance: "The workshop has not developed any agreed estimates." On the role of whales in the marine ecosystem, "relatively little progress has been made."

Yet the Japanese stand firmly by the science behind their whaling program. "We hear these criticisms all the time," says Morishita. "A lot of non-Japanese scientists are always calling for us to submit our data, and we present our research results every year to the Scientific Committee and at other scientific meetings. If they think our data is so useless, I don't think they'd demand it. We would also like to publish our papers in more leading Western science journals," but Morishita perceives these as being biased against scientific whaling. "We are also the only scientists collecting age data on these populations." Scientists determine a whale's age by its waxy ear plugs, which can only be studied if the whale is dead.

SOURCE: PAUL WADE/NMFS

Morishita argues that humpback and fin whales are now competing with the minke for krill and says their new program will test this idea.

Some researchers agree that the Japanese data are important. "They are doing valid science," says Norway's Walløe, pointing in particular to Japanese genetic data that suggest the minke whale numbers in the Southern Ocean are declining, and that minkes there are growing slimmer, losing blubber. "Whether or not it is necessary for their study to take so many hundreds of whales every year for science I cannot comment." Walløe adds that the Japanese also provide biopsy samples, which are rare from large baleen whales in the Southern Ocean.

But these data can be gathered without killing the whale, say Herman and others. "The Japanese want to ask which breeding populations the whales belong to, if these are growing, and where do they feed," says Gales. "These are all questions which can be answered using nonlethal techniques including observation, satellite tracking, and genetic studies." He and many others are unconvinced by the idea of food competition and say that it betrays an overly simplistic view of complex marine ecosystems.

Researchers on all sides agree that the humpback whales' numbers in the Southern Ocean are increasing. Indeed, the data should "make everyone happy," says Morishita. "Their numbers are so large now that their increase seems to be adversely affecting the minke whale. We want to see if that is the case."

Taken. Japanese ships catch minke whales like this one, as well as a few other species, under scientific programs.

But Clapham says not all southern humpback populations are rebounding. Whales from a variety of breeding populations congregate in the feeding area of the Southern Ocean. Most are part of two fairly large populations (totaling nearly 20,000) that travel from Antarctica to Australia's coasts, where they mate and birth their calves. Others, however, hail from far smaller populations that breed in the waters off Fiji, New Caledonia, and Tonga. "These stocks were devastated by illegal Soviet whaling in the late 1950s and '60s," says Clapham. "They've never recovered and still number in the mere hundreds or fewer. But they feed in Antarctica with the whales from Australia. It's impossible to tell them apart; they don't have signs on their backs. How are the Japanese going to be sure they don't take humpbacks from these highly endangered populations?"

Japan's program suggests to OSU's Baker that the science is "merely about managing whales for future harvest." Whaling "can be done sustainably, which is why Japan collects the kind of data it does," says Walløe. "If whales are going to be hunted in a sustainable manner, then we need this kind of information. But, if we're not going to kill any whales, then it could be argued we don't need it." And the killing of whales, he notes, has now become more of a political than a scientific question.

Because the scientific whaling program is "out of control," says former U.S. Whaling Commissioner Rollie Schmitten, it might be better to just phase it out and permit tightly controlled commercial whaling, while prohibiting any international trade in whale meat. IWC has attempted to negotiate similar agreements at its annual meetings since 1996 but it has always failed, partly because some countries, notably Australia, New Zealand, and the United Kingdom, refuse to consider removing the ban. Meanwhile, subsistence hunts by aboriginal peoples in the United States, Russia, Greenland, and the Caribbean nation of St. Vincent and the Grenadines are also up for renewal this year. All this sets the stage for a contentious meeting when the full IWC gathers at the end of May.

As a small island nation, Japan defends its right to marine resources. Japanese generally perceive antiwhaling sentiment as anti-Japanese, says Funahashi. But she holds out hope for change. "Most Japanese don't know that we hunt whales in Antarctica," she says. "They think it's only in Japanese waters. When they hear about this other, they don't approve. Now more Japanese are going whale watching, and this is changing people's attitudes." It's harder, after all, to eat an animal you know.

–VIRGINIA MORELL

CROSS CULTURAL RESEARCH

Pentagon Asks Academics for Help In Understanding Its Enemies

A new program at the U.S. Department of Defense would support research on how local populations behave in a war zone

The Iraq War was going badly in Diyala, a northern province bordering Iran, in late 2005. A rash of kidnappings and roadside explosions was threatening to give insurgents the upper hand. Looking for insights on how to quell the violence, the U.S. Department of Defense invited a handful of researchers funded by the agency to build computer models of the situation combining recent activity with cultural, political, and economic data about the region collected by DOD-funded anthropologists.

The output from one model, developed by sociologist Kathleen Carley and her colleagues at Carnegie Mellon University in Pittsburgh, Pennsylvania, connected a series of seemingly disparate incidents to local mosques. Results from another model, built by computer scientist Alexander Levis and his colleagues at George Mason University (GMU) in Fairfax, Virginia, offered a better strategy for controlling the insurgency. Getting Iraqis to take over the security of two major highways, and turning a blind eye to the smuggling of goods along those routes, the model found, would be more effective than deploying additional troops. The model also suggested that a planned information campaign in the province was unlikely to produce results within an acceptable period of time.

Researchers and DOD officials say these insights, however limited, demonstrate a role for the social and behavioral sciences in combat zones. And a new program called Human Social Culture Behavior Modeling will greatly expand that role. John Young Jr., director of Defense Research and Engineering and

CREDIT: IFAW

architect of the program, has asked Congress for $7 million for fiscal year 2008, which begins on 1 October, as a down payment on a 6-year, $70 million effort. Agency officials expect to direct an additional $54 million in existing funds to social science modeling over the next 6 years. Under the new program, the agency will solicit proposals from the research community on broad topic areas announced periodically, and grants will be awarded after an open competition.

Officials hope that the knowledge gained from such research will help U.S. forces fight what the Bush Administration calls a global war on terror and help commanders cope with an incendiary mix of poverty, civil and religious enmity, and public opposition to the U.S.-led occupation of Iraq. "We want to avoid situations where nation states have unstable governments and instability within populations, with disenfranchised groups creating violence on unsuspecting citizens," says Young. "Toward that goal, we need computational tools to understand to the fullest extent possible the society we are dealing with, the political forces within that government, the social and cultural and religious influences on that population, and how that population is likely to react to stimuli—from aid programs to the presence of U.S. troops."

The approach represents a broader and more scientific way to achieve military objectives than by using force alone, according to Young. "The military is used to thinking about bombs, aircraft, and guns," he says. "This is about creating a population environment where people feel that they have a voice and opportunity." Such tools would not replace the war games that military commanders currently use to simulate combat between conventional defense forces. Instead, the models would give military leaders knowledge about other options, such as whether improving economic opportunity in a disturbed region is more likely to restore order than imposing martial law and hunting down insurgents. Once developed in academic labs, the software would be installed in command and control systems.

The plan has drawn mixed reactions from defense experts. "They are smoking something they shouldn't be," says Paul Van Riper, a retired lieutenant general who served as director of intelligence for the U.S. Army in the mid-1990s. Human systems are far too complex to be modeled, he says. "Only those who don't know how the real world works will be suckers for this stuff."

But retired general Anthony Zinni, former chief of U.S. Central Command and a vocal critic of the Administration's handling of the Iraq War, sees value in the program. "Even if these models turn out to be basic," he says, "they would at least open up a way for commanders to think about cultural and behavioral factors when they make decisions—for example, the fact that a population's reaction to something may not be what one might expect based on the Western brand of logic."

The new program is not the first time the military has tried to integrate cultural, behavioral, and economic aspects of an adversary into its battle plans. During the Cold War, for example, U.S. defense and intelligence agencies hired dozens of anthropologists to prepare dossiers on Soviet society. Similar efforts were made during the U.S. war in Vietnam,

Beyond bombs and guns. DOD officials say social science models can supplement the use of force to reduce violence in Iraq.

with little success. But proponents say that today's researchers have a much greater ability to gather relevant data and analyze the information using algorithms capable of detecting hidden patterns.

A few such projects are already under way. At the University of Maryland, College Park, computer scientist V. S. Subrahmanian and his colleagues have developed software tools to extract specific information about violent incidents from a plethora of news sources. They then use that information to tease out rules about the enemy's behavior. For example, an analysis of strikes carried out by Hezbollah, the terrorist group in Lebanon, showed that the group was much more likely to carry out suicide bombings during times when it was not actively engaged in education and propaganda. The insight could potentially help security forces predict and counter suicide attacks. "This is a very coarse finding, not the last word by any means," cautions Subrahmanian, adding that a lot more data and analysis would be needed to refine that rule as well as come up with other, more useful ones. Last year, the researchers applied their tools to provide the U.S. Army with a detailed catalog of violence committed against the United States and each other by tribes in the Pakistan-Afghanistan region.

Other modeling projects are addressing more fundamental questions. With funding from the Air Force Office of Scientific Research, mathematical economist Scott Page of the University of Michigan, Ann Arbor, and his colleagues are modeling societal change under the competing influences of an individual's desire to act according to his or her values and the pressure to conform to social norms. The work could shed light on which environments are most supportive of terrorist cells, information that could help decide where to focus intelligence-gathering efforts and how to bust those cells. The research could also help estimate, by looking at factors such as rise in unemployment and growing social acceptance of violent behavior, when a population may be plunging into chaos. That in turn could help commanders and policymakers decide when and how to intervene.

Accomplishing those goals is a tall order, Page admits. "Despite tons and tons of data from U.S. elections," he says, "we are still not very good at predicting how people will vote."

Building comprehensive and realistic models of societies is a challenge that will require enormous amounts of empirical data, says GMU's Levis, a former chief scientist of the U.S. Air Force. But it is doable, he says, adding that the field will benefit greatly from linking social science researchers and computer scientists. "The goal here is to win popular support in the conflict zone," he says.

–YUDHIJIT BHATTACHARJEE

CREDIT: MAURICIO LIMA/AFP/GETTY IMAGES

CARBON EMISSIONS

Improved Monitoring of Rainforests Helps Pierce Haze of Deforestation

Deforestation produces a significant amount of greenhouse gas emissions through burning, clearing, and decay. But exactly how much?

Twenty-five years ago, the best way for Brazilian scientists to gauge the rate of deforestation in the Amazon was to superimpose dots on satellite photos of the world's largest rainforest that helped them measure the size of the affected area. INPE, the government agency responsible for remote deforestation monitoring data, didn't release regional maps and refused to explain its analytical methods. The result was data that few experts found credible.

Today, Brazil's monitoring system is the envy of the world. INPE has its own remote-sensing satellite, a joint effort with China launched in 1999, that allows it to publish yearly totals of deforested land that scientists regard as reliable. Using data from NASA's 7-year-old Terra satellite, INPE also provides automated weekly clear-cutting alerts that other tropical nations would love to emulate. And image-analysis algorithms have eliminated the need for measurement dots. "They've really turned things around," says forestry scientist David Skole of Michigan State University in East Lansing.

Generating good data on deforestation is more than an academic exercise. The process of cutting down forests and clearing the land—by burning the wood, churning soil for agriculture or grazing, and allowing the remaining biomass to decay—produces as much as 25% of the world's yearly emissions of greenhouse gases. That makes keeping tabs on deforestation a crucial issue for government officials negotiating future climate agreements, including a meeting next month in Bonn, Germany, and one next year in Bali to extend the 1997 Kyoto agreement after its 2012 expiration.

Despite solid improvements by scientists in monitoring deforestation, the uncertainties are still substantial. The gap between remote-sensing data and field measurements on the amount of deforested land is between 5% and 10%, say researchers. And the error bars on estimates of the amount of CO_2 released by clear-cutting those tracts, they note, are 25% to 50%. Those errors, related to gaps in fundamental understanding of forest carbon, will make it harder for developing nations to verify the extent to which they have managed to reduce deforestation and thus reduce their output of greenhouse gases. In turn, the uncertainty undermines efforts to convince skeptical lawmakers in industrialized countries that efforts to diminish deforestation should be a part of future climate-change agreements.

"We need to get these error bars down," says climate negotiations veteran Annie Petsonk of Environmental Defense (ED), a New York City–based nonprofit. More precise satellite data for calculating carbon flux could also shed light on the role of trees in the global carbon cycle, a key ingredient in understanding whether global warming will accelerate.

Margins of error

When negotiators in 2001 agreed on what the Kyoto treaty would cover, they omitted deforestation. One reason was fear that clear-cutting halted in one country trying to achieve its Kyoto goals would move to another country under less pressure to curb the practice. But uncertainty about the science didn't help. At the time, INPE was releasing only totals, not maps, and few nations had experience turning visual data from Landsat 5 and other satellites (see chart, left) into integrated totals. "You'd have [negotiators] saying that it's impossible to measure deforestation," says ecologist Paulo Moutinho of the Amazon Institute of Environmental Research in Pará State, Brazil. "There was all this data but not enough know-how," adds regional ecologist Greg Asner of the Carnegie Institution of Washington in Stanford, California.

In the last 5 years, a growing cadre of researchers in rainforest nations has begun applying satellite data to monitor their forests; the list includes India, Thailand, and Indonesia. In addition to Brazil's weekly alert system, experts across the Americas are making increased use of NASA's medium-resolution Terra, which can scan any point on Earth roughly each day at a decent resolution.

Policymakers are taking notice of that increased capacity. A side presentation on detecting clearing that Asner offered at the international climate meeting in Montreal in

Peering Through the Clouds

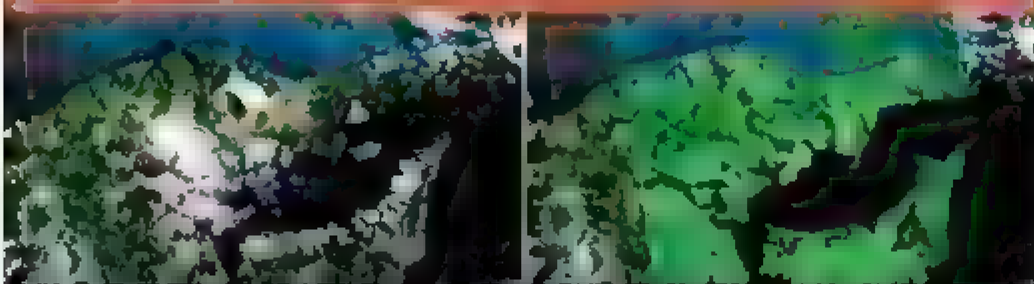

Not so hazy. An image of the Amazonian rainforest by Landsat 5 (left) includes clouds that obscure deforested areas visible on a radar image by ALOS (right). The two satellites are among a number of key sensors (below) that help researchers monitor deforestation in the tropics.

NATION	SATELLITE	SENSORS	RESOLUTION	FEATURES
U.S.	Landsat 5	Optical	30 m	The original workhorse offers images every 16 days to any nation with satellite receiving station
U.S.	Landsat 7	Optical	30 m	Some researchers have managed to use it effectively despite a crippled sensor
India	IRS-2	Optical	6–56 m	Experimental craft shows promise although images are hard to acquire
Japan	ALOS	Radar	50 m	Researchers hope cloud-penetrating radar could be key to deforestation studies
China/Brazil	CBERS-2	Optical	20 m	Experimental; Brazil uses on-demand images to bolster their coverage
U.S.	Terra	Optical	250–1000 m	Data easily available, almost daily
France	SPOT	Optical	20 m	Indonesia, Thailand use alongside Landsat data

CREDITS: (LEFT TO RIGHT) JAXA

December 2005 drew hundreds of negotiators. There, Papua New Guinea and Costa Rica proposed including credit, after 2012, for efforts to curb deforestation. The idea has gathered momentum, and environmentalists are hoping that next month's meeting in Bonn, convened by a United Nations technical body, will lay the groundwork to measure and credit action against deforestation by developing countries. "The science has really driven the policy," says ED's Stephen Schwartzman.

The Bonn delegates will confront a number of technical challenges. The first is how to reduce primary errors in detecting forest losses from space. Brazil's yearly survey, dubbed PRODES, is based on the situation each August, before fall clear-cutting season, and uses software that searches images for bare ground. But Landsat passes over any one forest area only twice in a month, and clouds can obscure areas during one or both passes. Any gaps are filled with data from July or September, massaged with algorithms. "You're providing the best of your knowledge," says mathematician Thelma Krug of INPE, which reported that 18,793 km² of Amazon forest, with a 4% margin of error, were destroyed in 2005. That figure includes only clear-cutting, because the satellites' 20- to 30-meter resolution cannot detect less dramatic disturbances.

One important omission is selective logging for timber, says Asner. In 2005, his team determined the fraction of green reflectance from each Landsat pixel, aided by considerable fieldwork to calibrate how nonvisual light frequencies could inform that calculation. They concluded that Brazil was omitting a whopping 12,000 km² or more of so-called selectively logged forest areas per year (*Science*, 21 October 2005, p. 480). Asner fears that any system rewarding efforts to halt deforestation could miss a substantial source of emitted carbon if selective logging is not included. Others believe that logging has less of an impact: Skole says Asner could have mistaken thin forests or wetlands for logged forests because their infrared image can "mimic … a logged forest." He also notes that many logged areas grow back. INPE estimates that the per-hectare emissions from selective logging are 2% of those from clear-cutting.

Even if scientists improve their monitoring of activities on the ground, however, they have only crude methods of calculating how much carbon a particular area of rainforest will emit once cleared. Estimates of the Amazon's total organic stock of carbon—including living and

Global Deforestation, 1990–2000

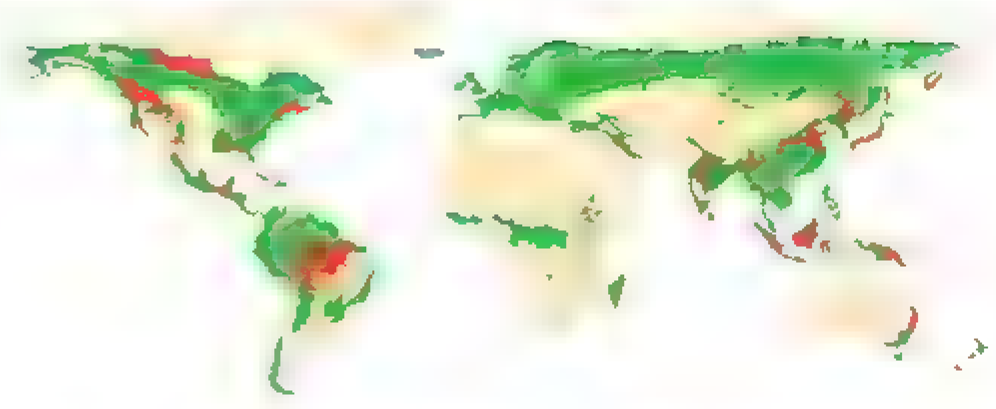

Going, going. Tropical deforestation in hot spots, including Brazil, Madagascar, Indonesia, and West Africa, is a big driver of rising CO_2 levels.

dead trees—range from 60 billion to 120 billion tons. National estimates are equally uncertain. Brazil calculated that deforestation and loss of grassland had emitted roughly a billion tons of CO_2 into the atmosphere in 2004, plus or minus 30%. Several experts told *Science* that the margin of error is even larger.

One problem is the heterogeneity of forests and the inability to identify denser, taller forest areas within larger regions. Historical sampling measurements in western Brazil only include trees at least 10 cm in diameter. "We need more science," says geographer Ruth DeFries of the University of Maryland, College Park. One low-tech step, says ecologist Richard Houghton of Woods Hole Research Center in Massachusetts, would be repeated sampling of trunks and better biomass equations that encompass the whole tree. "We don't have many studies that have looked below ground at the roots," he says. Even within a 1-hectare site, he says, the variability is maddening.

> "We need to **get these error bars down.**"
> —Annie Petsonk, Environmental Defense

Better eyes would also help. Japan's Advanced Land Observing Satellite (ALOS), launched last year, uses radar to see through the canopy and spot cleared sites that Landsat's cameras would miss. Initial results show decent contrast between forested and nonforested areas to a 50-meter resolution, says Woods Hole's Josef Kellndorfer. Upcoming ground studies in Brazil, Congo, and Uganda will aim to calibrate ALOS's ability to estimate biomass, aided by interferometry that could infer tree heights.

Radar would also be a boon to cloudy countries such as Gabon, whose rainforests have been largely hidden from satellites until now. And ALOS's youth is also welcome. Widely available and relied upon, Landsat 5 was built for a 3-year stint and is nearing a quarter-century of labor. It "could go any moment," worries DeFries. Christopher Justice of the University of Maryland, College Park, says that possibility highlights the need for "better international cooperation" to make sure data from other sources is just as easy to share.

Ground truth

DeFries says that those who care about rainforests shouldn't let the quest for improved detection stand in the way of making good use of what is already clearly visible. She's cheered by a campaign that has protected tens of thousands of square kilometers of Brazilian rainforest since 2004. A general trend of falling beef and soy prices has helped by cutting demand for land, environmentalists say. So has daily data from Terra, analyzed by INPE, that Brazilian officials have used to probe roughly 100 instances of possibly illegal deforestation, says INPE's Dalton Valeriano.

The government could step up its enforcement activities, says geographer Carlos de Souza Jr. of independent watchdog Imazon in Brazil, if its mapping work were more solid. Using the same data that INPE collects, de Souza has calculated monthly totals that exceed or fall short of the government's number by thousands of square kilometers. He fingers data-sampling techniques, clouds, or different aggregating methods as possible culprits. And he worries that the government is learning about some illegal clear-cutting belatedly, from the yearly PRODES survey. "The most important thing is stopping deforestation as it is happening, not after," says de Souza.

An international incentive system could strengthen Brazilian resolve, says Daniel Nepstad of Woods Hole. "If this is happening without a carrot, imagine what would happen with a carrot," he says. **—ELI KINTISCH**

SOURCE: THE NATURE CONSERVANCY AND HANSEN AND DEFRIES, 2004

Gravity Probe Researchers Report 'Glimpses' of Long-Awaited Payoff

[illegible]

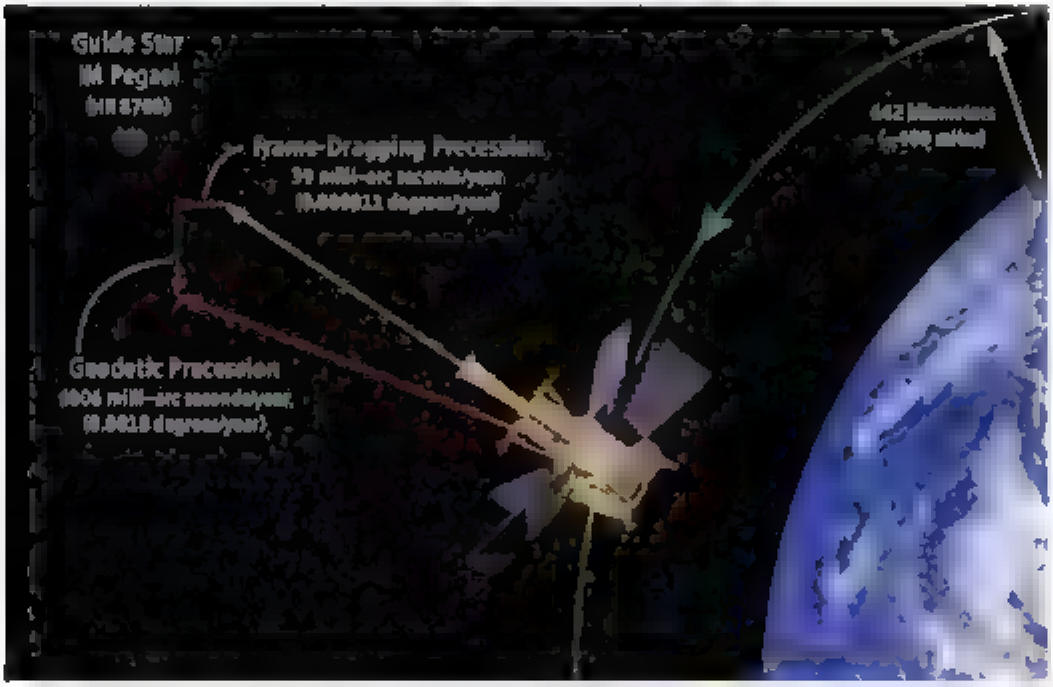

[illegible]

CREDIT: BOB KAHN/GRAVITY PROBE B, STANFORD UNIVERSITY

Snapshots From the Meeting >>

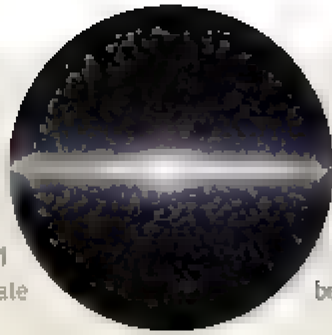

Safe zone? Galactic plane may block deadly rays

Top mass. Fermilab's Tevatron accelerator has reported a new value for the mass of the top quark, nature's heaviest basic particle. Combining data from the Tevatron's two experimental collaborations gives a top quark mass of 170.9 ± 1.8 giga–electron volts, Kevin Lannon of Ohio State University, Columbus, reported at the meeting.

Precise knowledge of the top quark's mass is important for determining the likely mass of the Higgs boson, the as-yet-undiscovered particle that physicists believe must exist in order for other particles to possess mass. Combined with the latest value for the mass of another relevant particle, the W boson, the new top mass implies that the Higgs may still lie in the range detectable by Fermilab experiments. The Higgs will be one of the main quarries of the more powerful Large Hadron Collider near Geneva, Switzerland, scheduled to begin operations later this year.

Cosmic extinction. For years, scientists have pondered fossil evidence that mass extinctions of life on Earth occur at regular intervals, suggesting some periodic cosmic influence. The latest analyses find a 62-million-year cycle in biodiversity, curiously close to the 64-million-year oscillation of the solar system above and below the plane of the Milky Way galaxy. But if radiation from sources within the galactic plane is to blame for biodiversity swings, the periodicity should be half as long, because Earth passes through the galactic plane twice each trip: on the way up, and on the way back. On the other hand, the 62-million-year cycle makes sense if the radiation attacks come from outside the galaxy, and only from one side, say Mikhail Medvedev and Adrian Melott of the University of Kansas, Lawrence.

"The oscillation of the solar system gives you the right periodicity but only if you have the effect on the north side," Medvedev said at the meeting. The reason, the Kansas scientists say, is that the whole galaxy is rushing toward the Virgo Cluster, north side foremost. When the solar system is north of the galactic plane, galactic magnetic fields no longer shield it from radiation assaults emanating from Virgo. A paper describing the analysis has been accepted for publication in the *Astrophysical Journal*.

–T.S.

we would leave other people to worry about it.

Everitt and other scientists on the Gravity Probe B team point out that the experiment has value beyond just measuring relativistic effects. It has produced technical advances already used on other space missions and has provided helpful lessons for planning future precision space probes, such as the proposed LISA mission to measure gravitational radiation from space.

And Will said that the very fact that the mission flew, and worked as well as it did after decades of waiting, should be considered a triumph.

"Everything worked almost perfectly," he said. "A few things didn't work as well. And there are these strange effects that nobody could have imagined beforehand. But that's physics."

Neutrino Study Finds Four's a Crowd

The family of self-effacing subatomic particles known as neutrinos should give up hope for the existence of an eccentric cousin, new results from the Fermi National Accelerator Laboratory (Fermilab) in Batavia, Illinois, suggest.

Physicists know of three types, or "flavors," of neutrino, designated electron, muon, and tau for their associations with other particles with those names. Neutrinos are notoriously difficult to detect and are very nearly massless. They must, however, possess at least a small mass, as they have shown the ability to switch identities in flight, a trick impossible for massless particles.

These identity shifts, or "flavor oscillations," have been well-established for years. Measurements of the oscillation rate provide clues to the differences in mass among the three known flavors. Such experiments at New Mexico's Los Alamos National Laboratory in the 1990s implied an unusually large mass difference, hinting that a fourth neutrino flavor ought to exist, in a "sterile" form that does not interact with other particles as ordinary neutrinos do.

Over the past decade, an international team of researchers using a neutrino beam at a Fermilab particle accelerator has sought evidence to confirm or refute the Los Alamos results. If correct, the Los Alamos findings imply that many of the muon neutrinos in the Fermilab beam should oscillate into electron neutrinos before reaching a detector 500 meters away. But the Fermilab experiment, known as MiniBooNE (for "Mini Booster Neutrino Experiment"), found no evidence for the brand of flavor shifting reported at Los Alamos.

"We do not see any evidence for muon neutrinos oscillating into electron neutrinos," Los Alamos physicist Heather Ray, a member of the MiniBooNE team, said at the meeting.

Although apparently ruling out the Los Alamos evidence for a sterile neutrino, the MiniBooNE experiment turned up a possible new mystery: a higher number of low-energy electron neutrinos than expected from "background" sources.

"They may be a misestimation of the background, but they may be interesting," said team member Eric Zimmerman of the University of Colorado, Boulder.

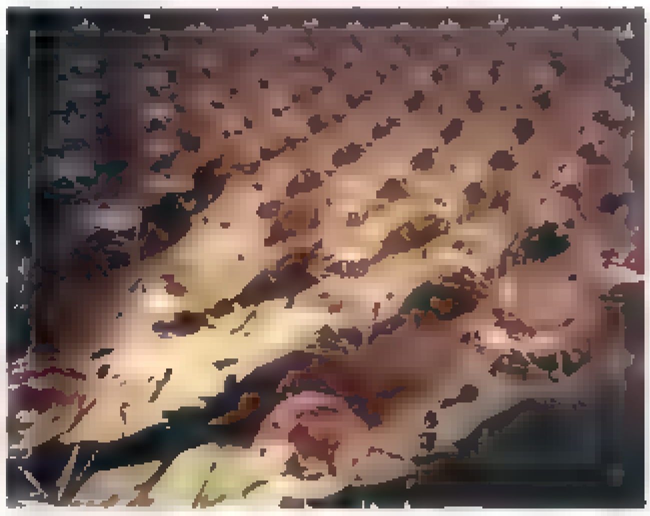

No trace. MiniBooNE's sensor array failed to confirm earlier hints of noninteracting "sterile" neutrinos.

Further analysis of the data and tests of new data now being gathered will be needed to clarify the reason for the low-energy anomalies, said Janet Conrad of Columbia University, one of the leaders of the MiniBooNE team. "There's still some possibility that there are some bizarre effects going on," she said.

–TOM SIEGFRIED

Tom Siegfried is a writer in Los Angeles, California.

CREDITS (TOP TO BOTTOM): THE COBE PROJECT, DIRBE, NASA; FERMILAB

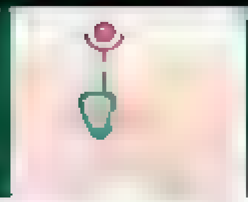

LETTERS

edited by Etta Kavanagh

Health Clues from Polar Regions

IN HIS EDITORIAL "CELEBRATING POLAR SCIENCE" ON THE FOURTH INTERNATIONAL POLAR YEAR (IPY) (16 Mar., p. 1465), Alan Leshner writes that the poles are among the scientifically richest places on Earth. Although we certainly agree, the Special Issue on Polar Science (16 Mar., pp. 1513–1540) misses the opportunity to mention another promise of circumpolar regions, namely, that they can provide options to better understand determinants of health and disease in humankind.

Indeed, one of the main health characteristics of Arctic populations (based on long-term monitoring of cancer data of some 100,000 Inuit in Alaska, Canada, and Greenland) appears to be the pronounced deficit of breast (*1*) and prostate (*2*) cancers when compared with populations from lower latitudes. Why two of the leading malignancies worldwide should be comparatively rare in the Arctic certainly ought to be investigated. It has already been speculated that winter darkness at the extremes of latitude may offer protection against these hormone-dependent cancers (*3*, *4*). The fact that the development of frequent "winter blues" among circumpolar inhabitants is also linked to the seasonal lack of light further suggests that the Arctic could offer unique opportunities to study light-related disorders and diseases.

Empirically, the differential geographic distribution of health has provided clues to disease before. Some 63 years ago, Kennaway alerted us to the different liver cancer incidences among Africans and African-Americans (*5*). Rather than being due to ethnic or genetic factors, this observation was later explained by the different geographic distribution of "extrinsic factors," namely, hepatitis B infections and the influence of aflatoxin on food products. In a similar vein, the possible effects of light (and darkness) on diseases, including cancers and seasonal affective disorders (SAD), could be studied more rigorously in populations that experience exposure to visible electromagnetic radiation that differs from that of other populations by virtue of geography. Although a considerable amount of work in these areas is already being carried out and an entire medical journal (the *International Journal of Circumpolar Health*) is devoted to health-related issues in the Arctic, more can, of course, be done. We should not have to wait for a possible 5th IPY to instigate concerted circumpolar studies of human health and disease.

THOMAS C. ERREN,[1] V. BENNO MEYER-ROCHOW,[2] MICHAEL ERREN[3]

[1]Institute and Policlinic for Occupational and Social Medicine, School of Medicine and Dentistry, University of Cologne, Kerpener Strasse 62, D-50937 Cologne, Lindenthal, Germany. [2]School of Engineering and Science, Jacobs University Bremen, D-28759 Bremen, Germany. [3]Institute of Clinical Chemistry and Laboratory Medicine, Westphalian Wilhelms University of Münster, Münster, Germany.

References

1. A. B. Miller, L. A. Gaudette, *Acta Oncol.* 35, 577 (1996).
2. A. Prener, H. H. Storm, N. H. Nielsen, *Acta Oncol.* 35, 589 (1996).
3. T. C. Erren, C. Piekarski, *Med. Hypoth.* 53, 1 (1999).
4. T. C. Erren, *Am. J. Prev. Med.* 31, 273 (2006).
5. E. L. Kennaway, *Cancer Res.* 4, 571 (1944).

Science, Religion, and Climate Change

A MOMENT OF AGREEMENT HAS ARRIVED FOR scientists to join forces with religious groups on issues of climate change. This is signaled by the summary for policy-makers from the Intergovernmental Panel on Climate Change (IPCC)'s Fourth Assessment Report, the AAAS Board's consensus statement on climate change, and the unanimity of scientists (*1*). Lynn White Jr. proposed in these pages in 1967 that (*2*) "we shall continue to have a worsening ecologic [sic] crisis until we reject the Christian axiom that nature has no reason for existence save to serve man." In their Policy Forum "Framing science" (6 Apr., p. 56), M. C. Nisbet and C. Mooney mention the more contemporary and less divisive efforts of some evangelical leaders to frame the problem of climate change as a matter of religious morality.

As faculty members at a Catholic university, we know the strong stance of Catholic documents on good science as the foundation for discussions of climate change. Two recent examples from the U.S. Conference of Catholic Bishops (USCCB) make IPCC findings their scientific basis. The IPCC Third Assessment Report led to the USCCB's *Global Climate Change: A Plea for Dialogue, Prudence, and the Common Good* (*3*), which states, "Global climate change is by its very nature part of the planetary commons. The earth's atmosphere encompasses all people, creatures, and habitats."

The scientific Summary for Policy Makers of the Fourth Assessment Report (*4*) was addressed by the chairman of the USCCB's international policy committee. He said in a letter to congressional leaders that the IPCC "has outlined more clearly and compellingly than ever before the case for serious and urgent action to address the potential consequences of climate change as well as to delineate the dangers and costs of inaction."

Additional reflections on climate change have come from numerous religious traditions. They are listening carefully to the science. Scientists ought to be in dialogue with them.

STEVEN A. KOLMES[1] AND RUSSELL A. BUTKUS[2]

CREDIT: DAVID MCLAIN/GETTY IMAGES


Performance
Simplicity
Elegancy
The new
Biometra Thermocycler
also available as basic version
TProfessional Thermocycler
Powered by
Biometras' 15-years experience
Large graphical display
High speed silver block
Easy spreadsheet programming
www.biometra.com

[1]Department of Biology, University of Portland, Portland, OR 97203, USA. [2]Department of Theology, University of Portland, Portland, OR 97203, USA.

References

1. N. Oreskes, *Science* **306**, 1686 (2004).
2. L. White Jr., *Science* **155**, 1203 (1967).
3. *Global Climate Change: A Plea for Dialogue, Prudence, and the Common Good* (United States Catholic Conference, Washington, DC, 2001) (available at www.usccb.org/sdwp/international/globalclimate.html).
4. Intergovernmental Panel on Climate Change, *Climate Change 2007: Summary for Policymakers, Contribution of Working Group I to the Fourth Assessment Report of the Intergovernmental Panel on Climate Change* (2007) (available at www.ipcc.ch).

Clarifying a Quote on Women in Science

THE ARTICLE "U.S. AGENCIES QUIZ UNIVERSITIES on the status of women in science" (News of the Week, 30 Mar., p. 1776) contains a quote from me that was taken out of context from a lengthy conversation and that does not represent my views on the subject.

While the specific issue I referred to in the quote (gender bias relating to which students may use what equipment) is, to my knowledge, not a problem in our department or other physics departments, the status of women is very important to us. We are committed to removing barriers to achievement and to increasing the diversity of our department. We are working hard to increase the representation of women and underrepresented minorities among our students, research associates, and faculty and to ensure that there is no discrimination nor any other barrier to achievement. We support the Title IX process as a way to help achieve these important goals.

ANDREW MILLIS

Professor and Chair, Department of Physics, Columbia University, New York, NY 10027, USA. E-mail: millis@tserver0.phys.columbia.edu

Notes on Modeling Light Water Reactors

AS A LONG-TIME EMPLOYEE OF THE IDAHO National Laboratory (INL), I wish to share my views on some of the characterizations made in the article "Former Marine seeks a model EMPRESS" (E. Kintisch, 9 Feb., p. 794) as they relate to modeling light water reactors. The assertions that "[e]xisting reactor computer models haven't been overhauled much since the heyday of the U.S. nuclear enterprise in the 1970s and 1980s" and that "nuclear engineers still depend on crude, 25-year-old computer programs" do not square with the facts. The RELAP5 computer code, developed at the INL for the U.S. Nuclear Regulatory Commission and the Department of Energy, has been under continuous improvement and refinement since the original release in 1978. Today's version, RELAP5-3D, is the current state of the art in modeling light water reactors and is the most widely used code of its kind in the world for safety analysis of current generation and next generation (Generation III) reactor designs.

RELAP5-3D includes a three-dimensional two-phase flow hydrodynamic model coupled to a three-dimensional nodal neutron kinetics model. The code has been extensively validated against experimental data as documented in hundreds of peer-reviewed technical papers. The mathematical models in the code are based on first principles and literature-based empirical correlations that were defined through traditional engineering practices and procedures and are thoroughly documented (www.inl.gov/relap5/r5manuals.htm).

GARY JOHNSEN

1950 Rose Circle, Idaho Falls, ID 83404, USA. E-mail: garyj@johnsen.myi.net

The Evolution of Eukaryotes

IN THEIR REVIEW "GENOMICS AND THE IRREducible nature of eukaryote cells" (19 May 2006, p. 1011), C. G. Kurland *et al.* purport to "review recent data from proteomics and genome sequences," but delivered only biased opinions. Asserting genomic sequence evidence to suggest "that eukaryotes are a unique primordial lineage," they present an introns-early (and eukaryotes-first) view of early evolution that was current in 1980 (*1*) and that was shown by conventional scientific criteria to be untenable over a decade ago (*2*). Their Fig. 1 indicates reductive evolution of prokaryotes from an ancestrally eukaryotic state; that idea was called streamlining in 1980, and its phylogenetic implications were drawn [Fig. 2 of (*1*)] in a fashion indistinguishable from its 2006 reincarnation.

The cellular structures and proteins that eukaryotes possess but that are lacking in prokaryotes are incorrectly asserted to "track the trajectory of eukaryote genomes from their origins." Uniquely derived characters lacking homologs in other taxa neither provide evidence of evolutionary relationships nor of genome trajectory, nor do they discriminate between alternative hypotheses. Were the host that acquired the mitochondrion a prokaryote, the origin of eukaryote-specific proteins and structures would follow mitochondrial origin (*3*–*5*); were the host a eukaryote (*1*, *6*), their origin would have been earlier.

The assertion that "most eukaryote proteins together with most prokaryote proteins diverge from a common ancestor" is unsubstantiated. Even at the level of protein structure, only 49 out of 1244 known protein folds (4%) are universal among 174 sequenced genomes (*7*). The claim that "[d]ifferent rates of evolution ... may account for the weak, shifting affinities between the molecular machineries encoded by eukaryote, archaeal, and bacterial genome sequences" However, they also claim that sequence comparisons can falsify particular models for eukaryote origins after all. Hence, they arbitrarily pick and choose among available observations relating to sequence similarity. The patterns of sequence similarity that fit their opinions are attributed to genuine evolutionary signals; the ones that counter their opinions are dismissed as rate fluctuation.

The statement that "[e]ukaryote proteins that are rooted in the bacterial or in archaeal clusters are few and far between" is inaccurate. The genomes of both yeast (*8*) and humans (fig. S1) (*9*) harbor many hundreds of proteins that have readily identifiable homologs among α-proteobacteria but not among archaebacteria, and vice versa.

They opine that "[i]t is an attractively simple idea that a primitive eukaryote took up the endosymbiont mitochondrion by phagocytosis," yet all testable predictions of that idea have failed (*4*). By contrast, examples of prokaryotes that live within other prokaryotes show that prokaryotes can indeed host endosymbionts in the absence of phagocytosis (*10*, *11*), as predicted by competing alternative theories (*4*).

They misattribute the notion that a eukaryotic "raptor" phagocytosed the mitochondrion to Stanier and van Niel's classical paper (*12*), which does not mention mitochondrial origin, and to de Duve's 1982 exposé (*13*), which argues for the endosymbiotic origin of microbodies while mentioning "alleged symbiotic adoption" of mitochondria in passing, but without mentioning phagocytosis. Their references (25) and (29) are misattributed as examples of "fusion" hypotheses; indeed, they indiscriminately label views on eukaryote origins that differ from their own as "fusion

Letters to the Editor

Letters (~300 words) discuss material published in *Science* in the previous 3 months or issues of general interest. They can be submitted through the Web (www.submit2science.org) or by regular mail (1200 New York Ave., NW, Washington, DC 20005, USA). Letters are not acknowledged upon receipt, nor are authors generally consulted before publication. Whether published in full or in part, letters are subject to editing for clarity and space.

hypotheses [see (4, 14, 15) for more differentiated discussion].

Finally, and most disturbing, if contemporary eukaryotic cells are truly of "irreducible nature," as Kurland *et al.*'s title declares, then no stepwise evolutionary process could have possibly brought about their origin, and processes other than evolution must be invoked. Is there a hidden message in their paper?

WILLIAM MARTIN,[1] TAL DAGAN,[1]
EUGENE V. KOONIN,[2] JONATHAN L. DIPIPPO,[3]
J. PETER GOGARTEN,[3] JAMES A. LAKE[4]

[1]Institute of Botany III, University of Dusseldorf, Düsseldorf 40225, Germany. [2]National Center for Biotechnology Information, National Library of Medicine, National Institutes of Health, Bethesda, MD 20894, USA. [3]University of Connecticut, Biology/Physics Building, 91 North Eagleville Road, Storrs, CT 06269–3125, USA. [4]Molecular Biology Institute, Departments of Molecular, Cell, and Developmental Biology, Human Genetics, and National Aeronautics and Space Administration Astrobiology Institute, University of California, Los Angeles, CA 90095, USA.

References

1. W. F. Doolittle, *Trends Biochem. Sci.* **5**, 147 (1980).
2. A. Stoltzfus, D. F. Spencer, M. Zuker, J. M. Logsdon, W. F. Doolittle, *Science* **265**, 202 (1994).
3. W. F. Doolittle, in *Evolution of Microbial Life*, 54th Symp. Soc. Gen. Microbiol. (Cambridge Univ. Press, Cambridge, 1996), pp. 1–21.
4. T. M. Embley, W. Martin, *Nature* **440**, 623 (2006).
5. W. Martin, E. V. Koonin, *Nature* **440**, 41 (2006).
6. W. F. Doolittle *et al.*, *Philos. Trans. R. Soc. London B* **358**, 39 (2003).
7. S. Yang, R. F. Doolittle, P. E. Bourne, *Proc. Natl. Acad. Sci. U.S.A.* **102**, 373 (2005).
8. C. Esser *et al.*, *Mol. Biol. Evol.* **21**, 1643 (2004).
9. See Supporting Online Material at www.sciencemag.org/cgi/content/full/316/5824/542c/DC1.
10. C. D. von Dohlen, S. Kohler, S. T. Alsop, W. R. McManus, *Nature* **412**, 433 (2001).
11. D. E. Wujek, *Trans. Am. Microsc. Soc.* **98**, 143 (1979).
12. R. Y. Stanier, C. B. van Niel, *Arch. Mikrobiol.* **42**, 17 (1962).
13. C. de Duve, *Ann. N.Y. Acad. Sci.* **386**, 1 (1982).
14. M. C. Rivera, J. A. Lake, *Nature* **431**, 152 (2004).
15. M. van der Giezen *et al.*, *Int. Rev. Cytol.* **244**, 175 (2005).

Response

OUR VIEW IS THAT CELLULAR AND MOLECULAR biology, especially genomics, reveals signs of an ancient complexity of the eukaryotic cell. This new information was not available to older hypotheses for eukaryote origins; they were answering questions that were incompletely formulated.

Our primary conclusions regarding the ancestral complexity of the eukaryote cell are illustrated in fig. S1 (1), which depicts a microsporidian cell and the subcellular location of its eukaryote signature proteins (ESPs) (2, 3). Even though Microsporidian genomes are among the most heavily reduced in eukaryotes, they still have many ESPs. An anaerobic endoparasitic life-style has reduced their mitochondria to mitosomes (4) and allowed the characteristic proteins of phagocytosis to be lost. Nevertheless, it is striking that characteristic ESPs are found throughout the cell; nothing in this picture suggests they are chimeric descendents of archaeal and bacterial ancestors.

We emphasize the role of molecular crowding [excluded volume effect (5)], which restricts the diffusion of macromolecules in cells. A dynamically efficient large cell is an impossibility unless it is highly compartmentalized. Yes, that reasoning also applies to the smaller prokaryote cells, but the problem increases with the cube of cell radius. Molecular crowding, like gravity, is ubiquitous. We infer that it is a major physicochemical reason for the evolution of functionally specialized, membrane-bound compartments in eukaryote cells.

We also challenge the use of Blast searches to infer deep phylogeny. For primary sequences, our Markov models use only a small number of parameters and so are both tractable mathematically and "identifiable" statistically (6). However, they rapidly saturate from random mutations and lose all information about deep phylogeny (7). Even for moderately deep phylogeny, whole genome data can give different trees for the deepest animal divergences; systematic errors exceed sampling error (8).

Tertiary structure maintains homology longer than primary sequences, which makes them suitable for Blast searches (9). Nevertheless, there is no theory to relate this signal to deep phylogeny, and it can mislead (10). Our general understanding of the relationship between protein structure and evolutionary rates was established by the early 1970s. Kimura's neutral model leads to basic principles of molecular evolution (11). And in the first issue of *Journal of Molecular Evolution* in 1971, Dickerson (12) relates the rate of protein evolution to the numbers of unconstrained amino acid sites (and outlined how this can change) and Fitch (13) expanded his covarion model where individual sites, over evolutionary time, change between constrained and unconstrained states.

However, there are too many free parameters to infer phylogeny from changes in tertiary structure. Because three-dimensional (3D) interactions vary, sites where mutations are nonlethal can differ between lineages. There is thus no limit on the number of parameters required for 3D models; there is no "common mechanism" for their evolution (14) as there is for primary sequences. The problem occurs in both experimental data (15) and simulations (16). For example, we used RNA-shape comparison metrics (17) to infer that the ribozyme MRP arose from RNase P in early eukaryotes (eukaryote RNase P was more similar in structure to RNase MRP than to bacterial or archaeal RNase P). We have had to revise that conclusion (18) because MRP is now found more widely in eukaryotes, as is its substrate. Yes, Blastology is brilliant at picking up distant homologies but it is not, by itself, a phylogenetic method.

It is still premature to decide between introns first, early, or late (19). Nevertheless, our primary conclusion is that there is good progress on understanding the complexity of the ancestral eukaryote cell ("Fred"). Despite his venerable pedigree, Fred is still alive and well.

C. G. KURLAND,[1] LESLEY J. COLLINS,[2]
DAVID PENNY[2]

[1]Department of Microbial Ecology, Lund University, Lund S 221 00, Sweden. [2]Allan Wilson Center for Molecular Ecology and Evolution, Massey University, Private Bag 11222, Palmerston North, New Zealand.

References

1. See Supporting Online Material at www.sciencemag.org/cgi/content/full/316/5824/542c/DC1.
2. A. Fedorov, H. Hartman, *J. Mol. Evol.* **59**, 695 (2004).
3. P. J. Kersey *et al.*, *Proteomics* **4**, 1985 (2004).
4. T. M. Embley, W. Martin, *Nature* **440**, 623 (2006).
5. N. A. Chebotareva, B. I. Kurganov, N. B. Livanova, *Biochemistry* **69**, 1239 (2004).
6. J. Chang, *Math. Biosci.* **137**, 51 (1996).
7. E. Mossel, M. Steel, in *Mathematics of Evolution and Phylogeny*, O. Gascuel, Ed. (Oxford Univ. Press, Oxford, 2005), pp. 384–412.
8. M. J. Phillips *et al.*, *Mol. Biol. Evol.* **21**, 1455 (2004).
9. C. Esser *et al.*, *Mol. Biol. Evol.* **21**, 1643 (2004).
10. L. B. Koski, G. B. Golding, *J. Mol. Evol.* **52**, 540 (2001).
11. M. Kimura, T. Ohta, *Proc. Natl. Acad. Sci. U.S.A.* **71**, 2848 (1974).
12. R. E. Dickerson, *J. Mol. Evol.* **1**, 26 (1971).
13. W. M. Fitch, *J. Mol. Evol.* **1**, 84 (1971).
14. M. A. Steel, D. Penny, *Mol. Biol. Evol.* **17**, 839 (2000).
15. P. J. Lockhart *et al.*, *Proc. Natl. Acad. Sci. U.S.A.* **93**, 1930 (1996).
16. E. Elhaik, N. Sabath, D. Graur, *Mol. Biol. Evol.* **23**, 1 (2006).
17. L. J. Collins, V. Moulton, D. Penny, *J. Mol. Evol.* **51**, 194 (2000).
18. M. O. Woodhams *et al.*, *BMC Evol. Biol.* **7** (suppl. 1), S13 (2007).
19. F. Rodriguez-Trelles, R. Tarrio, F. J. Ayala, *Annu. Rev. Genet.* **40**, 47 (2006).

CORRECTIONS AND CLARIFICATIONS

News of the Week: "Selfish genes could help disease-free mosquitoes spread" by M. Enserink (30 Mar., p. 1777). Kenneth Olson is not a faculty member at North Carolina State University in Raleigh, as the story said, but at Colorado State University in Fort Collins. Richard Beeman is a scientist at the Grain Marketing and Production Research Center in Manhattan, which is part of the U.S. Department of Agriculture's Agricultural Research Service, as well as an adjunct professor at Kansas State University.

News Focus: "Spinning a nuclear comeback" by D. Charles (30 Mar., p. 1782). GE Energy is located in Wilmington, North Carolina, not Wilmington, Delaware.

Special Section: Stardust: Reports: "Mineralogy and petrology of comet 81P/Wild 2 nucleus samples" by M. E. Zolensky *et al.* (15 Dec. 2006, p. 1735). An author was left out of the author list. Sirine Fakra should be listed between Stewart Fallon and Denton S. Ebel, and Fakra's affiliation should be Advanced Light Source, Lawrence Berkeley National Laboratory, 1 Cyclotron Road, Mail Stop 2-400, Berkeley, CA 94720, USA.

ECOLOGY

Sparrow Wars, Reptilian Eucalypts, and Xenophobes

Jessica Gurevitch

Over the past decade and a half, invasion ecology has come to dominate a great deal of both fundamental and applied ecology, as the enormous impacts of biological invasions have become more apparent in so many parts of the world. Invasions have presented seemingly insuperable challenges for conserving and restoring natural ecosystems, created hundreds of millions of dollars in damage, and caused the decline and extinction of species. They have also presented unprecedented opportunities for addressing basic questions in ecology and evolutionary biology. The reshuffling of biota has facilitated the ability of scientists to test what determines the limits to species' ranges, the number of species that can coexist in natural communities, the extent and rapidity of coevolutionary change, and other long-standing issues.

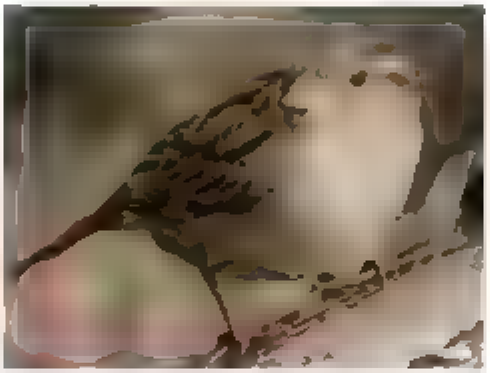

Deplored introduction. The house sparrow (*Passer domesticus*)

The study of biological invasions has also been the focus of heated controversies in ecology and in the social sciences. How important, relative to other factors such as habitat destruction, are invasions in causing species declines and extinctions? Do the responses of researchers to biological invasions reflect legitimate scientific concerns? Or are they merely an expression of underlying xenophobia and thus a question of debatable values?

In *American Perceptions of Immigrant and Invasive Species*, Peter Coates presents a lively and nuanced historical perspective on these issues. Coates (a historian at the University of Bristol) focuses on the changing interpretations and various voices among scientists, naturalists, and government workers from the mid-19th century to the present in the United States, with occasional discussions for perceptions in other countries. The book does not fall neatly into one area of contemporary history; rather, it incorporates environmental, social, and cultural history with history of science and a dash of philosophy (particularly rhetoric). For example, ecologists learn the dangers of anthropomorphism from their first ventures into the discipline as students, but Coates enlarges the issue by introducing its inverse, naturalization, "which refers to our proclivity for endowing people with the attributes, positive and negative, of natural entities (animate and inanimate)." Scientists will find this short history provides a general context and background for the current issues and debates and offers a number of surprising insights.

Many will be intrigued, for instance, to read about the acrimonious "sparrow wars" beginning in the 1870s, which pitted "cosmopolitanists" in favor of species introductions against nativists alarmed at the impact of invasives. Coates quotes William Dawson, a nativist, who wrote in 1903, "Without question the most deplorable event in the history of American ornithology was the introduction of the English Sparrow" (now called the house sparrow). Coates comments, "This may sound absurd to those acquainted with the passenger pigeon's fate. Yet Dawson insisted that the notorious extinctions of the pigeon and the great auk ... were mere 'trifles' compared to the frightful repercussions for various small native birds of the 'invasion of that wretched foreigner.'" And those who assume that sentiments deploring non-native plants are new will be enlightened and perhaps amused by the views expressed by a traveler in Italy in 1915 about non-native eucalyptus trees: "this particularly odious representative ... this eyesore ... this reptile of a growth with which a pack of misguided enthusiasts have disfigured the entire Mediterranean basin ... A single eucalyptus will ruin the fairest landscape."

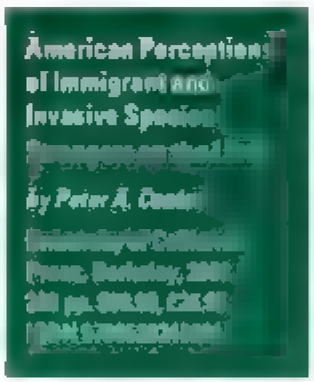

Such nativist sentiments were dramatically countered by others who vigorously championed the importation and establishment of non-native plants. It is sobering to read about "kudzu enthusiasts" and others who felt that native landscapes were depauperate and ugly and who worked enthusiastically to transform them by importing non-natives (some of which went on to become major invasives). But the good and the bad, the prescient and the misguided, are intriguingly tangled. Prominent and important figures promoted non-native species; equally prominent scientists and others defended natural environments and native species while espousing despicably racist and anti-foreigner opinions.

Coates does a reasonably good job in putting the human dimensions of the perceptions and controversies regarding alien species (or, to use the more neutral term he suggests, newcomers) into the context of the actual ecological invasions occurring at different times. It would have added to the book's depth had he also attempted to place this debate in the historical context of what was happening at the time in the science of ecology.

Perhaps the most interesting thread throughout *American Perceptions of Immigrant and Invasive Species* is the charge that the alarm about immigrant organisms stems from racist and xenophobic fears of human immigrants. Coates handles this question with nuance and subtlety, and he addresses it with evidence rather than emotion or political correctness. Prominent early scientists and opponents of the promotion of non-native species sometimes were racist, nationalistic xenophobes who equated human immigrants with undesirable imported insects, plants, and birds—or the converse—and Coates demonstrates the connections convincingly. The evidence for a modern connection is, apparently, weak to nonexistent, while there is considerable evidence to the contrary. Accusations that those advocating the promotion of native plants, for instance, are purists or, worse, fascists, racists, nativists, and Nazis are examined and found wanting (and, I would add, perpetuate the trivialization of the actions of the actual Nazis). To paraphrase Coates and Freud, sometimes a plant is just a plant, and the concern with its impacts on biodiversity is just that.

10.1126/science.1140898

The reviewer is at the Department of Ecology and Evolution, Stony Brook University, Stony Brook, NY 11794–5245, USA. E-mail: jgurvitch@life.bio.sunysb.edu

CREDIT: JOYCE GROSS/CALPHOTOS

ECOLOGY

Toward the Ideal of a Healthy Land

Frederick R. Davis

Citing Homer, Aldo Leopold noted that when Odysseus returned from the Trojan wars, he hanged a dozen slave girls on a single rope on suspicion of misbehavior. Such a brutal and callous act raised no questions of propriety as the slaves were considered property by the ancient Greeks. Similarly, 20th-century Americans felt no remorse at degrading what they considered to be their property, the land, although slavery had long since been abandoned. Leopold devoted most of his adult life to formulating a collective land ethic that incorporated an understanding of ecology and evolution. Most of us know Leopold through the posthumous collection of his writings, *A Sand County Almanac* (1), published in 1949 and still in print. As in those essays, Leopold's refined prose consistently captures the essence of conservation ethics.

Laying aside for the moment Leopold's gift for the written word, what were the sources for his ideas? We think of Leopold as a pioneer in the study and practice of game management, an acknowledgment he deserves. Yet no one's thoughts develop in a vacuum, least of all a distinguished professor with a strong commitment to practical applications.

In *Aldo Leopold's Odyssey*, Julianne Lutz Newton has meticulously traced the origins, evolution, and broader dissemination of Leopold's ideas regarding conservation. Newton's account opens with Leopold as a young assistant forester in the U.S. Forest Service. He had just graduated from Yale's School of Forestry, while retaining the rigorous classical education of its College. From the start, she focuses on Leopold's intellectual development rather than the details of his life and work, which can be found in Curt Meine's monumental biography (2).

To capture the intellectual milieu in which Leopold embarked on his career, Newton looks to expected sources, such as the writings of Gifford Pinchot and William T. Hornaday, as well as to classical literature and the Bible—in all of which he was well versed. Beyond the direct influences, Newton discusses sources of the American ideals of independence and the frontier. This initially struck me as a bit excessive, but I gradually realized that elements of Leopold's philosophy elaborated certain core beliefs of Americans. Thus, Newton's references to Frederick Jackson Turner and his notion of forest clearings as "the seed plots of American character" and Walt Whitman's expansive and inexhaustible landscapes serve as counterpoints to Leopold's conservation ethic. The author's insights into Leopold's ideas are not limited to his published works. Often Leopold's manuscripts, drafts, and letters reveal stronger sentiments than those exhibited in his published writings.

Aldo Leopold's Odyssey
by Julianne Lutz Newton
Island Press/Shearwater Books, Washington, DC, 2006. 501 pp. $35. [illegible]

CREDIT: 'DING' DARLING FROM T. BECK, N. DARLING, A. LEOPOLD, A NATIONAL PLAN FOR WILDLIFE RESTORATION, 1934

Far from an ivory tower academic, Leopold remained connected with his experiences in wildlife and land management. He witnessed the deleterious effects of overpopulation among white-tailed deer and the impact of soil erosion on the farms of the Great Plains. In the case of the latter, Leopold argued that conservation required "both programs of public land acquisition *and* the cooperation of private landowners."

Like many biologists and wildlife scientists, Leopold was influenced by the progenitors of American ecology such as Victor Shelford, Frederic Clements, and Alfred Emerson as well as the English ecologists Arthur Tansley and Charles Elton. In developing his biotic or land pyramid, Leopold drew upon Elton's 1927 pyramid of numbers (with small, abundant herbivorous animals at the bottom and a few larger carnivores at the apex) and incorporated additional research. Building on their shared intellectual interests, Leopold and Elton became lifelong friends.

Leopold extended his biotic concept beyond the ecologists to include conservation. As Newton remarks, "No ecologist before had presented such a comprehensive and comprehensible concept of the land and explained its implications for the broad range of conservation concerns." At the University of Wisconsin, Leopold sought to instill basic values in his students as stewards of the land. His wildlife ecology courses introduced "a new perspective on land, science, and the values of the land as a whole." As a member of a subcommittee of the Wildlife Society charged with developing qualifications for wildlife practitioners (an endeavor in which Elton was one of his ardent supporters), he added a measure of professional authority to this approach.

In the years leading up to *A Sand County Almanac*, Leopold developed his land health concept, synthesizing decades of study. For Newton, Leopold's essay "Odyssey" (3) is the clearest distillation of these ideas, drawing together ecological knowledge and practical wisdom. Having illuminated the richly textured backdrop of Leopold's intellectual influences, she presents this essay as capturing the essence of his vision for "a new kind of conservation," one that integrates "enduring prosperity and ecological harmony among humans and the entire community of life."

Newton's account ends on the eve of Leopold's death, which is to say before the publication of his most influential work. But with its careful analysis of Leopold's various sources of inspiration, *Aldo Leopold's Odyssey* enriches our appreciation of both Leopold and *A Sand County Almanac*.

The reviewer is at the Department of History, Florida State University, Tallahassee, FL 32306–2200, USA. E-mail: fdavis@fsu.edu

References

1. A. Leopold, *A Sand County Almanac and Sketches Here and There* (Oxford Univ. Press, New York, 1949).
2. C. Meine, *Aldo Leopold: His Life and Work* (Univ. Wisconsin Press, Madison, 1988); reviewed by S. R. Schrepfer, *Science* 241, 1237.
3. A. Leopold, *Audubon* 44, 133 (May–June 1942).

10.1126/science.1141356

ENVIRONMENT

Building a "Green" Railway in China

Construction of the Qinghai-Tibet Railway, the world's highest railway, has been achieved with ecological protection at the top of the project's agenda.

Changhui Peng,[1,2*] Hua Ouyang,[2] Qiong Gao,[3] Yuan Jiang,[3] Feng Zhang,[2] Jun Li,[2] Qiang Yu[2]

The Qinghai-Tibet Railway (QTR) was built during China's Tenth Five-Year Plan (2001–05) and, in China, is considered a landmark project (1). The QTR, completed in October 2005 and in trial operation since 1 July 2006, is the world's highest-elevation railway and the longest highland railway, extending over 1956 km from Xining (Qinghai's capital in northwestern China) to Lhasa, the capital city of the Tibet Autonomous Region (see figure, right). The Chinese government has invested an unprecedented amount of money to protect the area's ecology. A total of 26.2 billion yuan (U.S. $3.39 billion) was budgeted, and 1.54 billion yuan was allocated to ecosystem restoration and environmental protection.

An Environment-Friendly Railway

The railway project has raised serious concerns about its possible environmental consequences because the Qinghai-Tibet Plateau, covering more than 360,000 km, is a unique and fragile high-altitude ecosystem (2). The mean annual temperature of the plateau ranges between −4° and 6°C, and the average altitude is 4000 m. As a result, the Chinese government and local officials took great pains to address environmental concerns during their preparation for the construction of the QTR. The railway planners developed a "green policy" that emphasized protection of soils, vegetation, animals, and water resources (3–5).

In total, 550 km of the tracks were laid on permafrost. To avoid disrupting the seasonal migration routes of animals, including the famous Tibetan antelope (*Pantholops hodgsonii*), planners added a network of tunnels to their blueprints. To minimize the negative impacts of the construction, the Chinese government implemented several key measures. (i) Locations where earth was removed and construction sites were placed were carefully selected. Vegetation was then removed from these sites and was restored after the work was complete (see figure, page 547). (ii) Where possible, the railway path was directed around sensitive natural zones, and construction work was confined to the smallest possible area surrounding the railway. (iii) Planners detoured around wetlands and lakes wherever possible, and when this was not possible, they built bridges rather than surface routes to minimize the impact. (iv) Insulation and temperature-reducing facilities for frozen layers were used below the tracks to stabilize permafrost along the railway line. (v) The number of stations established along the line was minimized to reduce the impact of human wastes, and water treatment facilities were installed at every station. Recycled water is prevented from directly entering natural bodies of water. (vi) Railway construction was monitored by a third-party environmental inspector (the Qinghai Environmental Protection Bureau). (vii) The trains that will use the railway are fully enclosed to provide additional environmental protection.

In addition, planners established five nature reserves along the route [Kekexili (Hoh Xil), Qinghai Sanjiangyuan, Chang Tang, Lin-chou Pengbo, and La-lu], and six more are planned (5). In these reserves, a large number of endangered species such as the Tibetan antelope and black-necked crane (*Grus nigricollis*) live. To protect animals and plants, additional bridges and passages for animals will be built in sections of the railway that go through the reserves.

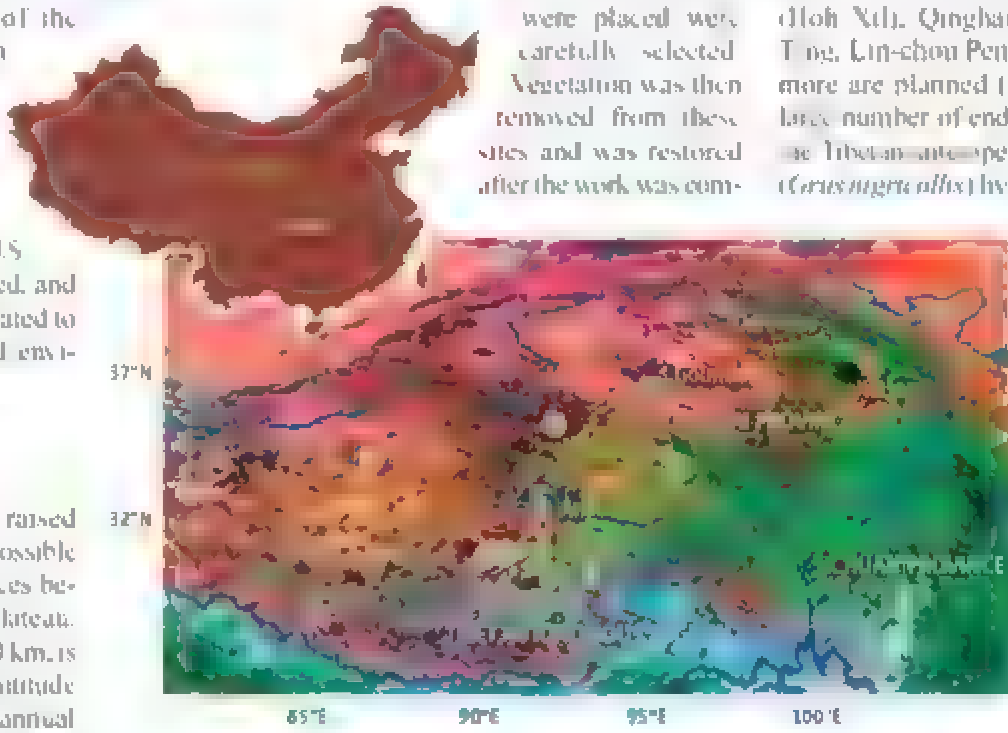

The highest railroad in the world. The Qinghai-Tibet railway from Xining to Lhasa (1956 km). Distribution of vegetation based on the MODIS product (MOD09A1 V4), 21 July 2005. Locations of the centers of five established natural reserves. (1) Kekexili (Hoh Xil), (92.3°E, 34.8°N); (2) Qinghai Sanjiangyuan (96 E, 34 N); (3) Chang Tang (87 E, 32 N); (4) Lin-chou Black Necked Crane (91.5°E, 29.9°N); and (5) La-lu wetland (90.8°E, 29.8°N).

During construction, efforts were made to reduce noise during the fieldwork and to avoid alarming animals. Moreover, planners identified areas where animals traveled, and built more than 33 passageways in the Hoh Xil nature reserve in Qinghai and the Chang Tang nature reserve in Tibet to permit undisturbed migration. The results of these measures were that the construction did not significantly affect species such as the Tibetan antelope. In 2006, the number of pregnant female antelopes was more than 30,000, the largest number ever recorded in this area (6).

Protection of bodies of water was also prioritized during the fieldwork. Construction of the railway bridge across three big rivers of the Clear-Water and Qumar was performed by the 12th bureau of China Railway Construction. Builders used 48 drilling machines to establish supports for the bridges in areas with permafrost. This approach prevented sedimentation of river water when drilling

[1]Institut des Sciences de l'Environnement, Département des Sciences Biologiques, Université du Québec à Montréal, Montréal, QC, Canada H3C 3P8. [2]Institute of Geographical Science and Natural Resources Research, Chinese Academy of Sciences, Beijing, 100101, China. [3]College of Resources Science and Technology, Beijing Normal University, Beijing 100875, China.

*Author for correspondence. E-mail: peng.changhui@uqam.ca

CREDIT: U.S. GEOLOGICAL SURVEY

establish underwater piers and when hauling sand along watercourses. In the tunneling work through Fenghuo Mountain, workers resorted to methods such as wet-spraying of cement and wet-drilling to reduce dust emissions.

In April 2001 the railway construction unit signed a letter of responsibility with the Qinghai Environmental Protection Bureau (7). This is the first letter of responsibility for environmental protection in the history of railway construction in China. It covered not only the underlying principles and main tasks (including protection of vegetation, wild animals, natural reserves, wetlands, permafrost, and the water quality of the main sources of China's five major river systems), but also detailed construction standards and regulations, the responsibilities of leaders, staff, and workers, and reporting, managing, and monitoring systems.

Grass restored. Grassland vegetation and its root soil layer were removed during construction then were replanted once the work was complete (12).

In addition, builders promoted the use of nonphosphate detergents at base camps and prevented discharge of untreated sewage. Workers used oil-burning boilers to stay warm and solar energy to power electrical equipment, rather than burning local woody vegetation such as trees. All daily waste generated by construction workers was collected and treated, and monitoring teams thus found no evidence of littering. A recent investigation conducted by the State Administration of Environmental Protection on the environmental protection work at the QTR construction sites reported no obvious changes in the water environment on the Qinghai-Tibet Plateau since the project started and stated that the area's vegetation and animals had been effectively protected (7). More measures will be taken to keep the environment clean, including the use of clean energy sources (e.g., solar power, wind power, and other non-fossil fuel sources of electric power) for railway stations built along the QTR, and passenger trains will have proper rubbish disposal facilities on board. However, long-term monitoring of the local environment and of wildlife must be carried out to provide advance warning of any developing problems and to permit timely improvements.

Local Transportation and Ecotourism

The new railway will greatly reduce transportation costs for materials entering and exiting Tibet, and this will help domestic and foreign enterprises that want to establish a presence in the Tibetan market. In addition, the QTR will boost cross-border trade with Nepal and India and will turn Tibet into a new economic frontier for southern Asia.

The QTR will also promote local tourism and related economic development. The tourism resources along the railway are very rich, with a wide range of landscapes, biology, and ethnic cultures. Regional authorities estimate that by 2010 the number of tourists will double from the 2006 total of 2.5 million, and tourist revenues in the region will rise to 5.8 billion yuan (U.S.$750 million) per year (8). Although tourism creates excellent opportunities, it also carries the risk of increasing pollution, habitat destruction, and the introduction of exotic species (9). It will need to be carefully managed to promote and ensure long-term ecosystem health and sustainability in the region.

Concerns for the Future

Recent studies indicate that plateau temperatures have risen remarkably since the 1980s and that winter temperatures could increase by another 1° to 2°C by 2050 (10). Such warming could cause permafrost to melt and might seriously threaten the stability of the railway's foundation. It will be necessary to find ways to stabilize the gradually thawing earth.

The most serious environmental problems created by the QTR, including garbage disposal, water treatment, and ecotourism, will only become apparent in the long run. These problems will not be identified in time unless the authorities assign clear responsibility for this task. The key to protecting the region's fragile environment from direct and indirect human damage will lie in tightly controlling the number of ecotourists and the speed of economic development.

In addition, mining and animal smuggling present a serious problem. There will need to be monitoring to ensure that Chinese local governments enforce environmental protection laws. Nongovernmental organizations (e.g., Green River) can also help to prevent local exploitation of animals and to protect biodiversity in the nature reserve areas.

Another concern is that construction of the QTR, by increasing movement of people into the region, could have a serious impact on the prevalence of diseases such as AIDS (11). Active disease surveillance and the ability to impose quarantine rapidly when warranted will be the most effective way to reduce the risk of disease spread.

If carefully managed, the Qinghai-Tibet railway will ultimately promote the sustainable ecological, social, and economic development of western China. We hope that it will be remembered as more than just an engineering accomplishment—that it will also be remembered as an ecological miracle and a successful example of a green railway that can be followed by other regions and developing countries.

References and Notes

1. National State Council, *Tibetan Ecological Construction and Environmental Protection* (Xinxin Press, Beijing, China, 2003), pp. 1–11 (in Chinese).
2. W. H. Li et al., in *Ecosystem of Qinghai-Xizang (Tibetan) Plateau and Approach for Their Sustainable Management* (Guangdong Science & Technology Press, Guangzhou, China, 1998), pp. 1–18 (in Chinese).
3. G. J. Xu, T. Z. Zhang, *Ecological Environment in Western China* (Chinese Central Party Univ. Press, Beijing, 2001), (in Chinese).
4. Z. Y. Zhang, Y. R. Lu, *Exploitation and Usage of Water Resources in Western China* (Chinese Water Conservancy and Water Electricity Press, Beijing, 2002) (in Chinese).
5. "Ecological protection on the Qinghai-Tibet railway," *China Through a Lens* (2006), www.china.org.cn/english/features/Tibet/1 2786.htm
6. Protection of endangered species, www.southcn.com/news/china/china05/qzlt/surround/200606280418.htm (in Chinese).
7. "Qinghai-Tibet railway: No harm to plateau ecology," *People's Daily* online (5 November 2002); available from www.People.com.cn (in Chinese) or http://english.peopledaily.com.cn/other/archive.html
8. Qinghai-Tibet Railway, environmental protection, www.chinaview.cn/qtr/environmental.htm
9. J. G. Liu, J. Diamond, *Nature* **435**, 1179 (2005).
10. J. Y. Liu et al., in *Integrated Ecosystem Assessment of Western China*, J. Y. Liu, T. X. Yue, H. B. Ju, W. Wang and X. B. Li, Eds. (China Meteorological Press, Beijing, 2005).
11. Z. Wu et al., *Science* **312**, 1475 (2006).
12. Restoring grassland vegetation, www.qh.xinhuanet.com/qztlw (in Chinese).

13. Supported by Chinese Academy of Sciences International Partnership Project "Human Activities and Ecosystem Changes" (CXTD-Z2005-1), the State Key Fundamental Science Funds of China (No. 2005CB422005), National Natural Science Foundation of China (No. 40228001 and 30590384), Natural Sciences and Engineering Research Council of Canada Discovery Grant, and Canada Research Chair Program. We thank J. Liu, H. Wu, and H. Jiang for valuable comments.

10.1126/science.1134134

THE PIPELINE

Benefits of Undergraduate Research Experiences

Susan H. Russell,[1*] Mary P. Hancock,[1] James McCullough[2]

Surveys indicate that undergraduate research opportunities help clarify students' interest in research and encourage students who hadn't anticipated graduate studies to alter direction toward a Ph.D.

Undergraduate students' participation in hands-on research is widely believed to encourage students to pursue advanced degrees and careers in science, technology, engineering, and mathematics fields. SRI International conducted a nationwide evaluation of undergraduate research opportunities (UROs) to understand who participates, what effects the experience has on them, and what factors favor positive outcomes. Our study included four Web-based surveys, conducted between 2003 and 2005 and involving almost 15,000 respondents. The survey instruments, detailed data tables, and analytical reports are available online (1).

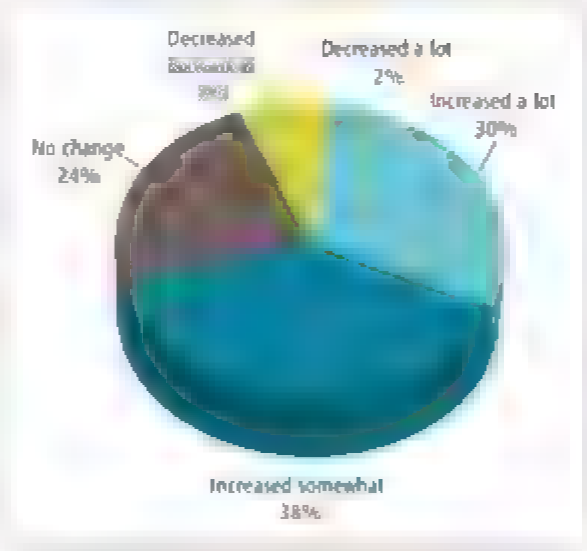

Raising interest. UROs often increase a student's interest in STEM careers.

Respondents to the first survey were approximately 4500 undergraduates and 3600 faculty, graduate student, and postdoc mentors who participated during 2002 or 2003 in UROs funded by any of eight NSF programs with a substantial undergraduate research component. Two years later, about 3300 individuals who were undergraduates in the initial survey responded to the follow-up survey.

In 2003, we surveyed a nationally representative sample of individuals (ages 22 to 35) who had received a bachelor's degree in science, technology, engineering, or mathematics (STEM) (n = 3400); in 2004, we conducted a parallel survey of individuals who had received a bachelor's degree in a social, behavioral, or economic science (SBES) (n = 3200). Of the STEM and SBES survey respondents, some (sponsored researchers) knew their research to be sponsored by NSF, NIH, or NASA. Others (nonsponsored researchers) did research that was not (as far as they knew) sponsored by NSF, NIH, or NASA. A third group (nonresearchers) did not participate in UROs.

About half of STEM and SBES survey respondents had participated in UROs. For about 1 in 15, this research was sponsored by NSF, NIH, or NASA. The experiences and outcomes reported by sponsored researchers in the STEM and SBES surveys proved to be similar to those of the NSF-participant surveys.

Profile of Undergraduate Researchers

The efforts of NSF and other entities to encourage the representation of groups historically underrepresented in STEM fields appear to have been effective. In all of our surveys, undergraduate researchers were demographically diverse, with women, blacks, and Hispanics/Latinos represented at rates at least equivalent to their rates in the overall college population. Those who began their undergraduate education at a 2-year college were as likely to participate in research as those who started at a 4-year college or university. However, URO participation rates differed across various disciplinary fields. In the STEM survey, participation rates ranged from 34% in mathematics and 37% in computer sciences to 72% in chemistry and 74% in environmental sciences. In the SBES survey, rates ranged from 38% in economics and political science to 63% in psychology.

Undergraduate researchers were mainly juniors and seniors, and they tended to have relatively high grade point averages, reflecting the competitive nature of many undergraduate research programs. They also were more likely than nonresearchers to expect to obtain an advanced degree (2). The STEM survey found that those who participated in UROs were twice as likely as those who did not to have pre-college expectations of obtaining a Ph.D. (14% versus 7%) (3).

Interest in STEM was likely to have begun in childhood: 59% of NSF researchers reported that they had been interested in STEM "since I was a kid," and another 29% said they became interested when they were in high school. This suggests that an effective time to attract students to STEM may well be while they are in elementary school (4). In contrast, interest in SBES was most likely to have developed during high school or college.

Undergraduate Research Outcomes

We found that UROs increase understanding, confidence, and awareness (5–8). Most (88%) of the respondents to the NSF follow-up survey reported that their understanding of how to conduct a research project increased a fair amount or a great deal; 83% said their confidence in their research skills increased, and 73% said their awareness of what graduate school is like increased.

UROs also clarify interests in STEM careers (9). Of respondents to the NSF follow-up survey, 68% said their interest in a STEM career increased at least somewhat as a result of their URO (see figure above).

Finally, UROs increase the anticipation of a Ph.D. (10). Of respondents to the NSF follow-up survey, 29% had "new" expectations of obtaining a Ph.D.—that is, they reported that before they started college they did not expect to obtain a Ph.D., but now (at the time of the survey) they did expect to obtain one. In the STEM survey, "new" expectations of obtaining a Ph.D. were reported by 19% of sponsored researchers, 12% of nonsponsored researchers, and only 5% of nonresearchers (see figure, page 549).

Students who participated in research because they were truly interested and who became involved in the culture of research

[1]SRI International, Menlo Park, CA 94025, USA. [2]SRI International, Arlington, VA 22209, USA. *To whom correspondence should be addressed. E-mail: susan.russell@sri.com

attending conferences, mentoring other students, authoring journal papers, and so on—were the most likely to experience the "positive" outcomes noted above, such as increased interest in a STEM career. The overall duration of research experiences and the variety of research activities also were related to positive outcomes (11). For example, in the STEM survey, 30% of researchers with more than 12 months of research experience reported that they expected to obtain a Ph.D., compared with only 13% of those with 1 to 3 months of research experience and 8% of those with no research experience. However, some of the commonly assigned research activities—preparing written final reports, in particular—tended to be unrelated to positive outcomes. The time of year in which the research experience took place (summer versus academic year) also was largely irrelevant.

We found little evidence of a relationship between mentoring characteristics and positive outcomes in responses to our structured (multiple-choice) questions. For example, neither involvement in decision-making nor perceived adequacy of mentor guidance was very strongly related to positive outcomes. However, in response to an open-ended question, by far the most common suggestions that students made about how to improve undergraduate research programs concerned increased or more effective faculty guidance. We suspect that the absence of strong relationships on the structured questions reflects the complexity of the mentor's role rather than its unimportance. Respondent comments, as well as other research (12), suggest that mentors who are able to combine enthusiasm with interpersonal, organizational, and research skills play a large role in facilitating positive outcomes.

Differential Group Needs

Among racial/ethnic groups, effects of UROs tended to be strongest among Hispanics/Latinos and weakest among non-Hispanic whites, but most racial/ethnic group differences that were statistically significant were nevertheless relatively small (typically less than 10 percentage points). Our surveys found almost no differences between men and women on any of the study variables, supporting observations of gender similarities in mathematics and science (13). Similarly, in our survey of NSF principal investigators (PIs) and mentors, only 4% identified differences in needs between men and women, and only 2% specified differences by racial/ethnic group.

We also explored whether it is important for women and minorities to have mentors who are similar to themselves (14). We found that women who had some female mentors or all female mentors were no more likely than those who had no female mentors to expect to obtain a Ph.D. or to gain new expectations of obtaining a Ph.D. The findings with regard to blacks and Hispanics/Latinos similarly showed no statistically significant differences. Across many comparisons, all groups—men, women, minorities, and nonminorities—who had both male and female mentors or both same- and different-race/ethnicity mentors tended to have slightly "better" outcomes (e.g., greater gains in confidence) than did those who had either only same or only different mentors. However, statistically significant differences were as common among men as among women and more common among non-Hispanic whites than among minorities. Thus, our findings suggest that having a mix of mentors (in terms of their sex and race/ethnicity) is likely to have a mildly beneficial effect for all students, not just women and minorities.

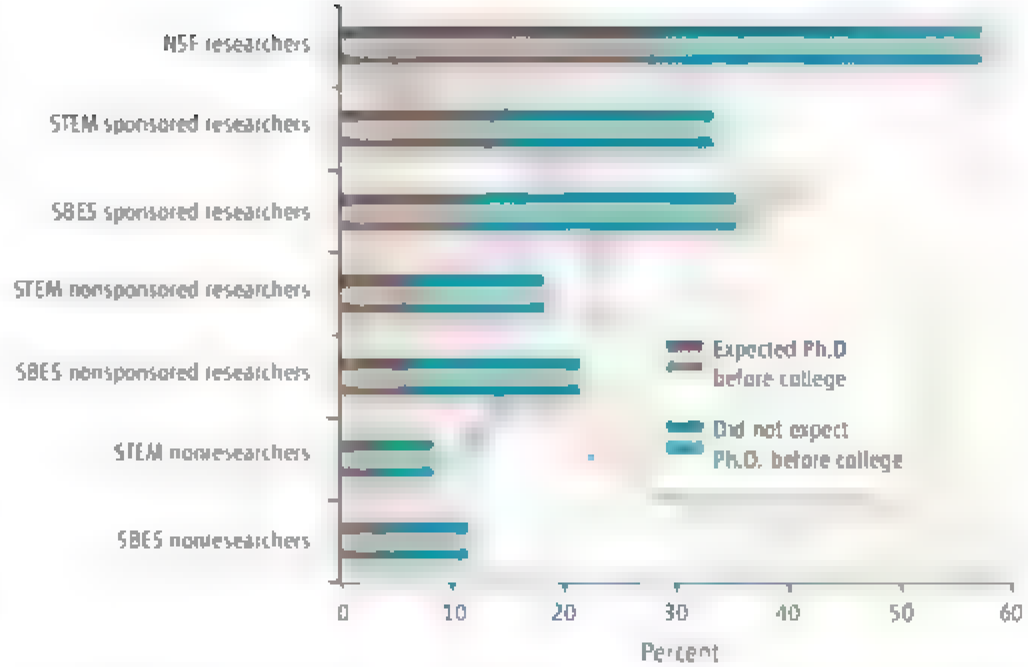

Ph.D. expectations. Participation in undergraduate research opportunities affects expectations of obtaining a Ph.D.

Conclusion

The large number and variety of students surveyed represented a variety of colleges and universities. Many types of undergraduate research experience fuel interest in STEM careers and higher degrees. No formulaic combination of activities optimizes the URO, nor should providers structure their programs differently for unique racial/ethnic minorities or women. Rather, it seems that the inculcation of enthusiasm is the key element—and the earlier the better. Thus, greater attention should be given to fostering STEM interests of elementary and high school students and providing UROs for college freshmen and sophomores.

References and Notes

1. Survey instruments, survey data, and analytical reports for all four surveys are available online (www.sri.com/policy/csted/reports/university/index.html#urosynthesis). An executive summary of the synthesis report also is available at that location as a subset of the overall synthesis report.
2. D. Lopatto, *Cell Biol. Educ.* 3, 270 (2004).
3. All differences cited here are significant at $P < 0.05$.
4. R. H. Tai et al., *Science* **312**, 1143 (2006).
5. E. Seymour et al., *Sci. Educ.* **88**, 493 (2004).
6. D. Lopatto, *Cell Biol. Educ.* 3, 270 (2004).
7. K. Bauer, J. Bennett, *J. Higher Educ.* **74**, 210 (2003).
8. S. Gregerman, *Improving the Academic Success and Retention of Diverse Students Through Undergraduate Research* (NSF, Arlington, VA, 2003); available online (http://uac.arizona.edu/gregerman.cfm).
9. A. Zydney et al., *J. Eng. Educ.* **91**, 151 (2002).
10. B. Hathaway et al., *J. Coll. Stud. Dev.* **43**, 614 (2002).
11. A. Zydney et al. (9) also found that participants' subsequent ratings of the benefits of UROs increased with the amount of time spent engaged in them.
12. A. Hunter et al., *Sci. Educ.* **91**, 36 (2007); available online (http://www3.interscience.wiley.com/cgi-bin/jhome/32122).
13. J. S. Hyde, M. C. Linn, *Science* **314**, 599 (2006).
14. B. Alexander, J. Foertsch, *The Impact of the EOT-PACI Program on Partners, Projects, and Participants: A Summative Evaluation* (Univ. of Wisconsin, Madison, WI, 2003); available online (www.eot.org/Summative.pdf).
15. This work was conducted under contract to NSF Directorate of Education and Human Resources, Division of Research, Evaluation and Communication (REC 9912172 and GS-10F-0554N). Any opinions, conclusions, or recommendations expressed in this material are those of the authors and do not necessarily reflect the views of the U.S. Government.

Supporting Online Material

www.sciencemag.org/cgi/content/full/316/5824/548/DC1

10.1126/science.1140384

GENETICS

Getting Closer to the Whole Picture

A quantitative data set of RNA, proteins, and metabolites provides an unprecedented starting point to understand, at a systems level, the effects of perturbations on a cell.

Uwe Sauer, Matthias Heinemann, Nicola Zamboni

A major challenge of biology is to unravel the organization and interactions of cellular networks that enable complex processes such as the biochemistry of growth or cell division. The underlying complexity arises from intertwined nonlinear and dynamic interactions among large numbers of cellular constituents, such as genes, proteins, and metabolites. As well, interactions among these components vary in nature (regulatory, structural, and catalytic), effect, and strength. The reductionist approach has successfully identified most of the components and many interactions but, unfortunately, offers no convincing concepts and methods to comprehend how system properties emerge. To understand how and why cells function the way they do, comprehensive and quantitative data on component concentrations are required to quantify component interactions. On page 593 of this issue, Ishii *et al.* (*1*) provide unsurpassed complete and quantitative data of components at the various constituent levels in a bacterial cell.

Rather than a reductionist viewpoint (that is, a deterministic genetic view), the pluralism of causes and effects in biological networks is better addressed by observing, through quantitative measures, multiple components simultaneously, and by rigorous data integration with mathematical models (*2*). Such a systemwide perspective (so-called systems biology) on component interactions is required so that network properties, such as a particular functional state or robustness (*3*), can be quantitatively understood and rationally manipulated.

The technical challenges of the systems biological approach (*4*) are mainly along four lines (see the figure): (i) systemwide component identification and quantification ("omics" data) at the level of mRNA, proteins, and small molecular weight metabolites; (ii) experimental identification of physical component interactions, primarily for information-processing networks; (iii) computational inference of structure, type, and quantity of component interactions from data; and (iv) rigorous integration of heterogeneous data. The last step is required to achieve a holistic, quantitative, and predictive understanding through mathematical models that enable an iterative cycle between prediction and experiments, the hallmark of systems biology.

The development of experimental methods relating to the first challenge has made tremendous advances in the past decade, but the level of sophistication and the associated costs have led to a situation where primarily single-component data—that is, data solely on genes, proteins, or metabolites—are available. Until the study by Ishii *et al.*, at best two different types of component data were reported for a given experiment, which severely limited progression along the iterative cycle between experiments and theory.

By joining forces among specialized labs, Ishii *et al.* report systemwide data on three main component layers of cells—transcriptome (mRNA), proteome (protein), and metabolome (metabolites)—with a particular focus on central carbon metabolism of the model bacterium *Escherichia coli*. Beyond component concentrations, the functional endpoint of gene, protein, and metabolite interactions—the intracellular metabolic fluxes—were quantified from ^{13}C-labeling experiments (*5*). In a laborious procedure, data on steady-state growth were collected from 24 mutant strains of *E. coli* in which a different gene that functions in carbon metabolism was removed from each strain. All mutants were grown at the same specific rate (*6*), thus minimizing indirect effects of the

The authors are at the Institute of Molecular Systems Biology, ETH Zurich, Switzerland. E-mail: sauer@ethz.ch

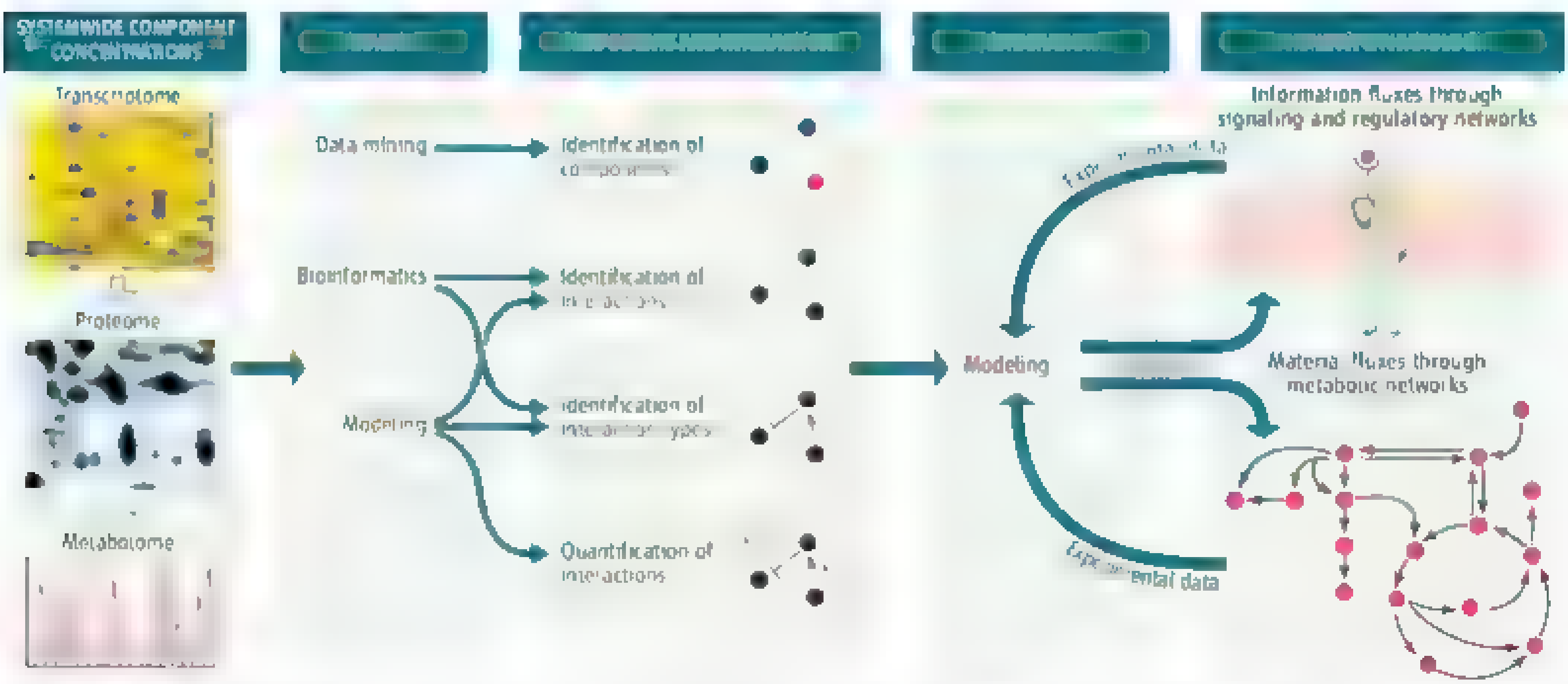

A systems roadmap. The comprehensive component concentrations reported by Ishii *et al.* provide input data for inferring component interactions using computational methods. The challenge for computational modeling methods yet to be developed is to predict the functional network state from the concentrations and to infer the information processing network that controls the functional state.

largely different mutant physiology that would otherwise hamper data interpretation from batch cultures.

The highly reproducible results from these genetic perturbation experiments were complemented with steady-state growth data from the wild-type bacterium grown at a range of growth rates in the same culture conditions, with the extreme cases of near starvation and almost unlimited supply of glucose (the limiting nutrient). An interesting observation is the active response of the bacterium's metabolic system to environmentally dictated changes in growth rate. There were global alterations in the expression level of many mRNAs and proteins. By contrast, upon genetic perturbation of the metabolic system, surprisingly few changes were observed at any component level (besides some obvious and inevitable local perturbations such as altered educt and product concentrations due to a deleted reaction). These results indicate that metabolic networks employ fundamentally different strategies to maintain active operation in the face of genetic or environmental perturbations. However, many important questions remain unanswered. Why does this particular distribution of flux in metabolism emerge from the determined component concentrations? What is actively regulated and by which mechanisms? Which mechanisms contribute to the observed robustness?

These questions remain open because the known component interactions have not yet been considered and because the regulatory network that controls metabolism is only partly known and qualitatively understood at best. But Ishii *et al.* provide, for the first time, a quantitative data set that includes both the constituting components and the functional state of a metabolic network. From these data, we can begin to unravel the conditional and quantitative relevance of regulatory interactions and discover new circuits, thereby addressing the question of how a functional state arises from the components. The call is thus open to integrate this heterogeneous data set into a coherent whole from which testable hypotheses on general principles and network regulation can be derived. Although this particular data set will not be sufficient—for example, it lacks time-resolved dynamic data, and the conditions studied are limited—its unprecedented completeness has the potential to become a cornerstone for computational systems biology.

A number of computational approaches are already available to integrate subsets of the Ishii *et al.* data. Statistical analyses of metabolic and transcriptional data, for example, can identify key features that are important for respiratory oscillations (7). Alternatively, computational mapping of transcriptome and metabolome data onto a graphic model of component interactions can provide guidance for dissecting control at the level of genetic regulation from regulation of protein activity (8). In contrast to statistical analyses, a method rooted in constraint-based modeling (4) allows combining metabolite concentrations with metabolite flux data using thermodynamic principles to derive hypotheses about active or new regulatory mechanisms (9).

The extensive data set reported by Ishii *et al.* now opens the way to use existing computational approaches and to develop new ones to extract new biological insights about a fundamental physiological process. From this starting point, model-based design of targeted experiments for further conditions will reduce the unrealistically tedious and expensive collection of large-scale data sets while working toward a truly holistic understanding of cellular behavior. We are one step closer.

References

1. N. Ishii *et al.*, *Science* **316**, 593 (2007).
2. H. Kitano, *Nature* **420**, 206 (2002).
3. J. Stelling, U. Sauer, Z. Szallasi, F. J. Doyle III, J. Doyle, *Cell* **118**, 675 (2004).
4. A. R. Joyce, B. O. Palsson, *Nat. Rev. Mol. Cell Biol.* **7**, 198 (2006).
5. U. Sauer, *Mol. Syst. Biol.* **2**, 62 (2006).
6. P. A. Hoskisson, G. Hobbs, *Microbiology* **151**, 3153 (2005).
7. D. B. Murray, M. Beckmann, H. Kitano, *Proc. Natl. Acad. Sci. U.S.A.* **104**, 2241 (2007).
8. T. Cakir *et al.*, *Mol. Syst. Biol.* **2**, 50 (2006).
9. A. Kümmel, S. Panke, M. Heinemann, *Mol. Syst. Biol.* **2**, 34 (2006).

10.1126/science.1142502

NEUROSCIENCE

How to Fill a Synapse

Philip J. Robinson

Knockout of a member of a family of proteins that support neuronal signal transmission reveals a number of unexpected pathways at work at distinct times during neuron stimulation.

The basis of almost all communication between neurons relies on vesicles containing chemical neurotransmitters. At the junction, or synapse, between two neurons, synaptic vesicles laden with neurotransmitter release their contents (exocytosis) from terminals of one neuron. The chemicals act on the opposing neuron, propagating a specific signal. Replenishing the presynaptic neuron with synaptic vesicles is critical to the signaling that underlies processes such as learning, and failure to control this cycle of vesicle formation and deployment can lead to conditions such as epilepsy. On page 570 of this issue, Ferguson and colleagues (1) show that the mechanism producing new synaptic vesicles is not as simple as once envisioned, but involves a family of proteins that manages the supply of vesicles both during and after a neuron is stimulated. Their discoveries reveal how a synapse maintains its full complement of synaptic vesicles to support all functions of the nervous system.

A protein called dynamin I has generally been considered the great ensurer of neurotransmitter-filled synaptic vesicles in a presynaptic nerve terminal. These vesicles are poised to fuse with the plasma membrane when the neuron is stimulated. Dynamin I acts after fusion and neurotransmitter release in a process called endocytosis. After the plasma membrane invaginates, dynamin I forms a helix around the neck of the new budding vesicle, acting as a spring. As dynamin I expands and twists, it pinches the membrane into a synaptic vesicle that can subsequently be filled with newly synthesized neurotransmitter (see the figure). But Ferguson *et al.* show that, unexpectedly, synaptic vesicles can form in the absence of dynamin I. By genetically engineering mice that lack dynamin I (knockout mice), they performed experiments that few thought would be fruitful. The mice appear normal at birth, with near-normal numbers of neurons and synaptic vesicles. However, the mice barely survive the first week after birth, and none survive two.

The data of Ferguson *et al.* are full of surprises. The first is that nerve terminals in the synapses of dynamin I knockout mice contain these vesicles at all. This reveals that another endocytosis mechanism can generate these vesicles. The next surprise is the heterogeneous size of the synaptic vesicles that are formed in the absence of dynamin I. Synaptic vesicles are considered the smallest cellular

The author is in the Cell Signalling Unit, Children's Medical Research Institute, Sydney, Australia. E-mail: probinson@cmri.com.au

vesicle, produced within a narrow size range of 40 to 43 nm. Indeed, the data of Ferguson *et al.* indicate that dynamin 1 is likely responsible for this by generating the highest possible membrane curvature through its helical assembly and twist (2). The larger synaptic vesicles in the dynamin 1 knockout mice were an average of 47 nm and up to two times larger than normal. This was matched by an increase in quantal size, an index of the quantity of transmitter in a vesicle, and they could still support synaptic transmission.

The most surprising observation in these animals is that synaptic vesicle endocytosis was almost totally absent during intense stimulation of neurons, yet resumed at a normal rate after the stimulus was terminated. Normally, endocytosis continues during and after neuron stimulation. This suggests that the dynamin 1–independent mechanism is suppressed by the influx of calcium ions that occurs when a neuron is stimulated.

The new observations show that dynamin 1 is dispensable for forming synaptic vesicles. It becomes indispensable when a burden is placed on the neuron by moderate or prolonged stimulation. Minimal neuronal activity of up to 10 stimuli in 1 s uses only about 10 to 20 vesicles. But when the frequency or duration exceeds this, exocytosis of many more synaptic vesicles occurs. Indeed, about a minute of stimulation is sufficient for the release of all 200 synaptic vesicles in the average nerve terminal (3). Without a mechanism for fast generation of new vesicles, neuronal activity cannot be sustained and nerve communication stops. Ferguson *et al.* suggest that very soon after stimulation ceases, dynamin 1 relinquishes its role in synaptic vesicle endocytosis to a dynamin 1–independent pathway. Dynamin 1 normally becomes activated during nerve stimulation, when it becomes dephosphorylated and is inhibited immediately after stimulation by phosphorylation (4). This phosphorylation cycle may allow the dynamin 1–independent

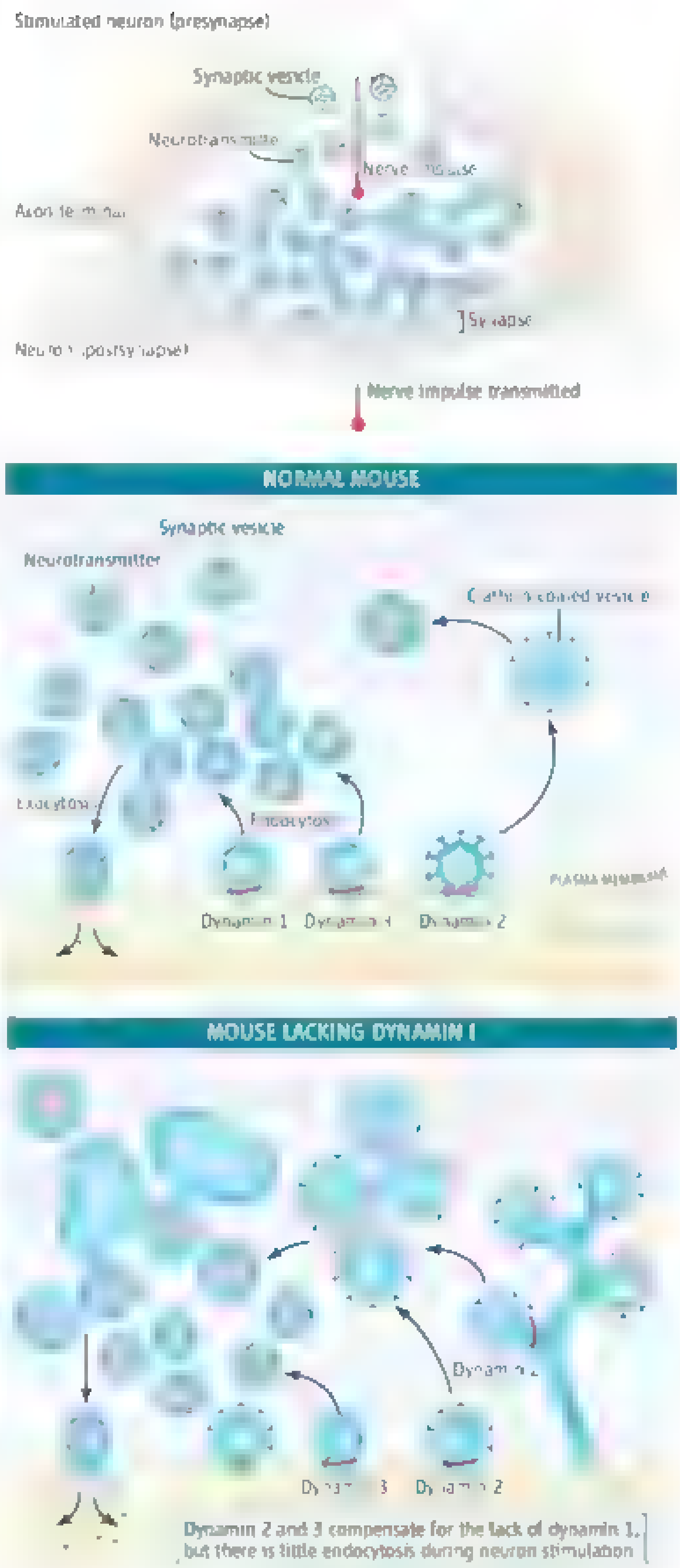

Synaptic vesicle cycling. (Top and Middle) A normal presynaptic neuron contains uniform, small synaptic vesicles. After electrical stimulation, vesicles release neurotransmitter. New vesicles are primarily produced by dynamin 1–dependent endocytosis. **(Bottom)** In the absence of dynamin 1, Ferguson *et al.* observe vesicles of heterogeneous sizes, some coated with clathrin, formed through dynamin 2 and 3 pathways.

mechanism to take over endocytosis.

Attention will now turn to the two other dynamin family members, dynamin 2 and 3, as likely mediators of the dynamin 1–independent mechanism(s). Ferguson *et al.* reveal important presynaptic roles for dynamin 3. The expression level of this protein does not change in the knockout mice, but it is recruited into the synapses, as if attempting to compensate for the lack of dynamin 1. In an elegant experiment, synaptic vesicle endocytosis that occurs during stimulation was fully rescued when dynamin 1 or dynamin 3 was expressed in neurons cultured from the brains of dynamin 1 knockout mice. Therefore, dynamin 3 may share a dynamin 1–like role in generating uniformly small synaptic vesicles. These two dynamins are also phosphorylated on analogous amino acids, further indicating similar control mechanisms (5). However, dynamin 3 expression is much lower than that of dynamin 1, and it cannot cope with the increased demands imposed at high neuronal activity in the knockout mice.

Dynamin 2 is ubiquitously expressed and in all cell types examined it mediates formation of vesicles, via endocytosis, that are coated with the protein clathrin. In presynaptic nerve terminals, clathrin is shed and the vesicles become synaptic vesicles filled with neurotransmitter. Ferguson *et al.* show that an average synapse contains less than one clathrin-coated vesicle. Expression of dynamin 2 does not change in the dynamin 1 knockout mice, nor can it rescue synaptic vesicle endocytosis during intense activation of neurons. Rather, it appears to play a role in the slow replenishment of synaptic vesicles after stimulation. Ferguson *et al.* found a 24-fold increase in the abundance of clathrin-coated vesicles, with occasional synapses showing up to 50 clathrin-coated profiles. In a few synapses lacking dynamin 1, synaptic activity produced

large membranous tubules in the presynaptic neuron, from which large numbers of clathrin-coated vesicles emerged. They appear trapped at the point just before dynamin normally acts. Although more clathrin is recruited into synapses of these neurons, dynamin 2 is not. Therefore, dynamin 2 abundance may be the rate-limiting factor in allowing the synapse to generate many vesicles after intense stimulation. This is in stark contrast to synapses forged by the neurons of normal mice, where dynamin 1 can maintain synaptic vesicle cycling for hours during sustained neuronal activity. If dynamin 2 mediates the bulk of slow synaptic vesicle formation, then why is this pathway suppressed during stimulation, only to operate again at normal rates after stimulation is terminated? There is no evidence that dynamin 2 is phosphorylated or dephosphorylated in nerve terminals (5). The simplest explanation is that a high calcium concentration in nerve terminals during stimulation suppresses dynamin 2 (or dynamin 3?) dependent endocytosis, while stimulating dynamin 1-dependent vesicle formation via dephosphorylation. In practice, this may divide the work load between two mechanisms of synaptic vesicle endocytosis.

The main discovery by Ferguson *et al.* is that there are at least two pathways mediating synaptic vesicle endocytosis, working in series: a high-capacity dynamin 1 (or dynamin 3?) pathway that works primarily during intense neuronal activity, and a low-capacity pathway, probably mediated by dynamin 2, that is suppressed during stimulation but is gradually activated when stimulation ceases. Thus, there is more than one way to fill a synapse with synaptic vesicles.

References

1. S. M. Ferguson *et al.*, *Science* 316, 570 (2007).
2. A. Rous, K. Uyhan, A. Frost, P. De Camilli, *Nature* 441, 528 (2006).
3. J. H. Koenig, K. Ikeda, *J. Neurosci.* 9, 3844 (1989).
4. M. A. Cousin, P. J. Robinson, *Trends Neurosci.* 24, 659 (2001).
5. M. E. Graham *et al.*, *J. Biol. Chem.* 10.1074/jbc.M609713200 (20 March 2007).

10.1126/science.1142705

CHEMISTRY

A Promising Mimic of Hydrogenase Activity

A chemical compound that mimics the active site of nickel-iron hydrogenases is catalytically active. Related compounds may serve as catalysts in a hydrogen economy.

Thomas B. Rauchfuss

Hydrogenases are enzymes that catalyze the reversible oxidation of dihydrogen (H_2). They have attracted intense interest because of their extraordinary efficiency and their unusual active sites, which feature carbon monoxide (CO) and cyanide (CN^-) as cofactors. Furthermore, a detailed understanding of the hydrogenases may lead to new kinds of biomimetic catalysts for the hydrogenation of organic compounds and for hydrogen production.

There are two types of widely distributed hydrogenases, which contain different metals in their active sites: nickel-iron (Ni-Fe) and iron-only hydrogenases (*1*). Progress on model compounds that capture the main features of iron-only hydrogenases has been rapid, but models for the more prevalent Ni-Fe hydrogenases have proven far more challenging to obtain. It has been difficult to introduce the most obvious feature of the Ni-Fe active sites—the hydride (H^-) ligand—into biomimetic models or to obtain any sign of catalytic activity. On page 585 of this issue, Ogo *et al.* (*2*) report the discovery of an easy-to-prepare biomimetic catalyst inspired by the Ni-Fe hydrogenases. More faithful structural replicas of the Ni-Fe active site are known (see the figure, top panel), but they are not catalytically active, in part because they lack the hydride ligand (*3*, *4*).

In the quest for biomimetic catalysts, scientists seek to replicate the coordination sphere that surrounds the metal centers, with the expectation that function will follow form. A straightforward approach to the assembly of models for the Ni-Fe active site follows from its structure (see the figure, bottom panel): Ni is bound to four cysteine residues, two of which bridge to the $Fe(CN)_2(CO)$ subunit.

Thus, it should be possible to generate mimics by combining nickel tetrathiolate compounds and $Fe(CN)_2(CO)$ fragments (*5*, *6*). However, because nickel complexes with four thiolate ligands are often labile, chemists

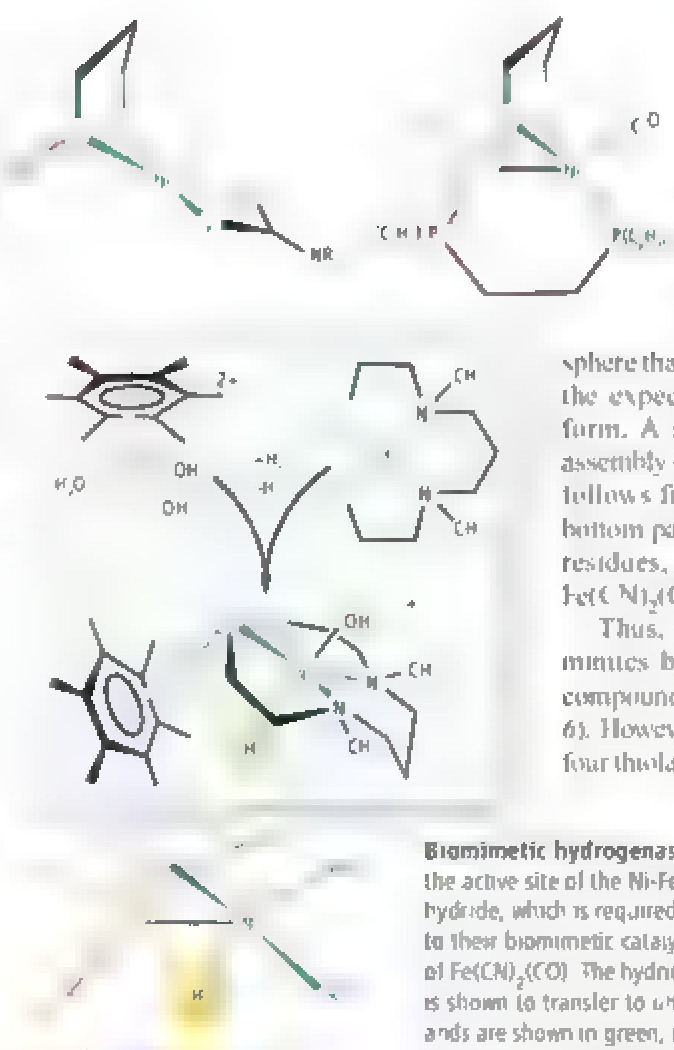

Ni-Fe hydrogenase active site

Biomimetic hydrogenases. (Top) Current structural models for the active site of the Ni-Fe hydrogenases. Note the absence of the hydride, which is required for activity. **(Middle)** Ogo *et al.*'s route to their biomimetic catalyst, with $Ru(C_6(CH_3)_6)^{2+}$ playing the role of $Fe(CN)_2(CO)$. The hydride ligand between the Ni and Ru centers is shown to transfer to unsaturated substrates. Nickel and its ligands are shown in green, iron and its ligands in red. **(Bottom)** The structure of the enzyme active site.

The author is at the School of Chemical Sciences, University of Illinois, Urbana, IL 61801, USA. E-mail: rauchfuz@uiuc.edu

have turned increasingly to the use of related $[Ni(S_2N_2)]$ complexes containing two amines and two thiolates (7) as building blocks for the assembly of bimetallic compounds. For the other half of the system, Ogo *et al.* mimic the $Fe(CN)_2(CO)H^-$ module with the electronically related fragment $(C_6Me_6)RuH^+$ (8), where Me denotes a methyl group. They assemble their model compound by simply combining aqueous solutions of the $Ni(S_2N_2)$ and $[(C_6Me_6)Ru(H_2O)_3]^{2+}$ building blocks.

Relative to other RuNi models (9, 10), the species reported by Ogo *et al.* is unique in that it undergoes the crucial reaction with H_2 to give the corresponding hydride (see the figure, middle panel). This conversion to the hydride entails scission of H_2 into H^- and H^+; as a result, the pH of the solution drops. Spectroscopic and crystallographic data show that the hydride ligand bridges the Ru and Ni centers, as expected. The results suggest that the RuNi-H core could be described as Ru-H$^-$→Ni, which indicates that the Ni(II) serves as a Lewis acid to stabilize the otherwise highly basic hydride. Such insights would be unattainable through studies on the enzyme itself, because protein crystallography cannot detect hydride ligands.

The greatest surprise from the results of Ogo *et al.* is that their compound is catalytically active: It catalyzes the hydrogenation of benzaldehyde to the corresponding alcohol. It is also intriguing that the catalyst features a sulfur-rich core. Sulfur compounds poison most industrial catalysts, but nature relies heavily on sulfur-rich environments for catalytic transformations involving CO and H_2. There is much interest in the development of sulfur-tolerant industrial catalysts for related transformations.

Given the progress reported by Ogo *et al.*, what is left to model? The answer is clear: a related complex, with Ru replaced by Fe, because nature always uses iron when working with hydrogen. The results reported by Ogo *et al.* show that such a feat should be achievable and that such advanced models can deliver new kinds of catalysts.

References

1. G. Jaouen, Ed., *Bioorganometallics: Biomolecules, Labeling, Medicine* (Wiley-VCH, Weinheim, Germany, 2006).
2. S. Ogo *et al.*, *Science* **316**, 585 (2007).
3. Z. Li, Y. Ohki, K. Tatsumi, *J. Am. Chem. Soc.* **127**, 8950 (2005).
4. W. Zhu *et al.*, *Proc. Natl. Acad. Sci. U.S.A.* **102**, 18280 (2005).
5. W.-F. Liaw *et al.*, *J. Am. Chem. Soc.* **124**, 1680 (2002).
6. A. Kayal, T. B. Rauchfuss, *Inorg. Chem.* **42**, 5046 (2003).
7. M. V. Rampersad *et al.*, *Angew. Chem. Int. Ed.* **44**, 1217 (2005).
8. G. Süss-Fink, B. Therrien, *Organometallics* **26**, 766 (2007).
9. Y. Oudart, V. Artero, J. Pécaut, M. Fontecave, *Inorg. Chem.* **45**, 4334 (2006).
10. M. A. Reynolds, T. B. Rauchfuss, S. R. Wilson, *Organometallics* **22**, 1619 (2003).

10.1126/science.1140733

PHYSICS

Factoring Numbers with Waves

Finding prime factors of a number by means of wave interference may have applications in quantum computing and security systems.

M. Suhail Zubairy

Although it may seem a mundane problem in number theory, the ability to factor a number into its primes lies at the heart of modern e-commerce. Anyone with a pocket calculator knows it is trivial to multiply two prime numbers together, but carrying out the reverse—finding the unknown prime factors given a large number—is extremely difficult. This difficulty is what enables some of the encryption systems used on the Internet, in which a secret key is exchanged between the sender and the receiver on a public channel. Any method for efficient factoring, therefore, attracts immediate attention. For example, the entire field of quantum computing (1), which had its beginnings in the early 1980s, did not receive much attention until Shor (2) demonstrated in 1994 how a quantum computer could potentially factorize a 1000-digit number relatively rapidly, whereas the same problem would take today's fastest computer several billion years. This theoretical development has caused the field of quantum computing to take off.

The author is in the Department of Physics, Texas A&M University, College Station, TX 77843, USA. Present address: Texas A&M University at Qatar, P.O. Box 23874, Education City, Doha, Qatar. E-mail: zubairy@physics.tamu.edu

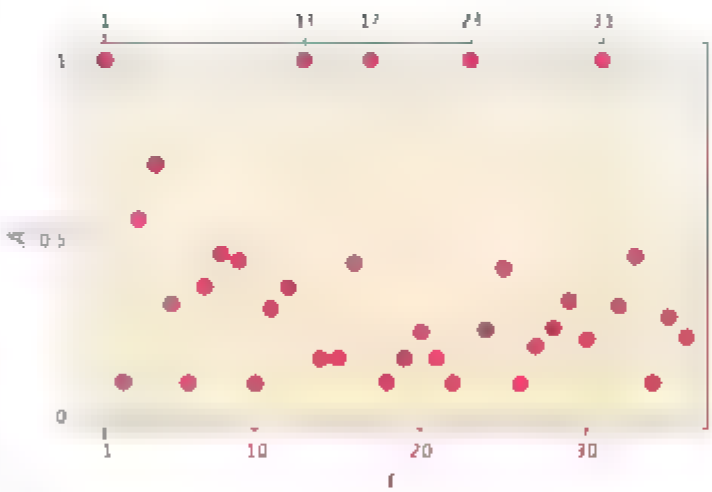

Peak factors. A plot of the absolute value of the truncated Gaussian sum *A* for *N* = 157 573 and truncation parameter *M* = 10. The sum is maximum for values of *l* that are the prime factors of *N* (13, 17, 23, and 31). This factorization method has been implemented with NMR techniques (3, 4). [Adapted from (3).]

An interesting but very different approach to factorization based on wave interference is reported in two recent papers (3, 4). When two waves are combined, they can create destructive or constructive interference, depending on their relative phase (that is, "in phase" the waves add up; "out of phase," they cancel out). When the number of waves becomes large and the relative phases between the waves have a wide range of values, the result is a combination of destructive and constructive interferences. The amplitude of the combined wave is substantially lower than when all the waves interfere constructively. But constructive interference causes a peak in the amplitude when all the relative phases are an integer multiple of 2π.

Mehring *et al.* (3) use this property of waves to factor numbers. They consider a quantity called the truncated Gaussian sum, which corresponds to the amplitude of a collection of *M* waves, where the phase of each wave depends on the number *N* that is to be factorized and another integer *l*. The total phase is chosen such that they are all equal to an integer multiple of 2π only if *l* happens to be a factor of *N*. Thus, the sum is maximized by constructive interference when *l* is a factor of *N*. A scan of the truncated Gaussian sum for different values of *l* will then yield the factors of *N* (see the figure).

How can this truncated Gaussian sum factoring method be implemented experimentally? Mehring *et al.* (*3*) and Mahesh *et al.* (*4*) do this with the techniques of nuclear magnetic resonance (NMR). They excite an ensemble of spins (specifically, protons in a molecular liquid) by a sequence of radio-frequency pulses. The spins rotate in small steps just as a mechanical pendulum would move under the action of periodic kicks. The number of pulses corresponds to the truncation parameter M, and the phase of the radio-frequency wave depends on N and l in such a way that, at the end of the pulse sequence, the collection of excited spins corresponds to a truncated Gaussian sum. The resulting signal emitted from the spins contains information about the various radio-frequency pulses used in the excitation. The maximum signal is obtained when l is a factor of N. Using this method, Mehring *et al.* factored the number 157,573 (*3*) and Mahesh *et al.* factored 52,882,363 (*4*).

This is essentially a classical scheme that employs the principle of superposition obeyed by the classical waves. Hence, it scales exponentially (that is, as the size of the problem increases, the time needed to solve it goes up exponentially). The quantum computing algorithms, however, are rooted in quantum entanglement, a notion peculiar to the nature of quantum mechanics. In an entangled system of several objects, the objects are highly correlated so that it is impossible to consider the objects independently. Their properties are intertwined. For example, in an entangled pair of atoms, we may not know the precise state of the individual atom before making the measurement. However, if the first atom is found in the ground state, then the other is necessarily in an excited state and vice versa. These nonclassical entangled states allow us, in principle, to do simultaneous manipulations on different states of the total system, a luxury not afforded in the classical world. This is the root cause of the speedup of quantum computers.

This inherent parallelism represents the good news. The bad news, however, is that it is very difficult to generate such entangled states, especially when many particles are involved. More important, entangled objects are among the most fragile objects in nature. Any interaction with the environment tends to destroy the high degree of correlation between the objects. So far, only the number 15 has been factored using Shor's algorithm (*5*), and an extension to larger numbers remains elusive.

A challenge is how to reduce the computational complexity of the scheme discussed by Mehring *et al.* (*3*) by using the parallelism offered by quantum entanglement. Can we prepare the system in such a way that the spins are in an entangled state and then manipulate different values of l simultaneously? This is indeed an exciting, but challenging, possibility. The ideas presented may, however, offer new possibilities in other directions, such as an efficient scheme to find the periodicity of a function, the key to finding prime factors in Shor's algorithm (*2*). Another interesting problem relates to searching for a marked object in a data base containing N objects. Classically, this is done on average with $N/2$ searches. However, quantum searches can lead a search in $\sqrt{N}$ steps (*6*, *7*). The question is whether one can do better than that and, at least in some special cases, recover the desired object in one or few steps. The work of research groups, including that of Mehring *et al.* and Mahesh *et al.*, may lead the way.

References and Notes

1. For background on quantum computing, see (*8*), for example.
2. P. Shor, in *Proceedings of the 35th Annual Symposium on Foundations of Computer Science*, Santa Fe, NM, S. Goldwasser, Ed. (IEEE Computer Society Press, New York, 1994), p. 124.
3. M. Mehring, K. Muller, I. S. Averbukh, W. Merkel, W. P. Schleich, *Phys. Rev. Lett.* **98**, 120502 (2007).
4. T. S. Mahesh, N. Rajendran, X. Peng, D. Suter, www.arxiv.org/quant-ph/0702205.
5. L. M. K. Vandersypen *et al.*, *Nature* **414**, 883 (2001).
6. L. K. Grover, *Phys. Rev. Lett.* **79**, 325 (1997).
7. M. O. Scully, M. S. Zubairy, *Phys. Rev. A* **64**, 022304 (2001).
8. S. Stenholm, K.-A. Suominen, *Quantum Approach to Informatics* (Wiley, New York, 2005).

9. This work is supported by the Air Force Office of Scientific Research grant FA9550-04-1-0206.

10.1126/science.1140915

PHYSICS

The End of an Entanglement

Observations of the early disappearance of quantum coherence between two systems may have implications for information processing.

J. H. Eberly and Ting Yu

In quantum physics, decoherence is a catch-all term that usually implies degradation of the purity of a quantum state. Over the past few decades it has been used as a guide to understand the loss of the two-body coherence called entanglement, which is an intrinsically quantum effect. In this context, it is relevant to fundamental questions such as, Why is the world mostly classical when we believe quantum theory provides all of the governing principles (*1*, *2*)? The answer lies in the critical role of "largeness"—simply put, larger bodies lose coherence more quickly. This is the essential ingredient in producing nearly instantaneous decay of entanglement between two large bodies or between a large body and a small one. The role of largeness is seen when decoherence occurs increasingly faster with the size of the environment. [See, for example, (*3*) for an instance of the effect.] Preservation of coherence is important in maintaining steady behavior of quantum systems whose coordinated action is critical, for example, among the working units of quantum computers when they become available.

A small body (spin, photon, atom, exciton, quantum dot, Cooper pair, etc.), on the other hand, can continue to behave as a quantum mechanical unit, even if not macroscopically entangled. A topic that remains open in almost all decoherence discussions, however, is the preservation or destruction of two-body quantum coherence when both bodies are small. For example, it has been predicted only recently that the one-body and two-body responses to a noisy environment can follow surprisingly different pathways to complete decoherence (*4*, *5*). Experimental entry into this new domain is needed, and impressive results are now reported on page 579 of this issue by Almeida *et al.* (*6*). They have devised an elegantly clean way to check and to confirm the existence of so-called "entanglement sudden death" (ESD) (*7*), a two-body disentanglement that is novel among known relaxation effects because it has no lifetime in any usual sense—that is, entanglement termi-

The authors are in the Department of Physics and Astronomy, University of Rochester, Rochester, NY 14627, USA. E-mail: eberly@pas.rochester.edu; ting@pas.rochester.edu

nates completely after a finite interval, without a smoothly diminishing long-time tail.

The lack of a smooth and lengthy degradation has to be regarded as unexpected and potentially troubling. Error correction technology applied to entangled quantum information networks (*8*, *9*) allows even the smallest amount of degraded entanglement to be restored to full usefulness. However, error correction comes up short in the face of exactly zero entanglement, i.e., sudden death. As a practical matter, familiar local (one-body) lifetimes have been commonly used to estimate all accompanying nonlocal (multibody entanglement) lifetimes. Until recently there has been no reason to think, and certainly no evidence, that these lifetimes would be substantially different. The experiment of Almeida *et al.* puts the first evidence on the table.

Since the discovery of ESD (*4*, *5*), a large number of instances of this surprising effect have been identified in the theoretical literature (see (*10*–*17*) and references in (*6*)). All of these share the property that while local (one-body) coherence decays smoothly to zero, requiring an infinite time to do so, nonlocal (two-body) entanglement vanishes after a finite time (see the figure for a schematic representation).

Although two-body entanglement is central to preservation of pairwise quantum correlations, there is an interesting unsolved problem in quantum mechanics related to it. Simply said, a computable quantity that universally measures entanglement of more than two bodies in partially relaxed (impure) states has yet to be identified by anybody. Along with Almeida *et al.*, we have used for ESD studies the two-body measure discovered by Wootters (*18*) and called concurrence (labeled *c* on the vertical axis of the right panel of the figure). It agrees about the boundary for zero entanglement with all other two-body measures and is more convenient than most.

It is often implied and sometimes said explicitly, in textbooks as well as in physics colloquia, that our evidence for the quantum character of natural phenomena comes from the existence of wave-particle duality in the microworld. But this is misleading at best. Wave mechanics is just optics for particles, and it contains effects no more exotic than are found in physical optics (rays, diffraction, tunneling, etc.). In striking contrast, quantum mechanics exhibits features that have no classical wave counterpart at all. Duality is no help in understanding the entangled nature of Schrödinger's Cat, which "exists" in a strange entangled state, equally likely dead and alive (*19*–*21*).

To investigate quantitatively the time development of a property such as the degree of entanglement of two or more quantum systems is to enter what is probably the largest nonclassical sector of the world we live in, and the report by Almeida *et al.* brings new evidence to bear on these questions. They have used a photonic Cat: a pair of qubits (quantum bits in the form of photon polarizations) whose degree of mutual entanglement they can study in the clear absence of mutual interaction. Each of these photonic qubits interacts only with its own individual environment, and this produces smooth dephasing of each individual photon's polarization angles. But this provides very misleading guidance to a quantitative understanding of the photons' Cat-like properties. One-body information about the photons is useless to explain the sudden death of their entanglement.

Different types of environmental noise can have different effects on two-body entanglement (*22*), and Almeida *et al.* have studied both phase- and amplitude-damping environments. They also mention that entanglement has a further unusual relaxation property in addition to sudden death. It can happen that different entangled states with the same initial degrees of entanglement may evolve to completely different final states, and examples of this are available (*4*) showing many pairs of mixed states with identical initial degrees of entanglements but with evolution pathways to very different final results. In addition, it is known that some two-qubit states are more robust against disentanglement than others (*23*) and that evolution to sudden death can be avoided in some cases by purely local (one-body) initializations (*22*).

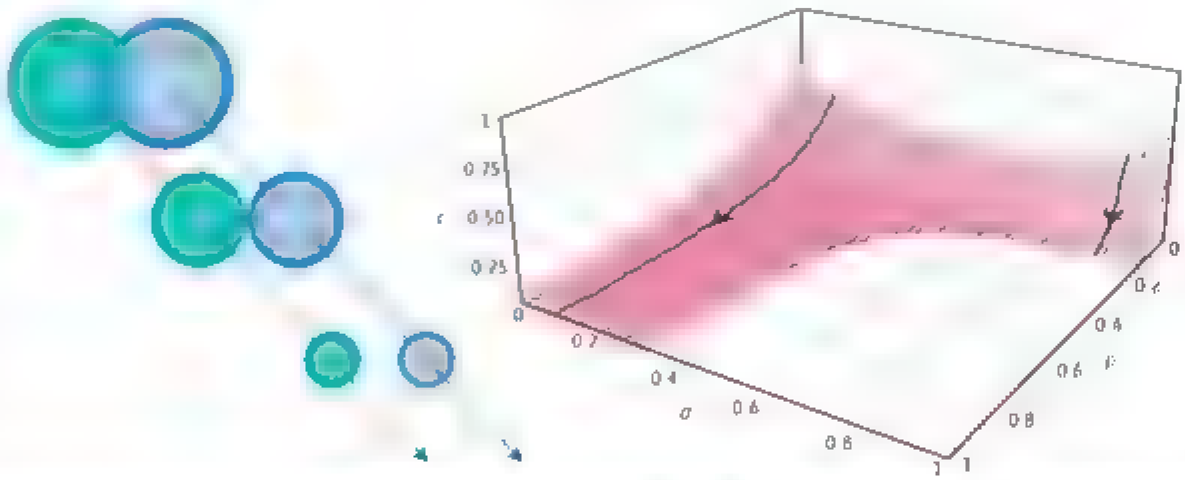

Parting ways. **(Left)** Sketch of entanglement sudden death, with spheres representing snapshots of the individual qubits [illegible] As [illegible] qubit [illegible] with [illegible] the [illegible] will shrink to the small [illegible] that represents its final state. However, [illegible] two spheres [illegible] overlapping. **(Right)** Entanglement sudden death [illegible] as reported by Almeida *et al.* (*6*). An [illegible] dependent [illegible] is shown [illegible] plotted [illegible] against the probability of decay *p* [illegible] under the [illegible] environmental amplitude [illegible] In this example, different values of α [illegible] correspond to [illegible] initial entanglements but lead to very different final conditions, some showing entanglement sudden death and some not (black lines).

Small-system entanglement dynamics is a domain with many borders. It touches on a wide spectrum of current research activities in coherence control, dynamic error correction, and experimental excursions in the vicinity of the quantum-classical interface, to name a few. The state of the theoretical frontier for entanglement dynamics is summarized in a review by Mintert *et al.* (*24*). The report by Almeida *et al.* is not the final word in studies in this domain, and given the central role of small-system entanglement in any quantum information network, it is likely that other experimental investigations will follow their work.

References and Notes

1. W. H. Zurek, *Rev. Mod. Phys.* **75**, 715 (2003).
2. E. Joos, H. D. Zeh, *Z. Phys. B* **59**, 223 (1985).
3. M. Brune *et al.*, *Phys. Rev. Lett.* **77**, 4887 (1996).
4. T. Yu, J. H. Eberly, *Phys. Rev. Lett.* **93**, 140404 (2004).
5. P. J. Dodd, J. J. Halliwell, *Phys. Rev. A* **69**, 052105 (2004).
6. M. P. Almeida *et al.*, *Science* **316**, 579 (2007).
7. T. Yu, J. H. Eberly, *Phys. Rev. Lett.* **97**, 140403 (2006).

8. P. Shor, *Phys. Rev. A* **52**, 2493 (1995).
9. A. Steane, *Phys. Rev. Lett.* **77**, 793 (1996).
10. O. Tolkunov *et al.*, *Phys. Rev. A* **71**, 060308 (2005).
11. K. Roszak *et al.*, *Phys. Rev. A* **73**, 022313 (2006).
12. M. Franca Santos *et al.*, *Phys. Rev. A* **73**, 040305 (2006).
13. L. Derkacz *et al.*, *Phys. Rev. A* **74**, 032313 (2006).
14. M. Yönaç *et al.*, *J. Phys. B* **39**, S621 (2006).
15. Z. Ficek *et al.*, *Phys. Rev. A* **74**, 024304 (2006).
16. K. Ann *et al.*, *Phys. Rev. B* **75**, 115307 (2007).
17. C. Pineda *et al.*, *Phys. Rev. A* **75**, 012106 (2007).
18. W. K. Wootters, *Phys. Rev. Lett.* **80**, 2245 (1998).
19. E. Schrödinger, *Naturwissenschaften* **23**, 807 (1935).
20. In Schrödinger's thought experiment, a cat is placed in a box with a randomly triggered poison. According to quantum theory, until an observation is made, the cat is in a superposition of two states, in effect both "alive" and "dead" simultaneously.
21. A. Einstein, B. Podolsky, N. Rosen, *Phys. Rev.* **47**, 777 (1935).
22. T. Yu, J. H. Eberly, http://arxiv.org/abs/quant-ph/0503089
23. T. Yu, J. H. Eberly, *Phys. Rev. B* **66**, 193306 (2002).
24. F. Mintert, A. R. R. Carvalho, M. Kus, A. Buchleitner, *Phys. Rep.* **415**, 207 (2005).
25. Supported by NSF grants PHY04-56952 and PHY06-01804 and Army Research Office grant W911NF-05-1-0543 to the Rochester Theory Center.

10.1126/science.1142654

EVOLUTION

Oxygen and Evolution

Changes in atmospheric oxygen concentration may be linked to key evolutionary events during the past 550 million years.

Robert A. Berner, John M. VandenBrooks, Peter D. Ward

The rise of atmospheric oxygen (O_2) concentrations during the Precambrian eon (~4500 to ~550 million years ago) was closely tied to biological evolution. Additional changes in atmospheric O_2 concentrations over the past ~550 million years (the Phanerozoic eon) have probably also been intertwined with biological evolution. Here we examine the evidence for changes in O_2 concentrations and their biological causes and effects during the Phanerozoic.

Evidence for variations in atmospheric O_2 concentrations over Phanerozoic time comes mainly from the geochemical cycles of carbon and sulfur. The weathering of organic carbon and pyrite sulfur results in O_2 consumption, and their burial in sediments results in O_2 production (*1*); organic burial represents an excess of global photosynthesis over global respiration. Existing combined carbon-sulfur-oxygen models all show distinct variation of O_2 over time, with a maximum centered around 300 million years ago, but with differences between models for the past 200 million years (*1*). They are based on either the abundance of reduced carbon and sulfur in sediments, the $^{13}C/^{12}C$ and $^{34}S/^{32}S$ values for the oceans, or the interaction of the carbon and sulfur cycles with cycles of other elements such as phosphorus.

The model shown in the figure is the most detailed for the entire Phanerozoic and lends itself readily to the discussion of evolutionary phenomena. Note the large rise in O_2 prior to 300 million years ago. The primary cause of this rise is believed to be the evolution of large vascular land plants (*1*). The plants caused increased burial of organic matter (and hence increased O_2 production) because of the introduction of a new biodegradation-resistant substance, lignin. The excessive burial of lignin and other plant debris in swamps during the late Paleozoic (~360 to 260 million years ago) led to the formation of vast coal deposits and to increased wildfires, as evidenced by abundant fossil charcoal (*2*). The drop in O_2 concentration across the Permian-Triassic boundary (~260 to 245 million years ago), and the relative lack of coal deposition during the last 5 million years of this time span, are believed to have been due mainly to a substantial reduction in the geographic extent of lowland forests and swamps. This resulted in a drop in global organic matter burial and in O_2 input to the atmosphere (*3*).

How has the variation in atmospheric O_2 concentration through the Phanerozoic affected the evolution and development of life on Earth? In 1970, McAlester (*4*) noted that to understand these effects, it is necessary to first run "long-term experiments on the effects of abnormally high or low O_2 partial pressures on the living representatives of the many groups which exist today."

Unfortunately, few scientists have heeded this call, and the effects of the modeled O_2 concentrations (~13 to 31%) on modern physiology and development are still poorly understood, especially in the hyperoxic range

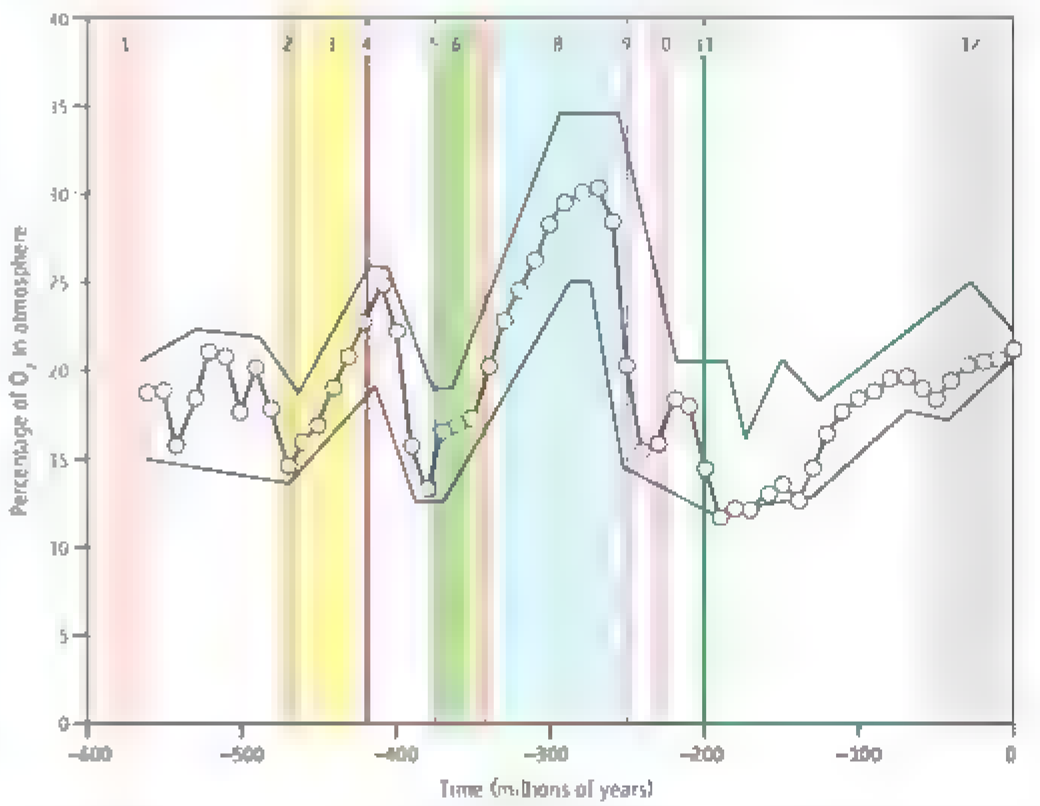

A possible link. The atmospheric O_2 curve is taken from (*2*). The upper and lower boundaries are estimates of error in modeling atmospheric O_2 concentration. The numbered intervals denote important evolutionary events that may be linked to changes in O_2 concentration (see text).

R. A. Berner is in the Department of Geology and Geophysics, Yale University, New Haven, CT 06520, USA. E-mail: robert.berner@yale.edu J. M. VandenBrooks is in the School of Life Sciences, Arizona State University, Tempe, AZ 85287, USA. P. D. Ward is in the Department of Biology, University of Washington, Seattle, WA 98195, USA.

(~21% O_2, the current atmospheric O_2 concentration). Furthermore, most studies have focused on the effect of O_2 on insect development, and even those limited studies examined O_2 levels outside the range of geologic variation (*5*). However, the existing studies point to a substantial effect of this range of O_2 variation on development and evolution.

Many studies have used *Drosophila melanogaster* to study these effects. For example, it has been shown that hyperoxia causes an increase in body size in *D. melanogaster* through multiple generations (*6*), whereas hypoxia decreases body size (*7*); O_2 concentration is negatively correlated with tracheal diameter in insects of the same body size (*8*), and hypoxia causes a decrease in cell size (*9*).

Fewer studies have investigated the effects of O_2 concentrations on vertebrates. For example, hyperoxia (35% O_2) induces regression of the external gills in tree frogs (*Agalychnis callidryas*) and causes early hatching when the frogs are subsequently exposed to air levels of O_2 (21%) (*10*). When juvenile trout (*Oncorhynchus mykiss*) are exposed to hyperoxia (38% O_2), their body weight increases compared to those at 21% O_2 (*11*).

One of us has studied the embryonic development of *Alligator mississippiensis* under seven different O_2 concentrations between 6 and 35% (spanning the entire Phanerozoic O_2 range) (*12*). The results show a positive effect of O_2 on body size, developmental rate, and bone composition, with a developmental optimum at ~27% O_2, beyond which the negative effects of increased O_2 concentration begin to play a larger role and cause increased mortality.

Four major events in the history of life illustrate the effects of rising, or high, concentrations of O_2 on evolution. First, the origin of the first animal body plans (see the figure, interval 1) coincided with a rapid rise in atmospheric O_2 concentration (*13*).

Second, the conquest of land by animals occurred during two independent phases of high O_2 concentration (*14*). The earliest, ~410 million years ago (interval 4), involved mainly arthropods; the other, which followed the Devonian mass extinction and a period of stasis (Romer's Gap, interval 6), involved both arthropods and vertebrates (interval 7).

Third, with increasing O_2 concentrations through the Carboniferous and Permian (interval 8), gigantism developed in several arthropod groups, and body size increased across primitive reptile-like animals and their descendants (*12, 15, 16*). The gigantism has classically been attributed to an increase in diffusive capacity caused by an increase in atmospheric O_2 concentration. This may explain the effect seen in egg-laying vertebrates, because diffusion across the eggshell will be increased and have an effect on hatchling and therefore adult body size. Alternatively, in some insects, body size is limited by the amount of their body that can be allocated to trachea. Because tracheal diameters decrease with increased O_2 concentration, a higher maximal body size can be achieved in times of higher O_2 concentration (*17*).

Lastly, the increase in mammalian body size in the Tertiary has been linked to rising O_2 concentrations (*18*) (interval 12), although the direct mechanism remains unclear, and community diversification occurred during the Ordovician rise in O_2 (interval 3).

Dropping O_2 or relatively low O_2 concentrations also had evolutionary consequences. Several extinctions appear to coincide with dropping O_2 concentrations superimposed on global warming from increased greenhouse gas concentrations (*19, 20*). Three of the major extinctions—in the Late Devonian (interval 5), Permian-Triassic (interval 9), and Triassic-Jurassic (interval 11)—were also followed by an extended period of low atmospheric O_2 concentration. The aftermath of a major extinction is often a time of rapid evolution, potentially producing novel body plans. Many of these new body plans may have supported more efficient respiratory systems, which may have been selected for under low-O_2 regimes that coincide with postextinction time periods.

For example, late Cambrian Ordovician lineages of fish and cephalopods evolved anatomical structures that took advantage of their swimming ability to force larger volumes of water across their gill surfaces, which in turn allowed for increased O_2 uptake (interval 2). Adaptations for more efficient respiration also occurred among terrestrial organisms. During the latter part of the Triassic (interval 10), a time of low modeled O_2 concentrations, the evolution of the dinosaur body plan involved a novel air-sac system (*21*), which was inherited in modified form by their descendants, the birds. Air-sacs allow highly efficient respiration even at high altitude (*22*). They may similarly have conferred a respiratory advantage to early dinosaurs as compared to other contemporary terrestrial animals.

In the past, respiratory structures were viewed as add-ons to body plans evolved largely to allow movement. Yet, the evidence discussed above suggests that the basic designs of many animals seems to maximize respiratory efficiency, with locomotion or protection (as with a mollusk or arthropod shell) as a secondary benefit.

To further this research, a better understanding of the effect of varying O_2 concentration on the physiology of present-day animals is needed. Multigenerational studies on a wide range of animals (both vertebrates and invertebrates) are necessary to accurately infer responses of fossil taxa to O_2 variation, to test evolutionary impacts of varying O_2 concentrations, and to understand the long-term effects of living under hyperoxic and hypoxic conditions. The results could be used to develop proxies for past O_2 concentrations, thereby improving O_2 modeling (which also needs constant updating based on better isotopic measurements). Once better modeling and more modern physiological studies have been carried out, we can begin to move from simple correlation to causation and truly test the hypotheses presented in the figure.

References and Notes

1. R. A. Berner, *The Phanerozoic Carbon Cycle: CO_2 and O_2* (Oxford Univ. Press, Oxford, 2004).
2. A. C. Scott, I. J. Glasspool, *Proc. Natl. Acad. Sci. U.S.A.* **103**, 10861 (2006).
3. R. A. Berner, *Geochim. Cosmochim. Acta* **69**, 3211 (2005).
4. A. L. McAlester, *J. Paleontol.* **44**, 405 (1970).
5. J. Harrison *et al.*, *Respir. Physiol. Neurobiol.* **154**, 4 (2006).
6. R. A. Berner, D. J. Beerling, R. Dudley, J. M. Robinson, R. A. Wildman Jr., *Annu. Rev. Earth Planet. Sci.* **31**, 105 (2003).
7. M. R. Frazier, H. A. Woods, J. F. Harrison, *Physiol. Biochem. Zool.* **74**, 641 (2001).
8. J. R. Henry, J. F. Harrison, *J. Exp. Biol.* **207**, 3559 (2004).
9. M. Farzin, S. A. Blatch, J. F. Harrison, paper presented at the Annual Meeting of the Society for Integrative and Comparative Biology, Phoenix, AZ, 5 January 2007.
10. K. M. Warkentin, *Physiol. Biochem. Zool.* **75**, 155 (2002).
11. K. Dabrowski, K. J. Lee, L. Guz, V. Verlhac, J. Gabaudan, *Aquaculture* **233**, 383 (2004).
12. J. M. VandenBrooks, thesis, Yale University (2007).
13. D. E. Canfield, S. W. Poulton, G. M. Narbonne, *Science* **315**, 92 (2007).
14. P. Ward, C. Labandeira, M. Laurin, R. A. Berner, *Proc. Natl. Acad. Sci. U.S.A.* **103**, 16818 (2006).
15. J. B. Graham, R. Dudley, N. Aguilar, C. Gans, *Nature* **375**, 117 (1995).
16. R. Dudley, *J. Exp. Biol.* **201**, 1043 (1998).
17. A. Kaiser *et al.*, paper presented at the Comparative Physiology Meeting: Integrating Diversity sponsored by the American Physiological Society, Virginia Beach, VA, 10 October 2006.
18. P. Falkowski *et al.*, *Science* **309**, 2202 (2005).
19. L. Kump, A. Pavlov, M. Arthur, *Geology* **33**, 397 (2005).
20. P. D. Ward, *Out of Thin Air* (Joseph Henry, Washington, DC, 2006).
21. P. M. O'Connor, L. P. A. M. Claessens, *Nature* **436**, 253 (2005).
22. Y. Jammes, *Poumon Coeur* **31**, 165 (1975).
23. R. A. Berner, *Geochim. Cosmochim. Acta* **70**, 5653 (2006).

24. The research of R.A.B. and J.M.V. was supported by the U.S. Department of Energy (grant DE-FG02-01ER15173) and that of P.D.W. by the NASA Astrobiology Institute.

10.1126/science.1140273

EDUCATION

Ambitious Joint Project Will Provide Science Support to School Boards

SAN FRANCISCO—Researchers call it an "urgency gap." While school officials and business leaders see a critical need for improved science, mathematics, and technology education, students and their parents are complacent.

Helping to close that gap will be one of the central goals in a historic new collaboration between AAAS and the National School Boards Association (NSBA), which have launched a 3-year project underwritten by the Ewing Marion Kauffman Foundation to give local school boards advice and resources for promoting science-related education in communities across the United States.

By February 2008, NSBA and AAAS expect to produce a set of resources on science, mathematics, and technology education, including a CD-ROM that can be tailored for different districts with different needs and a regularly updated Web site focused on science education news. Both will be based on extensive dialogue with school board members.

The program debuted 14 April before some 200 local school board members who attended a symposium at the NSBA annual conference in San Francisco. The biggest surprise to emerge from the 3-hour event: While Kansas City school board members interviewed for the project worry about the evolution issue emerging in their districts, most say that the need to improve science, mathematics, and technology education is a more pressing day-to-day and long-term issue, said Alison Kadlec, senior public engagement research associate at the civic research firm Public Agenda.

"What kind of jobs are out there, and what kinds of skills do kids need to be successful in those careers? That's what I want to know more about and think more about as I do my job," one of those board members told Public Agenda.

Board members at the San Francisco conference echoed that sentiment, and they welcomed the AAAS-NSBA project as a way to obtain expertise and training that will help them meet unprecedented challenges in preparing students for the 21st-century economy.

Divyesh N. Patel, a member of the Rio Rancho (NM) Board of Education, was among some 200 local school board members who discussed the challenges of improving science-related education.

The project creates a powerful partnership between NSBA, which represents 95,000 local school board members in nearly 15,000 local school districts serving more than 47 million public school students, and AAAS, the world's largest general scientific society and a global leader in science education. Other participants include AAAS's Education and Human Resources division, Project 2061, AAAS's science literacy initiative, and the International Technology Education Association.

"Our partnership with the NSBA is very exciting," said Connie Bertka, who oversees the project for AAAS as director of the association's Program of Dialogue on Science, Ethics, and Religion (DoSER). "The scientific community will now have an opportunity to discover firsthand what the needs and concerns of school board members are around science, math, and technology education. We can work collaboratively with school board leadership to respond to those needs."

"We have been working for the past 40 years to help school board members to recognize that student achievement is the top priority for school boards ... that's what they should focus on," added Joseph S. Villani, NSBA's deputy executive director. "Content expertise with science, math, and technology is something that we don't have a lot of experience with, and that's the value of working with AAAS."

AAAS initially had considered engaging with school boards about the issue of teaching evolution in schools. But in discussions with NSBA and other experts, the need emerged for a broader initiative, said Peyton West, a senior program associate with DoSER. The project is funded by a new $739,000 grant from the Kansas City–based Kauffman Foundation, which works to advance entrepreneurship and improve the education of children and youth.

The Foundation "recognizes the critical role that local school boards play in improving mathematics, science, and technology education through the decisions they make regarding funding, curriculum, and facilities," said Dennis Cheek, its vice president for education. "This grant will provide local school boards with high-quality, appropriate tools and information that can inform their local decisions to significantly improve programs ... at all levels of pre-K-12 education."

Erin Adams, a 10-year veteran of the school board in Minnetonka, Minnesota, said that the project could engage entire communities.

"The ultimate value of a project like this would be to give board members ... who are often not experts in these fields, and don't have the level of education that the students these days need ... a resource pool and training so that we can advocate these goals for our communities," Adams said. "If we have a more consistent, recommended policy, a definition of [illegible] mathematically and scientifically literate in the 21st century, we can achieve that vision."

AAAS

Regional Divisions Help Carry AAAS to the Grassroots

This September, before winter settles in, hundreds of scientists from Alaska, Canada, and other polar regions will travel to Anchorage for the 58th AAAS Arctic Science Conference. It won't be as big as the AAAS Annual Meeting, but the conference and the scientists who will attend it play a vital role in expanding the association's knowledge and extending its impact on polar science and policy issues.

AAAS's three other regional divisions—the Pacific, Caribbean, and the Southwestern and Rocky Mountain divisions—also are closely focused on environmental issues. They are engaging scientists and helping inform local policy-makers and the public not only about climate and sustainability, but also a range of issues that are priorities for AAAS and the world scientific community.

"For decades, our regional divisions have been doing important work for AAAS, with a great deal of energy but usually without a lot of fanfare," said AAAS CEO Alan I. Leshner. "They provide a forum for scientists in their regions. They engage with teachers, students, and the public, including many minorities and indigenous people. They help to carry the themes we set each year at the AAAS Annual Meeting to the grassroots, and that's very helpful to the scientific enterprise."

At Pacific Division's 88th Annual Meeting from 17 to 21 June, the theme will be "Science for a Green Future," said Executive Director Roger G. Christianson, professor of biology at Southern Oregon University. Among the featured programs will be symposia on "green cities," wilderness protection, and 150 years of human impact on the West's "sagebrush steppe."

The Southwestern and Rocky Mountain (SWARM) Division of AAAS held its 82nd Annual Meeting in Houston from 18 to 21 April, opening with a symposium on energy research and development; the closing symposia were on the teaching of evolution in public schools and stem cell research. SWARM Executive Director David T. Nash said that sessions on climate and sustainability are under consideration for the 2008 division meeting.

The Caribbean Division has cosponsored an exchange program involving environmental education teachers from Puerto Rico and Wisconsin. Like meetings in years past, this year's meeting — on 20 October in Puerto Rico — will feature environmental themes, said division President Margarita Irizarry-Ramírez, a researcher at the University of Puerto Rico Medical Sciences Campus.

The Arctic Division, founded in 1951 (as the Alaska Division), has emerged as a key forum on a range of polar environmental issues, including climate change. Its Arctic Science Conference in September will focus on the International Polar Year (IPY), a global scientific program that runs from March 2007 to March 2009.

Arctic Division President John Kelley, a professor of marine science at the University of Alaska Fairbanks (UAF), served on the National Academies of Science Planning Committee for U.S. participation in the IPY. "The IPY and the membership of the AAAS Arctic Division will have an opportunity to leave a legacy brought about by the presentation of results of international collaborative science and engineering through the publication of the proceedings of the Arctic Science Conference," Kelley said.

Arctic Division Executive Director Lawrence K. Duffy, professor of chemistry and biochemistry at UAF, noted that the annual AAAS Arctic conference also is an important forum for young scientists and science students.

"Learning about the role polar regions play in global climate processes and the resilience of Arctic peoples will inspire the next generation of scientists, science educators and policy leaders," Duffy said.

AAAS members who live or work within one of the regional divisions are automatically considered division members. To learn more about the regional divisions, visit www.aaas.org/go/divisions.

PROJECT 2061

New Atlas Maps Out Routes to Science Literacy

At this month's meeting of the National Science Teachers Association in St. Louis, AAAS's science literacy initiative Project 2061 released the second volume of its groundbreaking *Atlas of Science Literacy*. Like its 2001 companion *Atlas 1*, the new book is a collection of "roadmaps" that can help teachers build science literacy from kindergarten through the 12th grade.

The atlas debuts as new federal science learning standards are taking root in American classrooms. Beginning with the 2007–2008 school year, the U.S. No Child Left Behind Act requires science testing at least once in each of three grade spans: 3 to 5, 6 to 9, and 10 to 12.

Teachers may need to adjust when they teach certain topics to prepare their students for the new testing schedule, according to Elizabeth Petersen, a middle school science teacher in Ladue, Missouri, and past president of the Science Teachers of Missouri. The *Atlas* is "an enormously powerful tool to help teachers choose the most important science concepts at each stage," Petersen said. "The maps also underscore the fact that teachers at every grade level have such an important role to play in promoting science literacy."

Maps in the two-volume *Atlas of Science Literacy* connect the K–12 science learning goals recommended in Project 2061's respected *Science for All Americans* and *Benchmarks for Science Literacy*. Volume 2 contains maps for 44 new topics, including weather and climate, computation and estimation, and health technology.

"The maps chart the ideas and skills that students are expected to learn, when they might be able to learn them, and how the set of ideas and skills fit together to support science literacy," explained Jo Ellen Roseman, director of Project 2061.

St. Louis–area K–12 teachers who took part in an Earth Systems class praised the *Atlas* map format, according to course instructor Sharon Kassing of the St. Louis Zoo and the Center for Inquiry in Science Teaching and Learning. "They really liked the *Atlas* maps," she reported. "The way the information is arranged, and the notations about how and when related topics can be addressed with students were popular features among the teachers."

A preview of the new *Atlas* and information on ordering the volume is available at www.project2061.org. Project 2061's *Benchmarks of Science Literacy* and *Science for All Americans* are now freely available there, too.

SCIENCE CAREERS

Tap into Federal Funds with GrantsNet 2.0

Researchers can now use the ScienceCareers.org GrantsNet site to find U.S. government grant announcements, significantly expanding the funding opportunities available to GrantsNet visitors.

The new announcements, directly imported from the federal Grants.gov database, should increase the number of "live" grants on the site from 900 to 1400 by the end of the year, according to Alan Kotok, ScienceCareers managing editor. Many of these new grants are in the physical sciences, social sciences, and engineering — a change from GrantsNet's original focus on biomedical and life sciences.

Along with the site's extensive database of nongovernmental grants, the new GrantsNet "gives researchers and administrators a single location to find funding from all sources, with obvious savings in time and energy," Kotok said, noting that the number of visitors to the funding section of ScienceCareers is up 39% from this time last year.

The revamped database is only part of the site's transformation to "GrantsNet 2.0." The site also offers two new monthly RSS feeds that will alert users directly about new research funding and student and institutional support. But one thing hasn't changed: GrantsNet is still free of charge and requires no registration to use. To test-drive GrantsNet 2.0, visit http://sciencecareers.sciencemag.org/funding.

—Becky Ham

The Problem with Determining Atomic Structure at the Nanoscale

Simon J. L. Billinge[1*] and Igor Levin[2]

Emerging complex functional materials often have atomic order limited to the nanoscale. Examples include nanoparticles, species encapsulated in mesoporous hosts, and bulk crystals with intrinsic nanoscale order. The powerful methods that we have for solving the atomic structure of bulk crystals fail for such materials. Currently, no broadly applicable, quantitative, and robust methods exist to replace crystallography at the nanoscale. We provide an overview of various classes of nanostructured materials and review the methods that are currently used to study their structure. We suggest that successful solutions to these nanostructure problems will involve interactions among researchers from materials science, physics, chemistry, computer science, and applied mathematics, working within a "complex modeling" paradigm that combines theory and experiment in a self-consistent computational framework.

The "structure problem" can be stated simply as follows: Given a new material, what is the atomic arrangement inside it? Having this knowledge is a prerequisite to a clear theoretical understanding of the material's properties. In the case of crystals, there are robust and quantitative solutions to this problem, as far as the average atomic positions are concerned. In many cases, it is possible to put a crystal on a computer-controlled x-ray diffractometer (XRD) and have the computer retrieve the structure. This is not so for nanostructured materials, such as nanoparticles, mesoporous materials, and bulk crystals with short-range structural fluctuations. What emerges from the XRD when a sample of nanoparticles, for example, is loaded is not a structural model but a broad and continuous intensity distribution that is not amenable to a crystallographic structure solution. The need to determine atomic arrangements in nanostructured materials, quantitatively and with high precision, is what we call the "nanostructure problem." A number of powerful probes exist for studying local and nanoscale structures, but in general we have no widely applicable solution to the nanostructure problem.

Solving the crystal structure problem was far from trivial, the history of which is dotted with Nobel prizes. The reason is the "phase problem": the inherent loss of information that occurs when scattered intensities are measured. The challenge is to reconstruct the lost phase information from the intensity data. In most cases, this is done by solving a large, nonlinear, global optimization problem, where the degrees of freedom are the unknown phases, or atomic coordinates, and where the constraints come from the data (Bragg peak positions and intensities). Such a problem is solvable in principle if there are more constraints than degrees of freedom and solvable in practice if this condition is matched with suitable algorithms. Crystal structure problems are usually well conditioned because thousands of Bragg peaks are measured to determine hundreds of atomic positions in the unit cell (in the case of protein crystallography, these numbers are larger), and the existing algorithms work well.

This global optimization approach is completely generic and presents to us a road map for solving the nanostructure problem. First, we need to ensure that the particular nanostructure problem is well conditioned: We have more constraints from data, and other prior knowledge, than degrees of freedom in our model. Second, we need algorithms that can reconstruct the three-dimensional (3D) structure from the information at hand. In the case of nanostructures, both aspects present substantial challenges.

Many techniques exist for probing nanostructured materials. Some are inherently local, such as transmission electron microscopy (TEM) and scanning probe microscopies. Others are bulk average probes that are sensitive to local structure, such as the atomic pair distribution function (PDF) method or extended x-ray absorption fine structure (EXAFS) analysis. The principal difficulty with the application of these methods to solving the nanostructure problem is that, in general, any one technique does not contain sufficient information to constrain a unique structural solution. A coherent strategy is required for combining input from multiple experimental methods and theory in a self-consistent global optimization scheme, something that we refer to as "complex modeling."

Types of Nanostructure

Many crystals are now being made and studied that have local atomic arrangements substantially different from those inferred from the crystallographs (1). We refer to these as nanostructured bulk materials, and an example is shown in Fig. 1A. In these materials, domains of local structural order exist whose correlations extend over nanometer-length scales without destroying the average lattice. There is a growing realization that this behavior is not rare but widespread and can be extremely useful. For example, the most desirable ferroelectrics for transducers are relaxors with polar nanodomains (2); the most promising bulk thermoelectrics have nanoscale phase separations perfectly tuned to scatter heat-conducting long-wavelength phonons (3, 4); and nanoscale phase separation, possibly an intrinsic property of the electronic system, is thought to be essential for obtaining colossal responses in advanced electronic materials such as colossal magnetoresistant (CMR) manganites and high-temperature superconductors (5).

By definition, soft materials produce a large response to a mechanical load. The emerging nanostructured bulk materials can be thought of as hard materials that are electronically or magnetically (or in some other regard) soft. They are formed by nanoscale domains of order that can be easily flipped or switched, producing a large response (5). Because the structure is scale-dependent, the response also depends on the length and time scales of the probing excitation. Understanding the formation of nanostructures in (and their effects on the properties of) these materials is a complex problem because the different scales cannot necessarily be considered independently from each other. Multiscale modeling is a major frontier in computational materials science (6). The same could be said for multiscale studies in the experimental materials domain.

Mesoporous materials, illustrated in Fig. 1B, are bulk materials that contain porosity with nanometer-scale dimensions. They have a wide range of uses, including catalysis, chemical separation, waste remediation, hosts for hydrogen storage, passivation of reactive species, as well as hitherto unforeseen applications. Just about every bulk material is a candidate for being manufactured in mesoporous form, but most progress has been made in covalent network systems such as aluminosilicates (7), carbon (8), and silicon (9). Attention has recently been focused toward making narrow band gap semiconducting materials in the mesoporous form (10). The internal pores of these materials can also be functionalized with molecules to modify their reactive properties.

Structural questions are twofold in these systems: What is the structure of the framework, and what is the structure of species intercalated inside the pores? These are also multiscale problems. The performance of the material is not only sensitive to pore sizes (1 to 100 nm) and connectivity, but also to access to the pore network that depends on particle size (1 to 100 μm) and morphology. Except in the minority of crystalline

[1]Department of Physics and Astronomy, Michigan State University, East Lansing, MI 48824, USA. [2]Ceramics Division, National Institute of Standards and Technology, Gaithersburg, MD 20899–1070, USA.

*To whom correspondence should be addressed. E-mail: billinge@pa.msu.edu

cases, such as the zeolites, noncrystalline methods are needed. In general, the intercalated species are not arranged periodically in space, so noncrystallographic nanostructure methods are required to solve their structure.

Starting in the late 1980s, chemists began synthesizing nanoparticles, nanometer-scale crystals of semiconducting and metallic materials (Fig. 1C) (11). The synthetic ingenuity has developed rapidly, so that there is now enormous control and breadth of composition, size, shape, polydispersity, and self-assembly. Some nanoparticles even have their own substructure. Nanoparticles have already found application, for example, as nonquenching fluorescent tags for biological molecules. Assemblies of nanoparticles offer an entirely new and hardly explored frontier for applications.

The physical properties of the nanoparticles are modified as a result of their finite size that modifies the electronic structure through quantum confinement (11). However, equally important is the modification of the local atomic structure resulting from a substantial proportion of the sample being associated with a surface. The surface itself relaxes, but the presence of surfaces can also modify the "bulk" structure and the presence of stable extended defects (12). The nanoparticle structure can also depend on the chemical environment in which the nanoparticle resides and the nature of the passivating surfactant layers (13). However, because of the nanostructure problem, most structural studies have been semiquantitative at best and often rely on extrapolations from the bulk material. When considering discrete nanoparticles, it is also important to consider the true nature of the material and to formulate the pertinent structural question; for example, is the sample an ensemble of identical particles, a statistical distribution of similar particles, or a single nanoparticle in a device?

Experimental Methods for Nanostructure Elucidation

Experimental probes of nanoscale structure fall into a number of categories. Such probes can yield direct or indirect information about the atomic arrangement. XRD is an example of the former and Raman spectroscopy the latter. They can be methods that probe small, nanometer- to micrometer-sized regions of samples or bulk average probes of local structure. In general, methods from different categories provide highly complementary information and are much more powerful when used together. In Table 1, we list and categorize the different techniques described below.

One standard approach to crystal structure solution involves reconstructing the phase, as well as the known intensity, of each Bragg reflection. Lost phase information can also be reconstructed from nonperiodic systems in a process known as diffraction imaging (14, 15). The experimental requirement is a highly coherent x-ray beam with a cross-sectional area that is more than two times that of the nanoparticle under study. The nanoparticle or particles are mounted on a nonscattering (or weakly scattering) support. Powerful algorithms exist for reconstructing the lost phase information when the area illuminated by the coherent beam is more than twice that of the nanoparticle. This allows for a direct Fourier transform to reveal the density distribution, which is an image of the sample (16). The first successful experimental demonstration used soft x-rays to image 100-nm-diameter gold spheres arranged as letters (17). Currently, these techniques have not demonstrated atomic-scale resolution from x-ray measurements and show more promise in the short term as a nanoscale imaging method. In principle, with a probe of sufficiently short wavelength, individual atoms could be imaged, and this approach could be used for structure determination. Atoms on a carbon nanotube have already been imaged in this way by means of electron diffraction (18).

Nanostructures can also be solved from conventional diffraction data by computer modeling. For some time, it has been possible to extract nanoscale structure with the use of total scattering data that includes both Bragg (where it is present) and diffuse scattering intensities (6, 19). Such data yield the local and intermediate range structure and are often probed by Fourier-transforming to real space, yielding the atomic PDF (19). This function gives a measure of the probability of finding pairs of atoms separated by some distance. For example, a strong peak in the PDF can be seen at the nearest-neighbor distance between atoms, another at the second neighbor, and so on. Where a well-defined structure exists, peaks are observed at intermediate and long ranges, beyond 30 nm in some cases.

Total scattering data are rich in nanoscale structural information. The scattering pattern in reciprocal space and the PDF in real space are readily calculated from a model atomic configuration. The model can then be updated by moving atoms (or other parameters) until a good agreement is obtained between the calculated and measured patterns, a process called structure refinement. The diffuse scattering from nanostructured regions of single crystals can be studied with x-rays and neutrons (20); however, quantitative analysis of the data is a challenging computational problem that is under active development. Greater progress has been made with modeling the isotropic scattering from powders. When the analysis is carried out in reciprocal space, the model often consists of many atoms that are moved around with the use of a simulated annealing approach known as reverse Monte Carlo (21). This approach is widely used for extracting structural configurations from more highly disordered materials, such as glasses and liquids, with little a priori knowledge of the structure. Disorder in crystals is frequently modeled in real space in an approach that is similar to Rietveld refinement of regular powder x-ray or neutron diffraction data (22) but which yields the local structure because it is the PDF that is being fit (23, 24). The optimization method can be a local downhill-search method (24), such as Newton or Levenberg-Marquardt, or a global search method, such as Monte Carlo (25); the

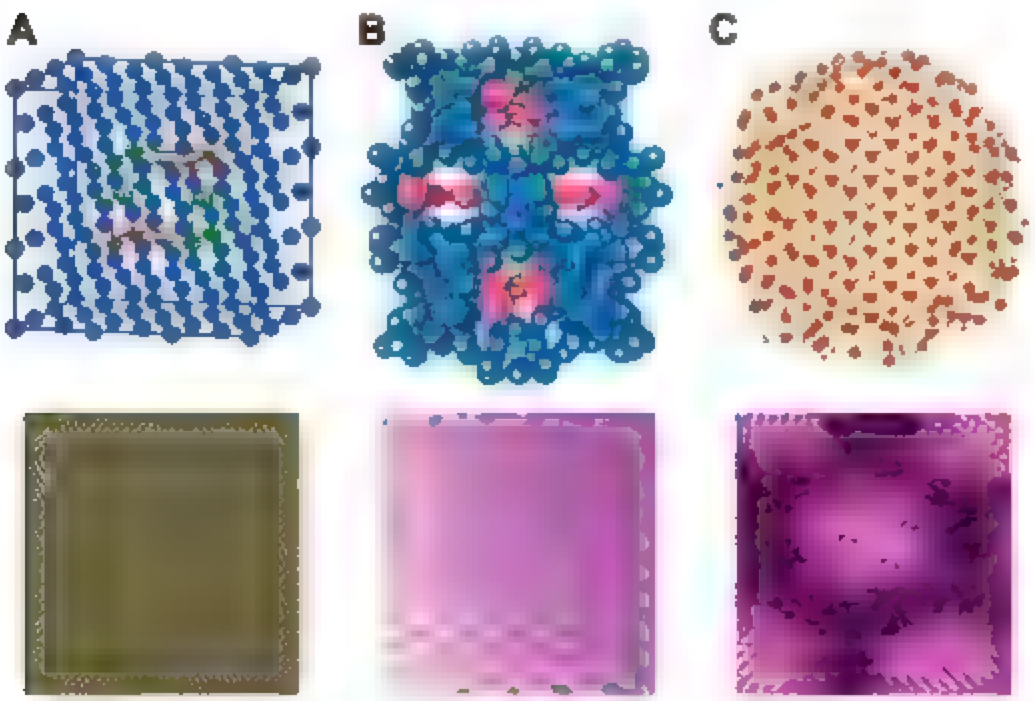

Fig. 1. Examples of nanostructured materials. **(A)** Nanostructured bulk materials. **(B)** Intercalated mesoporous materials. **(C)** Discrete nanoparticles. In each case, ball-and-stick renditions of possible structures are shown on the top, and TEM images of examples are shown on the bottom. Ball-and-stick images were reproduced with permission [in (A) and (B) from the American Physical Society [from (52) and (53), respectively] and in (C) [from (23)]].

former being much faster but requiring the initial guess to be rather close to the actual solution. There is sometimes benefit to fitting jointly in real and reciprocal space (25).

None of the above approaches allows for the ab initio solution of unknown nanoparticle structures from well-ordered nanoparticles (i.e., the case where a specific solution exists). However, by means of a recently developed algorithm, the 3D structure of C_{60} was determined from PDF data alone (26). In this case, the information content of the data (18 distinct atom-pair distances and their multiplicities) was enough to give a unique 3D reconstruction of the 60-atom buckyball, as illustrated in Fig. 2. The case of C_{60} proved to be well conditioned, though it was not obvious a priori that this would be the case. In general, total PDF data will have to be augmented with information from other sources such as EXAFS, nuclear magnetic resonance (NMR), TEM, or chemically resolved PDFs obtained from differential measurements making use of the different scattering strengths of isotopes (neutrons) or resonantly scattering elements (x-rays). The local structural methods described here are beginning to be applied to study excited-state structures of materials with the use of time-resolved pump-probe experiments (27, 28). Developments in nanostructure determination can therefore be quickly extended to excited-state structures in the future.

X-ray and neutron small-angle scattering, nanoscale tomographic imaging, and reflectivity measurements are widely used to study nanostructured systems. They do not yield atomic-resolution information but provide important ancillary data (for example, about the homogeneity of the sample) that will be important in constraining the proper atomic-scale structural solution. Similar highly complementary 3D information about materials with atomic resolution and chemical specificity but not quantitative bond-length information, is also available by means of the destructive atom probe tomographic technique (29).

EXAFS is a bulk probe that carries information about near-neighbor distance distributions, coordination numbers, and, less directly, bond angles. EXAFS probes only the first few coordination shells and therefore does not reveal nanometer-scale structure. However, it contains crucial chemical-specific local structural information and is sensitive to dilute species. Thus, it is a natural complement to the nanoscale, but chemically unresolved, PDF data. EXAFS is a widely applied local structural technique. Simultaneous quantitative analysis of diffraction and EXAFS data sets, currently rather rare (30), will certainly grow in importance in the future.

X-ray absorption near-edge structure (XANES) also reveals information on interatomic distances and coordination numbers but is substantially more sensitive to bond angles than EXAFS. XANES commonly serves as a fingerprint for the coordination type and oxidation state of a given chemical species, but it can also provide such structural details as the magnitudes of local metal displacements and chemical short-range order parameters (31) in transition metal oxides. Unlike EXAFS, the agreement between calculated and experimental XANES in many cases is still only semiquantitative, though the theory is rapidly developing (32). Full quantitative fitting will allow direct incorporation of this important information into nanostructure problems.

Raman spectroscopy in solids exploits the inelastic scattering of light by optical phonons. As such, it is an indirect probe of structure; however, Raman spectra are extremely sensitive to local deviations from the average periodicity, making this a valuable probe of local structure. Interpretation of Raman spectra requires accurate assignment of Raman peaks to specific vibrations from an independent preknowledge of the structure. Although group theoretical analyses provide insight into the nature of Raman-active modes, first-principles calculations are essential for a reliable peak assignment. First-principles calculations of Raman intensities are feasible (33) but still scarce, even for ideal crystals. Currently, Raman spectra serve as fingerprints for phase identification in nanostructures, providing important constraints for the correct structural model. Considering the broad availability of Raman spectroscopy and its sensitivity to local structural details, this technique has a potential to become a standard laboratory tool for rapid local structure analysis. Full access to the rich local structural information contained in Raman spectra necessitates development of theoretical models and efficient computer algorithms in systems that are distorted from the ideal structure.

Solid-state NMR (34) and related techniques, such as Mossbauer and muon spectroscopies, are other spectroscopic methods that are sensitive to local structure. They yield information about the local symmetry and coordination of the probe atom or site and can also be valuable for establishing and quantifying phase separation where it exists.

Advanced TEMs provide a multitude of complementary diffraction, imaging, and spectroscopic techniques—all available in a single instrument—that enable quantitative, atomically resolved, structural and chemical information over scales ranging from a micrometer to an angstrom. Real-space structural imaging from thin sections of material in high-resolution TEM (HRTEM) and scanning TEM (STEM) modes provides information on the nature of nanocrystals and nanostructures in bulk materials. Diffraction patterns are also available from these small areas.

The dynamical nature of the electron scattering means that HRTEM images contain all the phase information as well as the amplitudes of diffracted beams, which should facilitate ab initio crystal structure determination; however, the image contrast also depends on nonstructural factors such as sample thickness, lens aberrations, and imaging conditions. Only for sufficiently thin samples, as encountered in the studies of nanoparticles, can Fourier restorations of the electron wave at the exit surface of a sample enable direct interpretation of phase contrast in terms of the crystal potential. The power of this approach is highlighted in determinations of the chirality of single-walled carbon nanotubes (SWNTs) (35) and atomic arrangements in 1D semiconductor crystals (36). The phase information contained in HRTEM images can be combined with the amplitude information from electron diffraction patterns to solve the structure in a manner similar to the direct methods of x-ray crystallography (37). Despite considerable promise, ab initio solutions of the nanostructure problem with the use of HRTEM and electron crystallography are far from routine, and atomic arrangements are more commonly found by matching a computed phase contrast for a trial structure to the experimental images.

Table 1. Experimental probes of nanoscale structure categorized as direct versus indirect measures of structure and whether they probe the whole sample (bulk probe) or a small part of it (local probe).

Probe	Direct (D)/indirect (I) measures	Bulk (B)/local (L) probes
Total scattering/PDF	D	B
Diffuse scattering from single crystals	D	B
EXAFS	D	B
XANES	I	B
Raman spectroscopy	I	B
NMR/Mossbauer/μSR	I	B
Small-angle scattering*	I	B
Tomographic imaging*	I	B
Diffraction imaging	D	L
TEM/electron diffraction	D	L
Atom probe tomography	D	L
STM/AFM	I	L
X-ray/neutron reflectivity*†	I	L

*A direct measure of structure at low resolution that gives information that could be used indirectly in a nanostructure solution. †Local in the sense that it only probes surfaces and interfaces.

Annular dark-field STEM images, recorded by means of electrons scattered to large angles, exhibit a so-called Z contrast with the image intensity being approximately proportional to the atomic number, Z, squared. Atomic-resolution Z-contrast images carry both structural and chemical information that, in many cases, can be inferred directly from the image without computer simulations. Z-contrast imaging is often combined with electron energy-loss spectroscopy (EELS)—a technique analogous to soft x-ray absorption spectroscopy—to obtain additional element-specific chemical and structural information on the atomic scale. The Z-contrast EELS combination is particularly useful for determination of nanoscale chemical and charge ordering (38) and the location of dopant atoms (39). Recent dramatic advances in TEM instrumentation in the form of lens spherical-aberration correctors substantially improve the merits of both HRTEM- and STEM-based techniques for determination of local atomic arrangements, subject to sample limitations and radiation damage. Direct HRTEM imaging of nanoclusters (40), a 3D-like HRTEM imaging of SWNTs (41), and depth-resolved STEM imaging of a single dopant atom (42) are just a few examples that illustrate the potential contributions of aberration-corrected TEM to solutions of nanostructure problems.

Electron diffraction is a highly sensitive tool for the detection of diffuse intensity (43) because electrons are scattered by matter 1000 to 10,000 times more strongly than x-rays or neutrons. As with x-rays, the diffuse intensity encodes nanoscale structural information that can, in principle, be modeled to yield nanostructure, though fully quantitative analysis of the data is difficult. Precession methods that make the electron scattering more kinematical in nature (44) would help to make these analyses more quantitative, though this kind of analysis is in a fledgling state. Electron nanodiffraction in a STEM mode also contains structural information from nanometer-sized regions and can be used directly (45), or combined with STEM imaging in hybrid methods such as fluctuation microscopy (46), to determine medium-range structural correlations. As with the x-ray case, time-resolved measurements of excited-state structures are also possible with electrons and are especially apropos for nanoparticles (47).

In the world of nanostructures, TEM-based methods are positioned to play a critical role by providing single-crystal structural models that can be used in subsequent refinements by means of powder scattering and spectroscopic tools. Simultaneous quantitative analyses of TEM and other types of structural data (e.g., PDF and EXAFS) should greatly facilitate the determination of local atomic arrangements but will require the development of suitable computer software.

Surface imaging probes, such as scanning tunneling microscopy (STM) and atomic force microscopy (AFM), also provide valuable nanoscale information. They often have atomic resolution and can also give spectroscopic information on the nanoscale (48). Nanoscale-resolution x-ray imaging probes are under development that will give bulk projections and, combined with tomographic methods, will yield 3D reconstructions of nanostructures. These methods reach similar dimensions as diffraction-based lensless imaging techniques described above and currently have similar resolutions. X-ray imaging probes do not have atomic resolution, but combining the information with other atomic-resolution data is a powerful way to extract complex multiscale structures. Knowing the nanoscale morphology of the material can act as a constraint for other higher-resolution probes. In exceptional cases, it may be possible to get a multiscale structure solution by this approach, as has been demonstrated in the solution of virus structures by combining low-resolution cryogenic electron microscopy (cryo-EM) images with atomic-resolution structures of the individual proteins making up the viral capsid (49). A distribution of discrete but identical viral capsids that are frozen on a substrate in random orientations is imaged in the microscope, and software is used to reconstruct the low-resolution structure of a representative capsid. If the structure of the individual proteins making up the capsid has been solved by means of protein crystallography, then those protein structures can be superimposed on the low-resolution electron density map from the cryo-EM to give a more complete solution.

The Future: Complex Modeling

The complex nature of the nanostructure problem means that the solution will require a coordinated response from researchers with a broad range of scientific expertise. This currently happens but in an incoherent way. Multiple groups work independently on the same problem and interact through the literature and conferences. Coherence requires that experimental data are collected, to the extent possible, on the same or same-batch samples, and the data are shared in a common computational global optimization framework. The distinction between theory (predicting outcomes) and experiment (measuring outcomes) becomes blurred because both contribute to our state of knowledge of the system and can be used to regularize the problem. For example, theory can inform us of the presence of physically unreasonable structural solutions that are, nonetheless, consistent with data in an otherwise underconstrained situation. In principle, theoretical calculations can be included in the regression cycle, where approximations in the model are considered as degrees of freedom. Direct energy minimizations and data fitting in the form of χ^2 minimizations can be combined in the global optimization framework. This concept is not new: In crystallography, theoretical constraints (such as positivity of intensities) and prior knowledge from other methods (such as the amino acid sequence of a protein) are crucial in finding structural solutions. However, despite some initial efforts (50, 51), the approach is not being systematically exploited in materials science. Great strides toward more robust and widely applicable quantitative solutions to the nanostructure problem will be made as we learn how to combine the results of experimental methods and theory more effectively.

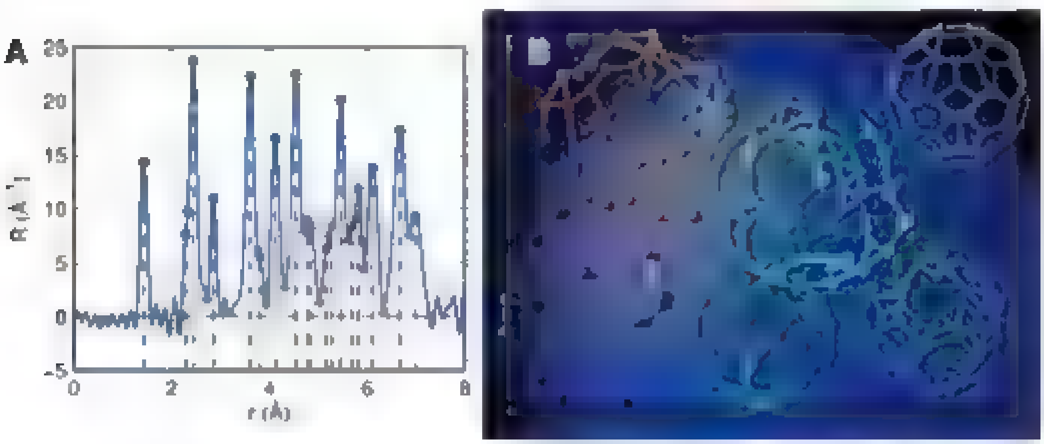

Fig. 2. Example of ab initio nanostructure determination with the use of PDF data and the "Liga" algorithm (26). (**A**) The PDF data are used to extract interatomic distances and multiplicities. This information is used by the algorithm to build up clusters that are consistent with that information, to backtrack by removing atoms in poorly performing clusters, and then to rebuild until a good solution is found. R is the radial distribution function, and r the interatomic distance. Black asterisks indicate the positions of PDF peak maxima and shoulders used to determine interatomic distances present (shown as dashed lines). Red and green triangles indicate the integration limits used to determine peak intensities and therefore multiplicities of those distances. The procedure is illustrated in (**B**) where a number of intermediate clusters are shown on the way to a successful reconstruction of C_{60} (top right corner). The colors of the spheres indicate the amount of error contributed to the atom at that position; it is a continuous color scale from dark blue (low error) to dark red (high error). Images were reproduced with permission [from (26)].

References and Notes

1. S. J. L. Billinge, M. G. Kanatzidis, *Chem. Commun.* **2004**, 749 (2004).
2. L. E. Cross, *Ferroelectrics* **76**, 241 (1987).
3. K. F. Hsu *et al.*, *Science* **303**, 818 (2004).
4. W. Kim *et al.*, *Phys. Rev. Lett.* **96**, 045901 (2006).
5. E. Dagotto, *Science* **309**, 257 (2005).

Fast Routing in Road Networks with Transit Nodes

Holger Bast,[1] Stefan Funke,[1] Peter Sanders,[2*] Dominik Schultes[2]

Computing the quickest route in a road network between a given source and a given target is an important problem used in diverse applications, such as car navigation systems, Internet route planners, traffic simulation, or logistics optimization. Dijkstra's classical algorithm for this problem (*1*) iteratively visits all nodes that are closer to the source than the target before reaching the target. On road networks for a subcontinent like Western Europe or the United States, this takes about 10 s on a workstation, which is too slow for many applications. Commercial systems instead use heuristics that are much faster but that do not guarantee optimal routes. There has been considerable interest in faster techniques for computing exact routes. The Supporting Online Material (SOM) text summarizes previous techniques. These use special properties of road networks and often precompute some connections.

Our approach, transit node routing, has its basis in a simple observation intuitively used by humans. When you drive to somewhere far away, you will leave your current location via one of only a few access routes to a relatively small set of transit nodes interconnected by a sparse network relevant for long-distance travel. We therefore precomputed the following connections: from each potential source or target to its access transit nodes and between all pairs of transit nodes. We also needed an effective notion of "far away." A locality filter determines when the precomputed information guarantees optimal results. Figure 1 gives an example.

For an efficient implementation, we adapted highway hierarchies, the fastest previous approach (*2*). A highway hierarchy consists of a sequence of levels, where level $\ell + 1$ is constructed from level ℓ by bypassing low-degree nodes and removing edges that never appear far away from the source or target of a quickest path. Interestingly, these levels are geometrically decreasing in size and otherwise similar to each other. Connection queries can be computed efficiently because, sufficiently far away from source and target, only high levels of the hierarchy need to be considered. The nodes of the highest level become the transit node set. For a commercial directed road network for Western Europe (results for North America are similar) with 18,010,173 nodes, we got 11,293 transit nodes, an average of 9.9 access transit nodes, and a locality filter allowing us to treat 98.7% of all queries by using a few table lookups (*3*).

We were not done yet because the remaining 1.3% of local queries are also important in applications. Therefore, we introduced an additional layer of secondary transit nodes. Because the secondary distance table only needs to store regional connections not covered by the primary layer, memory consumption remains reasonable: although in our example graph we have 323,356 secondary transit nodes. After applying a third layer with 2,954,721 tertiary transit nodes, the remaining local searches involve only a handful of nodes. We obtained query times between 5 μs for global queries and 20 μs for local queries (fig. S1). The precomputation needs less than 3 hours overall, and the precomputed information consumes 4.5 gigabytes. We also have versions with considerably lower space consumption at the cost of more expensive queries.

References and Notes

1. E. W. Dijkstra, *Numer. Math.* 1, 269 (1959).
2. P. Sanders, D. Schultes, in *Algorithms: ESA 2006*: 14th European Symposium on Algorithms (ESA), Zurich, Switzerland, 11 to 13 September 2006 (vol. 4168 of *Lecture Notes in Computer Science*, Springer, Berlin, 2006), pp. 804–816.
3. More details can be found at http://algo2.iti.uka.de/schultes/hwy.

4. This work was partially supported by Deutsche Forschungsgemeinschaft grant SA 933/1-3.

Supporting Online Material

www.sciencemag.org/cgi/content/full/316/5824/566/DC1
SOM Text
Fig. S1
References

13 November 2006; accepted 12 January 2007
10.1126/science.1137571

[1]Max-Planck-Institut für Informatik, 66123 Saarbrücken, Germany. [2]Universität Karlsruhe (TH), 76128 Karlsruhe, Germany.

*To whom correspondence should be addressed. E-mail: sanders@ira.uka.de

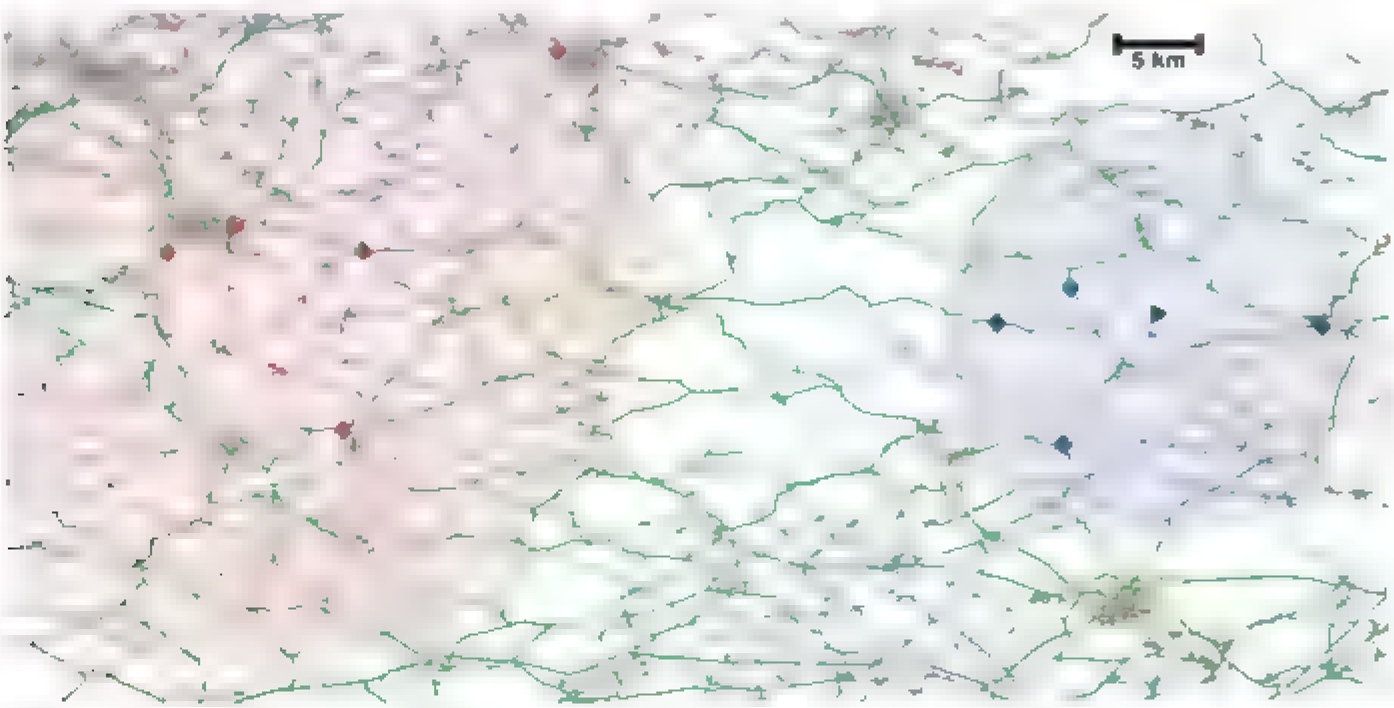

Fig. 1. Finding the quickest route between two points somewhere between Saarbrücken and Karlsruhe (triangle-shaped flags), Germany, amounts to retrieving the 2-by-4 access transit nodes (diamonds), performing 16 table lookups between all pairs of these nodes, and checking that the two disks defining the locality filter do not overlap. The levels of the highway hierarchy are drawn by using the colors gray, red, blue, and green for levels 0-1, 2, 3, and 4, respectively. The other transit nodes are drawn as small yellow squares.

Revisiting Carbon Flux Through the Ocean's Twilight Zone

Ken O. Buesseler,[1*] Carl H. Lamborg,[1] Philip W. Boyd,[2] Phoebe J. Lam,[1] Thomas W. Trull,[3] Robert R. Bidigare,[4] James K. B. Bishop,[5,6] Karen L. Casciotti,[1] Frank Dehairs,[7] Marc Elskens,[7] Makio Honda,[8] David M. Karl,[4] David A. Siegel,[9] Mary W. Silver,[10] Deborah K. Steinberg,[11] Jim Valdes,[12] Benjamin Van Mooy,[1] Stephanie Wilson[11]

The oceanic biological pump drives sequestration of carbon dioxide in the deep sea via sinking particles. Rapid biological consumption and remineralization of carbon in the "twilight zone" (depths between the euphotic zone and 1000 meters) reduce the efficiency of sequestration. By using neutrally buoyant sediment traps to sample this chronically understudied realm, we measured a transfer efficiency of sinking particulate organic carbon between 150 and 500 meters of 20 and 50% at two contrasting sites. This large variability in transfer efficiency is poorly represented in biogeochemical models. If applied globally, this is equivalent to a difference in carbon sequestration of more than 3 petagrams of carbon per year.

The transfer efficiency of the biological pump (1) depends upon how much sinking particulate organic carbon (POC) is remineralized and consumed by zooplankton and microbes within the ocean's twilight zone. This downward POC flux in the ocean comprises a complex mixture of living and dead cells, excretory products, detrital matter, and amorphous aggregates (2). Remineralization of POC and associated bioelements sets the concentration of deep ocean nutrients and via subsequent upwelling is a feedback on the strength of primary productivity. Since the 1980s there have been various attempts to parameterize this flux attenuation (3), the most common being $F = F_{100}(z/100)^{-b}$, where z is the trap depth, F_{100} is the POC flux at 100 m, and b is a unitless parameter determining the degree of flux attenuation with depth. A single empirical fit using six North Pacific sites yielded the Martin curve, with $F_{100} = 4.2$ mM C m^{-2} day^{-1} and $b = 0.86$ (4), which is still widely used in models to describe particle flux attenuation across regions and also globally (5–7).

In the past 10 to 20 years, concerns have grown over the validity of the Martin curve due in part to the possibility of collection biases in upper ocean sediment traps, which are open cylinders or cones tethered to surface floatation used to directly sample sinking particles (8). Moreover, flux predictions from global circulation and data assimilation models (9, 10) and measurements of flux variability in the deep ocean (11) have questioned the global applicability of this flux curve. Alternatives have since been proposed (11, 12), but their value is unclear because they have their basis largely in models and/or traps in the deep ocean, where flux collection biases are reduced but particle flux attenuation is much weaker (13).

VERTIGO (Vertical Transport in the Global Ocean). The VERTIGO project overcame many of the issues of trap collection biases in mesopelagic waters by using neutrally buoyant sediment traps (NBSTs) (14). These new-generation particle interceptors address the hydrodynamic concern of particle capture in a fluid moving several orders of magnitude faster laterally (km per day) than mean particle sinking rates (10 to 100 m day^{-1}) (2). NBSTs are free vehicles that sink to a predetermined depth, directly intercepting sinking particles in collection tubes for a preset period (days), after which the tubes close and the NBSTs surface (15) (figs. S1 and S2). We deployed NBSTs twice for 3 to 5 days using two to three instruments per depth (150 m for 3 days, 300 m for 4 days, and 500 m for 5 days). Such replication of flux measurements is rarely done. Another unique facet of VERTIGO was the 21-day occupation of each study site, which enabled us, with replicate deployments, to relate changes in flux at 500 m to processes in the surface water occurring several days prior [the majority of particles sink >100 m day^{-1} (16) and thus would reach 500 m within ~5 days].

VERTIGO studied two contrasting environments. ALOHA is within an oligotrophic subtropical gyre and is the site of the Hawaii Ocean time series (HOT) (17). At ALOHA, consistently low macronutrients within a warm surface ocean result in an ecosystem dominated by picophytoplankton and low seasonality, with relatively low and constant rates of primary production and POC flux at the base of the euphotic zone. K2 is situated in the Northwest Pacific subarctic gyre and is the site of a moored time-series program (18). K2 is characterized by cooler waters and high nutrient conditions, resulting in more seasonality in algal stocks, production, and export (18). Another important contrast is that the biomineral content of sinking particles at ALOHA was dominated by particulate inorganic carbon (PIC, i.e., carbonate; contents of 30% at 500 m and 60% at 4000 m, Table 1), whereas fluxes at K2 during summer were dominated by biogenic silica (bSi, i.e., opal) because of surface diatom productivity (80% at 500 and 4000 m).

K2 had higher POC fluxes than ALOHA at all depths (Fig. 1A). Fluxes at ALOHA were similar during both trap deployments, whereas at K2 POC flux decreased threefold between the two deployments, indicating substantial temporal phasing of export at this site. The normalized flux profiles display lower POC flux attenuation at K2 than at ALOHA (Fig. 1B). POC flux profiles from both K2 deployments collapse onto each other upon normalization to flux at 150 m (Fig. 1B), despite their difference in POC flux. This suggests that POC flux attenuation is not determined by the magnitude of flux but rather by the nature of the exported POC and the processes within the mesopelagic that are site specific. The degree of flux attenuation can be expressed as mesopelagic transfer efficiency (T_{eff}) or the ratio of POC flux at 500 to 150 m. At ALOHA, T_{eff} is only 20%, whereas for K2 T_{eff} equals 46 to 55% (Table 1).

This pattern of more rapid POC flux attenuation at ALOHA versus K2 holds for all associated bioelements and follows an internally consistent pattern (Fig. 2). At each site, attenuation follows the same relative order, with chlorophyll a > POC > particle mass > bSi > PIC, and tracks the lability of these elements, with chlorophyll flux decreasing fastest and much smaller losses of biominerals such as bSi and PIC as they sink. This implies that, for each component within the sinking particles, a larger proportion would sink to greater depth if associated with biomineral phases. All particle-associated elements reach greater depth at K2, which would enhance C sequestration at K2

[1]Department of Marine Chemistry and Geochemistry, Woods Hole Oceanographic Institution, Woods Hole, MA 02543, USA. [2]National Institute of Water and Atmospheric Research Centre for Physical and Chemical Oceanography, Department of Chemistry, University of Otago, Dunedin, New Zealand. [3]Antarctic Climate and Ecosystems Cooperative Research Centre, University of Tasmania and Commonwealth Scientific and Industrial Research Organisation, Marine and Atmospheric Research, Hobart, 7001, Australia. [4]Department of Oceanography, University of Hawaii, Honolulu, HI 96822, USA. [5]Earth Sciences Division, Lawrence Berkeley National Laboratory, Berkeley, CA 94720, USA. [6]Department of Earth and Planetary Science, University of California, Berkeley, CA 94720, USA. [7]Analytical and Environmental Chemistry, Free University of Brussels, B-1050 Brussels, Belgium. [8]Japan Agency for Marine-Earth Science and Technology (JAMSTEC), Mutsu Institute for Oceanography, Yokosuka, Kanagawa 237-0061, Japan. [9]Institute for Computational Earth System Science, University of California, Santa Barbara, CA 93106, USA. [10]Ocean Sciences Department, University of California, Santa Cruz, CA 95064, USA. [11]Virginia Institute of Marine Science, College of William and Mary, Gloucester Point, VA 23062, USA. [12]Department of Physical Oceanography, Woods Hole Oceanographic Institution, Woods Hole, MA 02543, USA.

*To whom correspondence should be addressed. E-mail: kbuesseler@whoi.edu

relative to ALOHA and consequently result in greater remineralization length scales at K2 for nutrients such as silicate.

The differences in particle flux attenuation between K2 and ALOHA must be related to the properties that characterize each site. These include pelagic food web structure, the proportion of fecal pellets versus phytoplankton aggregates, the fraction of export associated with ballast minerals and their sinking rates, water temperature, and C demand of the mesopelagic bacteria and zooplankton communities, or combinations thereof. Also, higher zooplankton abundances at K2 will have an impact on C transfer to depth via surface feeding and daily migration to mesopelagic depths.

Our observations demonstrate that the diatom-dominated ecosystem at K2 is associated with more efficient transport of POC through the twilight zone than the ecosystem at ALOHA. In addition to the high T_{eff} in the mesopelagic, the high efficiency of this "silica pump" in the Northwest Pacific for POC transport to the deep ocean has been noted previously (*19*). Thus, our mesopelagic data contrast with previous views of the POC carrying efficiency of different ballasting agents developed by using bathypelagic trap data, which suggested preferential deep ocean POC flux in association with PIC and not bSi (*11*, *20*).

The structure of the food web can also change temporally at any given site. Forty days after peak diatom production at K2 (*18*), we observed a continued decrease in primary production and a decrease in the fraction of C fixation attributable to >20 μm phytoplankton during deployment 2 (Table 1). A decrease in the export ratio from 21 to 11% [e ratio is trap-derived flux at base of euphotic zone divided by primary productivity (PP)] fits with lower export predicted with a shift to smaller cells (*21*, *22*). The constant T_{eff} at K2 in a changing flux environment suggests that flux attenuation processes below the euphotic zone respond proportionally and rapidly to the flux.

During both K2 deployments, most of the identifiable material intercepted by traps was fecal matter from larger zooplankton, in particular copepod species. In the water column above the traps at K2, both zooplankton size and the median size of fecal pellets were significantly larger (42% of zooplankton biomass from 0 to 150 m was >2 mm; 0.17 μg C per pellet at 150 m; fig. S3) than at ALOHA (18% of biomass was >2 mm; 0.036 μg C per pellet). Larger pellets tend to have higher gravitational sinking rates (*3*). Sinking rates would be further increased by the higher percentage of more dense biomineral phases within the sinking particles at K2 (80% opal and carbonate by mass at K2 versus 21% at ALOHA in 150-m trap; Table 1), although slower settling rates in colder, more viscous waters are a potential factor that would offset some of these density-driven changes in sinking rate. Therefore, a simple explanation that may account for much of the twofold higher T_{eff} at K2 compared with that at ALOHA is a faster sinking rate due to differences in ballasting and zooplankton pellet size. The impact of colder temperatures on the rate of heterotrophic metabolism may also contribute to this higher T_{eff} at K2 because of slower biological degradation of sinking particles.

The extent of flux attenuation at the two VERTIGO sites is not captured by the Martin curve. After normalizing the observed flux to 150 m, average *b* values for POC at ALOHA (*b* = 1.33 ± 0.15; fitted value ± 1SE) are higher than predicted (*4*), indicating greater flux attenuation, and lower at K2 (*b* = 0.51 ± 0.05), indicating more efficient C transfer to depth (Fig. 1B). Indeed, the contrast in POC flux attenuation between ALOHA and K2 exceeds the range seen across the six sites used to derive the Martin curve (*b* ranged from 0.64 to 0.97) (*4*). Applying the Martin curve at ALOHA would result in a POC flux at 500 m that is double (i.e., 36 mg C m^{-2} day^{-1}) our observations. At K2, POC fluxes would be 50% too small. The same over- and underpredictions would hold for other elements as well (Fig. 2) and thus would impact relative ratios of nutrients associated with remineralization of sinking particles.

Recent modeling studies based on extensive WOCE nutrient and alkalinity data (*10*) suggest that geochemical distributions in the deep ocean are highly sensitive to the choice of POC flux parameterization. By using global circulation models and simulated export production, Howard *et al.* (*10*) found differences of ~60 μmol dissolved inorganic carbon (DIC) kg^{-1} in the deep ocean between models and observations by using a Martin-like flux parameterization and increases of 30 μmol DIC kg^{-1} by increasing the

Table 1. VERTIGO site characteristics (*34*). Temp is temperature, S is salinity, and dep is trap deployment. ALOHA O_2 taken from HOT bottle data average for June and July 2004. POM is particulate organic matter and is calculated to be equal to 2.2 times mass of POC (*20*). Opal is calculated to be equal to mg of bSi times 2.4 (*26*). $CaCO_3$ is equal to 8.33 times PIC. Deep particle properties for ALOHA are from annual averages from a 4280-m trap (15.5°N, 151.5°E, Honjo *et al.* (*27*)), whereas K2 data are from 4810-m K2 trap samples corresponding to a VERTIGO cruise in 2005. Primary production from VERTIGO cruises are based on shipboard deck incubations using ^{14}C and ^{13}C methods and integrated to the 0.1% light level. For ALOHA, these are within 95% confidence intervals for HOT PP data for upper 100 m but >2 times lower than in situ PP on HOT cruises before and after VERTIGO. K2 PP are higher (D1) and similar to PP estimated by Honda *et al.* (*18*) for the same time period. Size-fractionated PP calculated as the percent of total PP attributable to >20 μm cells. Euphotic zone e ratio uses POC flux at 0.1% light level extrapolated using POC flux curve fits (Fig. 1) to mesopelagic data. Measured 150-m flux/PP ratios are 10 and 8% for ALOHA D1 and D2, and 12 and 6% for K2 D1 and D2, respectively. Mesopelagic transfer efficiency defined as 500-m/150-m POC flux.

	ALOHA			K2		
Dates on site	22 June to 9 July 2004			22 July to 18 August 2005		
Deployment start dates	23 June and 2 July 2004			30 July and 10 August 2005		
Mixed layer depth	49 m			26 m		
Depth of 0.1% light	~125 m			~50 m		
Physical properties						
	Temp (°C)	S	O_2 (μM)	Temp (°C)	S	O_2 (μM)
Mixed layer	26.10	34.63	210	9.61	32.91	285
150 m	21.93	35.26	204	2.17	33.46	198
300 m	13.55	34.33	210	3.37	33.97	29
500 m	7.62	34.04	115	3.17	34.18	21
1000 m	3.94	34.45	45	2.57	34.43	21
Particle properties (average by weight)						
	% POM	% $CaCO_3$	% Opal	% POM	% $CaCO_3$	% Opal
150 m	63.9	13.3	7.7	17.2	3.6	76.8
300 m	51.6	27.1	11.4	13.2	3.2	81.8
500 m	54.9	31.9	16.3	14.1	3.4	80.4
4000 m	13.3	59.9	26.9	7.6	8.5	77.0
POC fluxes (mg m^{-2} day^{-1})						
	First dep.	Second dep.		First dep.	Second dep.	
Integrated PP	180	220		530	365	
150-m POC flux	18	18		62	23	
300-m POC flux	7.2	6.0		47	17	
500-m POC flux	3.6	3.6		29	13	
Production, export, and flux ratios						
	First dep.	Second dep.		First dep.	Second dep.	
% PP >20 μm	12%	11%		30%	19%	
e ratio = flux at 0.1% light/PP	13%	11%		21%	11%	
T_{eff} = 500-m/150-m flux	20%	21%		46%	55%	

T_{eff} over a factor of 2.5. VERTIGO data confirm the existence of regional differences in POC T_{eff} of twofold or more. Our sites represent low-latitude oligotrophic and high-latitude mesotrophic regions and thus are unlikely to be singular end-member values for the global ocean or even seasonal extremes at these two sites.

Implications and conclusions. Our high and low T_{eff}, if applied to the global shallow export production estimate of Laws et al. of 11 Pg C year^{-1} (23), would result in a POC flux at 500 m ranging from 2.3 to 5.5 Pg C year^{-1}, or a difference in ocean C sequestration below 500 m of more than 3 Pg C year^{-1}. For comparison, global anthropogenic emissions of C are 6 to 7 Pg C year^{-1}. Certainly the entire ocean is not characterized by either single T_{eff}; however, this calculation shows that if climate-induced changes in ecosystem structure alter fluxes and shallow export changes to these oceanic contrasts, then T_{eff} would have a large impact on the magnitude of ocean C sequestration and hence be a potential feedback on climate. The predicted increase in ocean stratification and the decrease in nutrient supply because of climate change are thought to favor small phytoplankton at the expense of diatoms (24). Also, decreases in ocean pH with increased CO_2 would tend to decrease the fraction of ocean production attributed to calcium carbonate producers (25). Both of these effects would result in not only less efficient shallow export production but also likely lower mesopelagic T_{eff} and hence reduced ocean C sequestration, which would greatly amplify this positive feedback on climate change.

These data help connect surface water particle sources to mesopelagic fluxes. Both the fraction of production leaving the surface and the proportion of export reaching the deep ocean are highly variable and of similar importance to the sequestration of C in the deep ocean. Although process studies at contrasting sites using NBSTs can help unravel differences in particle flux generation and its fate, decadal mesopelagic time-series observations are necessary to catch episodic events and the full range of flux variability. This variability in the attenuation of sinking particle flux is not yet considered in ocean models and is poorly constrained by existing data from the twilight zone.

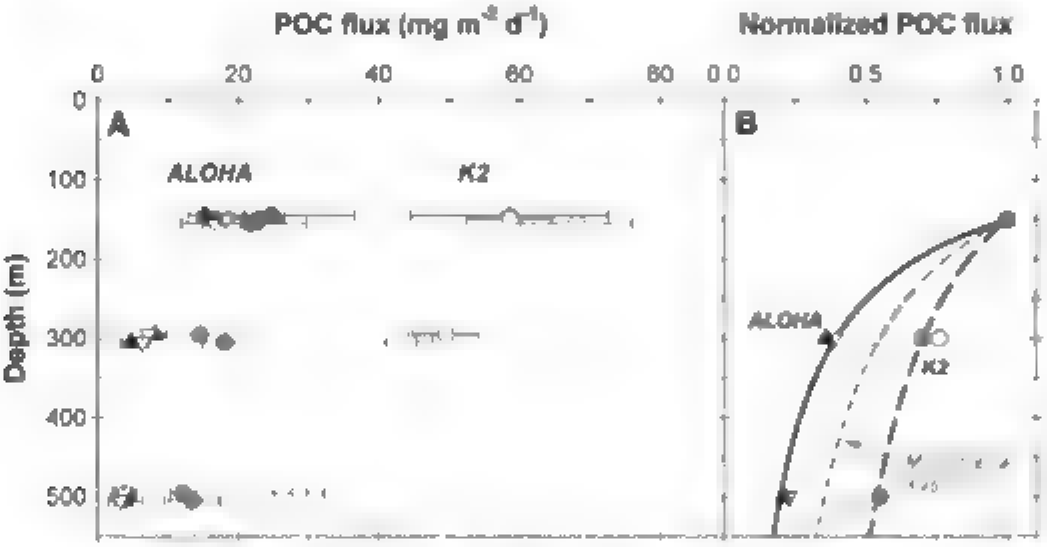

Fig. 1. POC flux versus depth at ALOHA (22°45′N, 158°W) and K2 (47°N, 160°E). (**A**) POC flux at ALOHA (triangles) and K2 (circles) with open and solid symbols for deployments 1 and 2, respectively (deployment start dates in Table 1). (**B**) Same data normalized to 150 m POC flux and compared with Martin *et al.* (4) (dashed line). For each depth, up to three independent NBSTs were deployed from the same launch site, and the POC fluxes are shown (A) for each NBST, with a slight vertical offset, as the mean and standard deviation of replicate POC measurements (*n* from 2 to 4). Fits to normalized data (B) used a power function of the form $F/F_{150} = (z/150)^{-b}$, where z is the depth of the trap, F_{150} is the POC flux at the 150 m reference depth, and b describes the rate of flux attenuation.

Fig. 2. Relative rates of flux attenuation as parameterized by power law fit of Martin *et al.* (4) for chlorophyll a, POC, mass, bSi, and PIC. These are calculated for deployment 1 (open) and 2 (solid) for ALOHA (**top**) and K2 (**bottom**) with an error bar derived from the curve fit to multiple NBST flux data at three depths. Also shown for comparison as a horizontal dashed line is the *b* value for the Martin curve of 0.86, with larger values of *b* indicating faster flux attenuation, i.e., increasing remineralization.

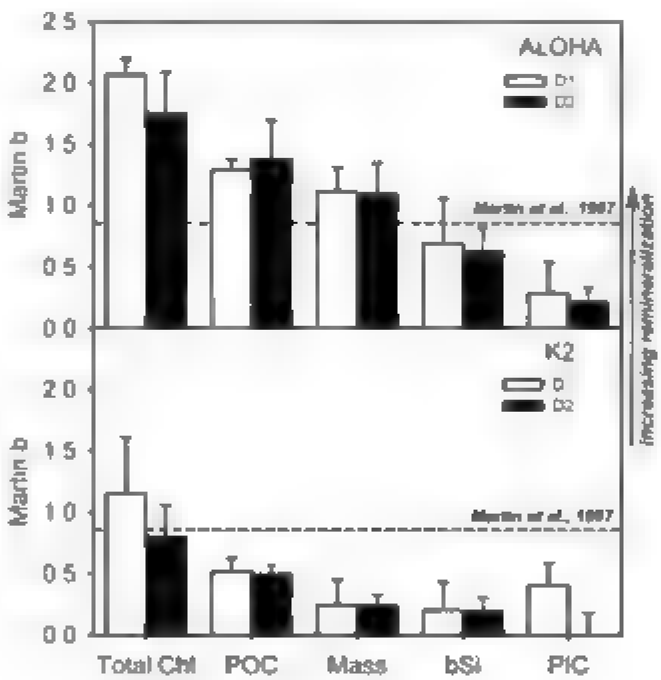

References and Notes

1. T. Volk, M. I. Hoffert, *Geophys. Monogr. Am. Geophys. Union 32* (American Geophysical Union, Washington, DC, 1985).
2. S. W. Fowler, G. A. Knauer, *Prog. Oceanogr.* **16**, 147 (1986).
3. J. Bishop, in *Productivity of the Ocean: Present and Past*, W. H. Berger, V. S. Smetacek, G. Wefer, Eds. (Wiley, New York, 1989), pp. 117–138.
4. J. H. Martin, G. A. Knauer, D. M. Karl, W. W. Broenkow, *Deep-Sea Res. A* **34**, 267 (1987).
5. R. W. Najjar, J. Sarmiento, J. R. Toggweiler, *Global Biogeochem. Cycles* **6**, 45 (1992).
6. Y. Yamanaka, E. Tajika, *Global Biogeochem. Cycles* **10**, 361 (1996).
7. T. Ito, M. J. Follows, *J. Mar. Res.* **63**, 813 (2005).
8. K. O. Buesseler, *Nature* **353**, 420 (1991).
9. R. Schlitzer, *Deep-Sea Res. II* **49**, 1623 (2002).
10. M. T. Howard, A. M. E. Winguth, C. Klaas, E. Maier-Reimer, *Global Biogeochem. Cycles* **20**, GB3011 (2006).
11. R. Francois, S. Honjo, R. Krishfield, S. Manganini, *Global Biogeochem. Cycles* **16**, 1087 (2002).
12. R. A. Armstrong, C. Lee, J. I. Hedges, S. Honjo, S. G. Wakeham, *Deep-Sea Res. II* **49**, 219 (2002).
13. P. W. Boyd, T. W. Trull, *Prog. Oceanogr.* 10.1016/j.pocean.2006.10.007 (2006).
14. Materials and methods are available on *Science* Online.
15. K. O. Buesseler *et al.*, *Deep-Sea Res. I* **47**, 277 (2000).
16. T. Trull *et al.*, in *ASLO-TOS-AGU Ocean Sciences Meeting Abstracts*, abstr. OS23H-05 (2006).
17. D. M. Karl *et al.*, *Deep-Sea Res. II* **43**, 539 (1996).
18. M. C. Honda, H. Kawakami, K. Sasaoka, S. Watanabe, T. Dickey, *Geophys. Res. Lett.* **33**, L16603 (2006).
19. M. C. Honda, *J. Oceanogr.* **59**, 671 (2003).
20. C. Klaas, D. E. Archer, *Global Biogeochem. Cycles* **16**, 1116 (2002).
21. A. F. Michaels, M. W. Silver, *Deep-Sea Res.* **35**, 473 (1988).
22. E. Peinert, B. von Bodungen, V. S. Smetacek, in *Productivity of the Ocean: Present and Past*, W. H. Berger, V. S. Smetacek, G. Wefer, Eds. (Wiley, New York, 1989), pp. 35–48.
23. E. A. Laws, P. G. Falkowski, W. O. Smith Jr., H. Ducklow, J. J. McCarthy, *Global Biogeochem. Cycles* **14**, 1231 (2000).

24. L. Bopp, O. Aumont, P. Cadule, S. Alvain, M. Gehlen, *Geophys. Res. Lett.* 32, 10.1029/2005GL023653 (2005).
25. R. A. Feely *et al.*, *Science* 305, 362 (2004).
26. R. A. Mortlock, P. N. Froelich, *Deep-Sea Res. A* 36, 1415 (1989).
27. S. Honjo, S. J. Manganini, J. J. Cole, *Deep-Sea Res. A* 29, 609 (1982).
28. VERTIGO would not have been possible without the field support obtained from the captain, crew, and shore-based support for the R/V *Kilo Moana* (2004) and R/V *Roger Revelle* (2005). Funding was obtained primarily through the NSF Ocean Sciences Programs in Chemical and Biological Oceanography, with additional support from the U.S. Department of Energy, Office of Science, Biological and Environmental Research Program, and other national programs, including the Australian Cooperative Research Centre program and Australian Antarctic Division. In addition, there are a number of individuals whose efforts at sea or in the laboratory made this VERTIGO program possible, including J. Andrews, C. Bertrand, R. Bidigare III, S. Bray, K. Casciotti, M. Charette, S. Coale, J. Cope, E. Fields, M. Gall, G. Jiao, T. Koban, S. Saitoh, M. Sann, S. Manganini, C. Moy, S. Okamato, S. Pike, L. Robertson, D. Ruddick, and Y. Zhang. We also thank the reviewers for their comments. More information can be found at http://cafethorium.whoi.edu.

Supporting Online Material
www.sciencemag.org/cgi/content/full/316/5824/567/DC1
Materials and Methods
SOM Text
Figs. S1 to S3
References

27 November 2006; accepted 8 March 2007
10.1126/science.1137959

A Selective Activity-Dependent Requirement for Dynamin 1 in Synaptic Vesicle Endocytosis

Shawn M. Ferguson,[1,2,3] Gabor Brasnjo,[5*] Mitsuko Hayashi,[1,2,3*] Markus Wölfel,[5] Chiara Collesi,[1,2,3,7] Silvia Giovedi,[1,2,3] Andrea Raimondi,[1,2,3] Liang-Wei Gong,[1,2,3] Pablo Ariel,[5,6] Summer Paradise,[1,2,3] Eileen O'Toole,[8] Richard Flavell,[1,4] Ottavio Cremona,[7] Gero Miesenböck,[3] Timothy A. Ryan,[5] Pietro De Camilli[1,2,3]†

Dynamin 1 is a neuron-specific guanosine triphosphatase thought to be critically required for the fission reaction of synaptic vesicle endocytosis. Unexpectedly, mice lacking dynamin 1 were able to form functional synapses, even though their postnatal viability was limited. However, during spontaneous network activity, branched, tubular plasma membrane invaginations accumulated, capped by clathrin-coated pits, in synapses of dynamin 1 knockout mice. Synaptic vesicle endocytosis was severely impaired during strong exogenous stimulation but resumed efficiently when the stimulus was terminated. Thus, dynamin 1–independent mechanisms can support limited synaptic vesicle endocytosis, but dynamin 1 is needed during high levels of neuronal activity.

Synaptic transmission is dependent on the continuous reformation of synaptic vesicles via local membrane recycling (*1, 2*). Although the precise mechanisms of synaptic vesicle reformation remain a matter of debate (*3–7*), there is strong evidence for a key role of the guanosine triphosphatase (GTPase) dynamin in this process (*8–12*), as well as in a variety of endocytic reactions in all cell types (*9, 13–16*). Dynamin is thought to oligomerize at the neck of endocytic pits and to mediate neck constriction and fission (*8, 9, 11*). However, previous studies have addressed the action of dynamin at synapses through dominant-negative interference or pharmacological inhibition strategies, which may also elicit dominant-negative effects from the inactivated protein. Thus, we investigated the importance of dynamin in membrane traffic at synapses in dynamin 1 null mutants.

Mammals express three dynamins with different expression patterns (fig. S1) (*17*). Dynamin 1 is expressed exclusively in the brain, whereas dynamin 2 is ubiquitously expressed and dynamin 3 is expressed selectively in brain and testis (fig. S1B) (*18*). In neurons, levels of dynamin 1 increase with synapse formation in parallel with the levels of synaptic vesicle proteins (fig. S1E). These and many other observations (*9, 18, 19*) strongly suggest that dynamin 1 plays a dedicated and essential role in the recycling of synaptic vesicles and thus a critical role in nervous system function.

Dynamin 1–KO mice appear normal at birth. A null allele of the mouse dynamin 1 gene was generated by deleting exon 1 (*17*) (fig. S1E). Heterozygous mice were viable, fertile, and without any apparent health defects. Their matings yielded wild-type (WT), heterozygous (Ht) and, surprisingly, knockout (KO) pups in the expected Mendelian ratio (table S1). At birth, KO mice breathed, moved, and suckled and were not distinguishable from their littermates (Fig. 1A). Thus, dynamin 1 is not required for either embryonic development or for the neurotransmission that supports perinatal life. However, a reduction in the ingestion of milk was apparent in KO pups within several hours after birth (Fig. 1A), and poor motor coordination became obvious over the following days. Overall, dynamin 1 KO pups failed to thrive and died within 2 weeks (fig. S2).

Immunoblot analysis of brain tissue and cortical neuron cultures demonstrated the absence of dynamin 1 in KO mice and a dramatic decrease of total dynamin levels (Fig. 1B and fig. S2), consistent with dynamin 1 being by far the predominant isoform in the nervous system. Levels of dynamin 2 and 3, as well as of a variety of proteins involved in synaptic transmission and endocytosis, were not changed (Fig. 1B and fig. S2).

Synaptic transmission in dynamin 1–KO neurons. Whole-cell voltage-clamp recordings from primary cortical cultures were carried out to study the impact of the loss of dynamin 1 on synaptic transmission. Recordings of miniature excitatory and inhibitory postsynaptic currents (mEPSCs and mIPSCs, respectively) revealed a large increase (Fig. 2, A and B), possibly due to increased vesicle size (see below). Next, evoked synaptic transmission was analyzed in paired recordings from low-density cortical cultures

[1]Howard Hughes Medical Institute, Kavli Institute for Neuroscience, Yale University School of Medicine, New Haven, CT 06510, USA. [2]Program in Cellular Neuroscience, Neurodegeneration and Repair, Yale University School of Medicine, New Haven, CT 06510, USA. [3]Department of Cell Biology, Yale University School of Medicine, New Haven, CT 06510, USA. [4]Section of Immunobiology, Yale University School of Medicine, New Haven, CT 06510, USA. [5]Department of Biochemistry, Weill Medical College of Cornell University, New York, NY 10021, USA. [6]David Rockefeller Graduate Program, The Rockefeller University, New York, NY 10021, USA. [7]IFOM, the FIRC Institute for Molecular Oncology Foundation, and Università Vita—Salute San Raffaele, Milano, Italy. [8]Boulder Laboratory for 3D Electron Microscopy of Cells, Department of Molecular, Cellular, and Developmental Biology, University of Colorado, Boulder, CO 80309, USA.

*These authors contributed equally.
†To whom correspondence should be addressed. E-mail: pietro.decamilli@yale.edu

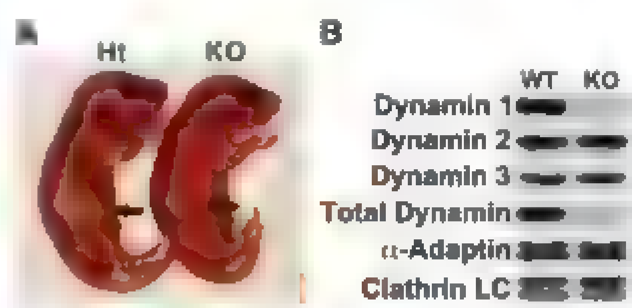

Fig. 1. Dynamin 1–KO mice appear normal at birth. (**A**) Ht and KO pups several hours after birth. Arrows highlight less milk in the stomach of the KO pup. (**B**) Immunoblot analysis of cell lysates from primary cortical neuron cultures (15 to 21 DIV) with dynamin isoform-specific antibodies and a pan-dynamin antibody. Clathrin LC, clathrin light chain.

Both EPSCs and IPSCs elicited by single presynaptic stimuli (Fig. 2C) were recorded, and a statistically significant reduction in peak amplitude was observed for IPSCs at KO synapses. Other characteristics of IPSCs were unchanged (table S2).

IPSCs were further recorded during trains of 1000 stimuli. Peak amplitudes of IPSCs tended to depress faster in KO neurons than in control (WT/Ht) neurons (time constants = 8.5 ± 2.5 s for control versus 3.9 ± 1.2 s for KO; $P = 0.26$, t test) (Fig. 2E). Furthermore, given the smaller initial peak amplitudes in KO synapses, synaptic transmission failed at earlier times in these synapses. IPSCs recovered (as assessed by test stimuli delivered at 0.1 Hz) within 100 s to 46.0 ± 6.[illegible] of the initial response in control cultures, but to only [illegible] ± 3.2% of their initial IPSC value in KO cultures (Fig. 2F). Thus, dynamin 1 is not essential for synaptic transmission, but is required for efficient and sustained evoked release.

Synaptic vesicles form without dynamin 1. Unexpectedly, in view of the predicted essential role of dynamin 1 in synaptic vesicle recycling, but consistent with the presence of a functional nervous system in KO mice, electron microscopy (EM) revealed an abundance of synaptic vesicles in both control and KO synapses in tissue sections examined at postnatal day 6 (fig. S5), as well as in primary cultures of cortical neurons at all ages examined (Fig. 3, A to E, and fig. S6). However, EM micrographs of cultured cortical neurons [mean age 21 days in vitro (DIV)] revealed a modest reduction (~20%) in synaptic vesicle numbers (38.9 ± 2.3 per active zone profile in WT versus 31.3 ± 2.1 in KO, $P = 0.018$, t test). In addition, synaptic vesicles had a more heterogeneous and generally slightly larger size in KO synapses (mean external diameter = 43.13 ± 0.19 nm for WT versus 47.27 ± 0.25 nm for KO; $P < 0.0001$, t test) (Fig. 3I; see also [illegible] fig. S5C), [illegible] size detected electrophysiologically (Fig. 2A).

Accumulation of clathrin-coated buds. A characteristic feature of KO synapses relative to controls was a much higher occurrence, striking at some synapses, of clathrin-coated vesicular profiles (Fig. 3, B to F and H). In ultrathin sections, many of the coated profiles appeared to be interconnected clathrin-coated buds rather than free coated vesicles (Fig. 3D, inset). Accordingly, they were accessible to extracellular tracers, such as horseradish peroxidase (HRP, a fluid phase tracer) (Fig. 4C) or HRP-labeled cholera toxin (a membrane tracer), even when cultures were labeled with the tracer on ice (Fig. 3E and fig. S6). Electron tomography unambiguously demonstrated that these structures were buds connected to the plasma membrane by narrow branched tubules (Fig. 3F). Thus, the fission of clathrin-coated vesicles was impaired.

The accumulation of assembled clathrin coats in KO neurons was also reflected in a modified distribution of clathrin and clathrin adaptors (e.g., α-adaptin subunit of AP-2) as shown by immunofluorescence (Fig. 4A and fig. S7). Although the abundance of these proteins was unchanged (Fig. 1B and fig. S2), their immunoreactivity had a much more punctate pattern in KO cultures. A similar change was observed for dynamin 3, which strongly colocalized with clathrin puncta in KO neurons (Fig. 4A and fig. S4); however, the dynamin 2 staining pattern was weak and diffuse in both KO and controls (fig. S4). These effects, together with the accumulation of coated intermediates revealed by EM, were more prominent when neuron density or culture age was increased. Hence, we suspected that the accumulation of coated intermediates reflected a backup of endocytic traffic in response to spontaneous network activity. Indeed, following blockade of action potential firing with tetrodotoxin (TTX), clustering of clathrin and dynamin 3 immunoreactivity and accumulation of clathrin-coated profiles were no longer observed (Fig. 4, A and B, respectively).

Impaired vesicle recycling during stimulation. To measure stimulation-dependent synaptic vesicle recycling directly, neurons that had been acutely stimulated in the presence of the extracellular tracer HRP were analyzed by EM. After a 90-s stimulation with high-potassium buffer, numerous labeled synaptic vesicles were observed in WT synapses (Fig. 4E). In contrast, in KO synapses, mainly clathrin-coated profiles and other endocytic intermediates were labeled, and the total number of synaptic vesicles was more steeply reduced (Fig. 4, C and H). However, after a recovery period of 10 min in HRP-containing control buffer, numerous labeled synaptic vesicles were visible in synapses of both genotypes (Fig. 4, C, F, and I). On average, recovery in KO synapses lagged behind that of the controls (Fig. 4C), consistent with the delayed recovery from depression observed electrophysiologically (Fig. 2F); nevertheless, robust dynamin 1–independent vesicle for-

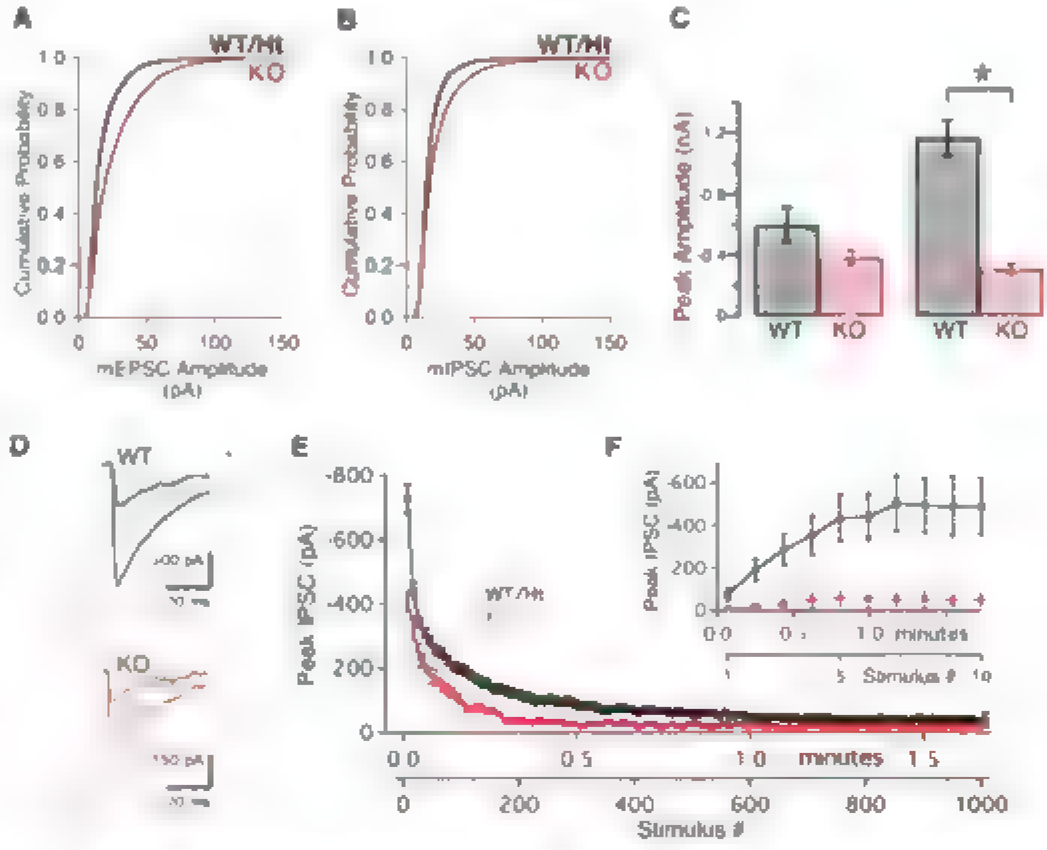

Fig. 2. Synaptic transmission in primary cultures of dynamin 1 KO cortical neurons. Cumulative probability histograms of peak mEPSC (**A**) and mIPSC (**B**) amplitudes from WT (black lines) and KO cultures (red lines). The mean mEPSC amplitude was increased from 17.0 ± 1.8 pA in WT neurons to 24.8 ± 2.5 pA in the dynamin 1 KO neurons (t test, $P = 0.011$, n = 2495 and 2435, respectively). A similar increase in amplitude was observed for mIPSCs (mean for WT = 17.3 ± 0.8 pA, n = 2369 versus 22.2 ± 1.0 pA, n = 2731, t test, $P = 0.0006$). (**C**) Modest reduction in single evoked (2-ms depolarization to +30 mV) EPSC amplitudes [WT n = 45, KO n = 40, $P = 0.0967$ (t test)] and significant reduction in single IPSC amplitudes in KO neuron pairs. *$P < 0.001$ (t test, n = 39, 38 for WT, KO). (**D**) Examples of evoked IPSCs for WT and KO, respectively. Shown are the 1st, 3rd, and 7th IPSC responses to stimulation at 10 Hz. Presynaptic stimulation is indicated as membrane voltage (gray dotted lines). (**E**) IPSC depression curves for control (black) and KO (red) during a sustained 10-Hz stimulation. Averaged data points represent 16 control and 7 KO cell pairs, binned into nonoverlapping groups of 10 responses. (**F**) Slower recovery of IPSCs from depression induced by 1000 action potentials at 10 Hz (shown in E) as assessed by 0.1 Hz stimulation. Averages represent unbinned data from 12 control and 6 KO cell pairs. The recovery (mean of the last five points) was markedly slower in the KO (t test, $P = 0.0024$).

nation was observed in some KO synapses (Fig. 4I).

Frequency-dependent endocytic blockade. To gain further quantitative and temporal insight into the synaptic vesicle recycling defect, we performed dynamic imaging assays of exo- and endocytosis. Cultured cortical neurons were transfected with synapto-pHluorin, a chimeric synaptic vesicle protein whose fluorescence is low in the acidic environment within the lumen of a synaptic vesicle and high when exocytosis exposes it to the cell surface (21). In WT neurons, the peak synapto-pHluorin fluorescence in response to a given number of action potentials was lower for a 10-Hz stimulation than for a 30-Hz stimulation, presumably because the ability of endocytosis to keep up with ongoing exocytosis was impaired with an increase of the stimulus frequency to 30 Hz (22) (fig. S8; see also Fig. 5F). In contrast, in dynamin 1 KO neurons, the extent of accumulation was almost identical following both stimulation conditions (fig. S8), which suggested that endocytic capacity was already saturated by stimulation at 10 Hz. Note, however, that the recovery kinetics after the end of the stimulus train were similar in WT and KO synapses (fig. S8).

This result was confirmed by a different experimental protocol involving both synapto-pHluorin and the H^+-ATPase (adenosine triphosphatase) inhibitor bafilomycin, which blocks synaptic vesicle reacidification, thus quenching the pHluorin signal after endocytosis (23). At WT but not at KO synapses, the increase in fluorescence produced by 300 action potentials delivered at 10 Hz was higher in the presence of bafilomycin, the "endocytosis-blind" condition (Fig. 5, A and C). Acid-quench experiments excluded the possibility that this difference was due to a defect in acidification (Fig. 5B). Similarly, this difference could not be attributed to differences in exocytosis rates during stimulation (Fig. 5C). As observed above (fig. S8), when the stimulus was removed, fluorescence declined in both sets of synapses at remarkably similar rates. Nonetheless, as 33% of the membrane that had undergone exocytosis had already been recovered by endocytosis during the stimulus, recovery to prestimulus levels was faster in the control synapses (Fig. 5C). Similar results were obtained using synaptotagmin-pHluorin (24) as the reporter of synaptic vesicle recycling (Fig. 5D). The endocytic blockade during stimulation was fully rescued if dynamin 1 was cotransfected into the KO neurons along with synapto-pHluorin (Fig. 5D). When cotransfected under the same conditions, i.e., conditions that result in overexpression, dynamin 3 produced an efficient rescue but dynamin 2, only a partial rescue (Fig. 5D). This result demonstrates that all three dynamin isoforms can participate in synaptic vesicle endocytosis but also reveals a greater functional similarity between dynamin 1 and 3. It further suggests that dynamin 1–independent recycling is mediated by dynamin 2 and/or consistent with the complete block of synaptic vesicle endocytosis by pharmacological inhibition of dynamin that is not isoform-specific (13, 25).

The endocytic defect in KO synapses during stimulation (as quantified by calculation of the endocytic/exocytic ratio) did not reach statistical significance following 300 action potentials at lower stimulation frequencies [2-Hz and 5-Hz stimulation (Fig. 5E)], and it was less severe during stimulation at 10 Hz when extracellular $[Ca^{2+}]$ was decreased to 0.75 mM (Fig. 5F). Under these conditions, the size of the exocytic responses and the accumulation of presynaptic $[Ca^{2+}]$ are both expected to be attenuated. Conversely, at a higher stimulation frequency (30 Hz), the endocytic/exocytic ratio was dramatically decreased also in WT synapses, as

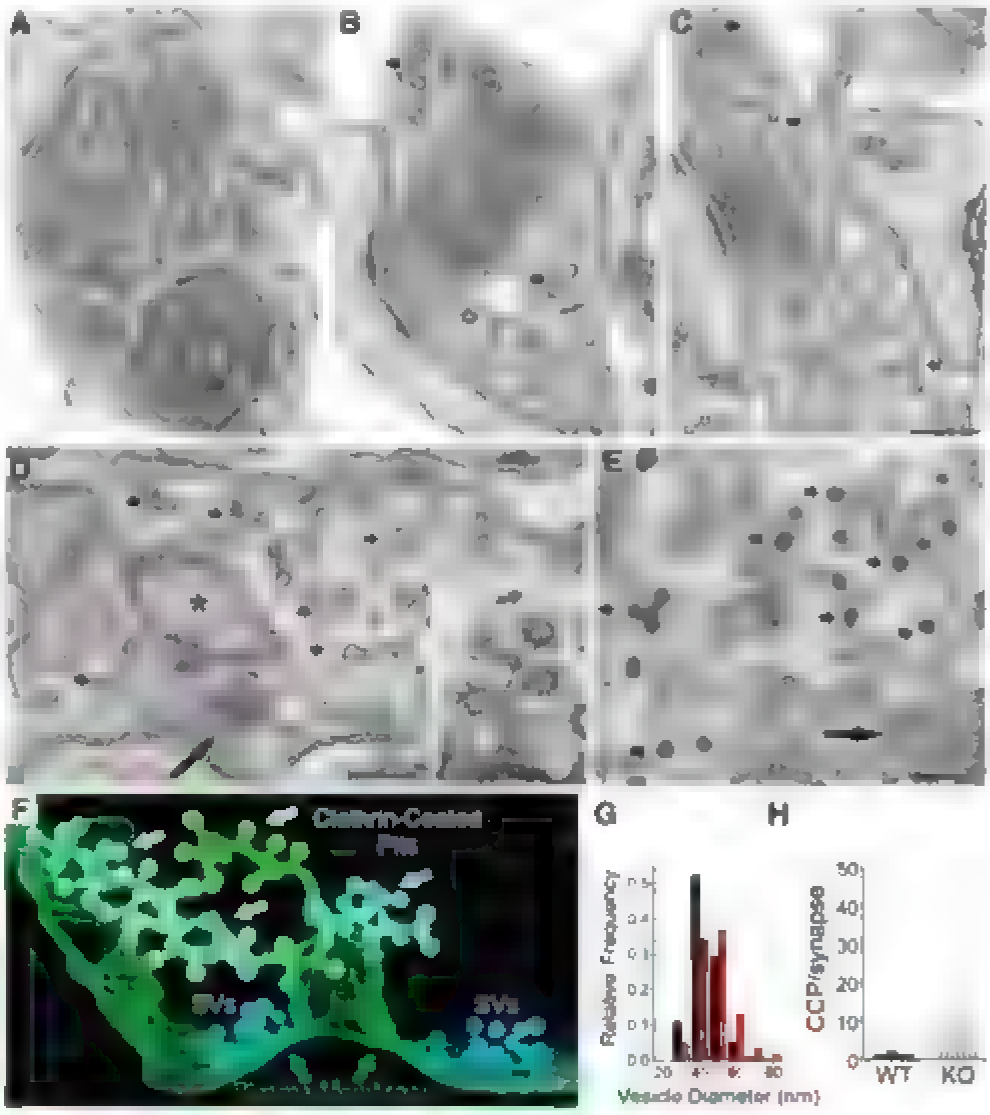

Fig. 3. Ultrastructural defects in dynamin 1 KO synapses of cultured neurons. **(A)** WT synapse. **(B** and **C)** KO synapses revealing an abundance of clathrin-coated profiles (arrows highlight stalks connecting clathrin-coated buds), an increase in the average synaptic vesicle size, and the presence **(C)** of several abnormally large vesicles. **(D)** A KO synapse with a massive accumulation of interconnected clathrin-coated buds (arrowheads) and only a small cluster (arrow) of heterogeneously sized synaptic vesicles. An asterisk indicates an evagination of an adjacent cell into this nerve terminal. (Inset) A plasma membrane connected network of clathrin-coated pits observed in a serial section from this same synapse (~200 nm away). **(E)** Accessibility of clathrin-coated profiles (arrowheads) in KO neurons to cholera toxin-HRP (10 μg/ml for 5 min on ice) supports their connection to the plasma membrane (the arrow indicates the location of the synaptic vesicle cluster within this synapse). **(F)** Partial reconstruction of a dynamin 1 KO synapse from electron tomography data shows three branched tubular networks (pale green, blue, and yellow) capped by clathrin-coated pits (white arrows) that are connected to the plasma membrane (green) in close proximity to two synaptic vesicle clusters (SVs, blue). **(G)** Quantification of synaptic vesicle external diameter (black, WT; red, KO; 10-nm bins). Vesicles exceeding 80 nm in diameter were 5.4 times as abundant in KO as in WT synapses (87 vesicles in KO versus 16 vesicles in WT) but were excluded from the analysis presented in (G) as their identification as synaptic vesicles remained questionable. **(H)** Histogram of clathrin-coated profile (CCP) counts from 75 WT and 87 KO synapses. WT = 0.2 ± 0.05, KO = 4.7 ± 0.89 CCPs/synapse (means ± SEM, $P < 0.0001$, t test). Data derived from three independent experiments. Horizontal black line is the mean. Scale bars, 200 nm.

expected (22–24) (Fig. 5F). Thus, the absence of dynamin 1 lowers the threshold of activity at which synaptic vesicle endocytosis becomes unable to compensate for exocytosis.

Discussion. Surprisingly, dynamin 1, the nervous system–specific dynamin, and by far the major dynamin in neurons, is largely dispensable for the biogenesis and endocytic recycling of synaptic vesicles. Dynamin 1 only becomes essential when an intense stimulus imposes a heavy load on endocytosis and only as long as the stimulus persists. The importance of dynamin 1 under these conditions is likely to be related to its abundance but also, at least in part, to its unique properties. Endocytosis occurs efficiently in both WT and KO synapses immediately after removal of the stimulus, when the endocytic load is still maximal. Thus, dynamin 1 may have a specific function within stimulated synapses. Strong stimulation produces a change in the state of phosphorylation of a variety of nerve terminal proteins (26). Several proteins implicated in endocytosis, including dynamin 1, undergo Ca^{2+}-dependent dephosphorylation by calcineurin, and this process, which is rapidly reversed upon cessation of the stimulus, enhances their recruitment to endocytic sites (26). Given the ability of dynamin 3, when overexpressed, to efficiently rescue the dynamin 1 KO phenotype, it is noteworthy that dynamin 1 and 3 share conserved phosphorylation sites on key residues controlling protein-protein interactions (27, 28). Furthermore, the coclustering of dynamin 3 with clathrin in nerve terminals favors the hypothesis that dynamin 3 has overlapping functions with dynamin 1, but is insufficient to support endocytosis at high levels of activity.

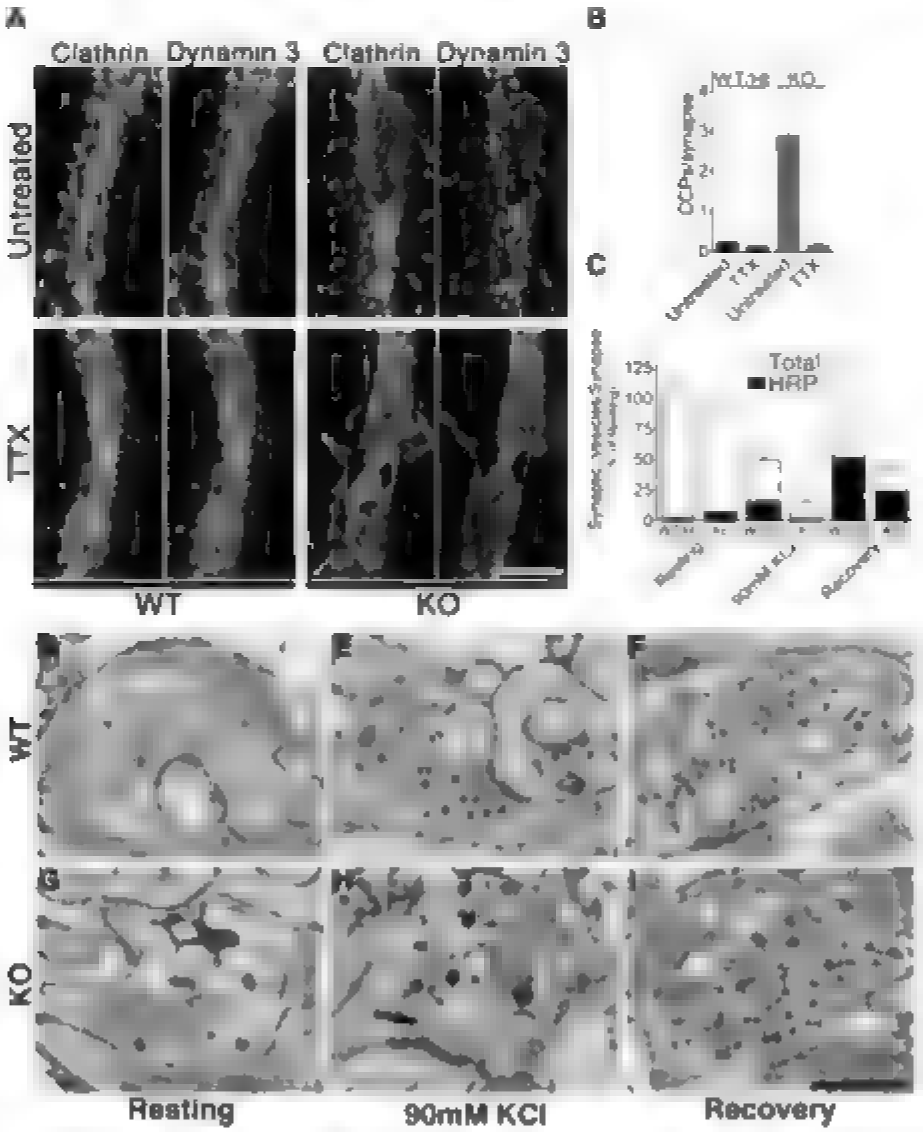

Fig. 4. Activity-dependent synaptic vesicle recycling defects in dynamin 1 KO synapses. **(A)** Immunofluorescence for clathrin light chain and dynamin 3 reveals a predominantly diffuse distribution in cultured WT neurons, but a punctate and overlapping distribution in KO neurons (see also fig. S4). Treatment with TTX (1 μM, 16 to 24 hours) caused clathrin and dynamin 3 in the KO neurons to redistribute to a diffuse localization resembling the localization of these proteins in untreated WT neurons (scale bar, 10 μm). **(B)** Morphometric analysis of EM images demonstrating that the accumulation of clathrin-coated profiles in KO synapses was reversed following TTX treatment (1 μM, 16 to 24 hours). **(C to I)** EM analysis of synapses from cortical cultures of WT and KO brains incubated with the extracellular tracer HRP (10 mg/ml) in control Tyrode's buffer (90 s), following a 90-s stimulation with 90 mM KCl, and then a further 10-min recovery period in Tyrode's buffer. (C) Quantification of changes in total synaptic vesicle number and in the number of vesicles positive for the extracellular tracer HRP. (D to I) Representative examples of HRP uptake by WT and KO synapses under the conditions described above. At rest, HRP-labeled clathrin-coated buds emerging from the labeled plasma membrane invagination are visible in the KO synapse (G). Following stimulation, the WT nerve terminal (E) contains labeled and unlabeled vesicles, whereas in the KO synapse (H) synaptic vesicles are nearly depleted (long arrow) and labeled clathrin-coated buds (short arrows) are visible. After recovery, synaptic vesicles including labeled vesicles are present in both genotypes (F and I). It is expected that, at this concentration, only a fraction of the endocytic vesicles should take up HRP. EM scale bar, 200 nm.

The morphological changes observed in nerve terminals of KO synapses under conditions of basal network activity are consistent with a role of dynamin in fission. The slightly larger and more heterogeneous size of synaptic vesicles raises the possibility that actions of dynamin 1 at the free edge of the clathrin coat of budding vesicles may help to control their size. The fidelity of this process may be disrupted when the overall dynamin content of the nerve terminal is drastically reduced. Indirect effects arising from the lack of dynamin 1 should also be considered because increases in synaptic vesicle size and size heterogeneity have been observed in neurons with other mutations that cause endocytosis defects (29, 30).

The most striking morphological change is the presence of deeply invaginated clathrin-coated endocytic pits, generally located at the tip of branched narrow tubules that are likely generated by the numerous clathrin accessory factors with membrane tubulating properties (31). This is in contrast to the collared but uncoated pits of the *Drosophila* Shibire mutant (a temperature-sensitive dynamin allele) synapses after stimulation at the nonpermissive temperature (32). Although the intense debate concerning the potential occurrence of two major pathways of synaptic vesicle recycling—kiss-and-run versus clathrin-mediated endocytosis—is ongoing (6, 7, 33), our results strongly support an important role of clathrin-mediated endocytosis.

The selective requirement for dynamin 1 in stimulation-dependent synaptic vesicle reformation is in contrast with the powerful complete block of several forms of endocytosis produced by expression of mutant forms of either dynamin 1 or dynamin 2 in a variety of cell types (8, 13, 15, 16). These dominant-negative effects may reflect hetero-oligomerization of mutant dynamins with endogenous dynamin(s), leading to impairment of actions that require the coordinated function of subunits within a polymeric complex. Overexpressed mutant dynamins could additionally sequester critical

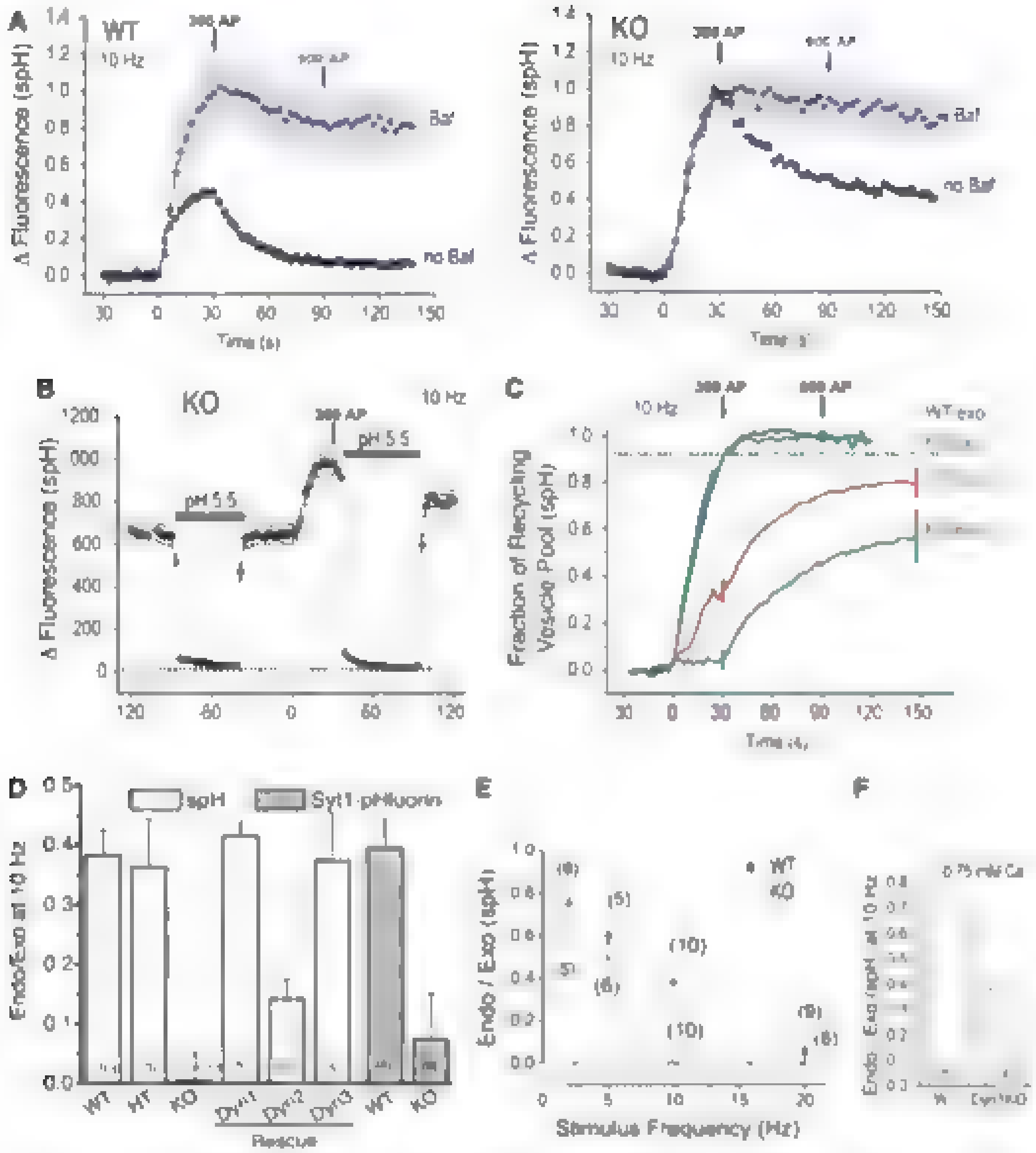

Fig. 5. Frequency dependent impairment of synaptic vesicle endocytosis in dynamin 1–KO neurons. (**A**) Representative traces from WT (left panel) and KO (right panel) synapto-pHluorin expressing neurons stimulated in the presence (blue circles) or absence (black squares) of bafilomycin (Baf). A 10-Hz field stimulation began at $t = 0$ and ended after 30 s (300 action potentials, no Baf) or 90 s (900 action potentials, Baf). (**B**) Brief application of extracellular membrane impermeant acid rapidly quenches all surface synapto-pHluorin in the prestimulus period (KO neuron). Following a 30-s stimulus (end marked by arrow), the fluorescence is quenched to the same level as the prestimulus period. The average degree of quenching poststimulus was 94.0 ± 1.4% in WT ($n = 5$) and 94.6 ± 1.0% in KO ($n = 8$). (**C**) The pooled average kinetics of exocytosis (exo = ΔF_{Baf}) from WT (blue) and KO (green) neurons after 900 action potentials (10 Hz in presence of bafilomycin) and the pooled average kinetics of endocytosis (endo = $\Delta F_{Baf} - \Delta F_{no\ Baf}$) from WT (red) and KO (cyan) neurons after 300 action potentials at 10 Hz (stimulus ends at first arrow). The dashed line indicates the extent of exocytosis at the 30-s time point where endocytosis to exocytosis ratios (endo/exo) are calculated. Error bars are shown at two time points on the endocytosis curves ($n = 9$ for both WT and KO). (**D**) The average endo/exo ratio after 300 action potentials at 10 Hz as determined by using either synapto-pHluorin (spH) or synaptotagmin1 (syt1)-pHluorin (gray bars). Rescue refers to dynamin 1–KO cells that were cotransfected with synapto-pHluorin and dynamin 1, dynamin 2, or dynamin 3. (**E**) Endo/exo ratios following 300 action potentials at different frequencies. (**F**) Mean Endo/exo ratios after 300 action potentials (10 Hz) in 0.75 mM Ca^{2+}. The numbers shown in parentheses in (D, E, and F) represent the number of independent experiments and error bars in this figure show ± SEM.

binding partners in nonfunctional protein complexes. In conclusion, dynamin 1, one of the most abundant synaptic proteins, is specifically dedicated to control plastic adaptation of the synaptic vesicle recycling machinery to high levels of activity.

References and Notes

1. V. N. Murthy, P. De Camilli, *Annu. Rev. Neurosci.* **26**, 701 (2003).
2. T. C. Sudhof, *Annu. Rev. Neurosci.* **27**, 509 (2004).
3. B. Ceccarelli, W. P. Hurlbut, A. Mauro, *J. Cell Biol.* **57**, 499 (1973).
4. N. C. Harata, A. M. Aravanis, R. W. Tsien, *J. Neurochem.* **97**, 1546 (2006).
5. J. E. Heuser, T. S. Reese, *J. Cell Biol.* **57**, 315 (1973).
6. M. Wienisch, J. Klingauf, *Nat. Neurosci.* **9**, 1019 (2006).
7. B. Granseth, B. Odermatt, S. J. Royle, L. Lagnado, *Neuron* **51**, 773 (2006).
8. J. E. Hinshaw, *Annu. Rev. Cell Dev. Biol.* **16**, 483 (2000).
9. G. J. Praefcke, H. T. McMahon, *Nat. Rev. Mol. Cell Biol.* **5**, 133 (2004).
10. S. Sever, H. Damke, S. L. Schmid, *Traffic* **1**, 385 (2000).
11. A. Roux, K. Uyhazi, A. Frost, P. De Camilli, *Nature* **441**, 528 (2006).
12. A. J. Newton, T. Kirchhausen, V. N. Murthy, *Proc. Natl. Acad. Sci. U.S.A.* **103**, 17955 (2006).
13. M. A. McNiven, H. Cao, K. R. Pitts, Y. Yoon, *Trends Biochem. Sci.* **25**, 115 (2000).
14. E. Macia *et al.*, *Dev. Cell* **10**, 839 (2006).
15. A. M. van der Bliek *et al.*, *J. Cell Biol.* **122**, 553 (1993).
16. J. S. Herskovits, C. C. Burgess, R. A. Obar, R. B. Vallee, *J. Cell Biol.* **122**, 565 (1993).
17. I. Cook, K. Mesa, R. Urrutia, *J. Neurochem.* **67**, 927 (1996).
18. H. Cao, F. Garcia, M. A. McNiven, *Mol. Biol. Cell* **9**, 2595 (1998).
19. K. Takei, P. S. McPherson, S. L. Schmid, P. De Camilli, *Nature* **374**, 186 (1995).
20. Materials and methods are available as supporting material on *Science* Online.
21. G. Miesenbock, D. A. De Angelis, J. E. Rothman, *Nature* **394**, 192 (1998).
22. J. Fernandez-Alfonso, T. A. Ryan, *Neuron* **41**, 943 (2004).
23. S. Sankaranarayanan, T. A. Ryan, *Nat. Neurosci.* **4**, 129 (2001).
24. T. Fernandez-Alfonso, R. Kwan, T. A. Ryan, *Neuron* **51**, 179 (2006).
25. T. Yamashita, T. Hige, T. Takahashi, *Science* **307**, 124 (2005).
26. M. A. Cousin, P. J. Robinson, *Trends Neurosci.* **24**, 659 (2001).
27. V. Anggono *et al.*, *Nat. Neurosci.* **9**, 752 (2006).
28. M. R. Larsen, M. E. Graham, P. J. Robinson, P. Roepstorff, *Mol. Cell. Proteom.* **3**, 456 (2004).
29. B. Zhang *et al.*, *Neuron* **21**, 1465 (1998).
30. K. E. Poskanzer, R. D. Fetter, G. W. Davis, *Neuron* **50**, 49 (2006).
31. T. Itoh, P. De Camilli, *Biochim. Biophys. Acta* **1761**, 897 (2006).
32. J. H. Koenig, K. Ikeda, *J. Neurosci.* **9**, 3844 (1989).
33. R. Fesce, F. Grohovaz, F. Valtorta, J. Meldolesi, *Trends Cell Biol.* **4**, 1 (1994).
34. N. C. Harata, S. Choi, J. L. Pyle, A. M. Aravanis, R. W. Tsien, *Neuron* **49**, 243 (2006).
35. S. P. Gandhi, C. F. Stevens, *Nature* **423**, 607 (2003).
36. D. K. Dickman, Z. Lu, I. A. Meinertzhagen, T. L. Schwarz, *Curr. Biol.* **16**, 591 (2006).
37. P. Verstreken *et al.*, *Cell* **109**, 101 (2002).

38. We thank R. Mata-Fitzsimonds, K. Howell, and N. Pypaert for advice and F. Wilson, L. Tomasini, L. Liu, L. Lucast, R. Kwan, and W. Yan for technical assistance. This work was supported in part by the G. Harold and Leila Y. Mathers Charitable Foundation, NIH grants to P.D.C. (NS36251, CA46128, DK45735 and DA018343), T.A.R. (NS036942), G.M. (DA17297), grant RR 000592 from the National Center for Research Resources of the National Institutes of Health to J. R. McIntosh, AIRC, AICR, Telethon, FIRB and COFIN/PRIN grants to O.C., a Canadian Institutes of Health Research fellowship to S.M.F., a Human Frontiers Science Program fellowship to M.H., and a Fondazione Italiana per la Ricerca sul Cancro (FIRC) fellowship to S.G.

Supporting Online Material

www.sciencemag.org/cgi/content/full/316/5824/570/DC1
Materials and Methods
Figs. S1 to S8
Table S1 to S3
References

31 January 2007; accepted 16 March 2007
10.1126/science.1140621

Control of Stress-Dependent Cardiac Growth and Gene Expression by a MicroRNA

Eva van Rooij,[1] Lillian B. Sutherland,[1] Xiaoxia Qi,[1] James A. Richardson,[1,2] Joseph Hill,[3] Eric N. Olson[1*]

The heart responds to diverse forms of stress by hypertrophic growth accompanied by fibrosis and eventual diminution of contractility, which results from down-regulation of α-myosin heavy chain (αMHC) and up-regulation of βMHC, the primary contractile proteins of the heart. We found that a cardiac-specific microRNA (miR-208) encoded by an intron of the αMHC gene is required for cardiomyocyte hypertrophy, fibrosis, and expression of βMHC in response to stress and hypothyroidism. Thus, the αMHC gene, in addition to encoding a major cardiac contractile protein, regulates cardiac growth and gene expression in response to stress and hormonal signaling through miR-208.

Cardiac contractility depends on the expression of two MHC genes, α and β, which are regulated in an antithetical manner by developmental, physiological, and pathological signals. βMHC, which encodes a slow myosin adenosine triphosphatase (ATPase), is the dominant isoform expressed in the embryonic heart, whereas αMHC, a fast ATPase, is up-regulated postnatally (1). Thyroid hormone (T3) signaling stimulates αMHC and inhibits βMHC transcription after birth (2). In contrast, hypothyroidism and various forms of cardiac stress increase βMHC expression with consequent diminution in cardiac performance (3–5). αMHC is the predominant adult cardiac isoform in rodents, whereas βMHC is the predominant isoform in adult human hearts and becomes even more abundant during cardiac disease when αMHC is down-regulated (6–9). Because even relatively subtle variations in the ratio of αMHC and βMHC can profoundly influence cardiac function, there has been great interest in deciphering the mechanisms that coordinate αMHC and βMHC expression and in strategies to therapeutically manipulate cardiac MHC expression (10).

MicroRNAs (miRNAs) are small, non-protein-coding RNAs that base pair with specific mRNAs and inhibit translation or promote mRNA degradation (11). MiRNAs arise from primary transcripts of variable sizes that are processed into 70- to 100-nucleotide hairpin-shaped precursors, which are processed into mature miRNAs of

[1]Department of Molecular Biology, University of Texas Southwestern Medical Center, Dallas, TX 75390–9148, USA. [2]Department of Pathology, University of Texas Southwestern Medical Center, Dallas, TX 75390–9148, USA. [3]Department of Internal Medicine, University of Texas Southwestern Medical Center, 6000 Harry Hines Boulevard, Dallas, TX 75390–9148, USA.

*To whom correspondence should be addressed. E-mail: eric.olson@utsouthwestern.edu

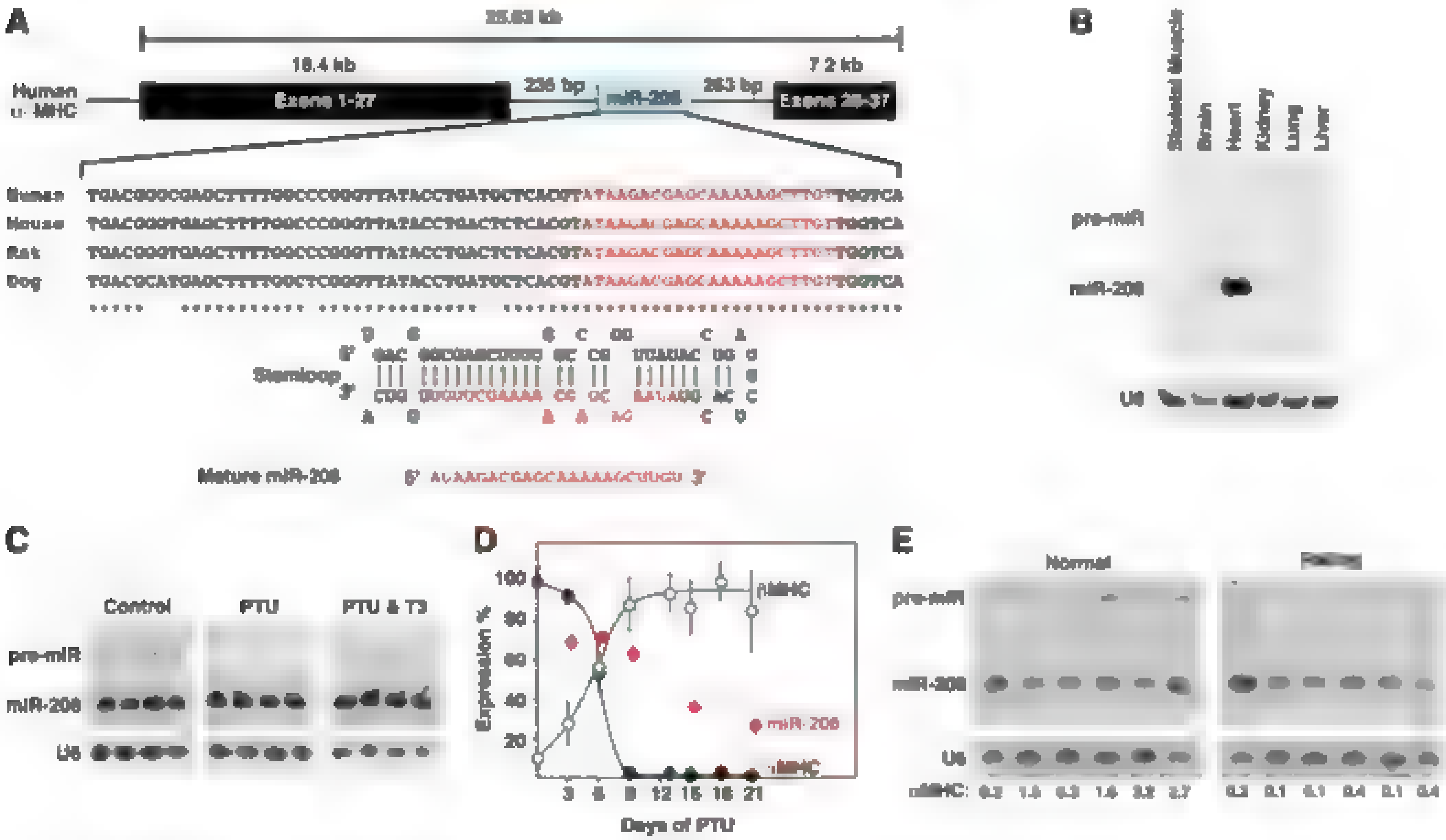

Fig. 1. Expression of miR-208 and coregulation with αMHC. **(A)** MiR-208 is encoded by intron 27 of the αMHC gene. Asterisks indicate sequence conservation. **(B)** Detection of miR-208 transcripts by Northern analysis of adult mouse tissues. U6 mRNA serves as a loading control. **(C)** Rats were treated with PTU or PTU + T3, as indicated, for a week, and the expression of miR-208 was detected by Northern blot. Hearts from four animals under each condition were analyzed. **(D)** Transcripts for αMHC and βMHC and miR-208 were quantified by real-time polymerase chain reaction (PCR) analysis at the indicated times after treatment with PTU. Expression of the miR-208 pre-miRNA parallels that of αMHC gene expression, whereas the mature miR-208 continues to be expressed even after the disappearance of αMHC mRNA. Values represent mean ± SEM of hearts of four animals at each time point. **(E)** Transcripts for αMHC and miR-208 were detected by Northern blot of cardiac tissue from six normal individuals and six individuals with idiopathic cardiomyopathy. Indicated αMHC levels were relative to average expression level in normal hearts. There is a close correlation between the level of expression of αMHC and pre–miR-208, whereas mature miR-208 expression is maintained after the latter RNAs have been down-regulated.

18 to 25 nucleotides. MiRNAs that base pair perfectly with target mRNA sequences result in mRNA degradation, whereas those that display imperfect sequence complementarity with target mRNAs generally result in translational inhibition (12). Overexpression experiments have implicated miRNAs in diverse cellular processes (13–19), but to date there have been no reports of the consequences of deletion of miRNA genes in vertebrate organisms. Recently, we identified a signature pattern of miRNAs associated with pathological cardiac growth and remodeling (19). Here, we describe miR-208 as an essential cardiac-specific regulator of *βMHC* expression and mediator of stress and T3 signaling in the heart.

Regulation of miR-208 expression. MiR-208 is encoded by intron 27 of the human and mouse *αMHC* gene. The sequences of miR-208 found in humans, mice, rats, and dogs are identical and the pre-miRNA is highly conserved in mammals (Fig. 1A). Consistent with the specific expression of *αMHC* in the heart and the pulmonary myocardium (20), miR-208 is expressed specifically in the heart and at trace levels in the lung (Fig. 1B). Blockade of T3 biosynthesis with propylthiouracil (PTU) represses *αMHC* and induces *βMHC* expression (21). After rats were treated with PTU for one week, the expression of *αMHC* mRNA declined in parallel with the level of the miR-208 stem loop, whereas mature miR-208 showed little or no change in expression. T3 treatment blocked the effects of PTU on expression of *αMHC* mRNA and pre-miR-208 (Fig. 1C and fig. S1A).

A time course of PTU treatment showed that *αMHC* and pre-miR-208 expression decreased and *βMHC* increased during the first 9 days of PTU treatment (Fig. 1D and fig. S1, B and C). Expression of pre-miRNA-208 paralleled *αMHC* mRNA expression, whereas even after 21 days of PTU treatment, long after *αMHC* mRNA expression had ceased, 30% of the mature miR-208 remained (Fig. 1D and fig. S1, B and C). We infer from the coregulation of pre-miR-208 and the *αMHC* transcript that miR-208 is processed from the *αMHC* intron rather than being transcribed as a separate RNA. The sustained expression of miR-208 after the pre-miRNA and *αMHC* transcripts are down-regulated by PTU suggests that it is extremely stable, with a half-life of ~12 days.

Although *αMHC* mRNA constitutes only about 30% of total *MHC* mRNA expressed in normal adult human heart (8), miR-208 expression was readily detectable in human cardiac tissue (Fig. 1E). Consistent with its relatively long half-life, miR-208 was also detectable in idiopathic failing human hearts in which αMHC levels were diminished relative to normal hearts.

Generation of miR-208 mutant mice. We deleted the miR-208 coding region by introducing loxP sites for Cre-mediated recombination at both ends of an 83 base pair (bp) region of intron 27 of the mouse *αMHC* gene, which encodes the complete pre-miRNA sequence of miR-208 (Fig. 2A and fig. S2A). Breeding of miR-208$^{flox/+}$ mice to mice bearing a ubiquitously expressed Cre recombinase transgene resulted in deletion of the miR-208 genomic sequence and the complete absence of miR-208 in homozygous mutant animals (Fig. 2B and fig. S2B). Disruption of the *αMHC* gene causes early embryonic lethality (22). Thus, it was important that the miR-208 targeting strategy not alter *αMHC* transcription or splicing. Deletion of miR-208 did not interfere with *αMHC* mRNA splicing or alter the expression of αMHC or βMHC proteins in hearts of newborn mice (Fig. 2C and fig. S2, C and D). A Western blot using an antibody against all striated myosins indicated no visible differences between wild-type and miR-208 mutant animals (fig. S3A).

Mice homozygous for the miR-208 deletion were viable and did not display obvious abnormalities in size, shape, or structure of the heart up to 20 weeks of age. Analysis of cardiac function by echocardiography showed a slight reduction in contractility, measured by fractional shortening, in miR-208$^{-/-}$ animals compared with the contractility of wild-type littermates at 2 months of age, which was attributable primarily to an increase in left ventricular diameter during systole (fig. S3B). At advanced age (>6 months), cardiac function declined further in mutant animals as a result of abnormalities in sarcomere structure.

Microarray analysis on hearts from wild-type and miR-208$^{-/-}$ animals at 2 months of age revealed that the removal of miR-208 resulted in pronounced expression of fast skeletal muscle contractile protein genes, including those encoding Troponin I2, Troponin T3, and myosin light chain-alkali, which are normally not expressed in the heart. Transcripts encoding the natriuretic peptides atrial natriuretic factor (ANF) and b-type natriuretic peptide (BNP), and heat shock proteins, which serve as markers of cardiac stress, were also up-regulated in the hearts of miR-208$^{-/-}$ animals (fig. S3, C and D, and table S1). None of the up-regulated transcripts contained predicted target sequences for miR-208, suggesting that they are regulated indirectly by miR-208.

MiR-208 regulates βMHC expression and cardiac remodeling. To further investigate the potential functions of miR-208, we compared the response of wild-type and miR-208 mutant mice to thoracic aortic banding (TAB), which induces cardiac hypertrophy by increased afterload on the heart and is accompanied by down-regulation of *αMHC* and up-regulation of *βMHC* (23). *αMHC* mRNA expression declined as expected after TAB (fig. S4A), but miR-208 was still abundantly expressed 21 days after TAB (fig. S4B), consistent with its relatively long half-life.

In response to TAB, wild-type mice showed a pronounced increase in cardiac mass accompanied by hypertrophic growth of cardiomyocytes

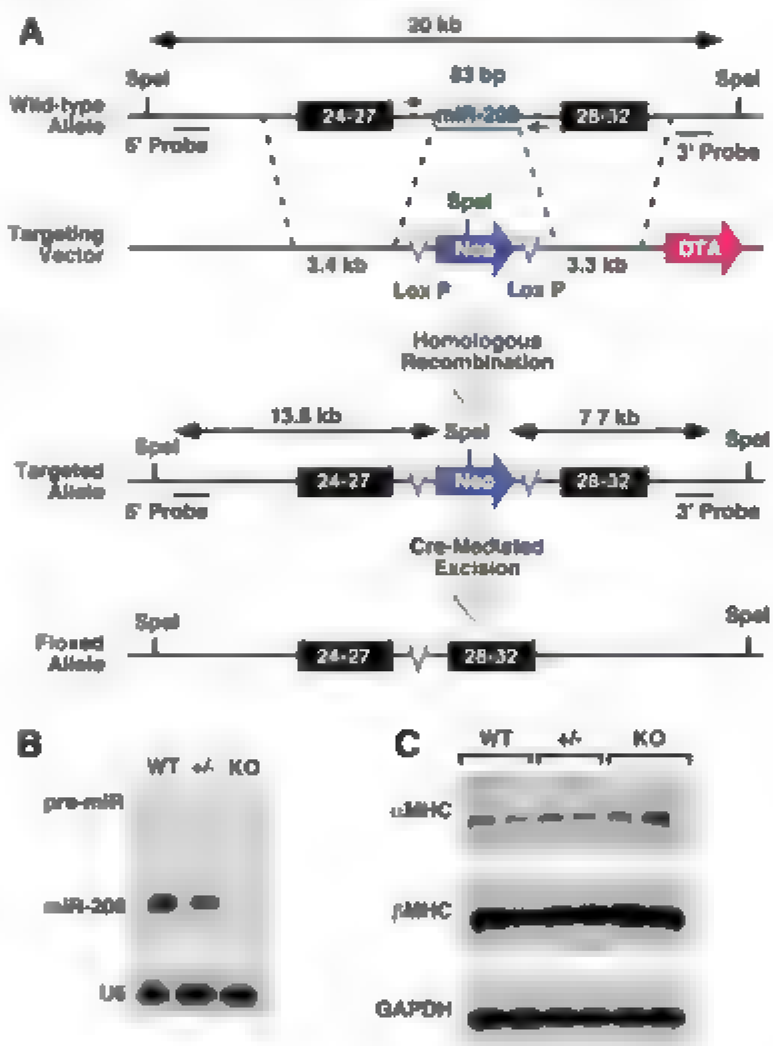

Fig. 2. Generation of miR-208 mutant mice. (**A**) Strategy to generate miR-208 mutant mice by homologous recombination. The pre-miRNA sequence was replaced with a neomycin resistance cassette (Neo) flanked by loxP sites. The neomycin cassette was removed in the mouse germ line by breeding heterozygous mice to transgenic mice harboring the CAG-Cre transgene. DTA, diphtheria toxin A. (**B**) Detection of miR-208 transcripts by Northern analysis of hearts from wild-type (WT) and miR-208 mutant (KO) mice. (**C**) Western analysis of αMHC and βMHC protein levels in hearts of neonatal mice of the indicated genotypes. Two mice of each genotype were analyzed. Glyceraldehyde-3-phosphate dehydrogenase (GAPDH) was detected as a loading control.

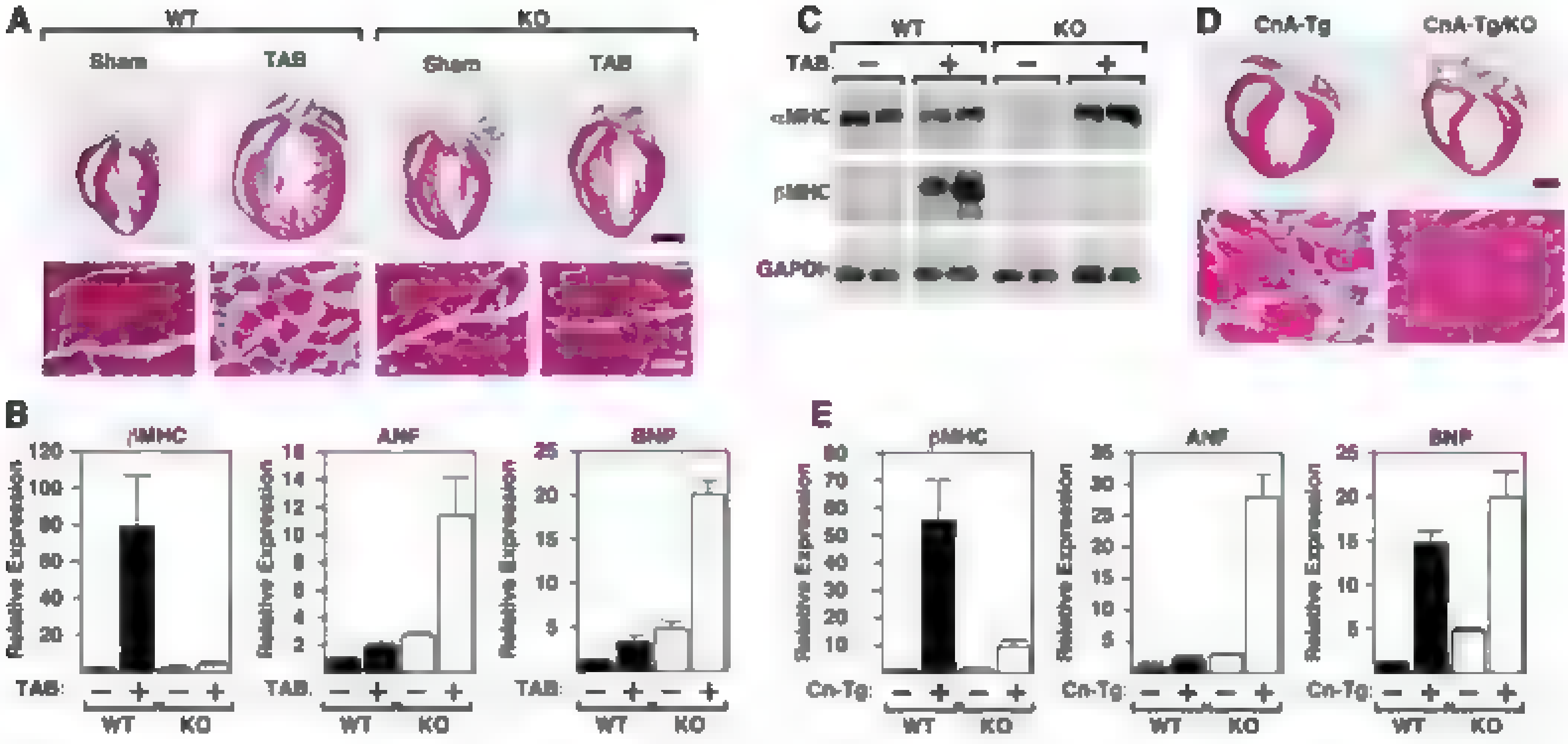

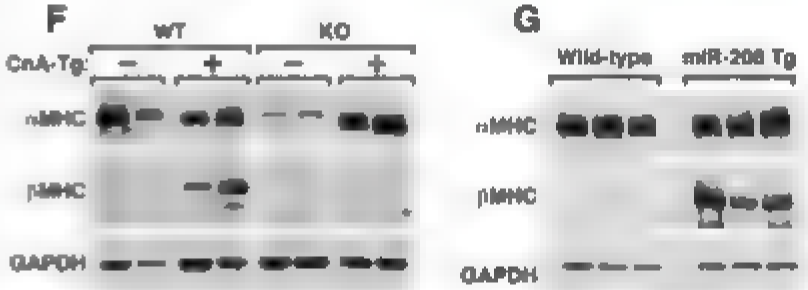

Fig. 3. MiR-208$^{-/-}$ mice show reduced cardiac hypertrophy in response to pressure overload. **(A)** Histological sections of hearts of wild-type (WT) and miR-208$^{-/-}$ (KO) mice stained for Masson trichrome. The absence of miR-208 diminishes hypertrophy and fibrosis seen in wild-type mice subjected to TAB for 21 days. Scale bars, 2 mm (top); 20 μm (bottom). **(B)** Transcripts for βMHC, ANF, and BNP were detected by real-time PCR in hearts from wild-type and miR-208$^{-/-}$ mice after sham or TAB surgery. Values are expressed as fold increase in expression (+SEM) compared with that of wild-type mice (n = 3) that underwent sham operations. **(C)** Western analysis of αMHC and βMHC protein levels in adult wild-type and miR-208 mutant mice 21 days after sham and TAB surgery. **(D)** Histological sections of hearts of 6-week-old mice expressing a calcineurin transgene (CnA-Tg) and hearts of miR-208$^{-/-}$/CnA-Tg mice stained for Masson trichrome. The absence of miR-208 diminishes hypertrophy and fibrosis seen in CnA-Tg mice. Scale bars, 2 mm (top); 20 μm (bottom). **(E)** Transcripts for βMHC, ANF, and BNP were detected by real-time PCR in hearts from the indicated genotype. Values are expressed as fold increase in expression (+SEM) compared with that of wild-type mice (n = 3). **(F)** Western analysis of αMHC and βMHC protein levels in adult wild-type and miR-208 mutant mice with and without the presence of the CnA transgene. **(G)** Western analysis of αMHC and βMHC protein levels in adult wild-type and miR-208 transgenic animals.

and ventricular fibrosis (Fig. 3A). In contrast, miR-208 mutant animals showed virtually no hypertrophy of cardiomyocytes or fibrosis in response to TAB (Fig. 3A). Echocardiography confirmed that miR-208$^{-/-}$ animals displayed a blunted hypertrophic response and a decrease in contractility (fig. S4C). Most notably, mutant animals were unable to up-regulate βMHC. Instead, αMHC protein expression increased in miR-208 mutant hearts in response to TAB, which may reflect a compensatory mechanism to maintain MHC expression in the absence of βMHC up-regulation. Other stress-responsive genes, such as those encoding the natriuretic peptides ANF and BNP, were strongly induced in miR-208 mutant animals (Fig. 3, B and C). Microarray analysis on hearts from wild-type and miR-208$^{-/-}$ animals confirmed that the absence of miR-208 resulted in a highly specific block to βMHC expression (table S2).

MiR-208$^{-/-}$ mice were also resistant to fibrosis and cardiomyocyte hypertrophy in response to transgenic expression of activated calcineurin (Fig. 3D), an especially powerful stimulus for cardiac hypertrophy and heart failure (24). Similarly, *βMHC* mRNA and protein failed to be up-regulated in hearts of miR-208$^{-/-}$/calcineurin transgenic mice at 6 weeks of age, whereas ANF and BNP were strongly induced (Fig. 3, E and F). Thus, miR-208 is necessary for up-regulation of *βMHC* and cellular remodeling, but not for expression of other markers of cardiac stress.

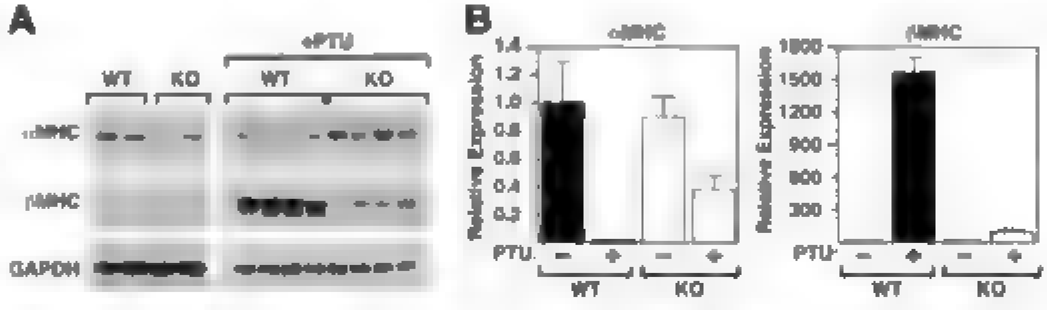

Fig. 4. Regulation of thyroid hormone responsiveness of the *βMHC* gene by miR-208. **(A)** Western analysis of αMHC and βMHC expression in wild-type (WT) and miR-208 mutant (KO) mice at baseline and 2 weeks after PTU treatment. **(B)** Transcripts for *αMHC* and *βMHC* were detected by real-time PCR in hearts from wild-type and miR-208$^{-/-}$ mice after PTU treatment. Values are expressed as fold increase in expression (+SEM) compared with that of wild-type mice that received regular chow (n = 3).

To test whether miR-208 was sufficient for up-regulation of *βMHC* expression, we generated transgenic mice that overexpressed miR-208 under control of the *αMHC* promoter. *αMHC-miR-208* transgenic mice were viable, and their miR-208 expression was about three times as high as that of wild-type hearts (fig. S4D). Hearts from a transgenic line representing the average over-

expression of the transgene showed no overt signs of pathological remodeling at 2 months of age but, notably, displayed a marked up-regulation of *βMHC* expression (Fig. 3G and fig. S4). This activity of miR-208 was specific, as shown by transgenic overexpression of miR-214, which is increased during cardiac hypertrophy (*19*), but had no effect on *βMHC* expression. Because the endogenous level of miR-208 in the adult mouse heart is insufficient to up-regulate *βMHC* expression, the finding that a threefold increase in miR-208 expression in these transgenic mice results in up-regulation of *βMHC* expression suggests that there is a sharp threshold for the control of *βMHC* expression by this microRNA.

MiR-208 regulates T3-dependent repression of βMHC. T3 signaling induces *αMHC* transcription through a positive T3 response element (TRE), whereas a negative TRE in the promoter of the *βMHC* gene mediates transcriptional repression (*25*). To test whether miR-208 was required for T3-dependent regulation of *βMHC*, we fed mutant and wild-type littermates PTU-containing chow for 2 weeks to block T3 signaling. Northern blot analyses revealed that miR-208 was modestly increased after 2 weeks of PTU treatment (fig. S5A). PTU, as expected, induced a decline in heart rate and contractility and an increase in dilation, with no marked differences between wild-type and mutant animals (fig. S5B). However, whereas wild-type animals showed the expected decrease in *αMHC* and increase in *βMHC* in response to PTU, the miR-208$^{-/-}$ animals again were resistant to up-regulation of *βMHC*, although a trace of *βMHC* expression was detectable (Fig. 4). *ANF* and *BNP* were up-regulated by PTU in miR-208$^{-/-}$ animals, confirming the specific role of miR-208 in *βMHC* expression (fig. S5C). Because PTU induces the *αMHC*-to-*βMHC* isoform switch by interfering solely with thyroid hormone receptor (TR) signaling (*27*), these findings suggest that miR-208 potentiates *βMHC* expression through a mechanism involving the TR.

MiR-208 targets TR-Associated Protein 1. Among the relatively few predicted targets of miR-208, the mRNA encoding thyroid hormone receptor Associated Protein 1 (THRAP1), also known as TRAP240, scored as the strongest predicted target with the PicTar target-prediction program (*26*). THRAP1, a component of the TR-associated TRAP complex, modulates activity of the TR by recruitment of RNA polymerase II and general initiation factors (*27*). The putative miR-208 binding site in the 3' untranslated region (UTR) of the *THRAP1* mRNA showed high complementarity with the 5' arm of miR-208, the most critical determinant of miRNA targeting, as well as evolutionary conservation (Fig. 5A). Based on the imperfect complementarity of miR-208 and *THRAP1* 3'-UTR sequence, miR-208 would be expected to inhibit translation of *THRAP1*.

To test whether the putative miR-208 target sequence in the *THRAP1* 3' UTR could mediate translational repression, we inserted the full-length 3' UTR of the *THRAP1* transcript into a luciferase expression plasmid, which we transfected into COS1 cells. Increasing amounts of CMV-driven miR-208 resulted in a dose-dependent decrease in luciferase activity, whereas comparable amounts of miR-126, which served as a control, had no effect (Fig. 5B). CMV-miR-208 also dose-dependently abrogated translation of a hemagglutinin (HA)-tagged malonyl coenzyme A decarboxylase (MCD) expression cassette linked to the *THRAP1* 3'-UTR binding sequence but not a mutant miR-208 target sequence (Fig. 5C). In addition, THRAP1 protein expression was increased in cardiac protein lysates from miR-208$^{-/-}$ mice compared with that in wild-type littermates (Fig. 5D), whereas THRAP1 mRNA was comparable in hearts of the two genotypes (fig. S6), consistent with the conclusion that miR-208 acts as a negative regulator of THRAP1 translation in vivo. Under situations of stress, the negative influence of miR-208 on THRAP1 protein expression may be even greater in light of recent studies showing that stress augments the repressive actions of miRNAs by promoting the association of miRNAs with Argonaute (*28*).

Discussion. Our results demonstrate that miR-208, which is encoded by an intron of the *αMHC* gene, regulates stress-dependent cardiomyocyte growth and gene expression. In the

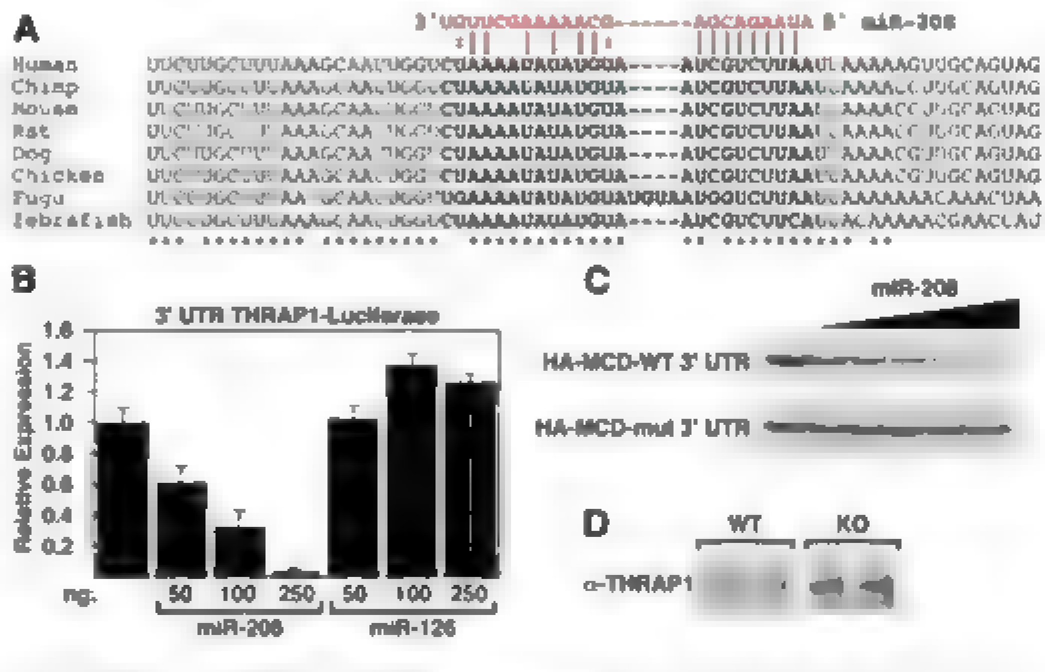

Fig. 5. MiR-208 targets THRAP1. (**A**) Sequence alignment of putative miR-208 binding site in 3' UTR of *THRAP1* shows a high level of complementarity and sequence conservation. (**B**) COS1 cells were transfected with a *THRAP1* 3' UTR luciferase construct, along with expression plasmids for miR-126 and miR-208. Values are fold change in luciferase expression (±SD) compared with the reporter alone. (**C**) COS1 cells were transfected with either HA-MCD-wild type (WT) UTR or HA-MCD-mutated UTR along with increasing dosages of pCMV-miR-208 (ranging from 0.1 to 2 μg). HA levels were detected using immunoblot. (**D**) THRAP1 Western blot using a THRAP1-specific antibody on THRAP1-immunoprecipitated cardiac cell lysates using 400 μg of protein from either wild-type or miR-208$^{-/-}$ (KO) animals.

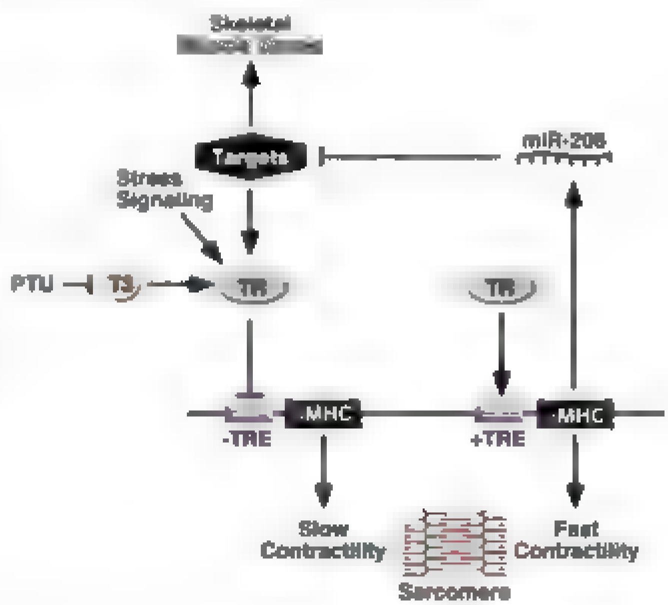

Fig. 6. A model for the role of miR-208 in cardiac gene regulation. The *αMHC* gene encodes miR-208, which negatively regulates expression of THRAP1 and skeletal muscle genes (and probably additional targets). The *αMHC* and *βMHC* genes are linked and miR-208 is required for up-regulation of *βMHC* in response to stress signaling and blockade to T3 signaling by PTU. *αMHC* and *βMHC* promote fast and slow contractility, respectively.

absence of miR-208, the expression of *βMHC* is severely blunted in the adult heart in response to pressure overload, activated calcineurin, or hypothyroidism, suggesting that the pathways through which these stimuli induce *βMHC* transcription share a common miR-208–sensitive component (Fig. 6). In contrast, *βMHC* expression was unaltered in the hearts of newborn miR-208$^{-/-}$ mice, demonstrating that miR-208 participates specifically in the mechanism for stress-dependent regulation of *βMHC* expression.

A clue to the mechanism of action of miR-208 comes from the resemblance of miR-208$^{-/-}$ hearts to hyperthyroid hearts, both of which display a block to βMHC expression, up-regulation of stress-response genes (*29*, *30*), and protection against pathological hypertrophy and fibrosis (*31*, *32*). The up-regulation of fast skeletal muscle genes in miR-208$^{-/-}$ hearts also mimics the induction of fast skeletal muscle fibers in the hyperthyroid state (*33*). T3 signaling represses *βMHC* expression in the postnatal heart, and PTU, which causes hypothyroidism, induces *βMHC* (*2*, *27*). The inability of PTU to induce *βMHC* expression in miR-208$^{-/-}$ hearts further implicates miR-208 in the T3 signaling pathway.

Our results suggest that miR-208 acts, at least in part, by repressing expression of the TR coregulator THRAP1, which can exert positive and negative effects on transcription (*34*, *35*). The TR acts through a negative TRE to repress *βMHC* expression in the adult heart (*2*). Thus, the increase in THRAP1 expression in the absence of miR-208 would be predicted to enhance the repressive activity of the TR toward *βMHC* expression, consistent with the blockade to *βMHC* expression in miR-208$^{-/-}$ hearts. In contrast, the regulation of *αMHC* and *βMHC* expression during development is independent of T3 signaling (*2*) and is unaffected by miR-208. Notably, other TR target genes, such as *phospholamban* and *sarcoendoplasmic reticulum calcium ATPase 2a* and *glucose transporter 4* were expressed normally in miR-208$^{-/-}$ mice (fig. S7). It has been proposed that the *βMHC* gene may respond to specific TR isoforms (*36*–*38*). Perhaps THRAP1 acts on specific TR isoforms or selectively on a subset of TR-dependent genes through interactions with promoter-specific factors. Because miRNAs generally act through multiple downstream targets to exert their effects, additional targets are also likely to contribute to the effects of miR-208 on cardiac growth and gene expression.

Relatively minor increases in βMHC composition, as occur during cardiac hypertrophy and heart failure, can reduce myofibrillar ATPase activity and systolic function (*9*). Thus, therapeutic manipulation of miR-208 expression or interaction with its mRNA targets could potentially enhance cardiac function by suppressing βMHC expression. Based on the profound influence of miR-208 on the cardiac stress response and the regulation of numerous miRNAs in the diseased heart (*19*), we anticipate that miRNAs will prove to be key regulators of the functions and responses to disease of the adult heart and possibly other organs.

References and Notes

1. A. Weiss, L. A. Leinwand, *Annu. Rev. Cell Dev. Biol.* **12**, 417 (1996).
2. E. Morkin, *Microsc. Res. Tech.* **50**, 522 (2000).
3. M. Krenz, J. Robbins, *J. Am. Coll. Cardiol.* **44**, 2390 (2004).
4. H. Kinugawa, E. G. Kranias, *Annu. Rev. Physiol.* **62**, 321 (2000).
5. D. Fatkin *et al.*, *J. Clin. Invest.* **106**, 1351 (2000).
6. B. D. Lowes *et al.*, *J. Clin. Invest.* **100**, 2315 (1997).
7. S. Miyata, W. Minobe, M. R. Bristow, L. A. Leinwand, *Circ. Res.* **86**, 386 (2000).
8. K. Nakao, W. Minobe, R. Roden, M. R. Bristow, L. A. Leinwand, *J. Clin. Invest.* **100**, 2362 (1997).
9. W. T. Abraham *et al.*, *Mol. Med.* **8**, 750 (2002).
10. T. A. McKinsey, E. N. Olson, *J. Clin. Invest.* **115**, 538 (2005).
11. D. P. Bartel, *Cell* **116**, 281 (2004).
12. W. P. Kloosterman, R. H. Plasterk, *Dev. Cell* **11**, 441 (2006).
13. A. Esquela-Kerscher, F. J. Slack, *Nat. Rev. Cancer* **6**, 259 (2006).
14. S. Costinean *et al.*, *Proc. Natl. Acad. Sci. U.S.A.* **103**, 7024 (2006).
15. S. M. Hammond, *Curr. Opin. Genet. Dev.* **16**, 4 (2006).
16. V. Ambros, *Cell* **113**, 673 (2003).
17. Y. Zhao, E. Samal, D. Srivastava, *Nature* **436**, 214 (2005).
18. J. F. Chen *et al.*, *Nat. Genet.* **38**, 228 (2006).
19. E. van Rooij *et al.*, *Proc. Natl. Acad. Sci. U.S.A.* **103**, 18255 (2006).
20. A. Subramaniam *et al.*, *J. Biol. Chem.* **266**, 24613 (1991).
21. G. T. Schuyler, L. R. Yarbrough, *Basic Res. Cardiol.* **85**, 481 (1990).
22. W. K. Jones *et al.*, *J. Clin. Invest.* **98**, 1906 (1996).
23. J. A. Hill *et al.*, *Circulation* **101**, 2863 (2000).
24. J. D. Molkentin *et al.*, *Cell* **93**, 215 (1998).
25. K. Ojamaa, A. Kenessey, I. Klein, *Endocrinology* **141**, 2139 (2000).
26. A. Krek *et al.*, *Nat. Genet.* **37**, 495 (2005).
27. M. Ito, R. G. Roeder, *Trends Endocrinol. Metab.* **12**, 127 (2001).
28. A. K. Leung, J. M. Calabrese, P. A. Sharp, *Proc. Natl. Acad. Sci. U.S.A.* **103**, 18125 (2006).
29. T. Wei, C. Zeng, Y. Tian, Q. Chen, L. Wang, *J. Endocrinol. Invest.* **28**, 8 (2005).
30. C. Pantos *et al.*, *Horm. Metab. Res.* **38**, 308 (2006).
31. J. Yao, M. Eghbali, *Circ. Res.* **71**, 831 (1992).
32. W. J. Chen, K. H. Lin, Y. S. Lee, *Mol. Cell. Endocrinol.* **162**, 45 (2000).
33. A. Vadaszova, G. Zacharova, K. Machacova, I. Jirmanova, T. Soukup, *Physiol. Res.* **53** (suppl. 1), S57 (2004).
34. R. Pavri *et al.*, *Mol. Cell* **18**, 83 (2005).
35. S. W. Park *et al.*, *Mol. Cell* **19**, 643 (2005).
36. K. Kinugawa, C. S. Long, M. R. Bristow, *J. Clin. Endocrinol. Metab.* **86**, 5089 (2001).
37. A. Mansen, F. Yu, D. Forrest, L. Larsson, B. Vennstrom, *Mol. Endocrinol.* **15**, 2106 (2001).
38. K. Kinugawa *et al.*, *Circ. Res.* **89**, 591 (2001).

39. This work was supported by grants from the NIH and the Donald W. Reynolds Cardiovascular Clinical Research Center to E.N.O. We thank C. Plato at Gilead Colorado (Westminster, CO) for providing human and rat RNA samples, M. Arnold for advice, and J. Shelton, J. McAnally, and C. Nolen for technical assistance.

Supporting Online Material
www.sciencemag.org/cgi/content/full/1139089/DC1
Materials and Methods
Figs. S1 to S7
Tables S1 and S2
References

20 December 2006; accepted 7 March 2007
Published online 22 March 2007;
10.1126/science.1139089
Include this information when citing this paper.

REPORTS

Environment-Induced Sudden Death of Entanglement

M. P. Almeida, F. de Melo, M. Hor-Meyll, A. Salles, S. P. Walborn, P. H. Souto Ribeiro, L. Davidovich*

We demonstrate the difference between local, single-particle dynamics and global dynamics of entangled quantum systems coupled to independent environments. Using an all-optical experimental setup, we showed that, even when the environment-induced decay of each system is asymptotic, quantum entanglement may suddenly disappear. This "sudden death" constitutes yet another distinct and counterintuitive trait of entanglement.

The real-world success of quantum computation and communication relies on the longevity of entanglement in multiparticle quantum states. The presence of decoherence (*10*) in communication channels and computing devices, which stems from the unavoidable interaction between these systems and the environment, degrades the entanglement when the particles propagate or the computation evolves. Decoherence leads to local dynamics, associated with single-particle dissipation, diffusion, and decay, as well as to global dynamics, which may provoke the disappearance of entanglement at a finite time (*11*–*15*). This phenomenon, known as "entanglement sudden death," is strikingly different from single-particle dynamics, which occurs asymptotically, and has been studied in recent theoretical work (*11*–*15*). Here we demonstrate the sudden death of entanglement of a two-qubit system under the influence of independent environ-

Instituto de Física, Universidade Federal do Rio de Janeiro, Caixa Postal 68528, Rio de Janeiro, RJ 21941-972, Brazil.
*To whom correspondence should be addressed. E-mail: ldavid@if.ufrj.br

ments. Our all-optical setup allows for the controlled investigation of a variety of dynamical maps that describe fundamental processes in quantum mechanics and quantum information.

Consider a two-level quantum system S (upper and lower states $|e\rangle$ and $|g\rangle$, respectively) under the action of a zero-temperature reservoir R. At zero temperature, the reservoir R is in the $|0\rangle_R$ (vacuum) state, and the S-R interaction can be represented by a quantum map, known as the amplitude decay channel (*1*)

$$|g\rangle_S|0\rangle_R \rightarrow |g\rangle_S|0\rangle_R$$
$$|e\rangle_S|0\rangle_R \rightarrow \sqrt{1-p}\,|e\rangle_S|0\rangle_R + \sqrt{p}\,|g\rangle_S|1\rangle_R \quad (1)$$

Under this map, the lower state $|g\rangle$ is not affected while the upper state $|e\rangle$ either decays to $|g\rangle$ with probability p, creating one excitation in the environment (state $|1\rangle_R$), or remains in $|e\rangle$, with probability $1-p$. This would be the situation, for instance, in the spontaneous emission of a two-level atom. In this case, the state $|1\rangle_R$ would correspond to one photon in the reservoir. Under the Markovian approximation, $p = 1 - \exp(-\Gamma t)$, that is, the decay probability approaches unity exponentially in time. As an initial pure state $a|e\rangle + b|g\rangle$ decays, it gets entangled with the environment, gradually losing its coherence and its purity over time. Complete decay only occurs asymptotically in time ($p \rightarrow 1$ when $t \rightarrow \infty$), when the two-level system is again described by the pure state $|g\rangle$. Note that the map in Eq. 1 encompasses several other kinds of dynamics, which differ only by the time dependence of the parameter p.

Now consider two entangled qubits that decay according to this map. How does the entanglement of the two-qubit system evolve? Does it mimic the asymptotic decay of each qubit, disappearing at $t \rightarrow \infty$, or does it disappear at some finite time? This question has been explored theoretically (*11–15*), but up to now there has been no experimental investigation of the relation between the global entanglement dynamics and the local decay of the constituent subsystems.

To answer these questions, one first needs a formal definition of entanglement. A two-qubit pure state is entangled, or nonseparable, if and only if the total state cannot be expressed as a product of the individual qubit states, $|\psi\rangle \neq |\phi_1\rangle \otimes |\varphi_2\rangle$. Likewise, a mixed bipartite state represented by a density matrix ρ is separable if and only if it can be written as a convex sum of products of individual density matrices, $\rho = \sum_i p_i \rho_i^{(1)} \otimes \rho_i^{(2)}$, with $0 \le p_i \le 1$. A convenient measure of entanglement for a two-qubit state ρ is the concurrence C (*16*), given by

$$C = \max\{0, \Lambda\} \quad (2)$$

where

$$\Lambda = \sqrt{\lambda_1} - \sqrt{\lambda_2} - \sqrt{\lambda_3} - \sqrt{\lambda_4} \quad (3)$$

and the quantities λ_i are the positive eigenvalues, in decreasing order, of the matrix

$$\rho(\sigma_y \otimes \sigma_y)\rho^*(\sigma_y \otimes \sigma_y) \quad (4)$$

where σ_y is the second Pauli matrix and the conjugation occurs in the computational basis $\{|00\rangle, |01\rangle, |10\rangle, |11\rangle\}$. C quantifies the amount of quantum correlation that is present in the system and can assume values between 0 (only classical correlations) and 1 (maximal entanglement).

For the dynamics given by Eq. 1 and an initial state of the form $|\Phi\rangle = \alpha|gg\rangle + \beta\exp(i\delta)|ee\rangle$, the entanglement decay dynamics depends on the relation between α and β (*14*). Concurrence in this case is given by

$$C = \max\{0, 2(1-p)|\beta|(|\alpha| - p|\beta|)\} \quad (5)$$

From this expression, one can see that for $|\beta| \le |\alpha|$, entanglement disappears only when the individual qubits have completely decayed ($p = 1$), whereas for $|\beta| > |\alpha|$, entanglement disappears for $p = |\alpha/\beta| < 1$, which corresponds to a finite time. This phenomenon has been called "entanglement sudden death" (*15*). Because the concurrence of the initial state ($p = 0$) is $C = 2|\alpha\beta|$, the entanglement dynamics of two states with the same initial concurrence can be quite different.

Photons are a useful experimental tool for demonstrating these properties and, more generally, for studying quantum channels like the one given in Eq. 1, as the decoherence mechanisms can be implemented in a controlled manner. Let us associate the H and V polarizations of a photon, respectively, to the ground and excited states of the two-level system S. The reservoir R in turn is represented by two different momentum modes of the photon.

Figure 1A shows a Sagnac-like interferometer that implements the amplitude-decay channel for a single qubit. A photon, initially in the incoming part of mode a, is split into its horizontal (H) and vertical (V) polarization components by a polarizing beam splitter (PBS1). Let us ignore the half-wave plates HWP1 and HWP0 momentarily. The V-polarization component is reflected and propagates through the interferometer in the clockwise direction, and, if unaltered, reflects through PBS1 into the outgoing part of mode a. The H-polarization component is transmitted and propagates through the interferometer in the counterclockwise direction and transmits through PBS1 also into the outgoing part of mode a (*17*). The interferometer is aligned so that the two paths are spatially separated, making it possible to manipulate the H and V polarization components independently.

To realize the amplitude decay given in Eq. 1, we use HWP1 to rotate the polarization of the V component to $\cos(2\theta)|V\rangle + \sin(2\theta)|H\rangle$, where θ is the angle of HWP1. Suppose that an incoming photon is V-polarized. When this photon exits the interferometer through PBS1, it is transmitted into mode b with probability $p = \sin^2(2\theta)$ and reflected into mode a with prob-

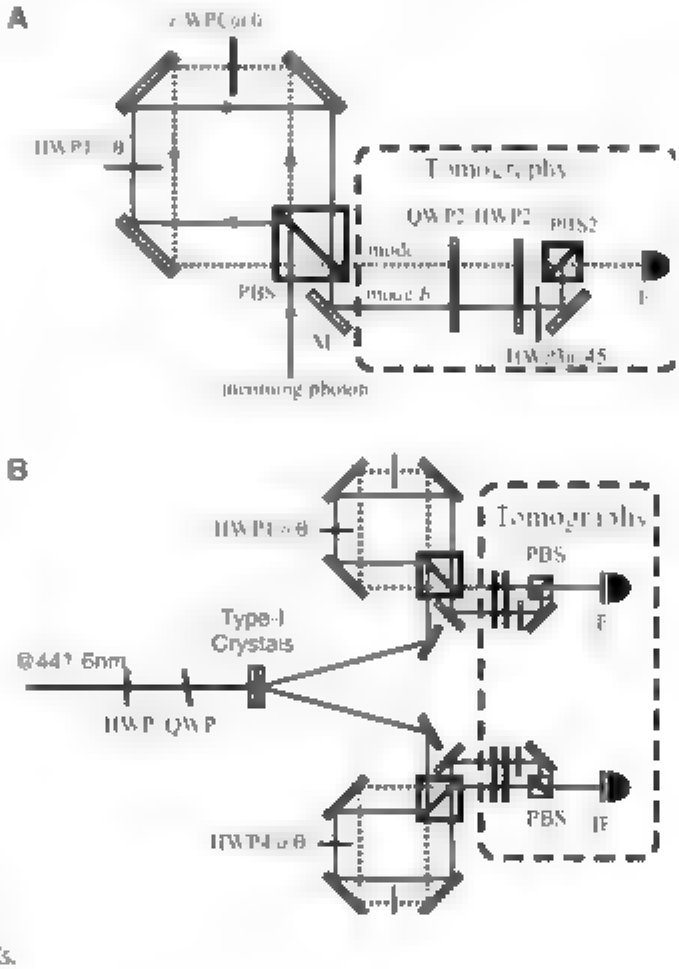

Fig. 1. Experimental setup. (**A**) Amplitude decay channel for a single photonic qubit. Because of the polarized beam splitter PBS1, the H and V components of polarized photons respectively propagate along counterclockwise and clockwise paths within the interferometer. With half-wave plate HWP1 set at 0°, they are coherently recombined into the outgoing spatial mode a, which represents the "vacuum state" of the reservoir. For other angles of HWP1, the V component undergoes a rotation, corresponding to its probabilistic "decay" into the H component, which PBS1 sends to outgoing mode b, representing the "one-excitation state" of the reservoir. Wave plates HWP2 and QWP2, together with PBS2, are used for tomography of the polarization state of outgoing modes a and b, which are recombined incoherently on PBS2 through HWP3 and are sent to the same detector. IF is an interference filter. (**B**) Amplitude decay channel applied to entangled qubits. The entangled state is generated by parametric down-conversion in type I nonlinear crystals.

ability $\cos^2(2\theta)$. This evolution can thus be described by $|V\rangle|0\rangle_a \rightarrow \sqrt{(1-p)}|V\rangle|0\rangle_a + \sqrt{p}|H\rangle|0\rangle_b$. Identifying the outgoing modes a and b (which correspond to orthogonal spatial modes) as the states of the reservoir with zero and one excitation, respectively, this operation is equivalent to that on the $|1\rangle|0\rangle_R$ state in Eq. 1. An incoming H-polarized photon is left untouched, corresponding to the first line in Eq. 1. This process therefore realizes the amplitude decay channel and is identical to the decay of a two-level system. Half-wave plate HWP0, oriented at 0°, is used solely to match the lengths of the two optical paths. The path lengths are adjusted so that if HWP1 is oriented at 0°, the polarization state in mode a after the interferometer is exactly the same as the input state. Photons in modes a and b are then directed to the same quantum state tomography (QST) system (18), composed of quarter-wave plate QWP2, half-wave plate HWP2, and polarizing beam splitter PBS2, and then registered using a single-photon detector equipped with a 10-nm (full width at half maximum) interference filter and a 1.5-mm-diameter aperture. Mode b is recombined incoherently with mode a on PBS2, so that both modes can be detected with a single detector. This is achieved by assuring that the path length difference between modes a and b is greater than the coherence length of the photons, which is determined by the width of the interference filters (~0.1 mm). The half-wave plate HWP3, aligned at 45°, transforms H-polarized photons into V-polarized ones. Because PBS2 transmits H-polarization and reflects V-polarization, the combination of HWP3 and PBS2 reflects photons that were originally H-polarized. This assures that the QST performed is identical for both modes a and b.

Using the interferometer described above, we studied both the decay of a single qubit and the dynamics of two entangled two-level systems interacting with independent amplitude-decay reservoirs. In the experimental setup (Fig. 1B), polarization-entangled photon pairs with wavelength centered around 884 nm were produced using a standard source (19) composed of two adjacent type-I $LiIO_3$ nonlinear crystals pumped by a 441.6-nm continuous-wave He-Cd laser. One crystal produces photon pairs with V-polarization and the other produces pairs with H-polarization. After propagation and spatial mode filtering, the H and V modes are spatially indistinguishable, and a photon pair is described by the pure state $|\Phi\rangle = \alpha|HH\rangle + \beta\exp(i\delta)|VV\rangle$ with high fidelity. A half-wave plate and a quarter-wave plate placed in the pump beam (Fig. 1B, left) allow the control of the coefficients α and β and the relative phase δ of the state (19).

The decay of a single qubit was investigated experimentally for both H- and V-polarized photons by generating states $|VV\rangle$ and $|HH\rangle$ and registering coincidence counts, with one photon propagating through the interferometer and the other serving as a trigger. The coincidence detection window ($\tau_c \approx 5$ ns ~ 1.5 m) was larger than the path difference between outgoing modes a and b (~5 cm). Figure 2A shows $P_V(V)$, $P_H(V)$, $P_V(H)$, and $P_H(H)$ as a function of p, where $P_J(K)$ is the probability of finding an input K-polarized photon in the J state after the interferometer. The linear behavior in p is characteristic of exponential decay in t, if $p = 1 - \exp(-\Gamma t)$.

For the investigation of entanglement dynamics, nonmaximally entangled states were produced and each photon was sent to a separate interferometer, which implemented an amplitude-damping reservoir, and then to a QST system. The half-wave plates HWP1 and HWP4 were set to the same angle θ, so that the reservoirs, although independent, acted with the same probability p. QST of the two-photon state followed the usual recipe of 16 coincidence measurements (18). Each measurement lasted 90 s, giving an average of about 250 coincidence events. We repeated the same procedure for different values of p, obtaining the tomographic reconstruction of the output two-photon polarization state in all cases. The concurrence was calculated using Eqs. 2 and 3. In all figures, horizontal error bars represent uncertainty in aligning the wave plates, and vertical error bars correspond to the standard deviations of Monte Carlo samples obtained from randomly generated counts following the statistics of the experimental data (20).

Figure 2B displays the concurrence and the quantity Λ, given by Eq. 3, as a function of the decay probability p, for two initial states that, although not pure, are very close to $|\Phi\rangle = \alpha|HH\rangle + \beta\exp(i\delta)|VV\rangle$; state I, defined by $|\beta|^2 = |\alpha|^2/3$ (triangles), and state II, defined $|\beta|^2 = 3|\alpha|^2$ (squares). Tomography of the initial states I and II showed them to have the same concurrence (~0.8) and similar purity (~0.91 to 0.97). The theoretical curves were obtained by applying Eq. 1 to the experimentally determined initial states, which correspond to $p = 0$. For initial state I, entanglement disappears asymptotically, and the concurrence goes to zero only when both individual systems have decayed completely ($p = 1$).

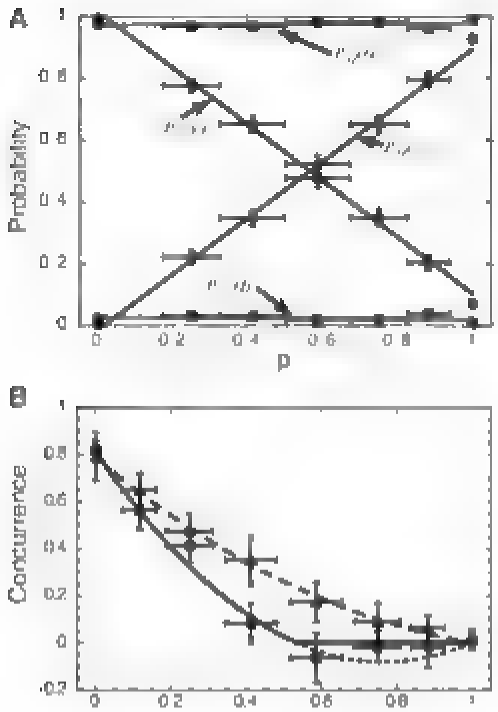

Fig. 2. Results for amplitude decay channel. **(A)** Experimental amplitude decay for a single qubit. $P_V(V)$ and $P_H(V)$ are the probabilities of detecting an input V-polarized photon in the V and H states, respectively; $P_V(H)$ and $P_H(H)$ are the probabilities for an input H-polarized photon. The points correspond to experimental data, and the lines are linear fits. **(B)** Entanglement decay as a function of the probability p. The squares correspond to experimentally obtained values of Λ for the case $|\beta|^2 = 3|\alpha|^2$. The solid line is the theoretical prediction of the concurrence for this state, given by Eq. 2; the dotted line shows the value of Λ, given by Eq. 3. The triangles are experimental values of Λ for the case $|\beta|^2 = |\alpha|^2/3$, and the dashed line is the theoretical prediction for Λ and C, which are equivalent for this state.

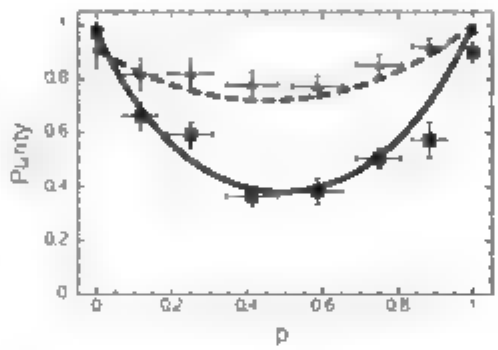

Fig. 3. Purity as a function of p for the amplitude damping channel. The squares correspond to experimentally obtained values of the purity for the case $|\beta|^2 = 3|\alpha|^2$; the solid line is the theoretical prediction. The triangles are experimental values of the purity for the case $|\beta|^2 = |\alpha|^2/3$, and the dashed line is the corresponding theoretical prediction.

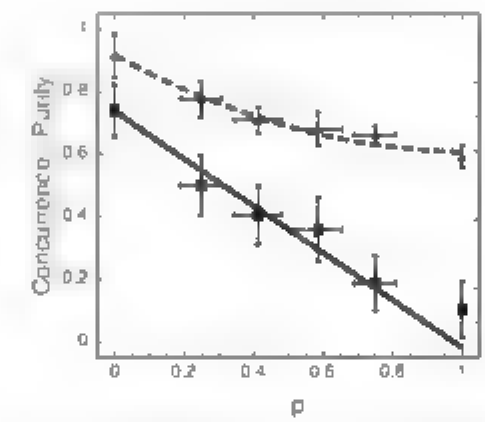

Fig. 4. Experimental results for the dephasing reservoir. Concurrence (squares) and purity (triangles) are shown for the case $|\beta|^2 = 3|\alpha|^2$. The solid line is the corresponding theoretical prediction for concurrence, given by Eq. 2. The dashed line is the theoretical prediction for purity, given by $\mathrm{tr}\rho^2$. The concurrence goes to zero asymptotically.

For initial state II, however, the entanglement behaves very differently. The concurrence goes to zero for $p < 1$, thus demonstrating "entanglement sudden death." We stress that the onset of separability ($C = 0$) occurs at the same point for all entanglement quantifiers and is not a particular artifact of the concurrence.

It is also illustrative to study the purity, defined as trρ^2, as a function of the decay probability (Fig. 3) for states I and II. In both cases the purity reaches a minimum but is restored when $p = 1$, when all photons have "decayed" to the H-polarization state. State II is more mixed than state I in the intermediate stages of this process because it has a larger $|1'\rangle$ component and thus becomes more entangled with the environment.

To further illustrate the usefulness of the present scheme for studying decoherence of entangled systems, we performed a second experiment studying the phase-damping channel, described by the map (*1*):

$$|0\rangle_S\otimes|0\rangle_R \rightarrow |0\rangle_S\otimes|0\rangle_R$$
$$|1\rangle_S\otimes|0\rangle_R \rightarrow \sqrt{1-p}\,|1\rangle_S\otimes|0\rangle_R + \sqrt{p}\,|1\rangle_S\otimes|1\rangle_R \quad (6)$$

This map could represent elastic scattering between atom and reservoir. States $|0\rangle$ and $|1\rangle$ are not changed by the interaction, but any coherent superposition of them gets entangled with the reservoir. There is no longer decay, but only loss of coherence between ground and excited states. The dephasing map can be implemented with the same interferometer through the addition of an extra HWP at 45° in mode b before the QST system (or, equivalently, through the removal of HWP3 and redefinition of the QST measurements). For the dephasing channel, pure states I and II present identical behavior, becoming completely disentangled only when $p = 1$. Figure 4 shows the concurrence (squares) and bipartite purity (triangles) as a function of p for the entangled state II.

In demonstrating the sudden disappearance of the entanglement of a bipartite system, induced by the interaction with an environment, our results show that entangled states with the same initial concurrence may exhibit, for the same reservoir, either an abrupt or an asymptotic disappearance of entanglement, even though the constituents of the system always exhibit an asymptotic decay. We have explicitly shown that this behavior also depends on the characteristics of the reservoir through two examples corresponding to amplitude decay and dephasing. The experimental setup represents a reliable and simple method for studying the dynamics of entangled systems interacting with controlled environments.

References and Notes

1. M. Nielsen, I. Chuang, *Quantum Computation and Quantum Information* (Cambridge Univ. Press, Cambridge, 2000).
2. C. H. Bennett, D. P. DiVincenzo, *Nature* **404**, 247 (2000).
3. C. H. Bennett, G. Brassard, *Proceedings of the International Conference on Computer Systems and Signal Processing, Bangalore, India* (IEEE, New York, 1984), pp. 175–179.
4. A. K. Ekert, *Phys. Rev. Lett.* **67**, 661 (1991).
5. N. Gisin, G. Ribordy, W. Tittel, H. Zbinden, *Rev. Mod. Phys.* **74**, 145 (2002).
6. C. H. Bennett *et al.*, *Phys. Rev. Lett.* **70**, 1895 (1993).
7. D. Bouwmeester *et al.*, *Nature* **390**, 575 (1997).
8. D. Boschi, S. Branca, F. DeMartini, L. Hardy, S. Popescu, *Phys. Rev. Lett.* **80**, 1121 (1998).
9. L.-M. Duan, M. D. Lukin, J. I. Cirac, P. Zoller, *Nature* **414**, 413 (2001).
10. W. H. Zurek, *Rev. Mod. Phys.* **75**, 715 (2003).
11. L. Diósi, in *Irreversible Quantum Dynamics*, F. Benatti, R. Floreanini, Eds. (Springer, Berlin, 2003), pp. 157–164.
12. P. J. Dodd, J. J. Halliwell, *Phys. Rev. A* **69**, 052105 (2004).
13. T. Yu, J. H. Eberly, *Phys. Rev. Lett.* **93**, 140404 (2004).
14. M. F. Santos, P. Milman, L. Davidovich, N. Zagury, *Phys. Rev. A* **73**, 040305 (2006).
15. T. Yu, J. H. Eberly, *Phys. Rev. Lett.* **97**, 140403 (2006).
16. W. K. Wootters, *Phys. Rev. Lett.* **80**, 2245 (1998).
17. A similar configuration, but with the addition of cylindrical lenses, was used to realize a direct measurement of entanglement for a pure state in (*21*).
18. D. F. V. James, P. G. Kwiat, W. J. Munro, A. G. White, *Phys. Rev. A* **64**, 052312 (2001).
19. P. G. Kwiat, E. Waks, A. G. White, I. Appelbaum, P. H. Eberhard, *Phys. Rev. A* **60**, R773 (1999).
20. J. B. Altepeter, E. R. Jeffrey, P. G. Kwiat, in *Advances in Atomic, Molecular and Optical Physics*, P. Berman, C. Lin, Eds. (Elsevier, San Diego, CA, 2005), vol. 52, pp. 107–161.
21. S. P. Walborn, P. H. S. Ribeiro, L. Davidovich, F. Mintert, A. Buchleitner, *Nature* **440**, 1022 (2006).

22. Supported by the Brazilian funding agencies CNPq, CAPES, PRONEX, FUJB, and FAPERJ. This work was performed as part of the Brazilian Millennium Institute for Quantum Information.

12 January 2007; accepted 20 March 2007
10.1126/science.1139892

Enantioselective Organocatalysis Using SOMO Activation

Teresa D. Beeson,[1,2] Anthony Mastracchio,[1,2] Jun-Bae Hong,[1,2] Kate Ashton,[1,2] David W. C. MacMillan[1,2]*

The asymmetric α addition of relatively nonpolar hydrocarbon substrates, such as allyl and aryl groups, to aldehydes and ketones remains a largely unsolved problem in organic synthesis, despite the wide potential utility of direct routes to such products. We reasoned that well-established chiral amine catalysis, which activates aldehydes toward electrophile addition by enamine formation, could be expanded to this important reaction class by applying a single-electron oxidant to create a transient radical species from the enamine. We demonstrated the concept of singly occupied molecular orbital (SOMO) activation with a highly selective α-allylation of aldehydes, and we here present preliminary results for enantioselective heteroarylations and cyclization/halogenation cascades.

Over the past four decades, the capacity to induce asymmetric transformations with enantioselective catalysis has remained a focal point for extensive research efforts in both industrial and academic settings. During this time, thousands of asymmetric catalytic reactions have been invented (*1*), in accord with the increasing need for enantiopure medicinal agents and the rapid advancement of the field of asymmetric synthesis. Most catalytic enantioinductive processes are derived from a small number of long-established activation modes. Activation modes such as Lewis acid catalysis (*2*), σ-bond insertion (*3*), π-bond insertion (*4*), atom transfer catalysis (*5*), and hydrogen bonding catalysis (*6*) have each spawned countless asymmetric reaction classes, thereby dramatically expanding the synthetic toolbox available to researchers in the physical and biological sciences. A necessary objective, therefore, for the continued advancement of the field of chemical synthesis is the design and implementation of distinct catalytic-activation modes that enable previously unknown transformations.

Over the past 8 years, our laboratory has been involved in the development of the field of organocatalysis, a research area that relies on the use of small organic molecules as catalysts for enantioselective transformations. As part of these studies, we introduced the concept of iminium catalysis (*7*): an enal or enone activation mode that lowers the energy of the substrate's lowest unoccupied molecular orbital, facilitating enantioselective C-C and C-N conjugate additions, cycloadditions, hydrogenations, and Friedel-Crafts alkylations (*8*). Simultaneously, Barbas and List (*9*) brought to fruition the concept of enamine catalysis (Fig. 1), which raises the energy of the highest occupied molecular orbital (HOMO) in aldehydes and ketones to promote enantioselective α-carbonyl functionalization with a large range of electrophiles (*10*). These two modes of catalyst activation (iminium and enamine) have provided, in total, more than 60 asymmetric methodologies over the past 7 years

[1]Merck Center for Catalysis, Department of Chemistry, Princeton University, Princeton, NJ 08544, USA. [2]Division of Chemistry and Chemical Engineering, California Institute of Technology, Pasadena, CA 91125, USA.

*To whom correspondence should be addressed. E-mail: dmacmil@princeton.edu

Given the established capacity of enamines and iminium ions to rapidly interconvert via a redox process (enamine has four π electrons and iminium has two π electrons), we recently questioned whether it might be possible to interrupt this equilibrium chemically and thereby to access a mode of catalytic activation that electronically bisects enamine and iminium formation. More specifically, we hypothesized that a one-electron oxidation of a transient enamine species (Fig. 2A) should generate a three π-electron radical cation with a singly occupied molecular orbital (SOMO) that is activated toward a range of enantioselective catalytic transformations not currently possible with established catalysis concepts.

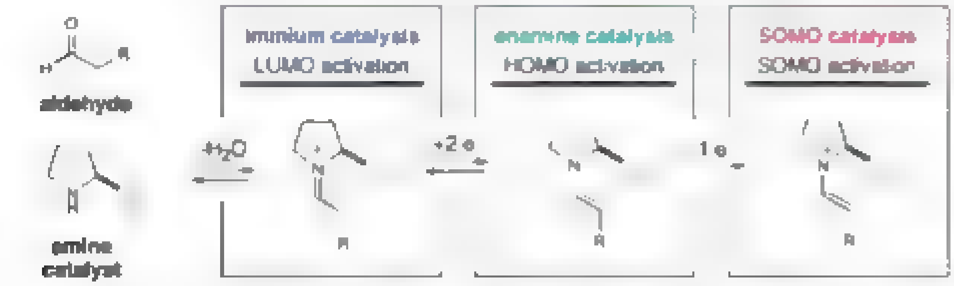

Fig. 1. SOMO catalysis via single-electron oxidation of a transiently formed enamine. LUMO, lowest unoccupied molecular orbital; R, an arbitrary organic substituent.

Table 1. Representative SOMO catalysis. Enantioselective aldehyde α-allylation is shown. Bz, benzoyl; Boc, *tert*-butyl carbamoyl; Et, ethyl.

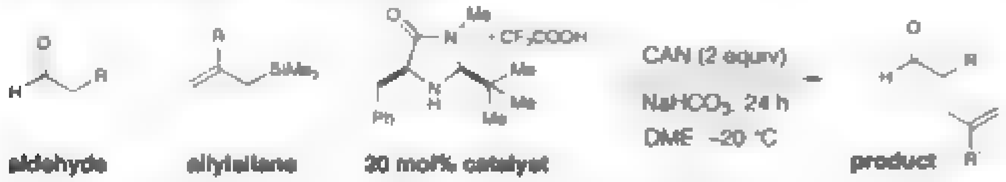

entry	aldehyde / product*	entry	aldehyde / product*
1	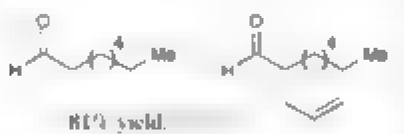 81% yield, [illegible]	4	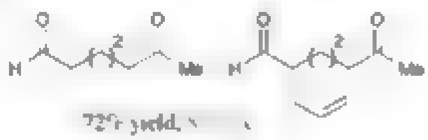 72% yield, [illegible]
2	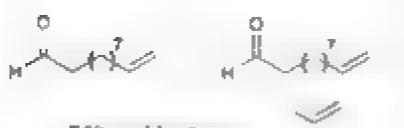 75% yield, [illegible]	5	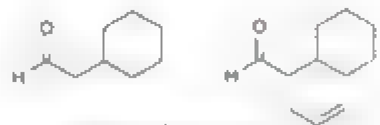 75% yield† [illegible]
3	 72% yield	6	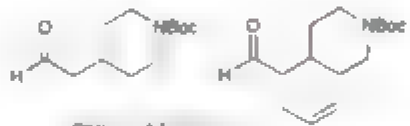 70% yield
entry	**allylsilane / product‡**	**entry**	**allylsilane / product‡**
7	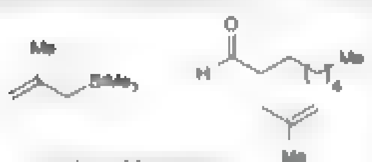 80% yield, [illegible]	9	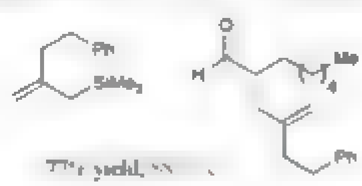 77% yield, [illegible]
8	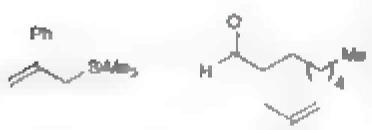 87% yield, [illegible]	10	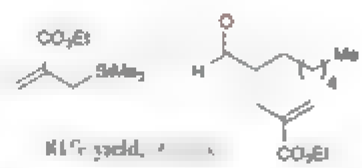 81% yield, [illegible]

*Reactions performed with allylsilane ($CH_2{=}CHCH_2SiMe_3$). †Yield determined by gas chromatographic analysis. ‡Reactions performed with octanal.

From the outset, we identified three key design elements to substantiate this proposal. First, we recognized the mechanistic requirement that an equilibrium population of enamine must undergo selective oxidation in the presence of an amine catalyst, an aldehyde substrate, and an iminium ion precursor. Theoretical support for such a chemoselective pathway was derived from the ionization potentials (IPs) of 1-(but-1-enyl)pyrrolidine (IP = 7.2 eV), pyrrolidine (IP = 8.8 eV), and butanal (IP = 9.8 eV) — data that reveal the transient enamine component to be sufficiently more susceptible to oxidation than the accompanying reaction partners (*11*, *12*).

Second, we understood that the widespread application of SOMO catalysis would require the identification of an amine catalyst that could generically enforce high levels of enantiocontrol in the coupling of the pivotal radical cation with a variety of π-rich nucleophiles. On the basis of density functional theory (DFT) calculations (*13*, *14*), we proposed that the imidazolidinone catalyst **1** (*8*) should selectively form a SOMO-activated cation, **DFT-2**, that projects the three π-electron system away from the bulky tert-butyl group, while the radical-centered carbon selectively populates an E configuration to minimize nonbonding interactions with the imidazolidinone ring (Fig. 2B). In terms of enantiofacial discrimination, the calculated **DFT-2** structure also reveals that the benzyl group on the catalyst system should effectively shield the *re* face of the radical cation, leaving the *si* face exposed for enantioselective bond formation.

Third, we knew that the intrinsic value of this activation mode would be defined by its capacity to enable useful enantioselective reactions. Radical cations show great potential in this vein, because they already participate in many noncatalytic C–C, C–O, C–N, C–S, and C–X (where X is a halogen) bond formations (*15*–*19*). Our analysis reveals the attractive prospect of applying asymmetric SOMO catalysis to important problems such as direct and enantioselective allylic alkylation, enolation, arylation, carbo-oxidation, vinylation, alkynylation, or intermolecular alkylation of aldehydes.

To test this activation concept, we selected the direct and enantioselective allylic alkylation of aldehydes as a representative transform (*20*, *21*). We recognized that the accompanying allylation products have been established as important chiral synthons in chemical synthesis (*22*, *23*). Experimentally, this allylation protocol was first examined in dimethoxy ethane (DME) solvent with octanal, imidazolidinone catalyst **1**,

ceric ammonium nitrate (CAN) as the stoichiometric oxidant, and allyltrimethylsilane as the SOMO nucleophile (Table 1) (24). Preliminary studies revealed the successful execution of our design ideas to provide (R)-2-allyl-octanal with excellent levels of enantioinduction and in good conversion [Table 1, entry 1, 81% yield, 91% enantiomeric excess (ee)]. Experiments that probed the scope of the aldehyde component in this reaction are summarized in Table 1, entries 1 to 6. There appears to be substantial latitude in the steric demand of the radical-cation substituent (compare entries 1 and 5, with the substituent being hexyl versus cyclohexyl), allowing access to a broad variety of 2-alkyl-substituted-4-pentenals (75 to 81% yield, 91 to 94% ee). Moreover, a variety of chemical functionalities appear to be inert under these mild oxidative conditions, including olefins, ketones, esters, and carbamates (entries 2 to 4 and 6, 70 to 75% yield, 87 to 95% ee).

Additionally, Table 1 reveals that a diverse array of π-rich olefinic silanes (25) will readily participate as allylic alkylating reagents in this catalytic protocol (entries 1 and 7 to 10). For example, methyl, phenyl, and 2-alkyl substituted allylsilanes can be tolerated without losses in reaction efficiency or enantiocontrol (entries 7 to 9; 77 to 88% yield, 88 to 91% ee). The electron-deficient olefin ethyl-2-(methyl-trimethylsilyl)-acrylate also functions effectively as a SOMO nucleophile to provide the corresponding alkylated adduct in 81% yield and 90% ee (entry 10). This last result provides circumstantial evidence for the generation and participation of a radical-cation species, given the capacity of ethyl-2-(methyl-trimethylsilyl)-acrylate to function as a viable SOMO nucleophile on account of the captodative effect (26), yet not as effectively as a HOMO nucleophile because of diminished π density at the olefin terminus. The sense of asymmetric induction observed in all cases (Table 1) is consistent with selective engagement of the allylsilane substrate with the *Si* face of the SOMO-activated species **2**, in complete accord with the calculated structure DFT-**2**.

A survey of reaction media for this organocatalytic allylation has revealed that a variety of solvents may be used without a substantial loss in reaction efficiency, provided that water is present as an addend (27). Although the use of DME provides optimal selectivity, reaction rate, and chemical yield (28), acetone can often be used as an alternative solvent without alkylation of the bulk medium (29). Moreover, extended reaction times do not lead to product epimerization or the formation of α,α-dialkylaldehydes or aldehyde dimerization adducts.

To highlight the anticipated broad scope of SOMO activation, we present preliminary results for the enantioselective α-heteroarylation of aldehydes (Fig. 3A). Specifically, exposure of octanal and N-tert-butyl carbamoyl pyrrole to our SOMO activation conditions enables formyl α-arylation with useful levels of enantioselectivity and excellent yields. Moreover, we have found that unsaturated aldehydes rapidly undergo enantioselective cyclization with trapping of an exogenous halide. As revealed in Fig. 3B, activation of *cis*-6-nonenal with our SOMO protocol in the presence of LiCl leads to the formation of a stereochemically dense cyclopentyl ring system with excellent stereocontrol [85% yield, >10:1 diastereomeric ratio (dr), 95% ee]. This latter result again provides circumstantial evidence for the generation and participation of a radical-cation species, given the propensity of radicals to undergo cyclization with unactivated olefins.

We have undertaken studies to more definitively investigate the participation of the putative radical-cation intermediate in this catalytic process. Specifically, aldehyde activation-addition experiments were performed with the vinyl cyclopropane substrate **3**, an established radical clock that was designed by Newcomb *et al.* (30) to differentiate between radical-mediated pathways and cationic mechanisms (Fig. 3C). Addition of the activated aldehyde intermediate to the olefin **3** occurs with subsequent scission of the benzylic cyclopropyl bond and not the α-methoxy cyclopropyl bond. This result is in complete accord with a radical pathway and not a cationic addition mechanism.

These results highlight the substantial scope of SOMO activation for useful transformations in organic synthesis. We anticipate a wide range of applications for pharmaceutically important compounds and intermediates. After our initial submission of this work, a similar approach was also applied to aldehyde α-oxidation (31).

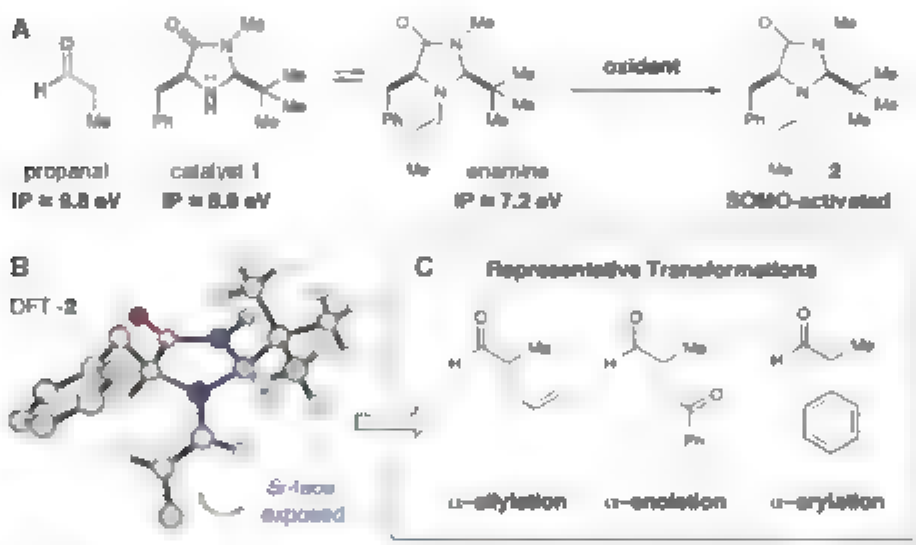

Fig. 2. **(A)** Catalytic chemical steps leading to formation of the SOMO-activated intermediate. Me, methyl; Ph, phenyl. **(B)** DFT-calculated three-dimensional structure of the enantio-differentiated radical cation. **(C)** Possible transformations arising from enantioselective organocatalytic SOMO catalysis.

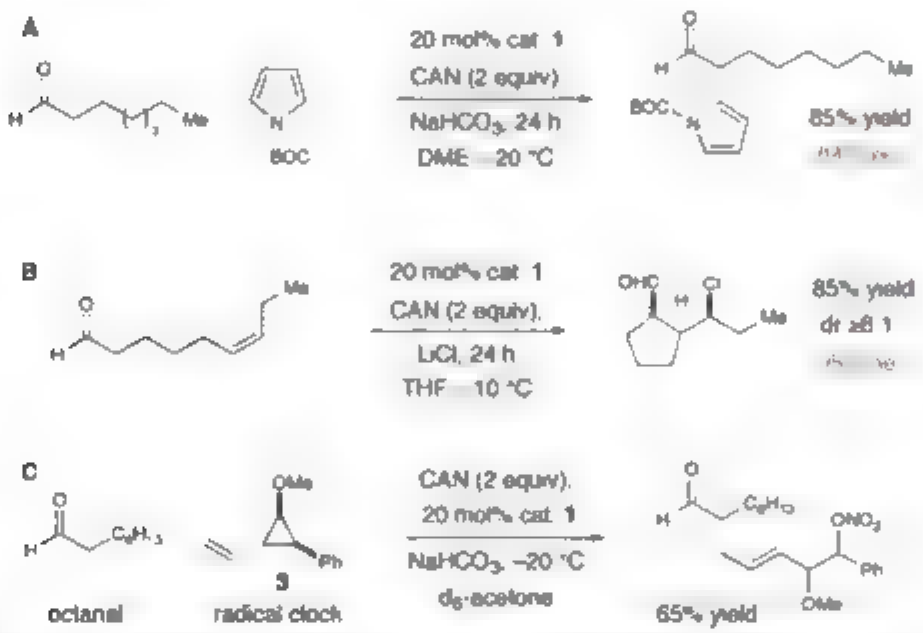

Fig. 3. **(A)** Enantioselective α-heteroarylation of aldehydes via SOMO catalysis. CAN, ceric ammonium nitrate. **(B)** Enantioselective olefin cyclization via SOMO catalysis. THF, tetrahydrofuran. **(C)** Mechanistic investigation to determine the intermediacy of a radical cation versus a carbocation.

References and Notes

1. E. N. Jacobsen, A. Pfaltz, H. Yamamoto, Eds., *Comprehensive Asymmetric Catalysis* (Springer, Berlin 1999), vol. 1 to 3
2. H. Yamamoto, Ed., *Lewis Acids in Organic Synthesis* (Wiley-VCH, New York, 2000)
3. R. H. Crabtree, *The Organometallic Chemistry of the Transition Metals* (Wiley-Interscience, Hoboken, NJ, ed. 4, 2005)
4. R. Noyori, in *Asymmetric Catalysis in Organic Synthesis* (Wiley-Interscience, New York, 1994), pp. 123–173
5. I. Ojima, Ed., in *Catalytic Asymmetric Synthesis* (Wiley-VHC, New York, ed. 2, 2000), chap. 6
6. M. S. Taylor, E. N. Jacobsen, *Angew. Chem. Int. Ed.* **45** 1520 (2006)
7. K. A. Ahrendt, C. J. Borths, D. W. C. MacMillan, *J. Am. Chem. Soc.* **122**, 4243 (2000).
8. G. Lelais, D. W. C. MacMillan, *Aldrichim. Acta* **39**, 79 (2006), and references therein
9. B. List, R. A. Lerner, C. F. Barbas III, *J. Am. Chem. Soc.* **122**, 2395 (2000)
10. B. List, *Chem. Commun.* **2006**, 819 (2006) and references therein
11. K. Müller, F. Previdoli, H. Desilvestro, *Helv. Chim. Acta* **64**, 2497 (1981).
12. D. R. Lide, Ed., in *Handbook of Chemistry and Physics* (CRC Press, New York, ed. 76, 1995), pp. 220–221.
13. DFT calculations were performed at the B3LYP/6-311+G(2d,p)//B3LYP/6-31G(d) level of theory using Gaussian 03 software (*14*)
14. M. J. Frisch *et al.*, Gaussian 03 software (Gaussian, Wallingford, CT, 2004)
15. K. Narasaka, T. Okauchi, K. Tanaka, M. Murakami, *Chem. Lett. (Jpn.)* **92**, 2099 (1992)
16. M. Kirchgessner, K. Sreenath, K. R. Gopidas, *J. Org. Chem.* **71**, 9849 (2006
17. A. Sutterer, K. D. Moeller, *J. Am. Chem. Soc.* **122**, 5636 (2000
18. H. B. Lee, M. J. Sung, S. C. Blackstock, J. K. Cha, *J. Am. Chem. Soc.* **123**, 11322 (2001)
19. P. Renaud, M. P. Sibi, Eds., *Radicals in Organic Synthesis* (Wiley-VCH, Weinheim, Germany, 2001), vol. 2, pp. 144–205
20. Organocatalysis in combination with organometallic catalysis has previously been applied to the nonasymmetric allylation of aldehydes.
21. I. Ibrahem, J. A. Córdova, *Angew. Chem. Int. Ed.* **45** 1952 (2006)
22. B. M. Trost, M. L. Crawley, *Chem. Rev.* **103**, 2921 (2003).
23. J. Seyden-Penne, in *Chiral Auxiliaries and Ligands in Asymmetric Synthesis* (Wiley-Interscience, New York, 1995), pp. 166–195
24. Materials and methods are available as supporting online material on *Science* Online
25. Mechanistically, we speculate that addition of the π-rich allylsilane to the radical cation species results in the formation of a β-silyl radical that undergoes rapid oxidation to the corresponding β-silyl cation before silyl elimination with concomitant olefin formation
26. H. G. Viehe, R. Merényi, Z. Janousek, *Pure Appl. Chem.* **60**, 1635 (1988)
27. The introduction of 1 to 5 equivalents of water is required to achieve useful levels of reaction efficiency in most solvents (e.g., ethyl acetate, tetrahydrofuran, and CH_2Cl_2)
28. Bench-grade DME was found to contain sufficient water to achieve optimal results. The exclusion of water by the use of rigorously dried DME results in substantially lower chemical yields
29. The coupling of octanal with allylsilane using acetone as the bulk medium provided the corresponding allylation product in 79% ee (75% conversion after 24 hours)
30. M.-H. Le Tadic-Biadatti, M. Newcomb, *J. Chem. Soc. Perkin Trans.* **2**, 1467 (1996)
31. M. P. Sibi, M. Hasegawa, *J. Am. Chem. Soc.* **129**, 395 (2007); published online 16 March 2007 (10.1021/ja069245n)

32. We thank R. A. Pascal for invaluable assistance in performing Gaussian DFT calculations and M. Amatore for a late-stage experimental contribution. Financial support was provided by NIH National Institute of General Medical Sciences (grant R01 GM078201-01-01) and by gifts from Amgen, Merck Research Laboratories, and the Astellas Foundation USA. T.D.B. is grateful for a Novartis predoctoral fellowship, J.-B.H. is grateful for a KRF postdoctoral fellowship, and K.A. is grateful for a Merck overseas postdoctoral fellowship

Supporting Online Material

www.sciencemag.org/cgi/content/full/1142696/DC1
Materials and Methods
References and Notes

20 February 2007; accepted 20 March 2007
Published online 29 March 2007
10.1126/science.1142696
Include this information when citing this paper

A Dinuclear Ni(μ-H)Ru Complex Derived from H_2

Seiji Ogo,[1*] Ryota Kabe,[1,2] Keiji Uehara,[2] Bunsho Kure,[1,2] Takashi Nishimura,[2] Satja C. Menon,[2] Ryosuke Harada,[1] Shunichi Fukuzumi,[2] Yoshiki Higuchi,[3] Takashi Ohhara,[4] Taro Tamada,[4] Ryota Kuroki[4]

Models of the active site in [NiFe] hydrogenase enzymes have proven challenging to prepare. We isolated a paramagnetic dinuclear nickel-ruthenium complex with a bridging hydrido ligand from the heterolytic cleavage of H_2 by a dinuclear NiRu aqua complex in water under ambient conditions (20°C and 1 atmosphere pressure). The structure of the hexacoordinate Ni(μ-H)Ru complex was unequivocally determined by neutron diffraction analysis, and it comes closest to an effective analog for the core structure of the proposed active form of the enzyme.

Hydrogenases are bacterial enzymes that catalyze the activation of H_2 into two protons (H^+) and two electrons (e^-) (*1*–*3*). Hydrogen isotope exchange experiments implicate as a first step the heterolytic cleavage of H_2 into a proton and a hydride ion (H^-) (*1*–*3*). Hydrogenases are classified into two major families on the basis of the metal content of their respective dinuclear active sites—that is, [FeFe]hydrogenases (*4*) and [NiFe]hydrogenases (*5*, *6*). Recent progress toward the structures and function of the hydrogenases has been provided by x-ray analysis, spectroscopic techniques, theoretical methods, and model studies (*7*).

X-ray crystallographic studies have shown that the resting-state core structure of [NiFe]hydrogenase from *Desulfovibrio gigas* consists of one nickel atom and one iron atom, which are bridged by two cysteic thiolates and one unidentified ligand (depicted as X in Fig. 1) (*2*, *5*, *6*). The bridging ligand X in the resting state is proposed to be an oxygen ligand such as H_2O, OH^-, or O^{2-} (*8*). The role of metal atoms and bridging S and X ligands in the H_2 cleavage has so far been the subject of controversy (*8*).

Many synthetic modeling efforts have been devoted to elucidating the core structure of the active form of the [NiFe]hydrogenase, such as preparation of [NiRu]complexes by Rauchfuss and others (*9*–*15*). A Ni(μ-S)$_2$(μ-H)Fe species is one of the candidates for the active form (*1*, *5*, *16*, *17*). However, ^{10}M(μ-S)$_2$(μ-H)^{8}M complexes [where ^{10}M = group 10 metals (Ni, Pd, and Pt) and ^{8}M = group 8 metals (Fe, Ru, and Os)] as models for the active form of the [NiFe]hydrogenase have yet to be reported.

Here, we report the successful isolation and crystal structure of the paramagnetic Ni(μ-H)Ru complex $[(Ni^{II}L)(H_2O)(\mu\text{-}H)Ru^{II}(C_6Me_6)](NO_3)$ {$[2](NO_3)$} [where L = *N,N'*-dimethyl-*N,N'*-bis(2-mercaptoethyl)-1,3-propanediamine], which we synthesized by reaction of a diamagnetic dinuclear NiRu aqua complex $[(Ni^{II}L)Ru^{II}(H_2O)(\eta^6\text{-}C_6Me_6)](NO_3)_2$ {$[1](NO_3)_2$} with H_2 in water under ambient conditions (20°C and 0.1 MPa) (Fig. 2).

We obtained the highly water-soluble NiRu aqua complex $[1](SO_4)$ by reaction of the ruthenium triaqua complex $[Ru(\eta^6\text{-}C_6Me_6)(H_2O)_3](SO_4)$

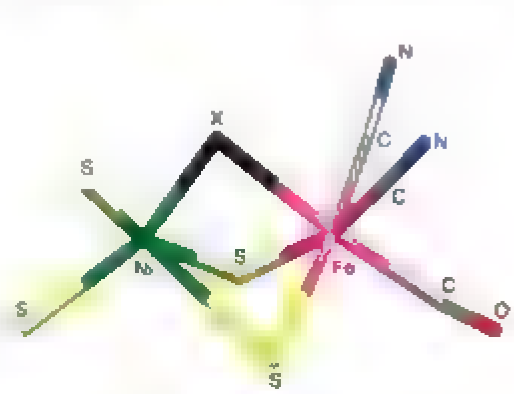

Fig. 1. Core structure of the resting form of [NiFe]hydrogenase from *D. gigas*, determined by x-ray analysis. [Adapted from (*6*)]

[1]Center for Future Chemistry, Kyushu University, Fukuoka 819–0395, Japan. [2]Department of Material and Life Science, Division of Advanced Science and Biotechnology, Graduate School of Engineering, Osaka University, Solution-Oriented Research for Science and Technology, Japan Science and Technology Agency (JST), Suita, Osaka 565–0871, Japan. [3]Department of Life Science, Graduate School of Life Science, University of Hyogo, Koto, Kamigori, Hyogo 678–1297, Japan. [4]Research Group for Molecular Structural Biology, Quantum Beam Science Directorate, Japan Atomic Energy Agency, Tokai, Ibaraki 319–1195, Japan.

*To whom correspondence should be addressed. E-mail: ogo-tcm@mbox.nc.kyushu-u.ac.jp

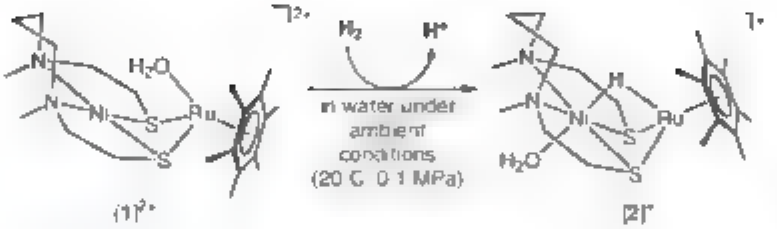

Fig. 2. Formation of a Ni(μ-H)Ru complex obtained from the reaction of a NiRu aqua complex with dihydrogen (H_2) in water under ambient conditions (20°C and 0.1 MPa).

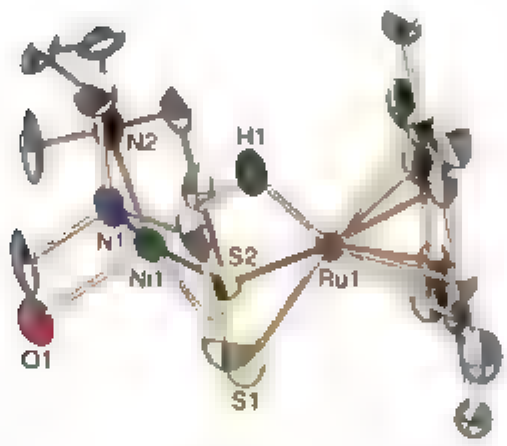

Fig. 3. Structure of [2](NO$_3$) as determined by neutron diffraction analysis. The ellipsoids are cut open to reveal the three principal axes and are drawn to include 30% probability density. Selected bond lengths (d/Å) and angles (ω/deg): Ni1–H1, 1.859 ± 0.007; Ni1–O1, 2.122 ± 0.005; Ni1–S1, 2.359 ± 0.010; Ni1–S2, 2.362 ± 0.009; Ni1–N1, 2.119 ± 0.003; Ni1–N2, 2.117 ± 0.004; Ru1–H1, 1.676 ± 0.008; Ru1–S1, 2.375 ± 0.011; Ru1–S2, 2.388 ± 0.007; Ni1–H1–Ru1, 101.47 ± 0.043; Ni1–S1–Ru1, 70.7 ± 0.3; and Ni1–S2–Ru1, 70.4 ± 0.2.

[1](SO$_4$) (18) with the nickel complex [Ni^{II}L] (4, 19) in aqueous solution (20). Complex $[1]^{2+}$ was characterized by nuclear magnetic resonance (NMR) (figs. S1 to S3) and infrared (IR) spectroscopy (fig. S4), as well as by electrospray mass ionization spectrometry (ESI-MS) (figs. S5 to S7) and x-ray photoelectron spectroscopy (XPS) (fig. S8, A and C). Magnetic susceptibility measurements confirmed that the complex was diamagnetic (fig. S9A). The solid state structure of $[1]^{2+}$ was characterized by x-ray diffraction from a red crystal of [1](OTf)$_2$ (where OTf = CF_3SO_3), obtained from an aqueous solution of [1](OTf)$_2$, prepared by an anion exchange [1](SO$_4$) with NaOTf in water (fig. S10). A variety of anions (such as SO_4^{2-}, OTf^-, or NO_3^-) were investigated with regard to their ability to induce isolation of the complexes as crystals (fig. S11). The Ni center of [1](OTf)$_2$ sits in the pocket of the tetradentate ligand in a square planar arrangement (fig. S10). The Ru1–O1 (aqua ligand) bond length is 2.154 ± 0.003 Å (where 0.003 is SD), whereas the Ni1–O1 distance is 2.858 ± 0.003 Å. (Further parameters are given in tables S1 and S2.)

The dinuclear NiRu aqua complex [1](NO$_3$)$_2$ was quantitatively obtained from anion exchange of [1](SO$_4$) in water at approximately pH 7 (fig. S11). H_2 (0.1 MPa) was bubbled through the phosphate buffer solution (pH 6.8) of [1](NO$_3$)$_2$ at 25°C to gradually precipitate dark-red crystals of [2](NO$_3$), which were isolated by filtration [34% isolated yield based on [1](NO$_3$)$_2$]. As the reaction progressed (without the addition of the phosphate buffer), the pH of the solution steadily decreased (from pH 6.4 to pH 4.6), indicating the heterolytic H_2 cleavage (21), which generated H^+ as a coproduct. The H_2O ligand of [1](NO$_3$)$_2$ may act as a base to release H_3O^+ ($H_2 + H_2O \rightarrow H^- + H_3O^+$) (22). We characterized [2](NO$_3$) by IR (fig. S12), ESI-MS (fig. S13), XPS (fig. S8, B and D), NMR (fig. S14), electron spin resonance (ESR) spectroscopy (fig. S15), and magnetic susceptibility measurements (fig. S9B).

Dark-red crystals of [2](NO$_3$) obtained from the aqueous solution of [2](NO$_3$) were characterized by x-ray (fig. S16) as well as neutron diffraction analysis, the latter chosen for its sensitivity to hydrides (Fig. 3 and fig. S17). The Ru–H distance (1.676 ± 0.008 Å by neutron diffraction analysis) in the Ni(μ-H)Ru moiety of [2](NO$_3$) is substantially shorter than the Ru–H distances (averaging 1.755 Å by neutron diffraction analysis) in the Ru(μ-H)Ru moiety of [{(η^5-C_5H_3)$_2$(SiMe$_2$)$_2$}{Ru$_2$(CO)$_4$(μ-H)}](BF$_4$) with a bulky dimethylsilyl linker (23). The Ni atom of [2](NO$_3$) adopts a distorted octahedral coordination geometry with the tetradentate ligand, one aqua ligand, and one hydrido ligand (Fig. 3). The bridging H atom is closer to the Ru atom (Ru–H = 1.676 ± 0.008 Å, Ni–H = 1.859 ± 0.007 Å) in the Ni(μ-H)Ru moiety. The Ru–H unit may serve as a two-electron donor to the Ni unit through the bridging H atom (24), much as in M(μ-H)B complexes (where M is a transition metal), in which the B–H unit acts as a two-electron donor to M (25). In this context, there are three examples of hexacoordinate Ni(μ-H)B complexes with S ligands whose structures have been determined by x-ray analysis (Ni–H = 1.83 to 1.98 Å) (26–28). The Ni–S–Ru angles (70.7° ± 0.3° and 70.4° ± 0.2°) for [2](NO$_3$) are substantially smaller than the Ni–S–Ru angles (86.81° ± 0.04° and 87.20° ± 0.05°) for [1](NO$_3$)$_2$. The tunable Ni–S–Ru angles allow such structural changes in these dinuclear complexes. The Ni–Ru distance (2.739 ± 0.003 Å) of [2](NO$_3$) is shorter than that (3.1611 ± 0.0006 Å) of [1](OTf)$_2$. A similar tendency has been observed in the [NiFe]hydrogenase, i.e., extended x-ray absorption fine-structure studies on the [NiFe]hydrogenase have shown that the Ni–Fe distance in the active form is 2.512 ± 0.007 Å, which is shorter than the Ni–Fe distance (2.906 ± 0.014 Å) in the resting form (29).

A positive-ion ESI mass spectrum of [2](NO$_3$) in H_2O is consistent with the above formulation and dinuclearity (fig. S13). A prominent signal at a mass-to-charge ratio (m/z) of 543.2 [relative intensity = 100% in the m/z range from 200 to 1000] has a characteristic distribution of isotopomers that matches well with the calculated isotopic distribution for $[2\text{-}H_2O]^+$. To confirm the origin of the hydrido ligand of [2](NO$_3$), we synthesized D-labeled [2](NO$_3$) by reaction of [1](NO$_3$)$_2$ with D_2 in H_2O for 30 min. In ESI mass spectra, the signal at m/z 543.2 shifts to 544.2 (fig. S18). This result indicates that the deuterium atom is incorporated into [2](NO$_3$). We have confirmed that there is no H-D exchange between D_2 and H_2O under the conditions of this experiment (at pH 7 to 9 in H_2O for 1 hour at 25°C at 0.1 MPa of D_2). An IR spectrum of [2](NO$_3$) in the region of 1000 to 2000 cm^{-1} shows a peak shift from 1740 to 1248 cm^{-1} after isotopic substitution of H by D in the hydrido ligand position. Magnetic susceptibility measurements of [2](NO$_3$) yield $\chi_M = 1.5 \times 10^{-3}$ electromagnetic units (emu) mol^{-1} at 300 K, corresponding to a magnetic moment of 2.32 BM. ^{1}H NMR and ESR measurements also indicate paramagnetism in [2](NO$_3$). The reason for paramagnetism is explained on the basis of the transformation of the nickel(II) spin state between a singlet ($S = 0$) square planar of $[1]^{2+}$ and a triplet ($S = 1$) pseudo-octahedral of $[2]^+$, triggered by the coordination of H^- and H_2O to the nickel ion. Complex [2](NO$_3$) is one of a few examples of stable paramagnetic metal hydride complexes (30). The binding energy of Ni $2p_{3/2}$ for XPS of [2](NO$_3$) indicates that a Ni atom has a similar charge (883.2 eV) to that of [1](OTf)$_2$ (882.9 eV), which corresponds to a Ni(II) species.

Previous studies of dinuclear transition metal complexes with two bridging sulfido ligands M(μ-S)$_2$M (where M = Ru or Ir), that activate H_2 to give M(μ-S)$_2$(μ-H)M species have been reported (31, 32). However, in those reported studies, the reactions have been carried out in organic solvent such as toluene. We attached an aqua ligand to the Ni(μ-S)$_2$Ru unit not only to gain water solubility but also to act as a base to form the Ni(μ-S)$_2$(μ-H)Ru species in water, because we assumed that the hydrogenases require the X ligand (H_2O, OH^-, or O^{2-}) in the resting state to activate H_2 in aqueous media in the same manner of this study.

References and Notes

1. R. Cammack, M. Frey, R. Robson, *Hydrogen as a Fuel: Learning from Nature* (Taylor & Francis, London, 2001).
2. M. Frey, *Structure and Bonding* (Springer-Verlag, Berlin, 1998), pp. 97–126.
3. S. P. J. Albracht, *Biochim. Biophys. Acta* **1188**, 167 (1994).
4. J. W. Peters, W. N. Lanzilotta, B. J. Lemon, L. C. Seefeldt, *Science* **282**, 1853 (1998).
5. A. Volbeda *et al.*, *Nature* **373**, 580 (1995).

6. A. Volbeda *et al.*, *J. Am. Chem. Soc.* **118**, 12989 (1996).
7. Special issue on Hydrogenases, C. J. Pickett, S. P. Best, Eds., *Coord. Chem. Rev.* **249**, 1517–1690 (2005).
8. M. Carepo *et al.*, *J. Am. Chem. Soc.* **124**, 281 (2002).
9. M. A. Reynolds, T. B. Rauchfuss, S. R. Wilson, *Organometallics* **22**, 1619 (2003).
10. E. Bouwman, J. Reedijk, *Coord. Chem. Rev.* **249**, 1555 (2005).
11. D. J. Evans, C. J. Pickett, *Chem. Soc. Rev.* **32**, 268 (2003).
12. A. C. Marr, D. J. E. Spencer, M. Schröder, *Coord. Chem. Rev.* **219-221**, 1055 (2001).
13. M. Y. Darensbourg, E. J. Lyon, J. J. Smee, *Coord. Chem. Rev.* **206-207**, 533 (2000).
14. Z. Li, Y. Ohki, K. Tatsumi, *J. Am. Chem. Soc.* **127**, 8950 (2005).
15. W. Zhu *et al.*, *Proc. Natl. Acad. Sci. U.S.A.* **102**, 18280 (2005).
16. S. Foerster *et al.*, *J. Am. Chem. Soc.* **125**, 83 (2003).
17. M. Brecht, M. van Gastel, T. Buhrke, B. Friedrich, W. Lubitz, *J. Am. Chem. Soc.* **125**, 13075 (2003).
18. M. Jahncke, G. Meister, G. Rheinwald, H. Stoeckli-Evans, G. Süss-Fink, *Organometallics* **16**, 1137 (1997).
19. G. J. Colpas, M. Kumar, R. O. Day, M. J. Maroney, *Inorg. Chem.* **29**, 4779 (1990).
20. Materials and methods are available as supporting material on *Science* Online.
21. A. C. Ontko *et al.*, *Organometallics* **17**, 5467 (1998).
22. S. Ogo, R. Nakai, Y. Watanabe, *J. Am. Chem. Soc.* **124**, 597 (2002).
23. A. Albinati *et al.*, *Inorg. Chim. Acta* **259**, 351 (1997).
24. M. H. Drabnis, R. Bau, S. A. Mason, J. W. Freeman, R. D. Ernst, *Eur. J. Inorg. Chem.* **1998**, 851 (1998).
25. T. J. Marks, J. R. Kolb, *Chem. Rev.* **77**, 263 (1977).
26. Y.-J. Wang, B. Cao, W.-H. Bi, *Polyhedron* **24**, 585 (2005).
27. H. M. Alvarez, M. Krawiec, B. T. Donovan-Merkert, M. Fouzi, D. Rabinovich, *Inorg. Chem.* **40**, 5736 (2001).
28. R. Cammi *et al.*, *Inorg. Chem.* **42**, 1769 (2003).
29. Z. Gu *et al.*, *J. Am. Chem. Soc.* **118**, 11155 (1996).
30. M. Peruzzini, R. Poli, *Recent Advances in Hydride Chemistry* (Elsevier, Amsterdam, ed. 1, 2001), pp. 139–188.
31. A. K. Justice, R. C. Linck, T. B. Rauchfuss, S. R. Wilson, *J. Am. Chem. Soc.* **126**, 13214 (2004).
32. R. C. Linck, R. J. Pafford, T. B. Rauchfuss, *J. Am. Chem. Soc.* **123**, 8856 (2001).

33. This work was supported by grants in aid 17350027, 19205009, 18033041, and 18065017 (Chemistry of Concerto Catalysis) from the Ministry of Education, Culture, Sports, Science, and Technology, Japan; and a Core Research for Evolutional Science and Technology program (Nano-Structured Catalysts and Materials) by JST. Crystallographic data for [3](OTf)$_2$ and [2](NO$_3$) have been deposited with the Cambridge Crystallographic Data Center under reference numbers CCDC-617674 (x-ray), 617675 (x-ray), and 637331 (neutron diffraction analysis).

Supporting Online Material

www.sciencemag.org/cgi/content/full/316/5824/585/DC1
Materials and Methods
Figs. S1 to S18
Tables S1 and S2
References

12 December 2006; accepted 12 March 2007
10.1126/science.1138751

Paleocene-Eocene Thermal Maximum and the Opening of the Northeast Atlantic

Michael Storey,[1] Robert A. Duncan,[2] Carl C. Swisher III[3]

The Paleocene-Eocene thermal maximum (PETM) has been attributed to a sudden release of carbon dioxide and/or methane. $^{40}Ar/^{39}Ar$ age determinations show that the Danish Ash-17 deposit, which overlies the PETM by about 450,000 years in the Atlantic, and the Skraenterne Formation Tuff, representing the end of 1 ± 0.5 million years of massive volcanism in East Greenland, are coeval. The relative age of Danish Ash-17 thus places the PETM onset after the beginning of massive flood basalt volcanism at 56.1 ± 0.4 million years ago but within error of the estimated continental breakup time of 55.5 ± 0.3 million years ago, marked by the eruption of mid-ocean ridge basalt–like flows. These correlations support the view that the PETM was triggered by greenhouse gas release during magma interaction with basin-filling carbon-rich sedimentary rocks proximal to the embryonic plate boundary between Greenland and Europe.

During the Paleocene-Eocene thermal maximum (PETM) (*1*), the sea surface temperature rose by 5°C in the tropics (*2*) and more than 6°C in the Arctic (*3*), in conjunction with ocean acidification (*4*) and the extinction of 30 to 50% of deep-sea benthic foraminiferal species (*5*). The onset of the PETM is marked by an abrupt decrease in the $\delta^{13}C$ proportion of marine and terrestrial sedimentary carbon (*1*, *6*), which is consistent with the rapid addition of >1500 gigatons of ^{13}C-depleted carbon, in the form of carbon dioxide and/or methane, into the hydrosphere and atmosphere (*7*). The PETM is thought to have lasted only 210,000 to 220,000 years, with most of the decrease in $\delta^{13}C$ occurring over a 20,000-year period at the beginning of the event (*8*).

A possible trigger for the initiation of the PETM is a period of intense flood basalt magmatism attending the opening of the North Atlantic (*9*, *10*), by generating metamorphic methane from sill intrusion into basin-filling carbon-rich sedimentary rocks (*11*). Here we present $^{40}Ar/^{39}Ar$ age determinations that allow the correlation of Early Tertiary volcanic rocks of East Greenland and the Faeroe Islands with the Danish Ash-17 deposit, which closely overlies PETM sequences in the North Atlantic. In East Greenland, a ~5-km-thick sequence of plateau basalts formed in 1.0 ± 0.5 million years (My). A surge in magma production, coupled with the eruption of mid-ocean ridge basalt (MORB)–like flows in the lower part of the flood basalt sequence, indicates the initiation of seafloor spreading at 55.5 ± 0.3 million years ago (Ma). The onset of the PETM correlates closely with this breakup-related magmatism.

The North Atlantic Igneous Province (NAIP) includes the basaltic and picritic lavas of Baffin Island and West Greenland; the ~7-km-thick predominantly tholeiitic lava flow sequences of the Blosseville Kyst of East Greenland; the seaward-dipping reflectors of the Greenland and northwest European volcanic rifted margins; the Faeroe Islands and British Tertiary basaltic lavas; and the aseismic ridges connecting Iceland to either margin of the central Northeast Atlantic (Fig. 1). The total area of the NAIP is 1.3 × 10^6 km^2 (*12*) and its volume is estimated to be 5 × 10^6 km^3 to 10 × 10^6 km^3 (*12*–*14*). The East Greenland (Blosseville Kyst) and Faeroe Islands flood basalts lie at opposite ends of the Greenland-Iceland-Faeroes Ridge (GIFR), the postulated Iceland hotspot track, and record volcanic activity leading up to, during, and after continental breakup between Greenland and Europe (Fig. 1).

$^{40}Ar/^{39}Ar$ age determinations show that pre-breakup volcanic activity in East Greenland and the Faeroes began at ~61 Ma (*15*–*17*). Seven lava flows cover the duration of magnetochron C25n (~500,000 years) in the uppermost part of the Faeroes lower series (FLS), indicating a very low eruption rate by ~57 Ma (*18*) (Fig. 2). The FLS extends into earliest C24r, as the lava flow immediately below the capping ~10-m-thick coal-bearing sediment horizon (*19*) is reversely magnetized (*18*). The volcanic hiatus as represented on the Faeroes, after the end of the initial phase of volcanism, has an estimated duration of 0.6 ± 0.4 My (Fig. 2). In East Greenland, volcaniclastic sediments overlie the FLS equivalent, the Nansen Fjord Formation (*20*), which includes lahars that contain coal fragments and plant imprints (*21*).

After the period of little or no volcanism, flood basalt eruptions commenced on a massive scale in East Greenland and the Faeroes (Fig. 2). Flood basalt activity in East Greenland is represented by four regionally extensive formations with a combined stratigraphic thickness of ~5 km. The Milne Land Formation (MLF), the oldest of these four formations, includes MORB-like low-Ti basalts halfway up the succession (*20*) that provide correlation with the Faeroes middle series (FMS) and upper series (FUS) (Fig. 2). Paleomagnetic data suggest a high eruption

[1]Quaternary Dating Laboratory, Department of Environment, Society and Spatial Change, Roskilde University Centre, Post Office Box 260, 4000 Roskilde, Denmark. [2]College of Oceanic and Atmospheric Sciences, Oregon State University, Corvallis, OR 97331, USA. [3]Department of Geological Sciences, Rutgers University, Piscataway, NJ 08854-8066, USA.

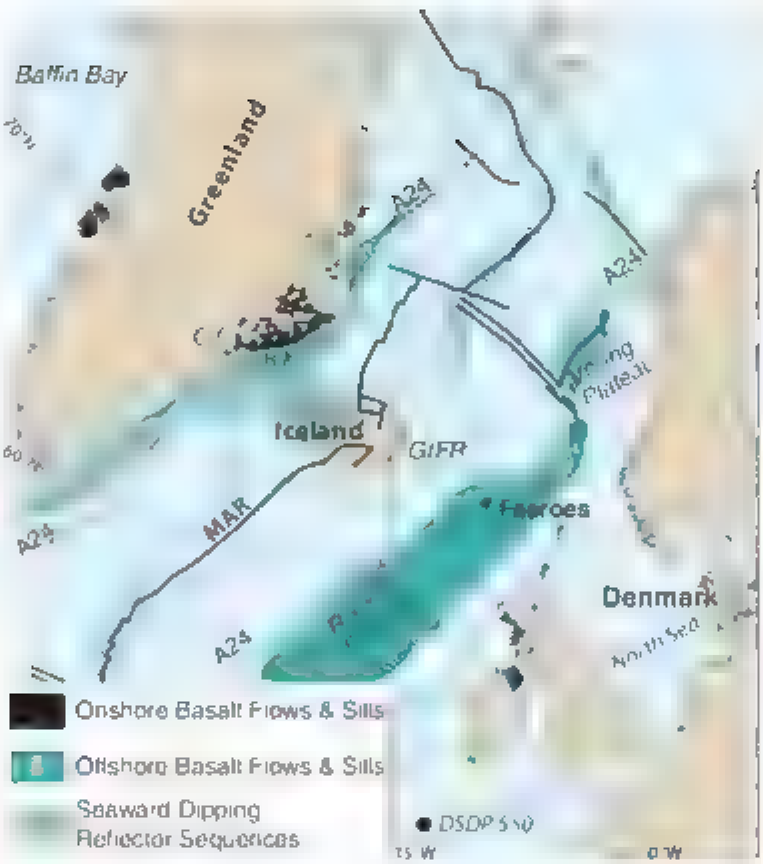

Fig. 1. Map of the North Atlantic region showing the distribution of igneous rocks related to the NAIP and DSDP site 550, where Danish Ash-17 closely overlies the PETM. A24, sea-floor magnetic anomaly 24r; BK, Blosseville Kyst; GC, Gardiner Complex; MAR, Mid-Atlantic Ridge.

rate at the onset of the FMS (18). In the MLF East Greenland, lavas show a regular decrease in the Dy/Yb ratio up through the section, indicative of a progressive drop in the mean pressure of partial melting (27) and consistent with rifting and thinning of the lithosphere. A $^{40}Ar/^{39}Ar$ age determination on plagioclase from a lava flow at the base of the MLF yielded an age of 56.1 ± 0.5 Ma (16), in agreement with age determinations for MLF-equivalent lavas inland (17). The weighted mean age is 56.1 ± 0.4 Ma [2σ internal standard error (SE) used throughout; all ages are reported relative to the currently accepted age of 28.02 Ma for the $^{40}Ar/^{39}Ar$ standard Fish Canyon Tuff Sanidine (23)]. A high-precision $^{40}Ar/^{39}Ar$ age of 55.12 ± 0.06 Ma (table S1) on sanidine from a tuff near the top of the Skrænterne Formation (SF), the uppermost of the four volcanic formations, indicates that the entire sequence was erupted in 1.0 ± 0.5 My (Fig. 2). The lowest stratigraphic occurrence of MORB-like flows, approximately 0.8 km above the base of the first flood basalts, was dated to 55.1 ± 0.5 Ma (16) on plagioclase from two samples of interlayered Fe-Ti basalts (Fig. 2). Further and more precise age constraints are provided by the Skaergaard intrusion age. The parental magma of the Skaergaard intrusion has been correlated with

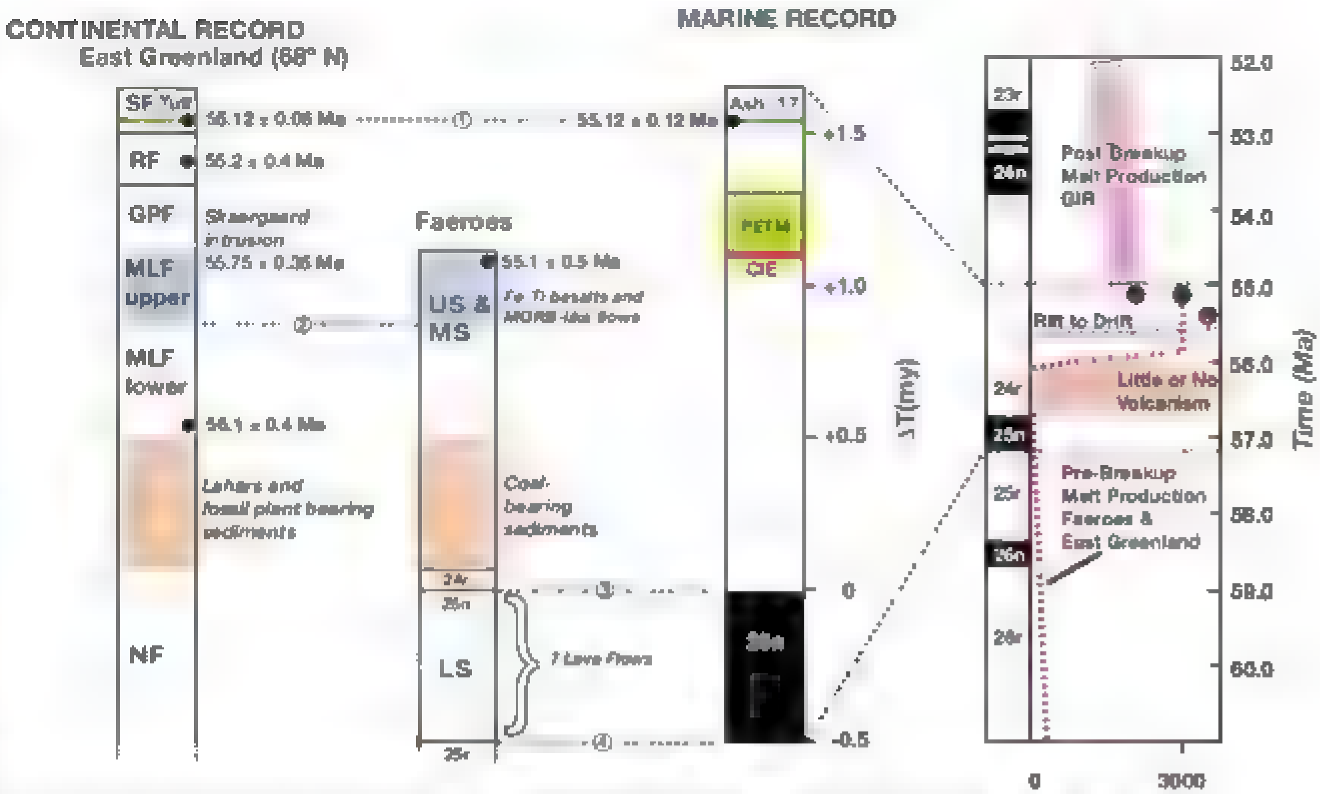

Fig. 2. Correlation of a composite marine record, which encompasses the PETM, Danish Ash-17, and magnetochrons C25n and lower C24r, with the continental East Greenland (68°N) and Faeroe Islands flood basalt record. Tie points are indicated by dashed horizontal lines. Tie point 1, correlation between the SF Tuff and the marine Danish Ash-17; tie point 2, correlation of the East Greenland and Faeroes flood basalts, based on the first occurrence of MORB-like flows in the respective volcanic records (20); tie points 3 and 4, top and base of C25n correlate the Faeroes volcanic record to the marine record. NF, Nansen Fjord Formation; RF, Romer Fjord Formation. Faeroes: LS, lower series; MS, middle series; US, upper series. Marine record: CIE, carbon isotope excursion. ΔT, change in time. $^{40}Ar/^{39}Ar$ age determinations for SF Tuff and Danish Ash-17 are given in tables S1 and S2 and Fig. 3. The $^{40}Ar/^{39}Ar$ age for the MLF is from (16, 17). The $^{40}Ar/^{39}Ar$ ages for the RF and Faeroes US/MS are from (16). The $^{40}Ar/^{39}Ar$ based Skaergaard intrusion age is from (26). The +1.11 My between the top of C25n and the beginning of the CIE is from (29). The +1.55 My between the top of C25n and Danish Ash-17 is based on the observation that Ash-17 occurs in the midpoint of C24r (32) and that C24r has a total duration of 3.11 My (29). The right panel shows magnetochron ages (30) and the estimated variation in magma productivity over time (from 16). There is a low melt production rate by the beginning of C25n and a surge in magmatism (curve 1) during early C24r. Curves 2 and 3 represent upper (6000 km³/km per My) and lower uncertainties on magma productivity during the rift-to-drift phase. Post-breakup melt production is based on seismic images of crustal thickness for the Greenland-Iceland Ridge (GIR) (14).

the Geike Plateau Formation (GPF) (24), which overlies the level of the MORB-like flows in East Greenland (Fig. 2). $^{40}Ar/^{39}Ar$ ages on biotite and hornblende from transgressive granophyres within the Skaergaard intrusion, in combination with models of cooling history (25), give an intrusion age of 55.75 ± 0.35 Ma (26). The weighted average of the Skaergaard intrusion age and the less precise age for the FLS FMS is 55.5 ± 0.3 Ma. This age for the MORB-like flows allows for the possibility that the majority of flood basalts were emplaced in <300,000 years as concluded from a fluid inclusion study on late-stage granophyres from the Skaergaard intrusion (27).

The average melt production rate for the flood basalts is 3000 (+3000/–1000) km^3/km of rift per My (Fig. 2), assuming that the hidden cumulates have a comparable volume to the lavas (28). Although there is a large degree of uncertainty, the figure is in accord with crustal thickness based estimates of magmatic productivity of 1800 ± 300 km^3/km of rift per My for the GIFR, proximal to the volcanic rifted margin (14) (Fig. 2). The surge in melt production after renewed volcanism in East Greenland and the Faeroes suggests a short-lived rift-to-drift phase beginning at 56.1 ± 0.4 Ma, with the eruption of MORB-like, low-Ti basalts at 55.5 ± 0.3 Ma marking the opening of the northeast Atlantic at 68°N, above the ancestral Iceland hot spot.

Although the PETM has been identified globally in marine and also in some continental sedimentary sections, there has been uncertainty about its timing relative to the on-land stratigraphy of the East Greenland–Faeroes flood basalts. Orbital-based calibration for magnetochrons C24r and C25n, using cores from multiple drill holes on the Walvis Ridge in the South Atlantic, indicates that the total duration of C24r is 3.12 ± 0.05 My and that the base of the PETM is 1.11 ± 0.04 My above the C24r/C25n boundary (29) (Fig. 2). This indicates an age of approximately 55.5 to 55.6 Ma for the onset of the PETM, relative to the geomagnetic polarity time scale value of 56.67 Ma for the C24r/C25n boundary (30). Further age constraints are provided by Danish Ash-17, a widespread stratigraphic marker horizon that is found in Early Tertiary marine sediments from the North Sea region and the North Atlantic. Danish Ash-17 overlies the PETM at Deep Sea Drilling Project (DSDP) site 550 in the middle of C24r (C24r.5) and has been used for the calibration of the PETM (Fig. 1) (31, 32). Danish Ash-17 has been correlated previously with an alkaline sanidine-bearing tuff in the SF near the top of the East Greenland Tertiary lava pile (Fig. 2) [illegible] $^{40}Ar/^{39}Ar$ ages [illegible] Ma [illegible] tic deposit is believed to originate from the Early Tertiary Gardiner melanephelinite-carbonatite volcanic complex on the East Greenland margin (Fig. 1). To test the correlation, with the aim of locating the stratigraphic position of the PETM in relation to the East Greenland and Faeroes flood basalts, we have redated both Danish Ash-17 and the SF Tuff, carrying out more than 50 individual age measurements (34). Figure 3 shows that $^{40}Ar/^{39}Ar$ laser-fusion age determinations on sanidines from the SF Tuff and Ash-17 are analytically indistinguishable. Of the 15 sanidine analyses from the SF Tuff, 1 is anomalously young with an age of 54.2 Ma, possibly reflecting ^{40}Ar loss by alteration. The remaining 14 analyses give ages ranging between 55.0 and 55.3 Ma and conform to a simple Gaussian distribution with a mean age of 55.12 ± 0.06 Ma (Fig. 3). Sanidine from Ash-17 is finer-grained, and overall the multiple- as well as single-grain analyses are less precise. However, the sanidine fusion ages for Ash-17 are mostly evenly distributed around 55.12 ± 0.12 Ma. There is a smaller fraction of older ages, which cluster around 56 Ma (fig. S1) and are considered to include an inherited (xenocrystic) component.

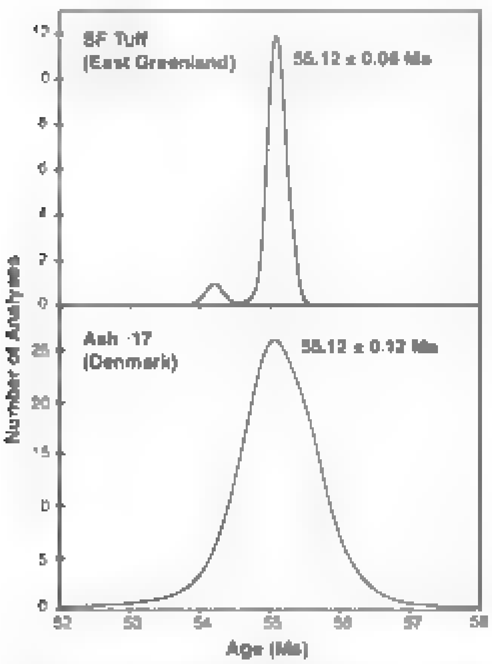

Fig. 3. Probability plot for sanidine $^{40}Ar/^{39}Ar$ ages for the SF Tuff (top) and Danish Ash-17 (bottom). With the exception of an anomalously young age, the SF Tuff ages conform to a simple Gaussian distribution. Ages are arithmetic mean ± 2 SE. Analyses are reported in tables S2 and S3.

The similar new high-precision ages for Danish Ash-17 and the SF Tuff indicate that they are coeval and, due to the rarity of sanidine-bearing tuffs in this time interval in the North Atlantic, most likely represent the same eruptive unit (33). Ash-17 occurs in the midpoint of C24r (30), which would place it approximately 450,000 years above the base of the PETM (29). Relative to the $^{40}Ar/^{39}Ar$ dates for the SF Tuff and Danish Ash-17, the start of the PETM would thus correspond to an age of 55.6 Ma. The onset of the PETM was most likely after the beginning of massive flood basalt volcanism at 56.1 ± 0.4 Ma, but is within error of the estimated age of continental breakup at 55.5 ± 0.3 Ma, marked by the eruption of MORB-like flows (Fig. 2). We suggest that rift propagation and magmatism (above the ancestral Iceland hot spot) during the final stages of breakup between Greenland and Europe triggered the PETM event, probably via the release of ^{12}C-enriched methane through massive sill intrusion and contact metamorphism of carbon-rich sediments contained in basins proximal to the embryonic plate boundary between Greenland and Europe (11).

References and Notes

1. J. P. Kennett, L. D. Stott, *Nature* **353**, 225 (1991).
2. J. C. Zachos *et al.*, *Science* **302**, 1551 (2003).
3. A. Sluijs *et al.*, *Nature* **441**, 610 (2006).
4. J. C. Zachos *et al.*, *Science* **308**, 1611 (2005).
5. E. Thomas, N. J. Shackleton, in *Correlation of the Early Paleogene in Northwestern Europe*, R. W. O'B Knox, R. M. Corfield, R. E. Dunnay, Eds. (Geological Society of London Special Publication, Geological Society of London, 1996), vol. 101, pp. 401–441.
6. P. L. Koch, J. C. Zachos, P. D. Gingerich, *Nature* **358**, 319 (1992).
7. G. R. Dickens, J. R. O'Neil, D. K. Rea, R. M. Owen, *Paleoceanography* **10**, 965 (1995).
8. U. Röhl, T. J. Bralower, R. D. Norris, G. Wefer, *Geology* **28**, 927 (2000).
9. D. K. Rea *et al.*, *Paleogeogr. Palaeoclimatol. Paleoecol.* **79**, 117 (1990).
10. O. Eldholm, E. Thomas, *Earth Planet. Sci. Lett.* **117**, 319 (1993).
11. H. Svensen *et al.*, *Nature* **429**, 542 (2004).
12. O. Eldholm, K. J. Grue, *J. Geophys. Res.* **99**, 2955 (1994).
13. R. S. White, D. P. McKenzie, *J. Geophys. Res.* **94**, 7685 (1989).
14. W. S. Holbrook *et al.*, *Earth Planet. Sci. Lett.* **190**, 251 (2001).
15. C. W. Sinton, R. A. Duncan, in *Proceedings of the Ocean Drilling Program*, H. C. Larsen *et al.*, Eds. (College Station, TX, 1998), vol. 152, pp. 387–402.
16. M. Storey, R. A. Duncan, C. Tegner, *Chem. Geol.* 10.1016/j.chemgeo.2007.01.016 (2007).
17. H. Hansen *et al.*, in *The North Atlantic Igneous Province: Stratigraphy, Tectonics, Volcanic and Magmatic Processes*, D. W. Jolley, B. R. Bell, Eds. (Geological Society of London Special Publication, Geological Society of London, 2002), vol. 197, pp. 183–218.
18. P. Riisager, J. Riisager, N. Abrahamsen, R. Waagstein, *Earth Planet. Sci. Lett.* **201**, 261 (2002).
19. J. Rasmussen, A. Noe-Nygaard, *Geology of the Faeroe Islands* (Danmarks Geologiske Undersøgelse, Copenhagen, Denmark, 1970), series 25.
20. L. M. Larsen, R. Waagstein, A. K. Pedersen, M. Storey, *J. Geol. Soc. London* **156**, 1081 (1999).
21. A. K. Pedersen, M. Watt, W. S. Watt, L. M. Larsen, *J. Geol. Soc. London* **154**, 565 (1997).
22. C. Tegner, C. E. Lesher, L. M. Larsen, W. S. Watt, *Nature* **395**, 591 (1998).
23. P. R. Renne *et al.*, *Chem. Geol.* **145**, 117 (1998).
24. T. F. D. Nielsen, *J. Petrol.* **45**, 507 (2004).
25. D. Norton, H. P. Taylor, *J. Petrol.* **20**, 421 (1979).
26. M. M. Hirschmann, P. R. Renne, A. R. McBirney, *Earth Planet. Sci. Lett.* **146**, 645 (1997).
27. R. B. Larsen, C. Tegner, *Lithos* **92**, 181 (2006).
28. K. G. Cox, *J. Petrol.* **21**, 629 (1980).
29. T. Westerhold *et al.*, *Paleoceanography* **22**, PA2201 (2007).
30. J. G. Ogg, A. G. Smith, in *A Geological Time Scale*, F. M. Gradstein, J. G. Ogg, A. G. Smith, Eds. (Cambridge Univ. Press, Cambridge, 2004), pp. 63–86.
31. R. W. O'B Knox, in *Initial Reports of the Deep Sea Drilling Project*, P. C. Graciansky *et al.*, Eds. (U.S. Government Printing Office, Washington, DC, 1985), vol. 80, pp. 845–850.
32. B. S. Cramer, J. D. Wright, D. V. Kent, M. P. Aubry, *Paleoceanography* **18**, 1097 (2003).
33. L. E. Heister *et al.*, *J. Geol. Soc. London* **158**, 269 (2001).
34. Materials, methods, and argon isotopic analyses are reported in the supporting material on *Science* Online.
35. The Villum Kann Rasmussen Foundation funded the establishment of QUAD-Lab and supports its continued operation. The U.S. NSF supported the age determinations at Oregon State and Rutgers Universities. F. A. Becker, L. Hogan, O. Stecher, J.-D. Nielsen, D. Vagner, and R. Bitsch are thanked for technical advice and support.

18 September 2006; accepted 21 March 2007
10.1126/science.1135274

NOV (CCN3) Functions as a Regulator of Human Hematopoietic Stem or Progenitor Cells

Rajeev Gupta, Dengli Hong, Francisco Iborra, Samantha Sarno, Tariq Enver*

Clinically successful hematopoietic cell transplantation is dependent on hematopoietic stem and progenitor cells. Here we identify the matricellular protein Nephroblastoma Overexpressed (Nov, CCN3) as being essential for their functional integrity. Nov expression is restricted to the primitive (CD34+) compartments of umbilical vein cord blood, and its knockdown in these cells by lentivirus-mediated RNA interference abrogates their function in vitro and in vivo. Conversely, forced expression of Nov and addition of recombinant Nov protein both enhance primitive stem and/or progenitor activity. Taken together, our results identify Nov (CCN3) as a regulator of human hematopoietic stem or progenitor cells.

A small population of self-renewing multipotent hematopoietic stem cells (HSCs) sustains blood production throughout life. They maintain a pool of multipotential progenitors that retain some features of HSCs, but that have the capacity to rapidly differentiate into mature cells (reviewed in *1*, *2*). Despite their clinical importance, a detailed molecular understanding of these primitive compartments in humans is lacking. Although the ex vivo expansion of transplantable human cells has been achieved, for example, by cytokine addition or forced expression of cell-intrinsic regulators such as Notch or *HoxB4* (*3*), no endogenous gene has been demonstrated to be an essential physiological regulator of human hematopoietic stem and/or progenitor cells (*3*). Such intrinsic regulators have been identified in murine HSCs by gene targeting (*3*–*6*); however, their roles in human HSCs remain untested.

Molecular profiling is a useful source of novel candidate regulators (*7*), and using such an approach, we have previously identified Nephroblastoma Overexpressed (Nov, CCN3) as a candidate marker of the undifferentiated state (*8*). The Nov gene was originally characterized as a site of proviral integration in an avian model of nephroblastoma (*9*), and it encodes an eponymous member of the CCN (Cyr61, CTGF, Nov) family of multimodular matricellular signaling proteins (*10*). Nov protein localizes both intracellularly and in the extracellular matrix; it is a normal component of human serum (*11*) and is a regulator of wound healing and angiogenesis (*12*, *13*).

Given the clinical importance of the human primitive hematopoietic stem and/or progenitor compartment in transplantation, and the differences in the growth and transplantation properties of human and mouse cells (*14*), including their responsiveness to stem cell active signaling pathways such as Wnt (*1*) and fibroblast growth factor (*15*), and that the increasing utility of cord blood in stem cell allografting (*16*), we used it as a system in which to understand the effects of Nov in primitive hematopoietic cells (*17*). Reverse transcription polymerase chain reaction (RT-PCR) analysis showed that Nov expression was highest in primitive (CD34$^+$) cells, which include HSCs and multipotential progenitors (fig. S1). To achieve stable knockdown of Nov in these cells, we cloned short-hairpin RNA (shRNA) oligonucleotides directed against human Nov into the lentilox3.7 lentiviral vector, which contains green fluorescent protein (GFP) as a reporter (Fig. 1A) (*18*). The resulting knockdown virus (Novi) reduced Nov protein expression in a cell line and in cord blood CD34$^+$ cells 7 days after infection (figs. S2 and S3), and this was confirmed by RT-PCR (fig. S4). Immunocytochemical analysis of primitive (CD34$^+$lineage$^-$) cord blood cells showed both nuclear and cytoplasmic expression of the Nov protein (Fig. 1B, left), which was abrogated after transduction with Novi (Fig. 1B, middle); the extent of knockdown is quantified in Fig. 1B (right). Taken together, these data show that Nov is expressed at the RNA and protein levels in primitive hematopoietic cells, and validate our knockdown strategy.

Cord blood CD34$^+$ cells transduced with Novi were functionally impaired in in vitro assays. Using quantitative limiting dilution analyses, we estimated the frequency of long-term culture–initiating cells (LTC-ICs), the most primitive human progenitor assessable in vitro; we saw that loss of Nov abrogated LTC-IC readout (Fig. 1, C and D). Expression of *Bmi1* and *Gfi1*, genes previously implicated in murine stem cell self-renewal (*4*, *5*), was similarly diminished (fig. S5). In contrast, loss of Nov did not abrogate the clonogenicity of more mature progenitors as tested in methylcellulose colony-forming cell (CFC) assays (performed 6 to 9 days after infection). Loss of Nov led to a modest increase in colony number (Fig. 1E), but without a difference in lineage distribution (fig. S6). However, cells from these primary colonies failed to generate secondary colonies in methylcellulose replating experiments (Fig. 1F), which implies a defect in progenitor self-renewal (*19*). This increase in primary CFC activity, but loss of secondary CFC activity, may represent a diversion of progenitor fate from self-renewal to differentiation in the absence of Nov. In other systems, NOV has been reported to regulate Notch signaling (*20*); this pathway plays a role in regulating hematopoiesis (*21*). Consistent with this

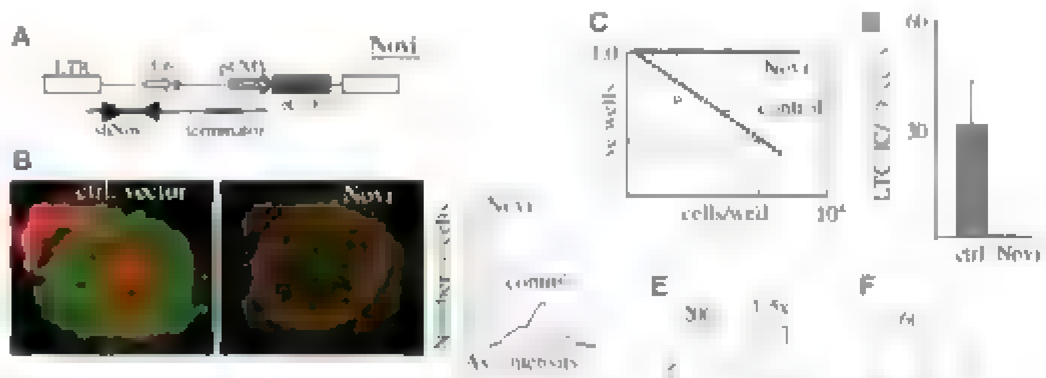

Fig. 1. Nov is required for stem and/or progenitor function in vitro. (**A**) The Novi vector. shRNA is transcribed from the U6 RNA–polymerase III promoter. (**B**) Immunofluorescence analysis of Nov expression in representative cord blood CD34$^+$lin$^-$ cells transduced with either control vector or Novi. Nov is labeled with Alexa-488 (green). Nuclei are stained with TO-PRO-3 (red). (Right) Average intensity of Nov staining in 500 cells transduced with either vector. (**C**) Representative LTC-IC assay by limiting dilution of cord blood CD34$^+$ cells transduced with either control or Novi virus. –ve wells, negative wells, fraction of wells showing no CFC activity. The LTC-IC frequency for control cells is 1/6260. Readout from Novi cells was not observed. (**D**) Mean LTC-IC frequency of control and Novi cells ($n = 6$, $P < 0.01$). Novi cells gave LTC-IC in only one of six experiments, which gives a computed frequency of 1/82 500 cells. (**E**) Methylcellulose CFC frequency in control and Novi cells. Novi cells showed a 1.5-fold increase in total CFC ($n = 6$, $P = 0.016$). (**F**) CFC replating frequency of primary control and Novi colonies ($n = 4$, $P = 0.015$).

Medical Research Council Molecular Haematology Unit, Weatherall Institute of Molecular Medicine, University of Oxford, John Radcliffe Hospital, Headington, OX3 9DS, UK.

*To whom correspondence should be addressed. E-mail: tenver@gwmail.jr2.ox.ac.uk

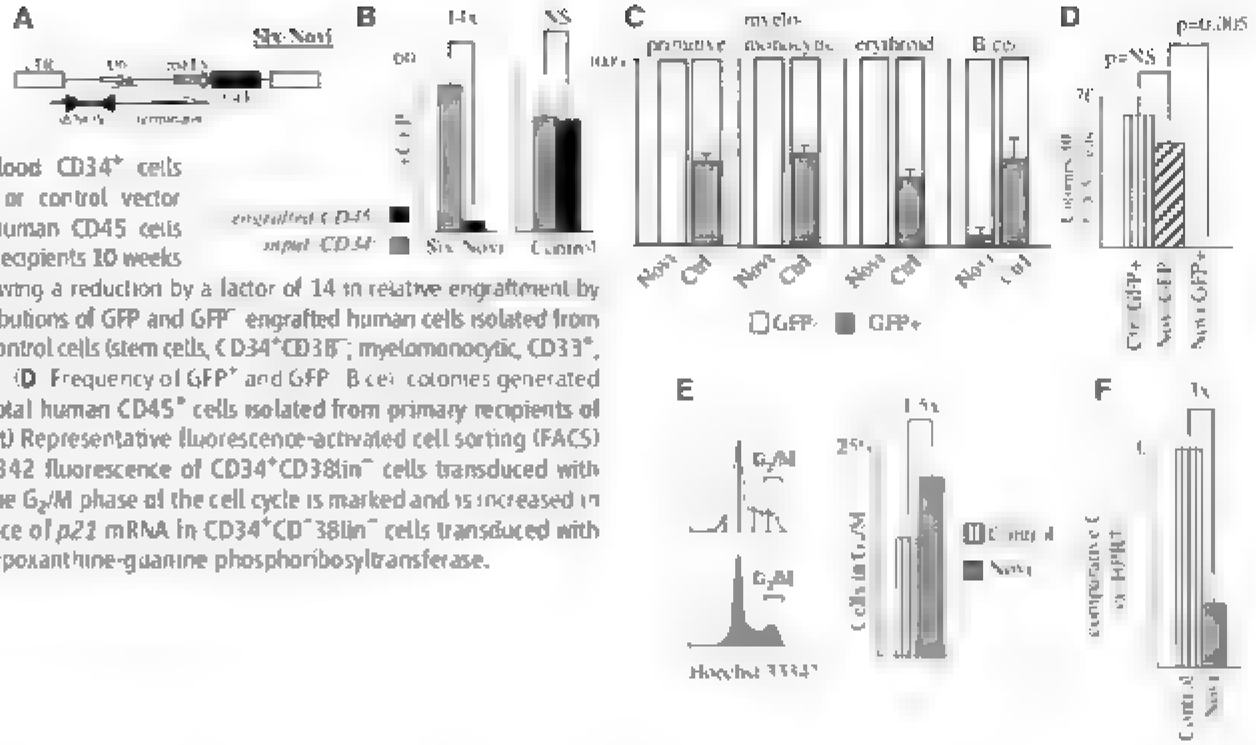

Fig. 2. Novi is required for stem and/or progenitor cell function in vivo. **(A)** Design of the six-Novi virus. The shRNAi sequence is identical to Novi's. **(B)** GFP expression in cord blood CD34$^+$ cells transduced with six-Novi (left) or control vector before transplantation and in human CD45 cells isolated from primary NOD/SCID recipients 10 weeks after transplantation (n = 4), showing a reduction by a factor of 14 in relative engraftment by GFP Novi cells. **(C)** Lineage contributions of GFP and GFP$^-$ engrafted human cells isolated from primary recipients of six-Novi or control cells (stem cells, CD34$^+$CD38$^-$; myelomonocytic, CD33$^+$; erythroid, CD235$^+$; B cell, CD19$^+$). **(D)** Frequency of GFP$^+$ and GFP$^-$ B cell colonies generated by MS-5–supported culture of total human CD45$^+$ cells isolated from primary recipients of control or six-Novi cells. **(E)** (Left) Representative fluorescence-activated cell sorting (FACS) histogram showing Hoechst 33342 fluorescence of CD34$^+$CD38lin$^-$ cells transduced with control vector or Novi. (Right) The G_2/M phase of the cell cycle is marked and is increased in Novi cells. **(F)** Relative abundance of *p21* mRNA in CD34$^+$CD$^-$38lin$^-$ cells transduced with control vector or Novi. *HPRT*, hypoxanthine-guanine phosphoribosyltransferase.

Novi hematopoietic cells were found to express less *Hes1*, a reporter of Notch activity, than controls. Furthermore, they exhibited a severely impaired *Hes1* transcriptional response after activation of Notch signaling by addition of the Notch ligand Jagged1 (fig. S7). These findings indicate that loss of Nov markedly diminishes the functional capacity of the primitive hematopoietic compartment, as tested by LTC-IC assays, and also abrogates the self-renewal, but not the differentiation capacity, of more mature cells in CFC assays.

Currently, the most primitive cell in the human hematopoietic hierarchy that is experimentally assessable in vivo is defined by its capacity for hematopoietic reconstitution of sublethally irradiated nonobese diabetic mice with severe combined immunodeficiency (NOD/SCID mice) (22, 23) and is termed a SCID repopulating cell (SRC) (24). Therefore, we further tested the effect of Nov knockdown on the function of the SRC-containing compartment in xenotransplantation experiments.

CD34$^+$CD38$^-$ cells infected with either control or Novi viruses were transplanted by intravenous injection into NOD/SCID mice. The contribution of Novi cells to engraftment assessed after 8 weeks was found to be lower than that of controls by a factor of 22, as determined by quantification of viral sequence in the genomic DNA of human cells isolated from recipient bone marrow (fig. S8). For a more extensive analysis of the impact of Nov abrogation on engraftment, we exchanged the cytomegalovirus (CMV)–driven GFP reporter cassette [which is known to function inefficiently in NOD/SCID mice (25)] for a spleen focus-forming virus (SFFV) GFP (26) to generate the six (empty vector control) and six-Novi viruses (Fig. 2A), and we repeated the experiments. Consistent with

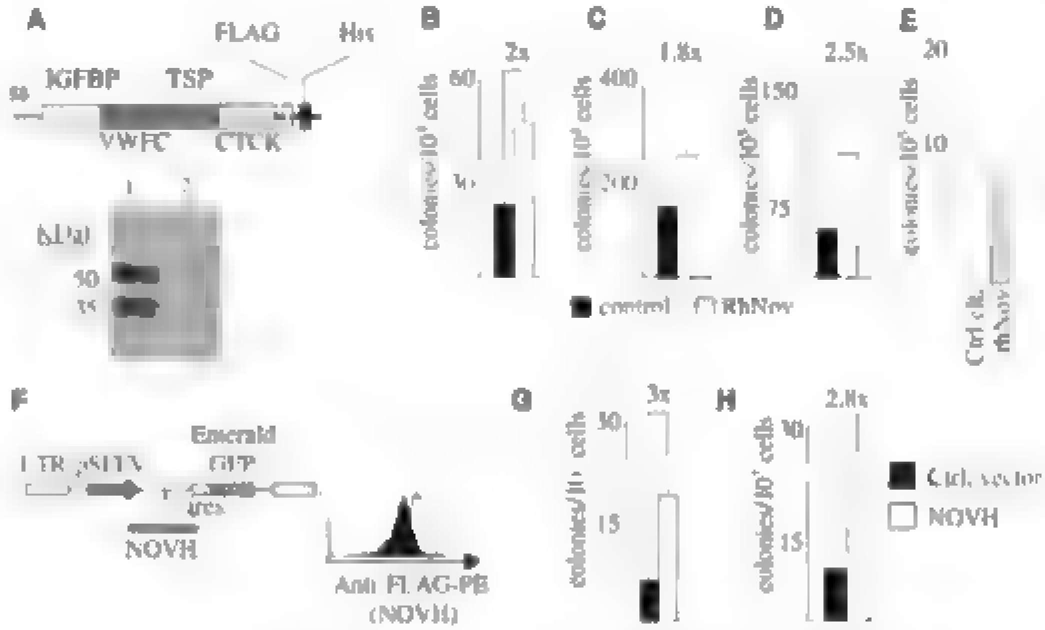

Fig. 3. In vitro effects of recombinant Nov on hematopoietic progenitors. **(A)** Recombinant Nov molecule showing domain structure (ss, signal sequence; IGFBP, insulin-like growth factor binding protein domain; VWFC, von Willebrand factor type C domain; TSP, thrombospondin-like domain; CTCK, C-terminal cysteine knot) and FLAG and histidine (His) epitope tags (upper). Western blot using FLAG-specific antibody of rhNov (lower) showing the two major isoforms described previously (32) (lane 1), and efficient depletion after passing over a histidine column (lane 2). **(B)** Methylcellulose CFU-GEMM output (n = 7, P < 0.01) and **(C)** Total CFC replating frequency (n = 4, P = 0.045) in cord blood CD34$^+$ cells after addition of rhNov or control eluate (17). **(D)** LTC-IC frequency in CD34$^+$ cells maintained for 10 days in the presence of rhNov or control eluate (n = 3, P = 0.06). **(E)** CFC replating frequency of Novi cells in the presence of rhNov or control eluate (n = 9, P = 0.001). **(F)** (Left) NOVH lentivirus showing how an internal ribosomal entry site (ires) links Nov expression to emerald-GFP. (Right) Intracellular expression of recombinant Nov protein in CD34$^+$ cells transduced with NOVH. **(G)** CFU-GEMM (n = 3, P = 0.05) and **(H)** LTC-IC frequency (n = 3, P = 0.07) in CD34$^+$ cells transduced with NOVH or control vector.

the analysis of engraftment by DNA, engraftment as assessed by GFP expression was dramatically reduced in six-Novi recipients; it was undetectable in half of the animals analyzed (Fig. 2B). This relative failure of primary engraftment by Novi cells was not attributable to an alteration in their homing capacity (figs. S9 and S10). In those animals where limited engraftment of Novi cells was detected, lineage analysis revealed that they did not contribute to the stem, myelomonocytic, or erythroid compartments. Those Novi cells that did persist in the graft were found to be

Fig. 4. Effects of recombinant Nov on human cord blood SRC function. Representative FACS traces showing similar GFP expression in CD34$^+$ cells transduced with either NOVH or control vector (**A**) before transplantation, similar intensities of GFP expression are indicated; (**B**) in primary recipients 6 weeks after transplantation overall GFP engraftment is unchanged, GFP^{hi} cells are indicated. (**C**) CD34 expression in GFP$^+$ cells from primary NOVH (mean 43%, n = 3) and control recipients (mean 16%, n = 2). (**D**) Sizes of CD34$^+$ CD38$^-$ pools in GFP$^+$ and GFP$^-$ human cells from NOVH recipients (n = 3). (**E**) Limiting dilution LTC-IC analysis of human cells from primary recipients of NOVH or control cells. In NOVH recipients, LTC-IC frequencies for GFP$^+$ and GFP$^-$ are 1/600 and 1/4000, respectively. (**F**) GFP and human CD34 expression in a representative secondary recipient 8 weeks after transplantation. (**G**) Secondary engraftment in unfractionated bone marrow from five NOVH recipients by genomic PCR; we used human chromosome 17 α satellite–specific oligonucleotides [α-satellite PCR product, 853 bp; mouse *glyceraldehyde-3-phosphate dehydrogenase* (*GAPDH*) PCR product, 872 bp]. NC, uninjected mouse.

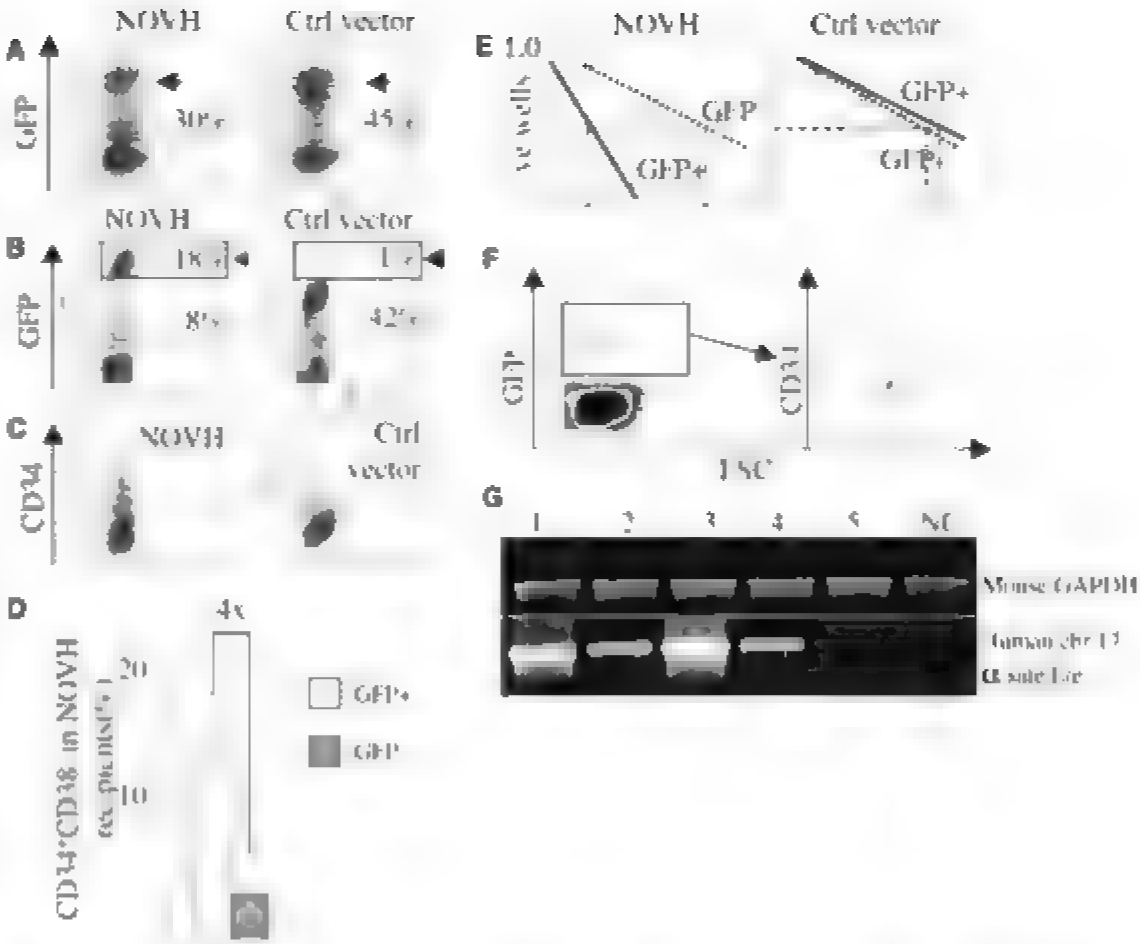

exclusively of the B lineage (Fig. 2C). Further immunophenotypic analysis showed that these B cells were predominantly long-lived mature B cells expressing immunoglobulin IgM (fig. S11). This was confirmed in functional experiments where little or no B cell progenitor activity could be detected in GFP cells from Novi recipients (Fig. 2D). To exclude the possibility of off-target effects of the particular short-hairpin sequence used, we used a second shRNA vector targeting independent Nov sequences, and we observed similar defects in engraftment (fig. S12). These data corroborate our in vitro findings and further indicate that Nov is required for persistent stem cell–dependent engraftment in vivo.

We next examined possible mechanisms for the failure in primary engraftment by Novi cells. Immunophenotypic analysis of cultured cells revealed a reduction in the primitive CD34 CD38 (lo) compartment after loss of Nov (fig. S13). The failure of engraftment could also reflect differences in cell cycle kinetics or cell survival, which are influenced by Nov in other systems (13). Cell survival was found to be unaffected by loss of Nov under the range of conditions tested (fig. S14). In contrast, cell cycle analysis showed an increased fraction of cultured CD34 CD38 (lo) cells in G_2/M phase in Novi compared with control vector, transduced cells (Fig. 2E). Consistent with this, we observed a reduction in *p21* expression in this population (Fig. 2F) (5).

Taken together, our studies suggest an intrinsic requirement for Nov in human stem or progenitor cell function and point to mechanistic defects in Notch signaling and cell cycling after Nov knockdown. Although it is already expressed in the primitive hematopoietic compartment, to corroborate this hypothesis, we performed gain-of-function studies to ask if increasing Nov levels could enhance stem and/or progenitor activity.

A FLAG-tagged recombinant human Nov protein (rhNov) was purified from transiently transfected 293T cells (Fig. 3A), and its effects on hematopoietic cells were studied. Addition of rhNov to CFC assays under serum-free conditions caused a twofold increase in mixed colony (colony-forming unit granulocyte, erythrocyte, monocyte, and megakaryocyte (CFU-GEMM)) formation by cord blood CD34 cells (Fig. 3B) and enhanced colony replating (Fig. 3C). There was no significant change in myelomonocytic or erythroid output, which suggested an effect on multipotential, but not more committed, progenitors. Furthermore, in the presence of rhNov, jagged1 increased total colony output 1.8-fold in CFC assays (fig. S15). Next, we expanded cord blood CD34 cells for 10 days under serum-free conditions with Flt3-L, stem cell factor, thrombopoietin, and interleukin 6, with or without rhNov, before assessing LTC-IC cultures. The mean LTC-IC frequency measured by limiting dilution, after 6 weeks, in cells that had been exposed to rhNov was 2.5 times that of controls (Fig. 3D); these effects on LTC-IC frequency of Nov are comparable to those reported for HoxB4 on human cells (27). These data suggest that extracellular Nov enhances the function of primitive hematopoietic cells in vitro. In addition, rhNov was able to reverse the functional defect shown by Novi cells in the progenitor replating assay (Fig. 3F), which provided further evidence for the specificity of the shRNA effects.

To score any additional effects of enforced endogenous expression of *Nov*, we constructed the NOVH plasmid, in which expression of the recombinant tagged *Nov* gene is controlled by the SFFV promoter in the pHR SIN-CSGW lentiviral vector (Fig. 3F) (26). Cord blood CD34 cells transduced with NOVH expressed the *Nov* transgene (Fig. 3E) and, in CFC assays, exhibited a threefold increase in CFU-GEMM (Fig. 3G). Mimicking the effects seen with purified Nov protein, these cells also showed increased LTC-IC frequency when quantified by limiting dilution (Fig. 3H). These data suggest that enforced intracellular expression of Nov also enhances the function of primitive hematopoietic cells in vitro.

To test the effects of persistent Nov expression in vivo, we transduced CD34 cells with either NOVH or empty-vector control viruses and xenotransplanted them by intravenous injection into NOD/SCID recipients. The viral transduction efficiencies and levels of GFP expression were similar (Fig. 4A), which implied similar genomic integration frequencies for each virus (28). When mice were analyzed, the levels of GFP expression in human CD45$^+$ cells were now considerably higher in the NOVH than in the control vector recipients (Fig. 4B), which suggested that, in vivo, high levels of *Nov* expression (Nov^{hi} cells) confer a selective engraftment advantage over low *Nov*-expressing cells. CD34

expression was, on average, three times as high in GFP cells from NOVH recipients as in those from control (CSGW) recipients (Fig. 4C). In addition, in each animal, this population exhibited a CD34 CD38 fraction four times that of GFP cells, which suggested an expanded stem and/or progenitor compartment in the virally transduced population (Fig. 4D). A similar increase was observed using a more stringent immunophenotype (CD34$^+$CD38 lin Thy1$^+$) for stem cells (fig. S16). Consistent with this, the LTC-IC frequency in GFP human cells isolated from NOVH recipients was almost seven times that in GFP human cells from the same animal (Fig. 4E). These NOVH GFP$^+$ cells isolated from primary recipients could be maintained in liquid culture for 4 weeks and still retained CD34 expression (fig. S17); by this time, GFP cells from NOVH recipients and GFP$^+$ cells from control recipients had expired.

In view of the preferential engraftment of Nov^{hi} cells, their enhanced LTC-IC capacity, and their ability to maintain high CD34 expression in liquid culture, we assessed the effects of enforced Nov expression on stem cell self-renewal, as classically measured in secondary transplantation assays. Therefore, we intravenously transplanted NOVH GFP cells that had been isolated from engrafted animals and subsequently cultured for 4 weeks into secondary recipients at a dose of 15,000 cells per mouse. The frequency of SRC has been estimated to be 1 per 20,700 in cord blood CD34 cells in primary engraftment assays (29), and is ≤1/10th that amount in secondary transplantation (30). Thus, we consider 15,000 cells in a secondary transplant setting to be a stringently limiting dose. After 8 weeks, engraftment was assessed in recipient bone marrow by GFP fluorescence (Fig. 4F), and, remarkably, given the limited cell dose and the intervening culture period between the primary harvest and the secondary transplantation, was seen in five out of five mice injected. To confirm engraftment, genomic DNA from total bone marrow in each mouse was purified and tested for the presence of human DNA by PCR using primers specific for human chromosome 17 α-satellite sequences (31). Evidence for engraftment was seen in each secondary recipient (Fig. 4G). About 20% of engrafted cells also expressed CD34 (Fig. 4F), and expression of human CD33 and CD19 could also be detected, which suggested that multilineage engraftment had occurred.

Using complementary approaches, we have identified a role for Nov in human hematopoietic stem or progenitor cell function, which implicates it as an essential regulator. The key findings are that loss of Nov abrogates primitive progenitor function, both in vitro and in vivo. Homing, survival, and differentiation appear intact, but defects in cell cycling and Notch signaling are apparent. The requirement for Nov in assays that functionally test several types of primitive cell raises the possibility that it has an impact on generic self-renewal machinery common to all of these subsets. Mirroring these observations, the addition of Nov either extracellularly or by enforced intracellular expression, enhances stem or progenitor read-out in vitro. In transplantation assays, enforced expression enhances stem cell and progenitor cell activity within the graft, as judged by immunophenotype and LTC-IC frequency, as well as secondary transplantability at limiting dose.

Although the role of NOV in the function of primitive hematopoietic cells in other species is yet to be tested, our results support the notion that Nov is a central regulator of these cells in humans. NOV thus provides a hitherto unexplored axis for understanding the critical cell fate decisions of the hematopoietic stem and progenitor compartments.

References and Notes

1. I. Lapidot, I. Petit, Exp. Hematol. 30, 973 (2002).
2. X.-B. Zhang et al., PLoS Med. 3, e173 (2006).
3. E. C. Attar, D. T. Scadden, Leukemia 18, 1760 (2004).
4. I. K. Park et al., Nature 423, 302 (2003).
5. H. Hock et al., Nature 431, 1002 (2004).
6. H. Hock et al., Genes Dev. 18, 2336 (2004).
7. N. B. Ivanova et al., Science 298, 601 (2002).
8. L. Bruno et al., Mol. Cell. Biol. 24, 741 (2004).
9. V. Joliot et al., Mol. Cell. Biol. 12, 10 (1992).
10. B. Perbal, Lancet 363, 62 (2004).
11. H. Thibout et al., J. Clin. Endocrinol. Metab. 88, 327 (2003).
12. C. G. Lin, C. C. Chen, S.-J. Leu, T. M. Grzeszkiewicz, L. F. Lau, J. Biol. Chem. 280, 8229 (2005).
13. C. G. Lin et al., CCN3, J. Biol. Chem. 278, 24200 (2003).
14. W. C. Hahn et al., Nature 400, 464 (1999).
15. G. de Haan, personal communication.
16. H. E. Broxmeyer, Cytotherapy 7, 209 (2005).
17. Materials and methods are available as supporting material on Science Online.
18. D. A. Rubinson et al., Nat. Genet. 33, 401 (2003).
19. L. Lu, M. Xiao, D. W. Clapp, Z. H. Li, H. E. Broxmeyer, J. Exp. Med. 178, 2089 (1993).
20. K. Sakamoto et al., J. Biol. Chem. 277, 29399 (2002).
21. K. Ohishi et al., Semin. Cell Dev. Biol. 14, 143 (2003).
22. M. Bhatia, J. C. Wang, U. Kapp, D. Bonnet, J. E. Dick, Proc. Natl. Acad. Sci. U.S.A. 94, 5320 (1997).
23. R. H. Cho, C. E. Muller-Sieburg, Exp. Hematol. 28, 1080 (2000).
24. J. E. Dick, G. Guenechea, O. I. Gan, C. Dorrell, Ann. N. Y. Acad. Sci. 938, 184 (2001).
25. A. Sirven et al., Mol. Ther. 3, 438 (2001).
26. C. Demaison et al., Hum. Gene Ther. 13, 803 (2002).
27. S. Amsellem et al., Nat. Med. 9, 1423 (2003).
28. O. S. Kustikova et al., Blood 102, 3934 (2003).
29. P. A. Denning-Kendall et al., Br. J. Haematol. 116, 218 (2002).
30. G. Guenechea, O. I. Gan, C. Dorrell, J. E. Dick, Nat. Immunol. 2, 75 (2001).
31. P. E. Warburton, G. M. Greig, T. Haaf, H. F. Willard, Genomics 11, 324 (1991).
32. B. Y. Su et al., Mol. Pathol. 54, 184 (2001).

33. We thank A. Atzberger, C. Waugh, I. Titley, and Y.-P. Guo for technical assistance; and N. Rodrigues, C. Heyworth, G. May, D. Higgs, M. Greaves, K. Humphries, M. Bhatia, M. Dexter, and S.-E. Jacobsen for advice and critical reading of the manuscript. This work was supported by the Leukaemia Research Fund, the Medical Research Council, and Eurostemcells.

Supporting Online Material
www.sciencemag.org/cgi/content/full/316/5824/590/DC1
Materials and Methods
Figs. S1 to S17
References

10 October 2006; accepted 26 March 2007
10.1126/science.1136011

Multiple High-Throughput Analyses Monitor the Response of *E. coli* to Perturbations

Nobuyoshi Ishii,[1,2]* Kenji Nakahigashi,[1,2]* Tomoya Baba,[1,2,3]* Martin Robert,[1,2]* Tomoyoshi Soga,[1,2,4]* Akio Kanai,[1,2]* Takashi Hirasawa,[1,2]* Miki Naba,[1] Kenta Hirai,[1] Aminul Hoque,[1,2] Pei Yee Ho,[5] Yuji Kakazu,[1] Kaori Sugawara,[1] Saori Igarashi,[1] Satoshi Harada,[1] Takeshi Masuda,[1,2] Naoyuki Sugiyama,[6] Takashi Togashi,[1] Miki Hasegawa,[1] Yuki Takai,[1] Katsuyuki Yugi,[1,2] Kazuharu Arakawa,[1] Nayuta Iwata,[1,2] Yoshihiro Toya,[1,2] Yoichi Nakayama,[1,2] Takaaki Nishioka,[1,2,4] Kazuyuki Shimizu,[1,2,5] Hirotada Mori,[1,2,3] Masaru Tomita[1,2,4]†

Analysis of cellular components at multiple levels of biological information can provide valuable functional insights. We performed multiple high-throughput measurements to study the response of *Escherichia coli* cells to genetic and environmental perturbations. Analysis of metabolic enzyme gene disruptants revealed unexpectedly small changes in messenger RNA and proteins for most disruptants. Overall metabolite levels were also stable, reflecting the rerouting of fluxes in the metabolic network. In contrast, *E. coli* actively regulated enzyme levels to maintain a stable metabolic state in response to changes in growth rate. *E. coli* thus seems to use complementary strategies that result in a metabolic network robust against perturbations.

The complex relationships between different layers of biological information that give rise to cellular functions can only be captured by combining global measurements across these different levels (1–8). Moreover, most current global methods such as DNA microarray and shotgun proteomic analyses aim to interrogate the composition of intracellular components rather than to accurately determine the quantities of molecules in cells. More quan-

titative methods such as quantitative reverse transcription polymerase chain reaction (qRT-PCR) and metabolic flux analysis, which have the advantage that they are essential to detect small changes in response to perturbation. In the present study, we measured the global responses of *E. coli* K-12 cells to genetic and environmental perturbations at the level of protein and gene expression, and compared this with a detailed quantitative analysis of specific metabolic pathways.

To monitor the global cellular response, we determined the relative quantities of gene and protein expression using DNA microarray analysis and two-dimensional differential gel electrophoresis (2D-DIGE) (9, 10). For more detailed analysis, in addition to qRT-PCR and metabolic flux analysis, we used capillary electrophoresis time-of-flight mass spectrometry (CE-TOFMS) for metabolome analysis (11) and liquid chromatography tandem mass spectrometry (LC-MS/MS) for absolute quantification of proteins (12). As molecular targets for these more detailed quantitative analyses, we selected genes, proteins, metabolites, and fluxes that make up the bulk of reactions of the central carbon metabolism of *E. coli* K-12, including glycolysis, the pentose phosphate pathway, and the tricarboxylic acid cycle (TCA), because these pathways play a crucial role in energy generation and in the production of important macromolecular precursors. We sought to characterize the cellular response to disruptions in order to fulfill basic metabolic needs and maintain the growth phenotype.

We collected data using these multiple high-throughput analyses for wild-type *E. coli* K-12 and 24 single-gene disruptants, which were selected from the Keio collection (13) and cover most viable glycolysis and pentose phosphate pathway disruptants (i.e., *galM, glk, pgm, pgi, pfkA, pfkB, fbp, fbaB, gapC, gpmA, gpmB, pykA, pykF, ppsA, zwf, pgl, gnd, rpe, rpiA, rpiB, tktA, tktB, talA,* and *talB*). The cells were grown at a single fixed dilution rate of 0.2 hours^{-1} in glucose-limited chemostat cultures, and wild-type cells cultured at the same specific growth rate were used as a reference sample for comparison. To allow a comparison of the effects of these genetic perturbations with the effects of environmental perturbations, wild-type cells were examined at several different dilution rates (0.1, 0.2, 0.4, 0.5, and 0.7 hours^{-1}). In chemostat cultures, the concentration of growth-limiting substrate can be controlled by the dilution rate. The dilution rate was thus varied in this study from an almost glucose-sufficient state to a heavily limited glucose supply. Changes in dilution rate, therefore, alter growth rate and can be considered a specific type of environmental change.

To evaluate differences between samples in the various perturbation experiments, we used an expression index (EI) (17), which scales the data to the same range for all molecules examined, regardless of the measurement (SOM text), so that changes in mRNA, protein, and metabolite levels can be compared more easily. Fig. 1 shows the EIs derived from the targeted analyses of the network components. For mRNA and protein, the effects of changes in growth rate are obvious and appear to be greater than the effects of most gene disruptions. In contrast, except for nucleotides, changes in metabolites did not show any distinctive patterns, which could indicate different responses in metabolite levels against various perturbations. The lower levels of nucleotides observed in some disruptants (e.g., *gnd, rpe, rpiA,* and *pgl*) may reflect problems in the maintenance of owing to the chemical instability or inconsistent extraction efficiencies of these molecules. We thus provide results calculated including and excluding nucleotide measurements.

To capture the magnitudes of the effects seen in Fig. 1, we calculated an average EI, the average expression index (AEI) (17), for each type of component (mRNA, protein, and metabolite) and compared them between samples (fig. S2 and tables S7 and S8). One-way analysis of variance (one-way ANOVA) and post hoc tests (Games-Howell test) were performed for all comparisons to test for statistically significant differences ($P < 0.05$; SOM text).

At higher growth rates, the AEI for mRNAs and proteins gradually increased for both targeted and global quantification analyses, suggesting that *E. coli* actively regulates the gene ex-

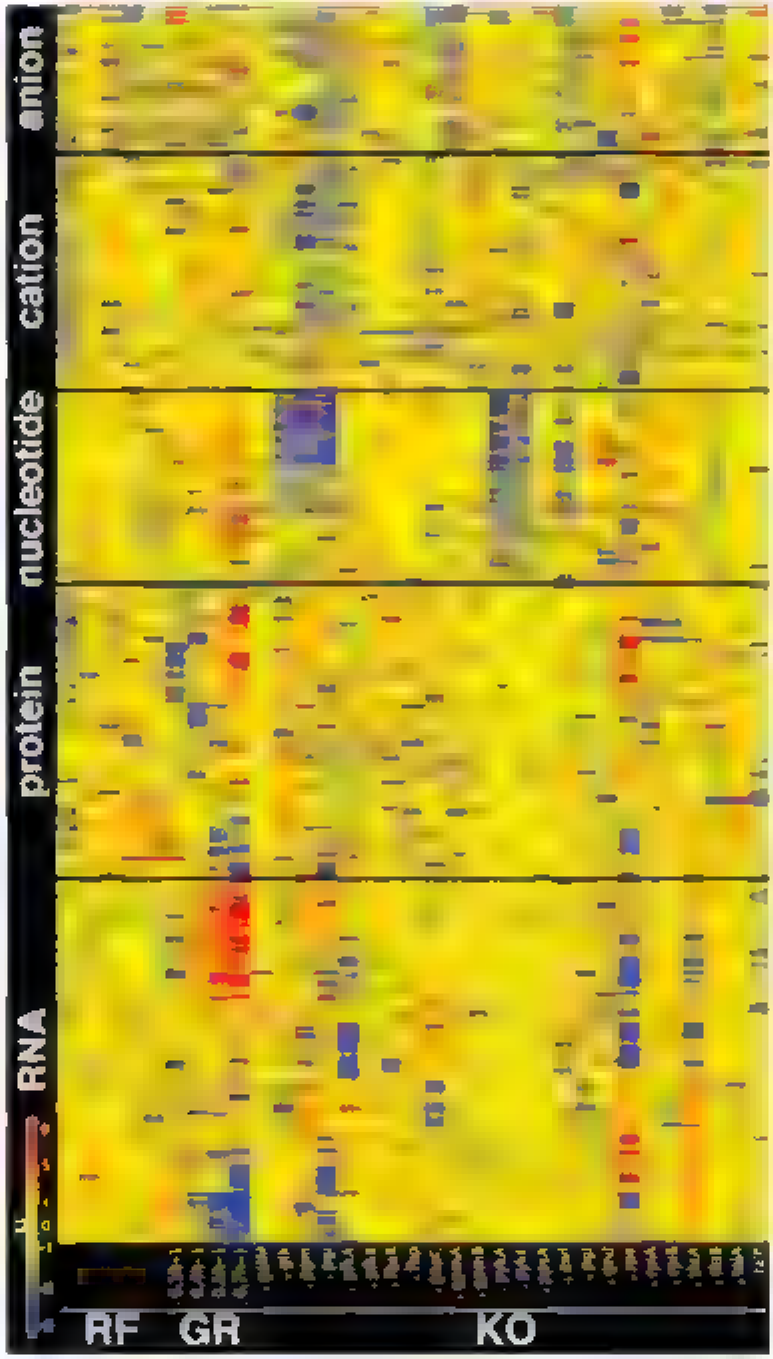

Fig. 1. Overall representation of changes in the targeted cellular components. The heat map shows the EI values of intracellular components that were detected in more than half the samples. RF, reference sample (wild-type cells cultured at a specific growth rate of 0.2 hours^{-1}); GR, wild-type cells cultured at the indicated specific growth rates; KO, single-gene knockout mutants cultured at a specific growth rate of 0.2 hours^{-1}. The numbers of individual components shown are metabolites, 130; proteins, 57; and mRNA transcripts, 85. The same type of representation including all component names is shown in fig. S3, and all EI values are shown in table S8.

[1]Institute for Advanced Biosciences, Keio University, Tsuruoka, Yamagata 997-0017, Japan. [2]Systems Biology Program, Graduate School of Media and Governance, Keio University, Fujisawa 252-8520, Japan. [3]Graduate School of Biological Sciences, Nara Institute of Science and Technology, Ikoma, Nara 630-0101, Japan. [4]Graduate School of Agriculture, Kyoto University, Kyoto 606-8502, Japan. [5]Department of Bioscience and Bioinformatics, Kyushu Institute of Technology, Iizuka, Fukuoka 820-8502, Japan. [6]Human Metabolome Technologies, Inc., Tsuruoka 997-0017, Japan.

*These authors contributed equally to this work.
†To whom correspondence should be addressed. E-mail: mt@sfc.keio.ac.jp

protein levels to meet increasing metabolic demands (Fig. 2, A, C, and D). In contrast, the AEI values for metabolites did not change significantly with growth rate. This relative stability in metabolite level may be a consequence of the observed regulation of enzyme levels. Closer examination of particular components revealed the induction and repression of mRNAs and specific enzymes after a change in specific growth rate (figs. S5 and S6). The levels of proteins involved in glucose uptake (PtsH and PtsI) were induced considerably when the specific growth rate increased. This is to be expected, because substrate uptake is the first step in fulfilling nutrient demands. The observed increase in the expression of phosphoenolpyruvate carboxylase (Ppc), decrease in the expression of phosphoenolpyruvate carboxykinase (PckA), and repression of glyoxylate shunt enzymes are also logical responses to enhance the tricarboxylic acid cycle flux (2), which corresponds to energy production under aerobic conditions and the components of which are important precursors in biomass production.

In contrast to the changes observed in wild-type cells cultured at various growth rates, most gene disruptants showed only subtle changes in AEIs for both mRNA and protein of central carbon metabolism enzymes, which fell within the range of variations observed in wild-type samples at the same specific growth rate (Fig. 2C). The AEI values for these targeted analyses of mRNAs and proteins in all disruptants were smaller than the AEI values observed for wild-type cells at a specific growth rate of 0.7 hours^{-1}, and the difference was significant in 23 disruptants for mRNAs and in 16 disruptants for proteins. Similar results were obtained for the AEI values representing the global analysis of mRNA and protein expression (Fig. 2D). These findings suggest that *E. coli* does not appreciably respond to the loss of a single central carbon metabolism enzyme by regulating the abundance of other compensatory enzymes. This was especially apparent when examining changes in the expression of genes encoding isozymes of the respective disrupted enzymes (fig. S5). Isozymes that might be expected to compensate for the loss of an important enzyme were not up-regulated, although many were induced at higher growth rates. The two exceptions to this general pattern were the induction of *pfkB* in the *pfkA* disruptant and the very considerable induction of *rpiB* in the *rpiA* disruptant. However, in both cases, we found that cells accumulated additional mutations that are known to induce expression of the isozymes (*15*, *16*). Therefore, the induction of these genes was not solely dependent on direct regulation (SOM text). It seems apparent that except for these genes, enzymatic capacity is already expressed in the cell through structural redundancy (presence of isozymes and/or alternative routes).

The AEI values for metabolites in three disruptants (*pgm*, *pgi*, and *rpe*) were higher than those of wild-type cells at high specific growth rates (0.5 and 0.7 hours^{-1}) (Fig. 2C). This phenomenon does not appear to be caused by the problems associated with nucleotide measurements in some disruptants, because similar results were obtained even when nucleotides were excluded from the AEI calculation (Fig. 2C). In the *rpe* disruptant, which had a particularly high AEI for metabolites, the levels of a few linked metabolites were increased to a large extent (Fig. 3A, *rpe*). However, these local changes were not responsible for the large metabolite AEI for this particular disruptant. Also, an overall stability in metabolic levels, i.e., low AEI, was maintained in most disruptants, even if the local metabolic network was perturbed (Fig. 2B and Fig. 3B, *talB*). This stability of metabolite levels is likely achieved through structural robustness of the metabolic network itself (*17*, *18*), even when considerable rerouting of fluxes occurs. For ex-

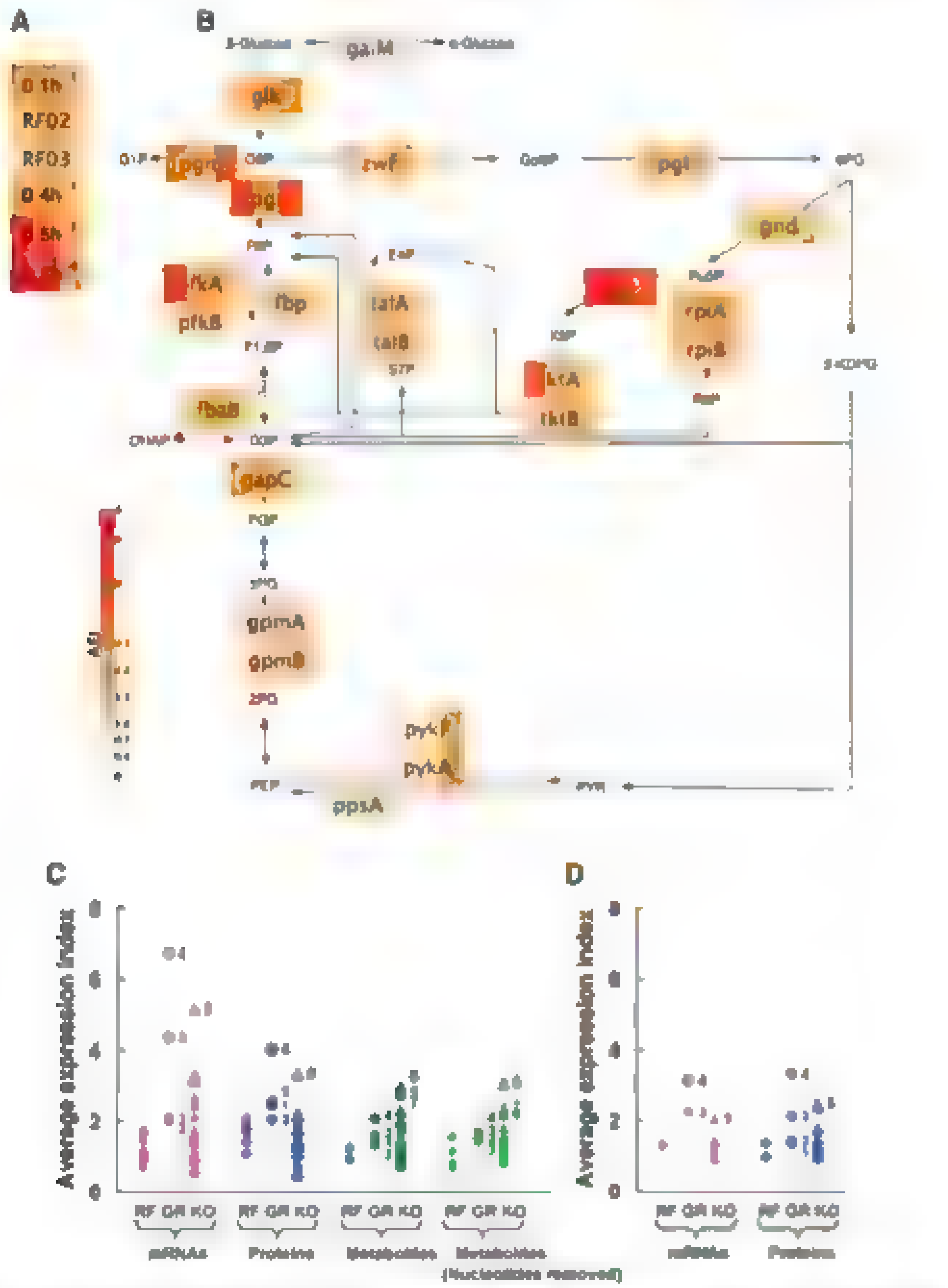

Fig. 2. AEI values for mRNA, protein, and metabolite levels. RF, GR, and KO are defined in the legend of Fig. 1. (**A** and **B**) The AEI values of a specific sample are represented as a heat map. The three panels in each box show three quantitative values corresponding to the AEI for mRNAs as determined by qRT-PCR (left panel), proteins as determined by LC-MS/MS (middle panel), and metabolites as determined by CE-TOFMS (right panel), respectively. (A) AEI values for GR. The labels in each row of the heat map correspond to either a specific growth rate (hours^{-1}) or the two reference samples (RF02 and RF03). (B) AEI values for all gene disruptants displayed at their respective locations on the metabolic pathway map. Abbreviations for metabolites are as shown in table S1. (**C**) Quantitative measurements obtained by targeted analysis. (**D**) Semiquantitative cell-wide measurements. The numerical values are provided in table S9. In (C) and (D), numbers 1, 2, 3, and 4 correspond to specific growth rates of 0.1, 0.4, 0.5, and 0.7 hours^{-1}, and numbers 5, 6, and 7 correspond to *rpe*, *pgi*, and *pgm* disruptants, respectively.

ample, in the *zwf* disruptant, the overall flux within the pentose phosphate pathway was reversed to compensate for the blocked route for the production of essential molecules, but, interestingly, this task can be achieved without large changes in enzyme levels in the pathways involved (Fig. 3C and table S5).

Our results reveal that the intracellular metabolic network of *E. coli* is remarkably stable and robust in the face of various types of disturbances. Highlighting the functional importance of this global stability for efficient cell growth, *E. coli* can actively respond to changes in the concentration of growth-limiting substrate by regulating the level of enzyme expression to maximize growth rate, which is reflected in the observed stability of metabolite levels. Using this strategy, *E. coli* can react quickly and effectively to this environmental change, but the strategy might be costly, because the cell must provide additional systems (such as sensor proteins, signal mediators, and transcriptional regulators) to detect and react appropriately to each specific perturbation. Because active response to the environment at the level of gene expressions is a widespread phenotype of *E. coli*, this might be a common strategy that the cell can use when it faces environmental changes. This strategy contrasts with the finding that *E. coli* does not appear to react significantly to the disruption of most single metabolic genes by regulating multiple other mRNA or protein levels. In this case, structural redundancy in the metabolic network itself provides the necessary robustness (*19*, *20*), allowing the levels of most metabolites to remain constant, although some localized perturbations are inevitable. This strategy is likely to be less costly than the one mentioned above, because it requires no specific sensors for each mutation, while providing resistance against many of these mutations. Even if this strategy appears insufficient in the face of some mutations, *E. coli* may survive by accumulating additional mutations, as we observed for *pfkA* and *rpiA* disruptants. Using multiple strategies may thus enable *E. coli* to maintain a stable state when exposed to various types of perturbations. Additional information is available at the project Web site (*21*).

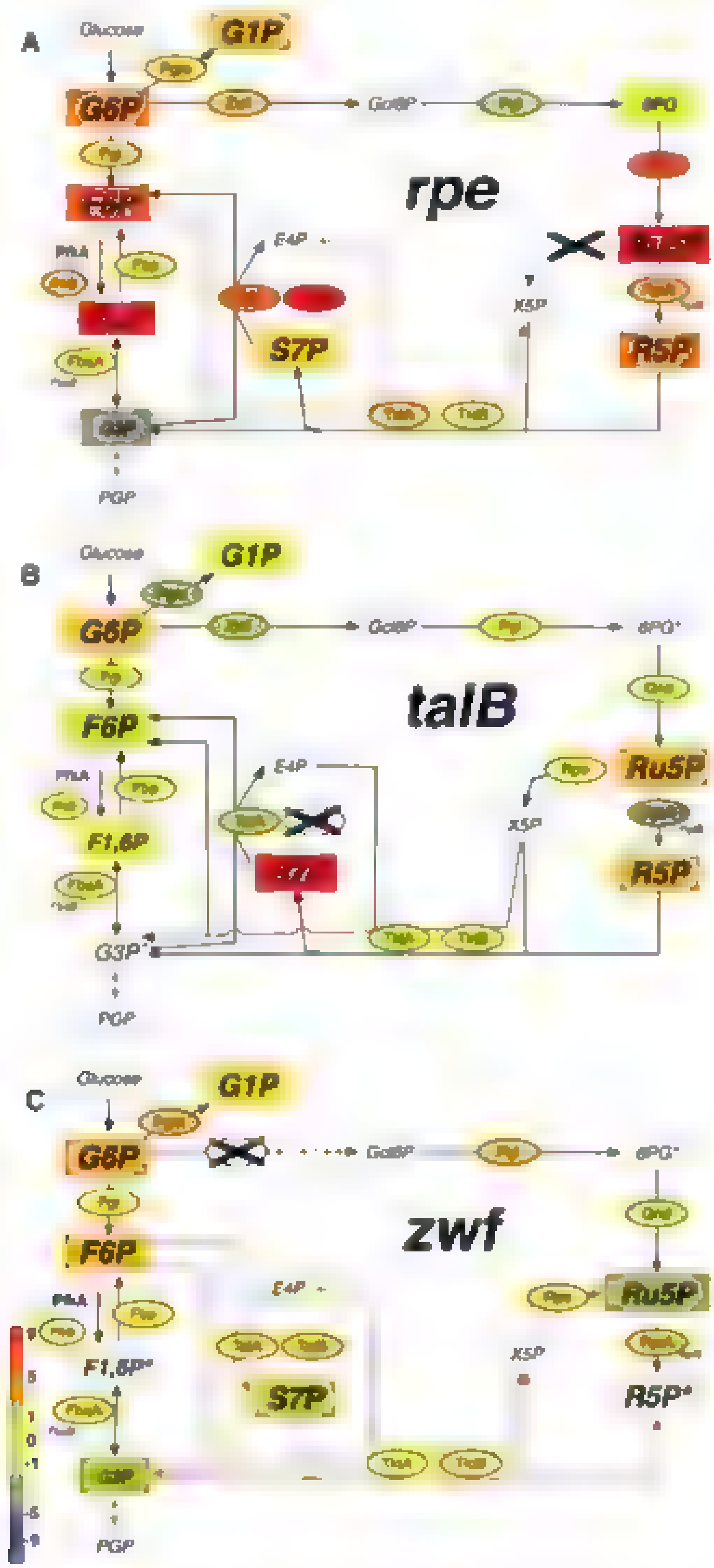

Fig. 3. Perturbations in the local metabolic network caused by enzyme gene disruptions. The EI values for proteins (circled) and metabolites (boxed) in *rpe* (**A**), *talB* (**B**), and *zwf* (**C**) disruptants are shown mapped onto the local metabolic network. The disrupted enzymes are highlighted with an X, and the specific reaction eliminated by the disruption is shown with a dashed line. Reactions indicated with red arrows are running in the direction opposite to that in the wild-type. Colorless symbols represent components that were not measurable, and components not detected in the specific mutant are shown with an asterisk.

References and Notes

1. A. R. Joyce, B. O. Palsson, *Nat. Rev. Mol. Cell Biol.* **7**, 198 (2006).
2. S. S. Fong, A. Nanchen, B. O. Palsson, U. Sauer, *J. Biol. Chem.* **281**, 8024 (2006).
3. G. N. Vemuri, A. A. Aristidou, *Microbiol. Mol. Biol. Rev.* **69**, 197 (2005).
4. A. Mukhopadhyay *et al.*, *J. Bacteriol.* **188**, 4068 (2006).
5. M. Y. Hirai *et al.*, *Proc. Natl. Acad. Sci. U.S.A.* **101**, 10205 (2004).
6. H. Ge, A. J. Walhout, M. Vidal, *Trends Genet.* **19**, 551 (2003).
7. T. Toyoda, A. Wada, *Bioinformatics* **20**, 1759 (2004).
8. T. Ideker *et al.*, *Science* **292**, 929 (2001).
9. R. Marouga, S. David, E. Hawkins, *Anal. Bioanal. Chem.* **382**, 669 (2005).
10. T. Soga *et al.*, *J. Proteome Res.* **2**, 488 (2003).
11. T. Soga *et al.*, *J. Biol. Chem.* **281**, 16768 (2006).
12. Materials and Methods are available as supporting material on *Science* Online.
13. T. Baba *et al.*, *Mol. Syst. Biol.* **2**, published online 21 February 2006 (10.1038/msb4100050).
14. P. A. Hoskisson, G. Hobbs, *Microbiology* **151**, 3153 (2005).
15. A. J. Skinner, R. A. Cooper, *J. Bacteriol.* **118**, 1183 (1974).
16. F. Daldal, *J. Mol. Biol.* **168**, 285 (1983).
17. Z. Gu *et al.*, *Nature* **421**, 63 (2003).
18. J. Stelling, S. Klamt, K. Bettenbrock, S. Schuster, E. D. Gilles, *Nature* **420**, 190 (2002).
19. H. Kitano, *Nat. Rev. Genet.* **5**, 826 (2004).
20. D. Becker *et al.*, *Nature* **440**, 303 (2006).
21. http://ecoli.iab.keio.ac.jp

22. The authors thank M. Li and M. J. Arauzo-Bravo for help with the metabolic flux calculations, Y. Ishihama for proofreading the manuscript and for advice about LC-MS/MS absolute quantification of proteins, and T. Ogawa, Y. Suga, A. Hagiya, and M. Yoshino for experimental support for protein analyses. This study was carried out as part of a grant from the New Energy and Industrial Technology Development Organization (NEDO) of the Ministry of Economy, Trade, and Industry of Japan (METI) (Development of a Technological Infrastructure for Industrial Bioprocess Project). The work was also

supported by a grant from Core Research for Evolutional Science and Technology (CREST), Japan Science and Technology Agency (JST) (Development of Modeling/Simulation Environment for Systems Biology); a grant from Japan Society for the Promotion of Science (JSPS); and "grant-in-aid" research grants from the Ministry of Education, Culture, Sports, Science, and Technology (MEXT) for the 21st Century Centre of Excellence (COE) Program (Understanding and Control of Life's Function via Systems Biology), Scientific Research on Priority Areas "Systems Genomics," and Scientific Research on Priority Areas "Lifesurveyor" as well as funds from the Yamagata Prefectural Government and Tsuruoka City. We thank the faculty and students of the Systems Biology Program at Keio University for useful discussions, as well as members of the International E. coli Alliance (IECA).

Supporting Online Material
www.sciencemag.org/cgi/content/full/1132067/DC1
Materials and Methods
SOM Text
Figs. S1 to S7
Tables S1 to S12
References

5 July 2006; accepted 12 March 2007
Published online 22 March 2007;
10.1126/science.1132067
Include this information when citing this paper.

A Synthetic Maternal-Effect Selfish Genetic Element Drives Population Replacement in *Drosophila*

Chun-Hong Chen,[1] Haixia Huang,[1] Catherine M. Ward,[1] Jessica T. Su,[1] Lorian V. Schaeffer,[1] Ming Guo,[2] Bruce A. Hay[1]*

One proposed strategy for controlling the transmission of insect-borne pathogens uses a drive mechanism to ensure the rapid spread of transgenes conferring disease refractoriness throughout wild populations. Here, we report the creation of maternal-effect selfish genetic elements in *Drosophila* that drive population replacement and are resistant to recombination-mediated dissociation of drive and disease refractoriness functions. These selfish elements use microRNA-mediated silencing of a maternally expressed gene essential for embryogenesis, which is coupled with early zygotic expression of a rescuing transgene.

Mosquitoes with a diminished capacity to transmit human pathogens have been identified in the wild and/or created in the laboratory, demonstrating that endogenous or engineered mosquito immunity can be harnessed to attack these pathogens (*1*–*5*). However, it will be necessary to replace a large percentage of the wild mosquito population with refractory insects to achieve substantial levels of disease control (*6*–*8*). Mosquitoes carrying genes that confer disease refractoriness are not expected to have a higher fitness than native mosquitoes, implying that Mendelian transmission is unlikely to result in an increase in the frequency of transgene-bearing individuals after their initial release into the wild (*4*, *9*). Thus, effective population replacement will require the coupling of genes conferring disease refractoriness with a genetic mechanism for driving these genes through the wild population at greater than Mendelian frequencies (*10*, *11*).

Maternal-effect selfish genetic elements [first described in the flour beetle *Tribolium castaneum* and known by the acronym *Medea* (maternal-effect dominant embryonic arrest)] select for their own survival by inducing maternal-effect lethality of all offspring not inheriting the element-bearing chromosome from the maternal and/or paternal genome (*12*) (Fig. 1A). Current models predict that if *Medea* elements are introduced into a population above a threshold frequency, determined by any associated fitness cost, they will spread within the population (*12*–*14*) (Fig. 1, C and D). When introduced into a population at relatively high frequencies, *Medea* elements are predicted to rapidly convert the entire population into element-bearing heterozygotes and homozygotes (Fig. 1C). *Medea* in *Tribolium* is hypothesized to consist of a maternal lethal activity (a toxin) that kills non-*Medea*–bearing progeny and a zygotic rescue activity (an antidote) that protects *Medea*-bearing progeny from this maternal lethal effect (*12*, *15*) (Fig. 1A).

To create a *Medea*-like maternal-effect selfish genetic element in *Drosophila*, we generated a *P* transposable element vector in which the maternal germline–specific *bicoid* (*bcd*) promoter drives the expression of a polycistronic transcript encoding two microRNAs (miRNAs) designed to silence expression of *myd88* (the gene producing the toxin) [Fig. 1B and (*16*)]. Maternal Myd88 is required for dorsal-ventral pattern formation in early embryo development. Females with germline loss-of-function mutations for *myd88* give rise to embryos that lack ventral structures and thus fail to hatch, even when a wild-type (WT) paternal allele is present (*17*). This vector (known as *Medea*[myd88]) also carries a maternal miRNA-insensitive *myd88* transgene expressed under the control of the early embryo–specific *bottleneck* (*bnk*) promoter (the gene producing the zygotic antidote) (Fig. 1B). Our analyses focused on flies carrying a single autosomal insertion of this element, *Medea*[myd88-1].

Matings between heterozygous *Medea*[myd88-1]/+ males (where + indicates a chromosome that does not carry *Medea*[myd88-1]) and homozygous +/+ females resulted in high levels of embryo viability, similar to those for the w^{1118} strain used for transformation (Table 1). In addition, 50% of the adult progeny carried *Medea*[myd88-1], as expected for Mendelian segregation without dominance. Matings among homozygous *Medea*[myd88-1] flies also resulted in high levels of egg viability. In contrast, when heterozygous *Medea*[myd88-1]/+ females were mated with homozygous +/+ males, ~50% of progeny embryos had ventral patterning defects (fig. S1) and did not hatch (Table 1). All adult progeny (*n* > 12,000 flies) carried *Medea*[myd88-1] (Table 1). On the basis of these data and the results of several other crosses (Table 1), we inferred that a single copy of *bcd*-driven miRNAs targeting maternal *myd88* expression was sufficient to induce maternal-effect lethality and a single copy of zygotic *bnk*-driven *myd88* expression was sufficient for rescue.

The above observations, in conjunction with the lack of any obvious fitness effects (lethality) in individuals carrying one or two copies of *Medea*[myd88-1], suggested that *Medea*[myd88-1] should be able to drive population replacement. To test this prediction, we mated equal numbers of WT (+/+) and *Medea*[myd88-1]/*Medea*[myd88-1] males with homozygous +/+ females, giving rise to a progeny population with *Medea*[myd88-1] present at an allele frequency of ~25% (*16*). This level of introduction, although high, is not unreasonable, given previous insect population suppression programs (*18*). Replicate population cage experiments, carried out in a darkened incubator to prevent *Medea*[myd88-1]-bearing flies (which are P^{w+} and thus red-eyed) from obtaining any vision-dependent advantage over their +/+ counterparts (which are w^{1118} and white-eyed) (*19*), followed three replicates for 20 generations. A second set of four replicates, which were initiated by crossing heterozygous *Medea*[myd88-1] males with homozygous +/+ females, was followed for 15 generations. In both experiments, non-*Medea*[myd88-1]–bearing flies permanently disappeared from the population between generations 10 and 12 (Fig. 1E), without a loss of non-*Medea*–bearing + chromosomes (in *Medea*[myd88-1] individuals) in the population (Fig. 1F). The observed changes in *Medea*[myd88-1] were not significantly different from the null hypothesis that the element had no fitness cost [(*16*) and fig. S2], although we cannot exclude the possibility that a *Medea*[myd88-1]-associated cost is counterbalanced by an unknown negative effect associated with

[1]Division of Biology, Mail Code 156-29, California Institute of Technology, Pasadena, CA 91125, USA. [2]Departments of Neurology and Pharmacology, Brain Research Institute, David Geffen School of Medicine, University of California, Los Angeles, Los Angeles, CA 90095, USA.

*To whom correspondence should be addressed. E-mail: haybruce@caltech.edu

the w^{1118} mutation in +/+ individuals. Finally, we carried out three further replicate population cage experiments in which the $Medea^{myd88-1}$ transgene was introduced at a frequency of 25% into the Oregon-R strain, which is WT with respect to the endogenous w locus (and thus members of which are red-eyed). Evidence for population replacement by generation 12 was observed in this context as well (16), suggesting that $Medea^{myd88-1}$ associated P^{w+} expression is unlikely to be a major contributor to the ability of $Medea^{myd88-1}$ to drive population replacement.

For any gene-drive mechanism to be successful in reducing parasite transmission, there must be tight linkage between the genes that mediate drive and effector functions (10). If the driver becomes separated from the effector gene through chromosome breakage and nonhomologous end joining (as in a reciprocal translocation) (Fig. 2A) and the effector gene carries a fitness cost, selection will favor and promote the spread of chromosomes carrying Medea elements that lack the effector ($Medea^{\Delta eff}$). Locating the effector gene between the toxin and antidote prevents a single chromosome breakage and end joining event from creating a $Medea^{\Delta eff}$-bearing chromosome (Fig. 2B). However, it does not prevent the creation of $Medea^{ins}$-bearing chromosomes that carry the antidote, and perhaps the effector, but not the toxin (Fig. 2B). $Medea^{ins}$-bearing chromosomes are insensitive to Medea-dependent killing. If the presence of the toxin and/or the effector results in a fitness cost, then $Medea^{ins}$-bearing chromosomes gain a fitness advantage with respect to those carrying the complete Medea element, thereby promoting spread of the former. This outcome can lead to the reappearance of pathogen-transmitting insects (14).

One way to prevent chromosome breakage and end joining–mediated formation of $Medea^{\Delta eff}$ and $Medea^{ins}$ elements is to put the toxin and effector genes into an intron of the antidote (Fig. 2C). To test this approach, we generated flies carrying $P^{w+}Medea^{myd88-int}$, in which the toxin, a transcript generating maternally expressed miRNAs targeting myd88, was placed in an intron of the zygotically expressed antidote, bnk-driven myd88, in the opposite orientation (Fig. 2D). We characterized the behavior of one autosomal insertion of this element $Medea^{myd88-int-1}$, which behaved as a maternal-effect selfish genetic element (Table 2). Females heterozygous for $Medea^{myd88-int-1}$ gave rise to a high frequency of $Medea^{myd88-int-1}$ carrying progeny (~99%), and the maternal-effect lethality associated with a single copy of $P^{w+}Medea^{myd88-int-1}$ was rescued by zygotic expression of the antidote from either the maternal or paternal genome (Table 2). However, when homozygous element-bearing females were crossed with non-element-bearing males, progeny embryo survival was very poor (~20%), suggesting an inefficient zygotic rescue, perhaps resulting from inefficient splicing of the myd88 artificial intron. Population replacement for an element with these fitness characteristics is still expected to occur, though with some delay (fig. S3) as compared to that for an element in which the fitness costs are a simple function of copy number in either sex (Fig. 1, C and D).

$Medea^{ins}$-bearing chromosomes can also arise if the toxin mutates to inactivity. Although toxin mutation cannot be prevented, the use of

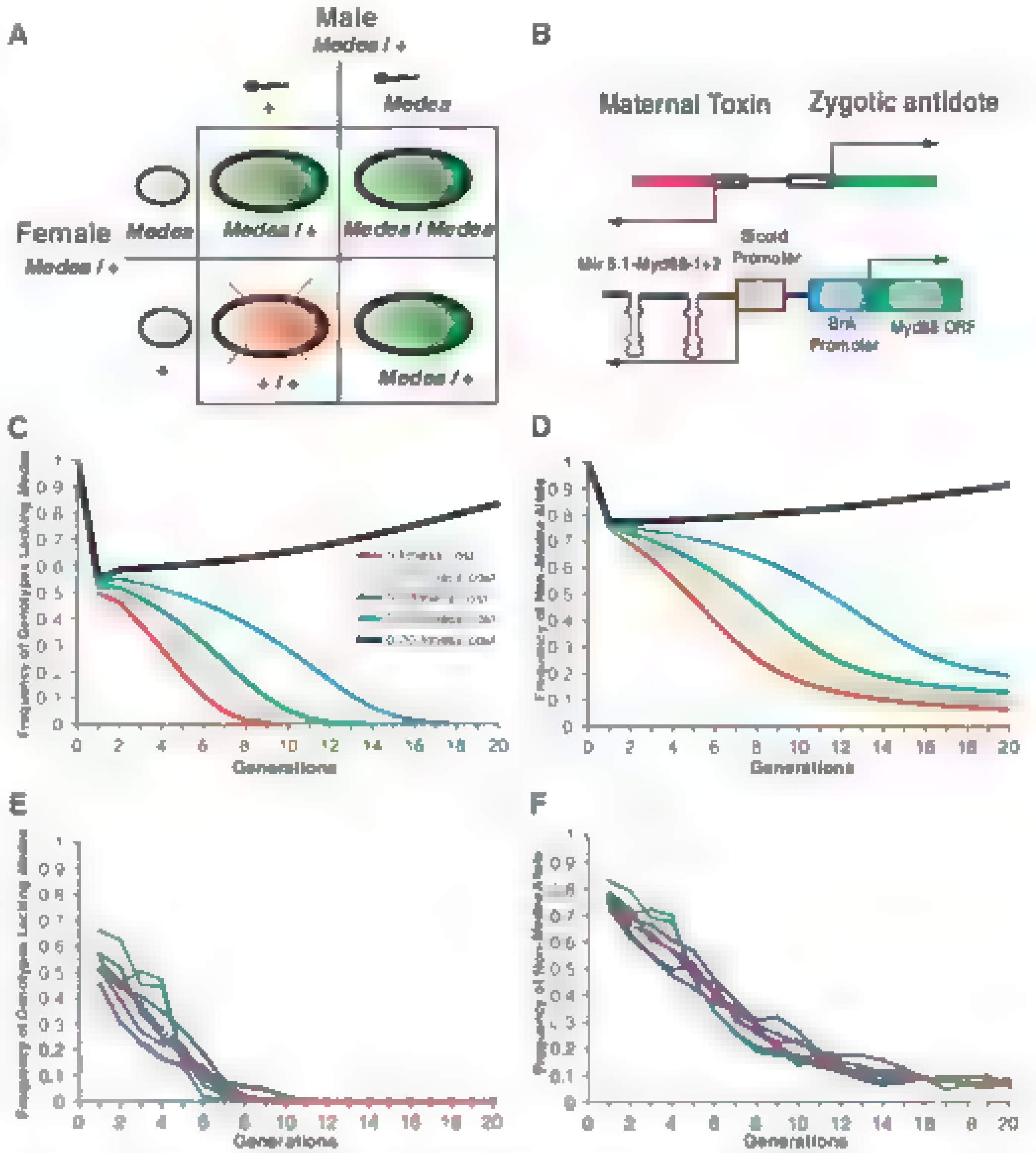

Fig. 1. Characteristics of a maternal-effect selfish genetic element (Medea) and a synthetic Medea element in Drosophila. (**A**) It is postulated that females heterozygous for Medea (Medea/+) deposit a protoxin or toxin (red dots) into all oocytes. Embryos that do not inherit a Medea-bearing chromosome die because toxin activation or activity is unimpeded (bottom left square). Embryos that inherit Medea from the maternal genome (top left square), the paternal genome (bottom right square), or both (top right square) survive because zygotic expression of a Medea-associated antidote (green background) neutralizes toxin activity. (**B**) (Top) Schematic of a simple molecular model that accounts for Medea behavior postulates the existence of two tightly linked loci. One locus consists of a maternal germline–specific promoter that drives the expression of RNA or protein that is toxic to the embryo. The second locus consists of a zygotic promoter that drives the expression of an antidote. (Bottom) Schematic of $Medea^{myd88}$ is shown. ORF, open reading frame; Mir 6.1-Myd88 1+2, transcript encoding two copies of Drosophila miRNA 6.1 modified to target the myd88 5′ untranslated region. (**C**) Frequency of genotypes lacking Medea for an element carrying the additive fitness costs indicated, over generations, with Medea introduced at a 1:1:2 ratio of homozygous Medea-bearing males, non-Medea–bearing males, and females lacking Medea. Generation zero refers to the wild population (non-Medea/non-Medea = 1) before population seeding. Generation one refers to the progeny of crosses between these individuals and homozygous Medea-bearing males. (**D**) Frequency of the non-Medea–bearing chromosome for the populations described in (C). (**E** and **F**) $Medea^{myd88-1}$ drives population replacement in Drosophila. $Medea^{myd88-1}$ was introduced into seven population cages at an allele frequency of ~25% (16). (**E**) The frequency of genotypes lacking Medea (+/+) over generations is indicated for two separate sets of population cage experiments involving three (green lines, 20 generations) or four (blue lines, 15 generations) population cages each. The predicted frequency of genotypes lacking Medea for a Medea element with zero fitness cost (introduced at an allele frequency of 25%) is indicated by the red line. (**F**) The frequency of the non-$Medea^{myd88-1}$–bearing chromosome (+/Medea and +/+) over generations from the population cage experiments in (E) is indicated as above, as is the predicted frequency for an element with zero fitness cost.

Table 1. *Medea*$^{myd88\text{-}1}$ shows maternal effect selfish behavior. Progeny of crosses between parents of several different genotypes (M refers to the *Medea*$^{myd88\text{-}1}$–bearing chromosome; + refers to the non–element-bearing homolog) are shown. The maternal copy number (0 to 2) of *bic*-driven miRNAs targeting the endogenous *myd88* transcript (maternal toxin) and zygote copy number (0 to 2) and percentage of embryos inheriting *bnk*-driven *myd88* (zygotic antidote) are indicated, as are the adult progeny genotypes predicted for Mendelian inheritance of *Medea*$^{myd88\text{-}1}$ and the percent embryo survival. –, not measured. The asterisk denotes that embryo survival was normalized with respect to percent survival (± SD) observed in the w^{1118} stock used for transgenesis (97.1 ± 0.7%).

Parental genotype		Inherited by the Oocyte	Inherited by the Embryo	Adult M progeny (%)		Embryo survival (%)*
Male	Female	Maternal toxin	Zygotic antidote (*n*, %)	Predicted	Observed	
M/+	+/+	0	0, 50	50	50	99.6 ± 1
			1, 50		(*n* > 7000)	
M/M	M/M	2	2, 100	100		98.1 ± 0.4
+/+	M/+	1	0, 50	50	100	48.3 ± 2
			1, 50		(*n* > 12,000)	
M/M	M/+	1	1, 50	100	–	98 ± 1
			2, 50			
M/+	M/+	1	0, 25	75		74.3 ± 0.5
			1, 50			
			2, 25			
M/+	M/M	2	1, 50	100	–	98.3 ± 1
			2, 50			
+/+	M/M	2	1, 100	100	–	99.1 ± 0.4
M/M	+/+	0	1, 100	100		98.8 ± 0.5

miRNAs as toxins can provide a degree of redundant protection because multiple miRNAs, each processed and functioning as an independent unit, can be linked in a polycistronic transcript [(Fig. 1B and (16)]. The use of miRNAs as toxins also provides a basis by which selfish genetic element drive can be limited to the target species. *Medea* elements only show drive when maternal-effect lethality creates an opportunity for zygotic rescue of progeny that inherit the element. Therefore, drive can be limited to a single species [illegible] miRNAs that are [illegible] the [illegible] the [illegible].

Perhaps the most likely point of failure in any population-replacement strategy involves the [illegible] creating *Medea*$^{\Delta eff}$-bearing chromosomes. In addition [illegible] selection for [illegible]. These events, as well as the possible appearance of *Medea*^{ins}-bearing chromosomes discussed above, will lead to the reappearance of permissive conditions for disease [illegible] it is important [illegible] strategies be available for removal of an element from the population, followed by its replacement with a new element. One potential strategy for [illegible] *Medea* elements located at a common site in the genome [illegible].

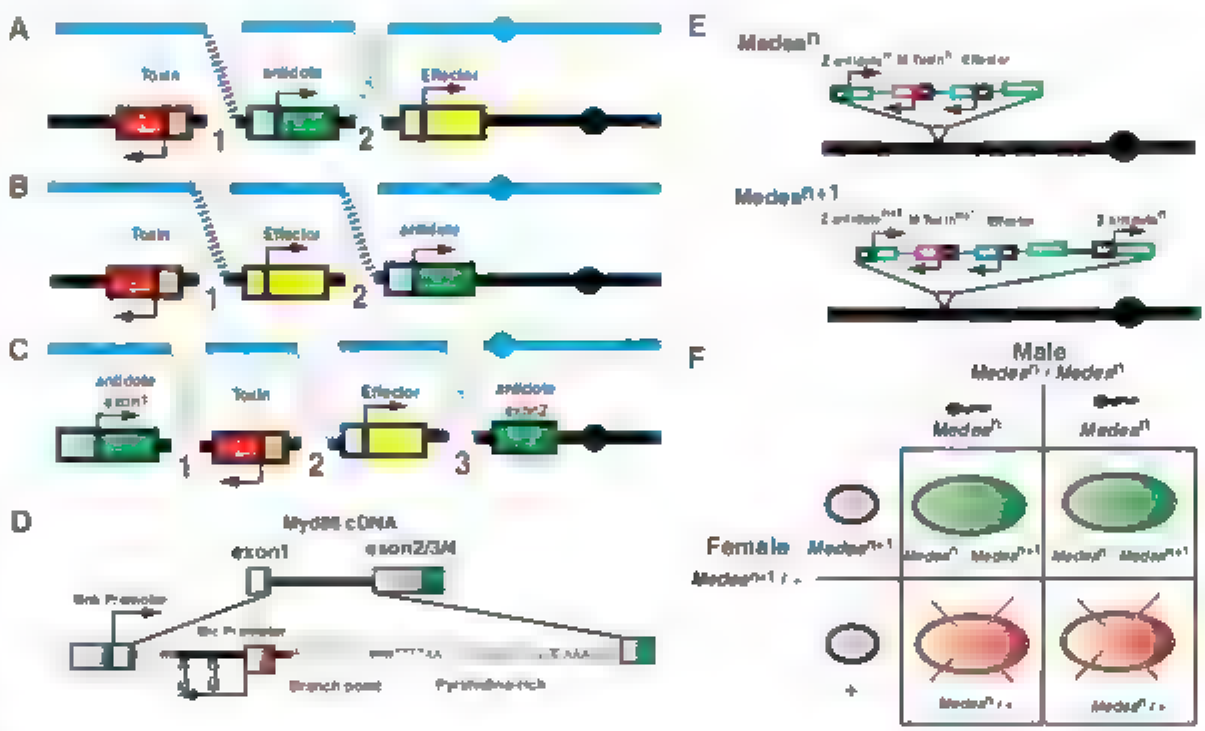

Fig. 2. A strategy for enhancing the functional lifetime of *Medea* elements in the wild and for carrying out cycles of population replacement. (**A** to **D**) Locating *Medea* toxin and effector genes in an intron of the antidote prevents chromosome breakage and end joining–mediated separation of drive and effector genes and creation of *Medea*^{ins}-bearing chromosomes. [(A) to (C)] *Medea* constructs with different gene arrangements are shown. Sites of chromosome breakage and end joining with a second nonhomologous chromosome are indicated by the crossed lines. Recombinant products referred to in the text are indicated by thick lines, the color of which indicates the centromere (solid circles) involved. (A) Recombination at site 1 generates a *Medea*^{ins}-bearing chromosome that carries the effector. Recombination at site 2 generates a *Medea*$^{\Delta eff}$-bearing chromosome. (B) Recombination at site 1 or site 2 generates a *Medea*^{ins}-bearing chromosome. (C) Recombination at sites 1 to 3 generates benign chromosomes that cannot show *Medea*^{ins} or *Medea*$^{\Delta eff}$ behavior. (D) Schematic of *Medea*$^{myd88\text{-}int}$. Splice donor and acceptor sites are indicated in large red letters, with the branchpoint and polypyrimidine stretch in small red letters. (**E** and **F**) A strategy for carrying out cycles of population replacement with *Medea*. (E) A first-generation *Medea* element (*Medea*^{n}), driven by Toxin^n and Antidote^n, is integrated into the chromosome [thick black line with centromere (solid circle) at the right] at a specific position (triangle). A second generation *Medea* element (*Medea*$^{n+1}$), driven by Toxin^{n+1} and Antidote^{n+1}, can be integrated at the same position using site-specific recombination (24). Locating both elements at the same position limits the possibility of homologous recombination creating chromosomes that carry both elements. (F) Because progeny carrying *Medea*^{n} are sensitive to Toxin^{n+1}, the only progeny of females heterozygous for *Medea*$^{n+1}$ that survive are those that inherit *Medea*$^{n+1}$, regardless of their status with respect to *Medea*^{n}. In contrast, the progeny of *Medea*^{n} females that fail to inherit *Medea*^{n} survive if they inherit Antidote^n as a part of *Medea*$^{n+1}$.

Table 2. *Medea*$^{myd88\text{-}int\text{-}1}$ shows maternal-effect selfish behavior. Progeny of crosses between parents of several different genotypes are shown, and notations are the same as those in Table 1

Parental genotype		Inherited by the Oocyte	Inherited by the Embryo	Adult M progeny (%)		Embryo survival (%)*
Male	Female	Maternal toxin	Zygotic antidote (*n*, %)	Predicted	Observed	
M/+	+/+	0	0, 50	50	51	98.4 ± 0.6
			1, 50		(*n* = 5000)	
M/M	M/M	2	2, 100	100	-	98.6 ± 0.8
+/+	M/+	1	0, 50	50	99.5	48.7 ± 0.6
			1, 50		(*n* = 5000)	
M/M	M/+	1	1, 50	100	-	98.4 ± 0.7
			2, 50			
M/+	M/+	1	0, 25	75	-	73.6 ± 1.2
			1, 50			
			2, 25			
M/+	M/M	2	1, 50	100	-	57.2 ± 1.5
			2, 50			
+/+	M/M	2	1, 100	100	-	20.2 ± 1.1
M/M	+/+	0	1, 100	100	-	98.5 ± 0.7

sion in transheterozygous females, is illustrated in Fig. ...

Our data show de novo synthesis of a selfish genetic element able to drive itself into a population. This laboratory demonstration notwithstanding, several obstacles remain to the implementation of *Medea*-based population replacement in the wild. First, for pests such as mosquito species, there is little genetic or molecular information regarding genes and promoters used during oogenesis and early embryogenesis. This information is straightforward to generate, with the use of transcriptional profiling to identify appropriately expressed genes and transgenesis and RNA interference in adult females to identify those required for embryonic development, but it remains to be acquired. In addition, current models of the spread of *Medea* do not take into account important real-world variables, such as migration, nonrandom mating, and the fact that important disease vectors such as *Anopheles gambiae* consist of multiple partially reproductively isolated strains (*20, 21*). Although an understanding of the above issues is critical for the success of any population-replacement strategy, the problems are not intractable, as evidenced by past successes in controlling pests by means of sterile-male release (*18*) and as implied by our growing understanding of mosquito population genetics, immunity, and ecology (*20–23*).

References and Notes

1. M. de Lara Capurro *et al.*, *Am. J. Trop. Med. Hyg.* **62**, 427 (2000).
2. J. Ito, A. Ghosh, L. A. Moreira, E. A. Wimmer, M. Jacobs-Lorena, *Nature* **417**, 452 (2002).
3. L. A. Moreira *et al.*, *J. Biol. Chem.* **277**, 40839 (2002).
4. K. D. Vernick *et al.*, *Curr. Top. Microbiol. Immunol.* **295**, 383 (2005).
5. A. W. E. Franz *et al.*, *Proc. Natl. Acad. Sci. U.S.A.* **103**, 4198 (2006).
6. G. Macdonald, *The Epidemiology and Control of Malaria* (Oxford Univ. Press, London, 1957).
7. J. M. Ribeiro, M. G. Kidwell, *J. Med. Entomol.* **31**, 10 (1994).
8. C. Boëte, J. C. Koella, *Malar. J.* **1**, 3 (2002).
9. P. Schmid-Hempel, *Annu. Rev. Entomol.* **50**, 529 (2005).
10. A. A. James, *Trends Parasitol.* **21**, 64 (2005).
11. S. P. Sinkins, F. Gould, *Nat. Rev. Genet.* **7**, 427 (2006).
12. R. W. Beeman, K. S. Friesen, R. E. Denell, *Science* **256**, 89 (1992).
13. M. J. Wade, R. W. Beeman, *Genetics* **138**, 1309 (1994).
14. M. G. C. Smith, *J. Theor. Biol.* **191**, 173 (1998).
15. R. W. Beeman, K. S. Friesen, *Heredity* **82**, 529 (1999).
16. Materials and methods are available as supporting material on *Science* Online.
17. Z. Kambris *et al.*, *EMBO Rep.* **4**, 64 (2003).
18. F. Gould, P. Schliekelman, *Annu. Rev. Entomol.* **49**, 193 (2004).
19. B. W. Geer, M. M. Green, *Am. Nat.* **96**, 175 (1962).
20. A. della Torre *et al.*, *Science* **298**, 115 (2002).
21. M. Coetzee, *Am. J. Trop. Med. Hyg.* **70**, 103 (2004).
22. D. Vlachou, F. C. Kafatos, *Curr. Opin. Microbiol.* **8**, 415 (2005).
23. H. Pates, C. Curtis, *Annu. Rev. Entomol.* **50**, 53 (2005).
24. D. D. Nimmo, L. Alphey, J. M. Meredith, P. Eggleston, *Insect Mol. Biol.* **15**, 129 (2006).

25. This work did not receive specific funding. It was supported by NIH grants GM057422 and GM70956 to B.A.H. and NS042580 and NS048396 to M.G. C.-H.C. was supported by the Moore Foundation Center for Biological Circuit Design. We thank two reviewers for useful comments and improvements on the manuscript. GenBank accession numbers for *Medea*^{myd88} and *Medea*$^{myd88\text{-}int}$ are EF447106 and EF447105, respectively.

Supporting Online Material

www.sciencemag.org/cgi/content/full/1138595/DC1

Materials and Methods

Figs. S1 to S5

References

8 December 2006; accepted 20 March 2007

Published online 29 March 2007

10.1126/science.1138595

Include this information when citing this paper.

Modeling the Initiation and Progression of Human Acute Leukemia in Mice

Frédéric Barabé,[1,2,3,4*] James A. Kennedy,[1,5*] Kristin J. Hope,[1,5] John E. Dick[1,5]†

Our understanding of leukemia development and progression has been hampered by the lack of in vivo models in which disease is initiated from primary human hematopoietic cells. We showed that upon transplantation into immunodeficient mice, primitive human hematopoietic cells expressing a *mixed-lineage leukemia* (*MLL*) fusion gene generated myeloid or lymphoid acute leukemias, with features that recapitulate human diseases. Analysis of serially transplanted mice revealed that the disease is sustained by leukemia-initiating cells (L-ICs) that have evolved over time from a primitive cell type with a germline immunoglobulin heavy chain (IgH) gene configuration to a cell type containing rearranged IgH genes. The L-ICs retained both myeloid and lymphoid lineage potential and remained responsive to microenvironmental cues. The properties of these cells provide a biological basis for several clinical hallmarks of *MLL* leukemias.

In human leukemia, only a subset of leukemic blast cells have the potential to initiate and recapitulate disease when transplanted into immunodeficient mice (*1–3*). To date, these approaches have not permitted identification of the cell type(s) from which leukemia-initiating cells (L-ICs) originate or assessment of how these L-ICs phenotypically evolve during disease progression. In order to investigate these questions, we have developed an in vivo model of leukemia initiated from primary human hematopoietic cells.

Over 50% of infant acute leukemias exhibit rearrangements of the *mixed-lineage leukemia* gene (*MLL*, also termed *ALL-1* and *HRX*) at human chromosome 11q23 (*4*). Translocations of *MLL* to >40 different partner genes have been identified, and the resulting fusion proteins are strong transcriptional activators that drive the aberrant expression of homeobox family genes (*5*). In view of the potent oncogenic properties of *MLL* fusion genes, we tested the leukemogenic potential of *MLL eleven-nineteen*

leukemia (*ENL*), the product of t(11;19) that is found in both acute myeloid leukemias (AMLs) and acute lymphoid leukemias (ALLs). A lineage-depleted fraction of human umbilical cord blood enriched for stem and progenitor cells (Lin⁻ CB) was infected with either a retrovirus encoding *MLL-ENL* and an enhanced green fluorescent protein (*EGFP*) marker gene or a control retrovirus encoding *EGFP* only and then injected into sublethally irradiated immunodeficient mice (6).

[1]Division of Cell and Molecular Biology, University Health Network, Toronto, Ontario, M5G 1L7, Canada. [2]Department of Medicine, Laval University, Quebec, G1K 7P4, Canada. [3]Department of Hematology, Enfant-Jesus Hospital, Quebec, G1J 1Z4, Canada. [4]Research Center in Infectious Diseases, Centre Hospitalier Universitaire de Québec-Centre Hospitalier de l'Université Laval, Quebec, G1V 4G2, Canada. [5]Department of Molecular and Medical Genetics, University of Toronto, Toronto, Ontario, Canada.

*These authors contributed equally to this work.

†To whom correspondence should be addressed. E-mail: jdick@uhnres.utoronto.ca

The recipients of cells transduced with the control retrovirus (hereafter referred to as control mice) displayed no overt pathology. In contrast, >75% of the mice receiving *MLL-ENL*–transduced cells (hereafter referred to as *MLL-ENL* mice) were dying within 135 days of transplantation, appearing pale and lethargic (Fig. 1A). Postmortem analysis revealed splenomegaly and generalized lymphadenopathy (fig. S1), and in 26 out of 29 *MLL-ENL* mice, L1-type lymphoblasts were found in the blood and bone marrow (BM), which is consistent with the development of ALL. As in the human disease, these cells also infiltrated the liver, lungs, kidneys, brain, and testes (Fig. 1, B and C, and fig. S2A). To assess the lineage and maturation stage of the leukemic blasts, human grafts were studied by flow cytometry (Fig. 1, D and E, and fig. S3). In control mice, the human graft made up 76 ± 15% of the BM and consisted mainly of leukocytes expressing the pan-B cell marker CD19, with a minor population of myeloid cells (CD33⁺CD19⁻), as previously described (7). In contrast, in *MLL-ENL* mice, the human graft made up 96 ± 2% of the BM and consisted almost exclusively of B cells. The human B cell population in control mice showed evidence of normal terminal differentiation, whereas in *MLL-ENL* mice, these cells were arrested at the pro-B cell stage of differentiation (CD19⁺, CD20⁻, IgM⁻, and IgD⁻) (8). Thus, the cell surface phenotype and tissue-infiltration pattern of the leukemic blasts seen in this model resemble those observed in B-ALL patients with this translocation (9, 10). B-precursor ALL has rarely been observed in previous work where various *MLL* fusions were studied in transgenic mice or by murine BM transplantation (11–17).

We next tested the leukemogenic potential of *MLL-AF9*, a different fusion gene predominantly associated with AML (5, 10). Clinically, different *MLL* fusions are associated with distinct frequencies of myeloid and lymphoid leukemias. In contrast to our findings with *MLL-ENL*,

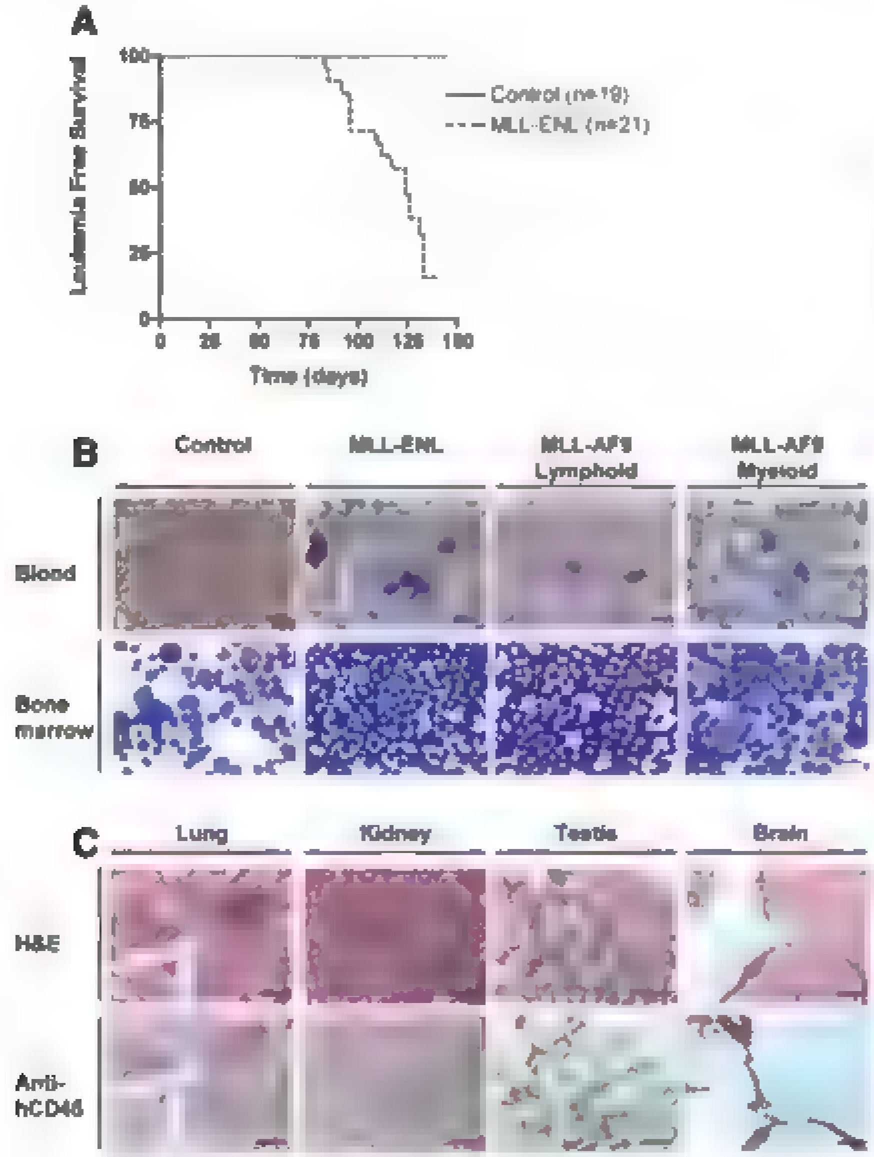

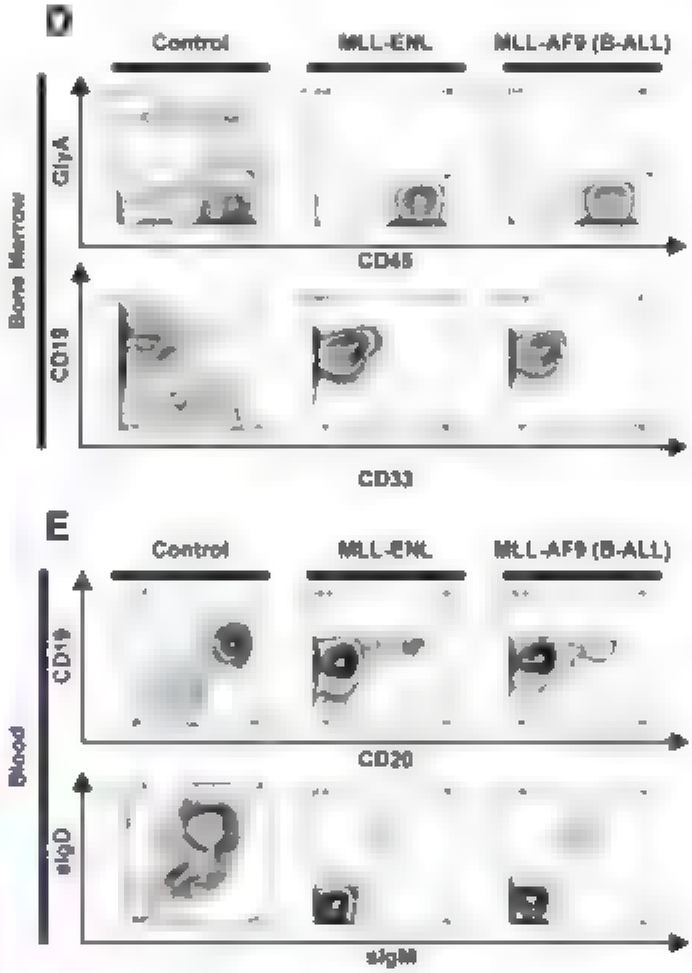

Fig. 1. Morphology, tissue infiltration, and immunophenotype of *MLL*-induced ALL and AML. **(A)** Kaplan-Meier survival analysis of control and *MLL-ENL* mice. *n*, number of mice. **(B)** Blood smears and BM cytospins [May-Grunwald-Giemsa (MGG) staining] of representative mice injected with control cells, *MLL-ENL*-transduced cells, and *MLL-AF9*-transduced cells. Scale bars, 10 μm. **(C)** Organ infiltration by lymphoblasts in a representative *MLL-ENL* mouse. Tissue sections are stained with hematoxylin and eosin (H&E) and with a human-specific antibody to CD45. Scale bars, 100 μm (lung, kidney, and testis) or 25 μm (brain). **(D** and **E)** Flow cytometric analysis of BM and blood from representative mice with *MLL*-induced B-ALL. The upper row in (D) shows the human erythroid cells (GlyA⁺ cells) and the human leukocytes (CD45⁺GlyA⁻ cells) that compose the human graft; the cells of mouse origin are in the lower left quadrant (CD45⁻GlyA⁻ cells). Contour plots are gated on all live cells [upper row in (D)] or on human CD45⁺ cells [(D), lower row, and (E)].

Lin− CB cells expressing *MLL-AF9* initiated both B-lymphoid and myeloid disease upon transplantation (Fig. 1, B, D, and E; figs. S2B, S3, and S4; and table S1). Eight of 16 *MLL-AF9* mice developed B-precursor ALL with features identical to those noted with *MLL-ENL*. Two mice developed AML, characterized by myelomonocytic blasts in the blood and BM with diffuse organ infiltration. This disease corresponds phenotypically to the myelomonocytic or monoblastic leukemias seen in the majority of patients with *MLL-AF9* translocations. A single *MLL-AF9* mouse developed a mixed leukemia composed of both B-lineage lymphoblasts and myeloblasts. Thus, as seen in mouse models of *MLL* leukemias and in patients, the identity of the fusion partner plays an instructive role in determining leukemia lineage in our model (*18*).

Table S1 summarizes the data corresponding to all primary mice from six independent transduction experiments. Using the clinical definition of human leukemia (>20% blasts in the BM), we found that 78% of mice (35 out of 45) injected with cells expressing *MLL* fusion genes developed leukemia in less than 19 weeks, and two mice were preleukemic when they were killed (<20% blasts in the BM but present in blood and peripheral organs). Among mice that were engrafted with transduced human cells, 95% developed disease (*8*). This high penetrance of leukemia and the short latency to disease suggest that *MLL* fusion genes efficiently initiate leukemogenic programs and that minimal cooperating events are required for the development of fully transformed leukemic stem cells that are capable of sustaining aggressive disease. These results clearly contrast with models of solid tumors that required at least three different oncogenes to transform primary human cells (*19*–*21*).

For L-ICs to sustain and propagate disease, they must self-renew. We assessed the self-renewal of *MLL*-derived L-ICs by serial transplantation. BM cells from control, *MLL-ENL*, and *MLL-AF9* primary mice were transplanted into 34 secondary recipients (table S2). After 15 weeks, the BM from controls generated no detectable human grafts in secondary mice. In contrast, recipients of BM from *MLL-ENL* and *MLL-AF9* mice were engrafted with human cells and developed leukemia of the same phenotype (cell surface markers and organ involvement) as the corresponding primary mouse but with a shorter latency (fig. S5). Secondary transplantation of limiting doses of leukemic blasts from primary mice allowed us to estimate that the L-IC frequency was 1/300 cells (table S3).

To investigate self-renewal at a clonal level, retroviral insertion sites were analyzed by Southern blotting. The transduced human graft in the BM of control primary mice was derived from two to five clones (Fig. 2A), as previously reported (*7*). In all *MLL* primary mice, the leukemic grafts were composed of either one or two major clones with variable numbers of minor contributors (Fig. 2, A and C, and fig. S6). In general, the predominant clone from a primary mouse persisted to generate monoclonal disease in its corresponding secondary mice. However, in two instances, a novel clone that was below the detection limit in primary mice made a substantial contribution in secondary recipients (Fig. 2C). One interpretation of this finding, supported by clonal tracking studies in human AML (*3*), is that such clones arose from L-ICs that were quiescent in primary mice and became activated after secondary transplantation.

To determine the type of cell transformed by *MLL* fusion genes, Southern blotting was used

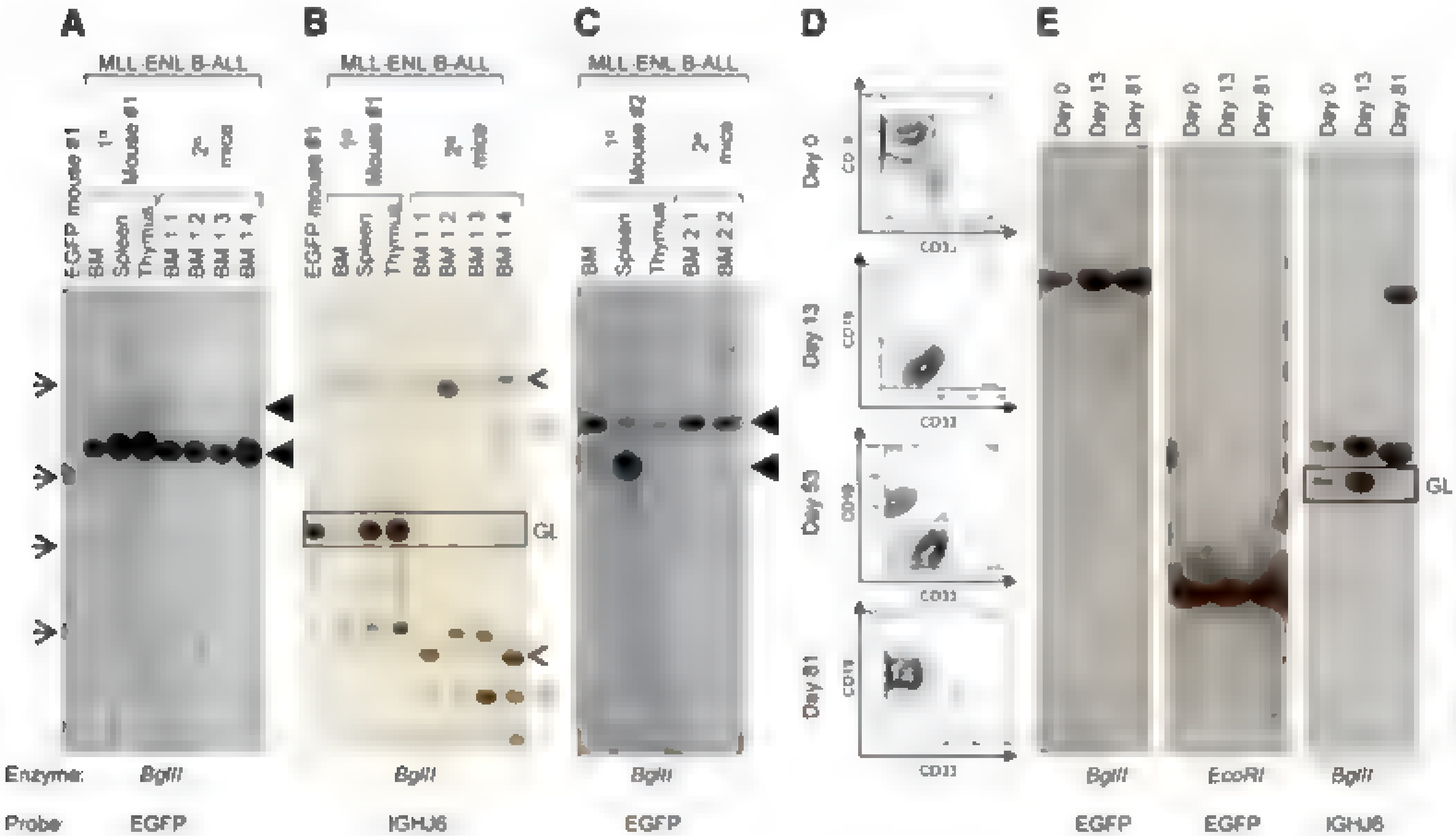

Fig. 2. Clonal analysis of *MLL*-induced leukemias. Southern blotting was performed by digesting DNA with the indicated enzymes and probing with either an *EGFP* cDNA probe (to assess retroviral integration) or a probe specific for the region 3′ to the J_H segments of the human IgH locus (IGHJ6) (to analyze IgH gene rearrangement). All secondary recipients were derived from BM cells of the primary mouse analyzed on the same membrane. (**A** and **C**) Black arrows (control mouse) and solid arrowheads (leukemic mice) indicate clones with unique proviral insertions. The open arrow in (C) indicates a novel clone present in a secondary mouse that was not detectable in the corresponding primary mouse. (**B**) The germline IgH configuration is surrounded by a rectangle. Open arrowheads indicate rearrangements common to primary and secondary mice. Gray arrows point to new rearrangements common to all secondary mice that were not detectable in the primary mouse. (**D**) Example of a spontaneous lineage switch that occurred during the in vitro culture of BM cells from an *MLL-ENL* mouse. (**E**) Clonal analysis of this culture for both proviral insertion and IgH rearrangement.

to study immunoglobulin heavy chain (IgH) gene rearrangement, an event that occurs at a stage of B-lymphoid differentiation between the common lymphoid progenitor (CLP) and the pro-B cell (22). Although control and *MLL-AF9* mice with AML displayed only the germline arrangement (fig. S6), all primary mice with B-precursor ALL displayed varying rearrangements of the IgH gene in addition to the germline band (Fig. 2B and fig. S6). In ~40% of the primary mice, the germline configuration accounted for >50% of all the IgH gene configurations. These data allow us to exclude the possibility that, in these cases, transformation occurred in a committed B cell with a rearranged IgH gene. Instead, they indicate that a more primitive cell type that had not initiated IgH gene rearrangement (such as the hematopoietic stem cell, CLP, or the early B cell) was the target of transformation.

A comparison of the IgH gene-rearrangement patterns in secondary mice and their corresponding primary mice showed a consistent decrease in the intensity of the germline configuration, accompanied by a greater contribution by clones with rearranged IgH alleles. The same rearrangements were often present in multiple secondary mice derived from the same primary animal (Fig. 2B and fig. S6), suggesting that the L-ICs in primary mice underwent self-renewal divisions and generated daughter L-ICs capable of initiating ALL upon transplantation. Thus, in leukemias where a primitive cell type was deemed to be the target of transformation, we can conclude that the L-ICs present at later time points were not identical to those initially generated, though they shared the same retroviral integration. Instead, it appears that the phenotype of the L-ICs evolved over time from a primitive (germline IgH) cell type to a cell type with rearranged IgH genes. This clonal evolution indicates that analysis of L-IC properties and phenotype at a single time point may not provide a complete picture of L-IC biology or insights into the identity of the cell of origin.

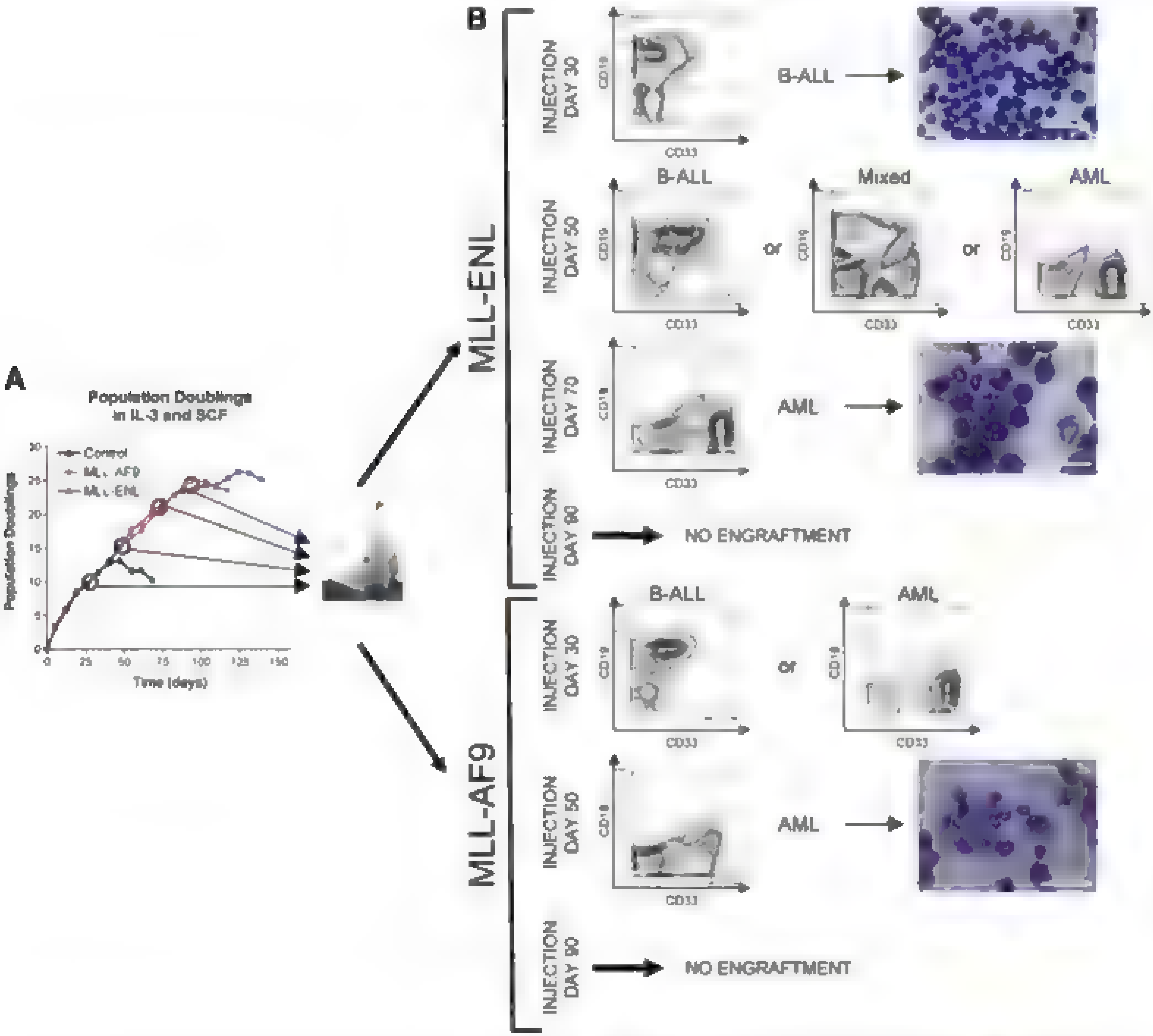

Fig. 3. *MLL-ENL* and *MLL-AF9* cells cultured in myeloid-promoting conditions generate different graft phenotypes upon injection into immunodeficient mice. **(A)** In vitro growth curves of control, *MLL-AF9*, and *MLL-ENL* cells under conditions that promote myeloid differentiation. At the indicated time points, cultured cells were injected into immunodeficient mice. IL-3, interleukin-3; SCF, stem cell factor. **(B)** Types of human grafts generated in mice. Contour plots are gated on live cells, and BM cytospins (MGG staining) illustrate the morphology of the indicated leukemias. Scale bars, 25 μm.

Because a primitive cell was the target for the transformation in ~40% of our experimental leukemias, we investigated the differentiation potential of *MLL*-derived L-ICs. Leukemic cells were harvested from the BM of primary mice and cultured in vitro under conditions supportive of both B-lymphoid and myeloid cells. Both AML and B-precursor ALL grew for >100 days (fig. S7, A and B), and in 10 out of 14 cultures initiated from mice with *MLL-ENL* B-ALL, a $CD33^+CD19^-$ myeloid population emerged. Three of these cultures underwent a complete switch from a B-lymphoid to a myeloid blastic population; in one instance, this was followed by a reversion back to B-lineage cells (Fig. 2D and fig. S7, C and D). Retroviral integration analysis showed that clonality was maintained during these lineage switches, but cells with either rearranged IgH alleles or strictly germline status were competent to switch lineages (Fig. 2E and fig. S7F). Consistent with these observations, intraclonal lineage switching has been documented in patients with *MLL* leukemias upon relapse (*23–25*) and was also found in our in vivo studies (fig. S8). Together these in vitro and in vivo data indicate that *MLL*-derived L-ICs, including those with rearranged IgH genes, retain both lymphoid and myeloid potential, a finding also observed in murine models (*11*).

Finally, to investigate the influence of microenvironment on *MLL* L-ICs, we seeded cells expressing *MLL-ENL* or *MLL-AF9* into myeloid-promoting suspension cultures immediately after transduction. Under these conditions, cells expressing *MLL* fusions outgrew controls, generating populations of monoblastic cells (*MLL-ENL*) and myelomonoblastic cells (*MLL-AF9*) (Fig. 3A and fig. S9). Analysis of the leukemia-initiating capacity of cells from different times in culture showed that at the earliest time point, cultured *MLL-ENL* cells generated B-precursor ALL in vivo; however, at later passages the phenotype of the human grafts shifted toward the myeloid lineage, with some mice showing monoclonal mixed-lineage leukemias and AML (Fig. 3, fig. S10, and table S4). Thus, exposure to myeloid-supportive conditions was permissive for the development of clones capable of generating myeloid disease in vivo. In contrast to *MLL-ENL*, the injection of *MLL-AF9* cells from culture resulted in strictly myeloid outgrowths in all but one engrafted mouse, again highlighting an instructive role for the *MLL* fusion partner in determining leukemia lineage.

Our data show that *MLL* fusion genes can initiate both myeloid and lymphoid leukemogenic programs in primary human hematopoietic cells. Which program is ultimately followed is influenced by the identity of the fusion partner, as well as by microenvironmental signals. The responsiveness of *MLL*-derived L-ICs to extrinsic cues, coupled with their lympho-myeloid potential, provides a biological basis for several hallmarks of *MLL* leukemias, including lineage switching at relapse and the high incidence of B-ALL in infants (*26*), where the intrinsic and extrinsic determinants of neonatal hematopoiesis favor B cell development (*27*). The finding that L-ICs undergo clonal evolution indicates that disease progression is linked to the biological properties of the leukemia stem cells that underlie the disease, rather than to the evolution of leukemic blasts. Thus, it will be essential to understand the cellular and molecular properties of L-ICs at all stages, from leukemic initiation to disease progression, in order to devise therapies to target their eradication.

References and Notes

1. T. Lapidot et al., *Nature* **367**, 645 (1994).
2. D. Bonnet, J. E. Dick, *Nat. Med.* **3**, 730 (1997).
3. K. J. Hope, L. Jin, J. E. Dick, *Nat. Immunol.* **5**, 738 (2004).
4. A. T. Look, *Science* **278**, 1059 (1997).
5. A. Daser, T. H. Rabbitts, *Genes Dev.* **18**, 965 (2004).
6. Materials and methods are available as supporting material on *Science* Online.
7. G. Guenechea, O. I. Gan, C. Dorrell, J. E. Dick, *Nat. Immunol.* **2**, 75 (2001).
8. Details pertaining to engraftment and leukemic phenotypes are available as supporting material on *Science* Online.
9. C. H. Pui et al., *J. Clin. Oncol.* **12**, 909 (1994).
10. J. E. Rubnitz et al., *J. Clin. Oncol.* **17**, 191 (1999).
11. C. W. So et al., *Cancer Cell* **3**, 161 (2003).
12. B. B. Zeisig, M. P. Garcia-Cuellar, T. H. Winkler, R. K. Slany, *Oncogene* **22**, 1629 (2003).
13. A. Cozzio et al., *Genes Dev.* **17**, 3029 (2003).
14. A. V. Krivtsov et al., *Nature* **442**, 818 (2006).
15. J. Corral et al., *Cell* **85**, 853 (1996).
16. W. Chen et al., *Blood* **108**, 669 (2006).
17. M. Metzler et al., *Oncogene* **25**, 3093 (2006).
18. L. F. Drynan et al., *EMBO J.* **24**, 3136 (2005).
19. J. M. Rich et al., *Cancer Res.* **61**, 3556 (2001).
20. B. Elenbaas et al., *Genes Dev.* **15**, 50 (2001).
21. Y. Chudnovsky, A. E. Adams, P. B. Robbins, Q. Lin, P. A. Khavari, *Nat. Genet.* **37**, 745 (2005).
22. T. W. LeBien, *Blood* **96**, 9 (2000).
23. J. G. Jiang et al., *Leuk. Lymphoma* **46**, 1223 (2005).
24. S. A. Ridge et al., *Leukemia* **9**, 2023 (1995).
25. G. Germano et al., *Haematologica* **91**, ECR09 (2006).
26. E. Forestier, K. Schmiegelow, *J. Pediatr. Hematol. Oncol.* **28**, 486 (2006).
27. E. M. Rego, A. B. Garcia, S. R. Viana, R. P. Falcao, *Cytometry* **34**, 22 (1998).

28. We thank M. Doedens for technical assistance, the University Health Network Pathology Research Program for tissue sectioning and immunohistochemistry; P. Marrano for karyotyping, members of the Dick lab, J. Hitzler, and M. Minden for critical comments on the manuscript; and M. Greaves for inspiring this study. This work was supported by a Canadian Institute of Health Research (CIHR) clinician-scientist award (to F.B.), an MD/PhD studentship (to J.A.K.), and grants from the CIHR, the Ontario Cancer Research Network, Genome Canada through the Ontario Genomics Institute, a Canada Research Chair, the Leukemia and Lymphoma Society, and the National Cancer Institute of Canada, with funds from the Canadian Cancer Society and the Terry Fox Foundation (to J.E.D.).

Supporting Online Material

www.sciencemag.org/cgi/content/full/316/5824/600/DC1
Materials and Methods
SOM Text
Figs. S1 to S10
Tables S1 to S4
References

22 August 2006; accepted 26 March 2007
10.1126/science.1139851

Regulation of the Germinal Center Response by MicroRNA-155

To-Ha Thai,[1] Dinis Pedro Calado,[1] Stefano Casola,[2] K. Mark Ansel,[3] Changchun Xiao,[1] Yingzi Xue,[3] Andrew Murphy,[3] David Frendewey,[3] David Valenzuela,[3] Jeffery L. Kutok,[4] Marc Schmidt-Supprian,[1] Nikolaus Rajewsky,[5] George Yancopoulos,[3] Anjana Rao,[3] Klaus Rajewsky[1]*

MicroRNAs are small RNA species involved in biological control at multiple levels. Using genetic deletion and transgenic approaches, we show that the evolutionarily conserved microRNA 155 (miR-155) has an important role in the mammalian immune system, specifically in regulating T helper cell differentiation and the germinal center reaction to produce an optimal T cell–dependent antibody response. miR-155 exerts this control, at least in part, by regulating cytokine production. These results also suggest that individual microRNAs can exert critical control over mammalian differentiation processes in vivo.

MicroRNAs are emerging as key players in the control of biological processes, and the stage-specific expression of certain microRNAs in the immune system suggests that they may participate in immune regulation. One such microRNA is miR-155, produced from the non–protein-coding transcript of the *bic* gene. *bic* was discovered as a recurrent integration site of avian leukosis virus in chicken lymphoma cells (*1*). The hairpin from which miR-155 is processed represents the only evolutionarily conserved sequence of the *bic* gene, indicating that miR-155 mediates *bic* function (*2–4*). *bic*/miR-155 has been shown to be highly expressed in a variety of human B cell lymphomas, including the Hodgkin Reed-

[1]CBR Institute for Biomedical Research, Harvard Medical School, Boston, MA 02115, USA. [2]IFOM–the FIRC Institute for Molecular Oncology, Milano, Via Adamello 16 Milan 20139, Italy. [3]Regeneron Pharmaceuticals, 777 Old Saw Mill River Road, Tarrytown, NY 10591, USA. [4]Department of Pathology, Brigham and Women's Hospital, Boston, MA 02115, USA. [5]Max Delbrück Center for Molecular Medicine, Robert-Rössle-Strasse 10, D-13125 Berlin, Germany.

*To whom correspondence should be addressed. E-mail: rajewsky@cbr.med.harvard.edu

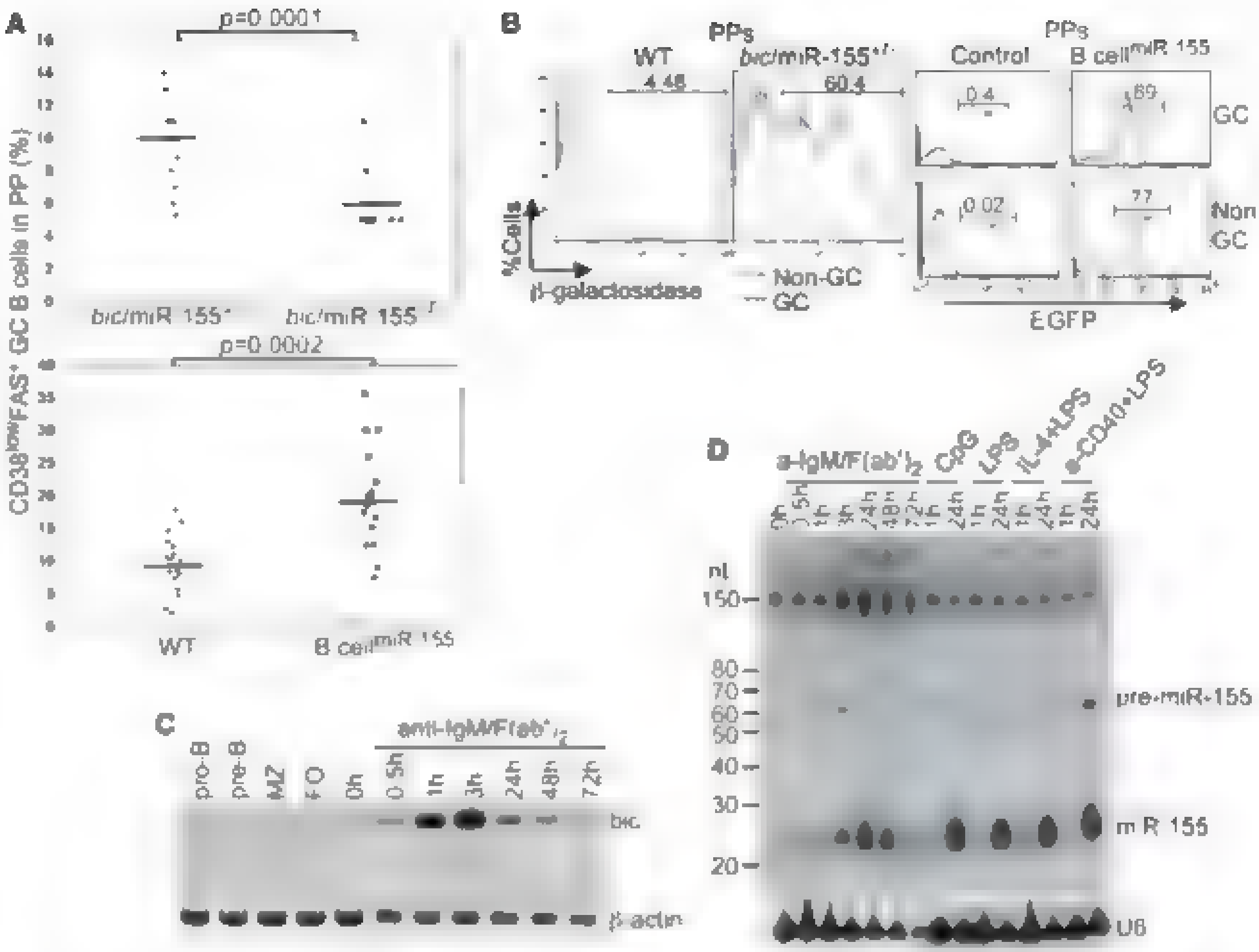

Fig. 1. *bic*/miR-155 regulates the GC response and is induced upon activation. **(A)** The percentage of PP GC B cells was determined by FACS in *bic*/miR-155$^{-/-}$ mice (n = 13) and controls (n = 15), and in B cell$^{miR\text{-}155}$ mice (n = 16) and controls (n = 17). **(B)** (Left panels) *bic* promoter activity was measured by LacZ staining in GC B cells with the use of FACS. (Right panels) In B cell$^{miR\text{-}155}$ mice, *bic*/miR-155 expression in mature B cells is reported by EGFP expression. **(C)** RT-PCR was used to detect *bic* in progenitor, resting B cells and anti–IgM-(Fab′)$_2$–stimulated mature spleen B cells (10 μg/ml). The smaller transcript represents the spliced form of *bic*. **(D)** miR-155 expression was detected by Northern blots in the same samples as in (C). LPS, lipopolysaccharide.

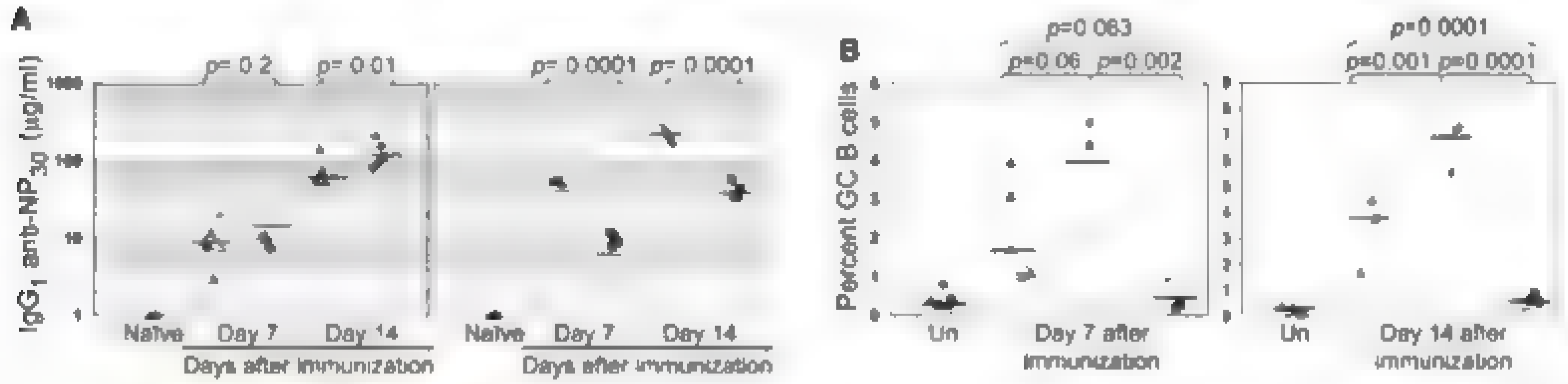

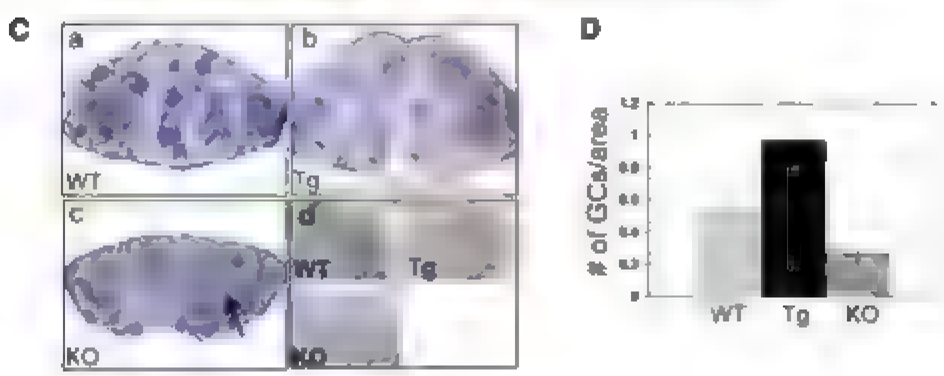

E

Genotype	V186.2 rearrangements	Mutation frequency (%)	W to L (%)
miR-155	13	1.0	64
miR-155	13	1.0	30
miR-155	15	0.9	80
miR-155	14	0.9	86
miR-155$^{-/-}$	13	0.8	21
miR-155	8	1.7	20
miR-155	16	1.0	12.5
miR-155	15	0.9	26

Somatic hypermutation analyses of IgH genes from NP-immunized spleen GC B cells

Number of unique rearrangements carrying the V186.2V$_H$ gene
Percent of rearrangements carrying the tryptophan to leucine substitution at position 33
Mutation frequency in non-GC B cells: 0.05%

Fig. 2. *bic*/miR-155$^{-/-}$ mice show impaired T cell–dependent antibody responses. **(A and B)** Mice were immunized intraperitoneally with NP-CGG/Alum and analyzed on days 7 and 14 after immunization. Open and closed symbols: experiments 1 and 2. Triangles: controls; diamonds: B cell$^{miR\text{-}155}$; squares: *bic*/miR-155$^{-/-}$. **(A)** NP-specific IgG$_1$ levels were measured by enzyme-linked immunosorbent assay. **(B)** The percentage of spleen CD38^{lo}Fas^{hi} GC B cells was determined by FACS. Un, unimmunized. **(C)** Immunohistochemistry was performed on day 14 NP-immunized spleen sections from wild-type (a), B cell$^{miR\text{-}155}$ (b), and knockout mice (c) to detect GCs (brown: PNA$^+$; blue: hemotoxylin). High-magnification image is shown in (d). Images are representative of three mice per group. **(D)** Number of GCs (+SEM) was determined from sections in (C); n = 3 mice per group. **(E)** The frequency of W33L replacement was determined by sequence analyses with spleen GC B cells 12 or 14 days after NP-CGG immunization.

Sternberg cells in Hodgkin's disease, and miR-155 transgenic mice develop B cell lymphomas (5, 8). In humans, *bic*/miR-155 expression was detected in activated mature B and T lymphocytes (7, 9), including germinal center (GC) B cells (3, 7), as well as in activated monocytes (10). Germinal centers represent sites of antibody affinity maturation and memory B cell generation in T cell dependent antibody responses (11).

To obtain insights into the physiological function of *bic*/miR-155, we generated two mutant mouse strains. In the first, a major portion of the *bic* second exon, including miR-155, was replaced by a β-galactosidase (lacZ) reporter (12), generating a loss-of-function allele designated *bic*/miR-155$^{-/-}$. The reporter allows one to study the *bic*/miR-155 expression pattern through lacZ expression (fig. S1) (13). Northern blots showed that miR-155 expression was completely ablated in activated *bic*/miR-155$^{-/-}$ B cells (fig. S1C). To generate the second mutant strain, we used a previously established knock-in strategy (14), to conditionally express miR-155 and an enhanced green fluorescent protein (EGFP) reporter in mature B cells in a Cre-dependent manner (fig. S2A) (15). For simplicity, mice carrying the miR-155 knock-in and the CD21-cre alleles will be referred to as B cell$^{miR-155}$ mice.

The gut-associated lymphoid tissue (GALT), including Peyer's patches (PPs) and mesenteric lymph nodes (mLNs), contains both B and T cells and activated, proliferating B cells undergoing GC reactions in response to chronic stimulation by gut-derived microbes. We found increased fractions of GC B cells in both PPs and mLNs of B cell$^{miR-155}$ mice (Fig. 1A and figs. S3 and S4A), and most of these cells, as well as the non-GC B cells, expressed the EGFP reporter. In contrast, in *bic*/miR-155$^{-/-}$ mice the fraction of GC B cells, determined by fluorescence-activated cell sorting (FACS) and immunohistochemistry, was significantly reduced in PPs and mLNs (Fig. 1A and figs. S3 and S4, A and B). In *bic*/miR-155$^{+/-}$ mice the vast majority of the non-GC B cells were negative for lacZ, whereas ~60% of GC B cells expressed the lacZ reporter (Fig. 1B and fig. S1B). Because the detection of β-galactosidase activity depends on the sensitivity of the assay as well as the persistence of the enzyme in dividing cells, we conclude that many or perhaps all GC B cells express *bic*/miR-155 in the course of the GC response.

To further characterize miR-155 expression, we isolated spleen B cells from wild-type mice stimulated through the B cell receptor (BCR), CD40, or with mitogens that bind Toll-like receptors (TLRs). Although little *bic*/miR-155 expression was seen in cells before activation, strong up-regulation was detected under each of these activation conditions (Fig. 1, C and D). The signaling requirements were different for BCR versus TLR/CD40-mediated *bic*/miR-155 induction. The former appeared to depend on the calcineurin-NFAT (nuclear factor of activated T cells) pathway, but not NEMO, an essential component of the nuclear factor κB (NF-κB) signaling pathway. The latter required both MyD88 and NEMO (fig. S5) (16). A kinetic analysis upon BCR cross-linking showed that both *bic* and miR-155 up-regulation was transient, with a maximum induction of the former at 3 hours and the latter at 24 hours, consistent with a precursor-product relationship (Fig. 1, C and D). Thus, in the GC response, B cells may up-regulate *bic*/miR-155 at its initiation or recurrently during proliferation and selection by antigen.

We have also observed that *bic*/miR-155 expression was absent in nonlymphoid organs (brain, kidney, lung, liver, and heart) as well as in resting naïve CD4$^+$ T cells, but strongly up-regulated upon activation of these cells by T cell antigen receptor cross-linking (fig. S6), in accord with earlier work in the human (9, 10).

The reduced fraction of GC B cells in the GALT of *bic*/miR-155$^{-/-}$ mice, together with its increase in mice overexpressing miR-155 in B cells, suggests that miR-155 may indeed mediate *bic* function and may also be involved in the control of the GC reaction. To determine whether *bic*/miR-155 is also involved in induced GC responses in the spleen, we immunized mice with alum-precipitated 4-hydroxy-3-nitro-phenylacetyl (NP) coupled to chicken gamma globulin (CGG), which normally initiates a GC response accompanied by the production of antigen-specific antibodies detectable at day 7 after immunization and reaching a peak 1 week later (17). Antigen-specific immunoglobulin G1 (IgG$_1$) antibody titers and the fractions of GC B cells were compared between immunized mutant and wild-type mice. In mice overexpressing miR-155, the antibody response was marginally enhanced at both time points (Fig. 2A). In contrast, the *bic*/miR-155$^{-/-}$ mice produced about one-fifth as much NP-specific antibody titers as their littermate controls (Fig. 2A). The percentages and numbers of spleen GC B cells were increased in the miR-155 overexpressing mice, but reduced in the knockouts, compared to controls, most notably on day 14 after immunization (figs. 2B and S7). Furthermore, *bic*/miR-155$^{-/-}$ spleens displayed reduced numbers of GCs that appeared

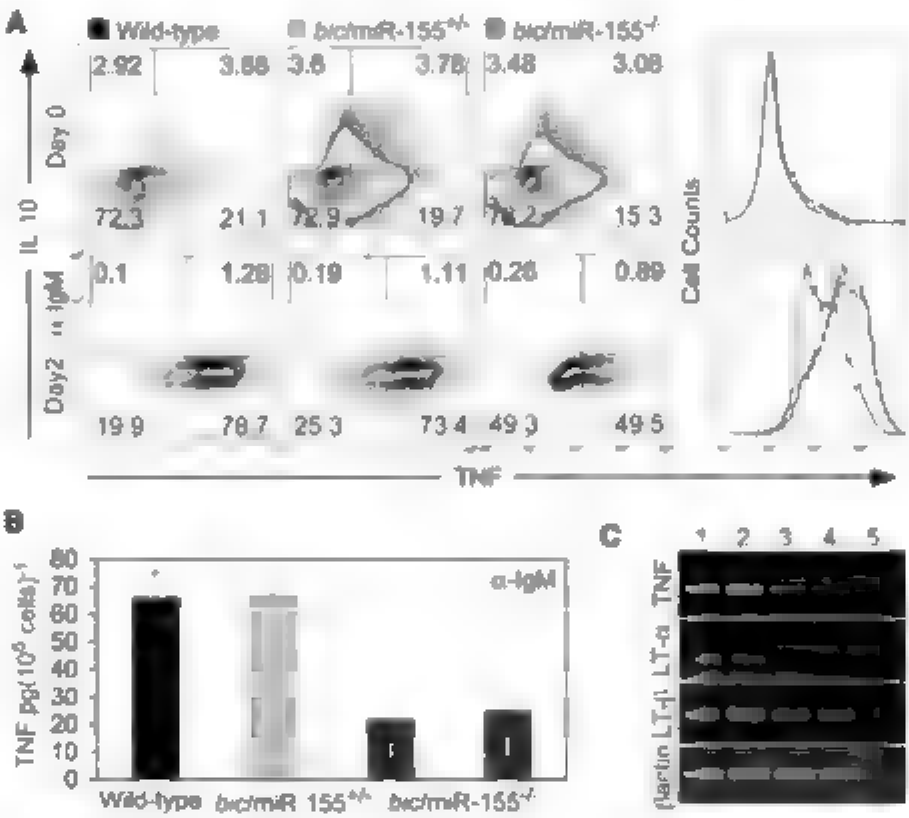

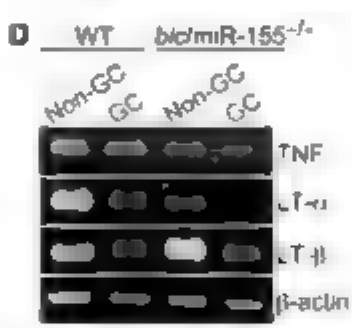

Fig. 3. *bic*/miR-155$^{-/-}$ B cells are deficient in TNF and LT-α production. All experiments were done with CD19$^+$ mature spleen B cells. (**A**) TNF expression determined by FACS was analyzed before and after stimulation with anti-IgM-F(ab′)$_2$ antibodies for 2 days (gated on blasted cells). Numbers in panels represent the percentage of cells. Histograms display the amount of TNF expressed at the indicated time points after stimulation. (**B**) TNF production was measured with the Beadlyte mouse cytokine kit in supernatants from (A). (**C**) mRNAs were detected by RT-PCR in cells from (A). Lanes, WT (lane 1), *bic*/miR-155$^{+/-}$ (lane 2) and *bic*/miR-155$^{-/-}$ mice (lanes 3 and 4), and no cDNA input (lane 5). Data are representative of five independent experiments. (**D**) mLNs non-GC and GC B cells were sorted, and RT-PCR was performed as in (C).

smaller than those of controls and B cell$^{miR-155}$ mice (Fig. 2, C and D). Together, these results complement those obtained for GC formation (bic/GAL mice) and indicate that miR-155 plays a specific role in the control of the GC reaction in the context of a T cell–dependent antibody response.

We next investigated a possible molecular basis for the effects of miR-155. With no obviously relevant predicted miR-155 targets in hand, we focused on basic features of the GC response, namely, B cell proliferation, the generation of somatic antibody mutants, and selection of mutated B cells that bound antigen with high affinity. We also examined the production of tumor necrosis factor (TNF) and lymphotoxin-α (LT-α) and LT-β by mutant and control B cells, because it is known that TNF and LT-α, produced by B cells, are critical for GC formation (*18–20*). When *bic*/miR-155$^{-/-}$ B cells were induced to proliferate in vitro by a variety of stimuli, their proliferation profile, determined by dilution of a cell-bound carboxyfluorescein diacetate succinimidyl ester (CFSE) label, was indistinguishable from that of control cells (fig. S8). There was thus no indication from these experiments that miR-155 expression is directly involved in the control of B cell proliferation. The anti-NP response is characterized by the preferential usage of the V_H186.2 gene segment of the IgH^b haplotype. Furthermore, high-affinity anti-NP antibodies acquire a tryptophan-to-leucine mutation at position 33 (W33L) (*17*). GC B cells were thus isolated from *bic*/miR-155$^{+/+}$ and *bic*/miR-155$^{-/-}$ mice on day 12 or 14 after immunization with NP-CGG, and rearranged V_H186.2 gene segments were sequenced (*17*). Although there were no notable differences in overall mutation frequency between control and mutant cells, the selection for the W33L mutation was compromised in *bic*/miR-155 knockout cells (Fig. 2E). Therefore, although miR-155 is not required for somatic hypermutation of antibody genes in GC B cells, it contributes to an optimal selection of cells acquiring high-affinity antibodies. A possible clue to an understanding of the defective GC reaction in *bic*/miR-155 knockout mice came from the analysis of cytokine production by activated B cells from knockout and control mice. Two days after in vitro activation by BCR cross-linking, TNF production by *bic*/miR-155$^{-/-}$ B cells was noticeably reduced when compared with that of the controls (Fig. 3A). Consistent with this, the concentration of TNF in culture supernatants of the mutant B cells was about one-third of that in control supernatants (Fig. 3B). The differences in TNF production between knockout and wild-type cells were also apparent at the level of gene expression, as demonstrated by reverse transcription polymerase chain reaction (RT-PCR) analysis of TNF-specific transcripts (Fig. 3C). We further showed, by RT-PCR, that *lt-α* but not *lt-β* expression is also compromised in the mutant cells. These defects were also observed in ex vivo sorted GC and non-GC B cells from mLNs of the knockout mice, where B cells may be chronically activated by exposure to bacterial antigens (Fig. 3D). Together, these data suggest that miR-155 controls the GC response at least in part at the level of cytokine production. Although this control may follow pathways of posttranscriptional gene silencing, we note that fragile-X mental retardation related protein 1 (FXR1) and Argonaute-2, an RNA-binding protein involved in the microRNA pathway, were shown to associate with an AU-rich element in the 3′ untranslated region (UTR) of the TNF mRNA during translation activation (*21*). A conserved miR-155 binding site (AGCAUUA) downstream of this element could contribute to the targeting of Argonaute-2 and FXR1 to the TNF mRNA.

Because miR-155 is also expressed in T cells upon activation and differential cytokine production is a hallmark of T cell differentiation into T helper cell 1 (T_H1) and T_H2 effector cells, we tested T_H1 and T_H2 differentiation of knockout and control T cells in vitro (*22, 23*). We found that T cell differentiation proceeded normally in both cases (Fig. 4A). However, when T cells were cultured under conditions that promote neither differentiation pathway or suboptimally promote T_H2 differentiation, *bic*/miR-155$^{-/-}$ cells produced more interleukin-4 (IL-4) and less interferon-γ (IFN-γ), suggesting that they were more prone to T_H2 differentiation than controls (Fig. 4 and fig. S9). In addition, mutant T cell cultures generated more cells producing IL-10, a cytokine known to dampen immune responses (*24, 25*).

Although it remains to be seen whether these observations relate to the impaired GC response in the mutants, the present experiments establish, through a combined genetic loss- and gain-of-function approach, that miR-155 is critically involved in the in vivo control of specific differentiation processes in the immune response and that it exerts its functions at least partly at the level of control of cytokine production.

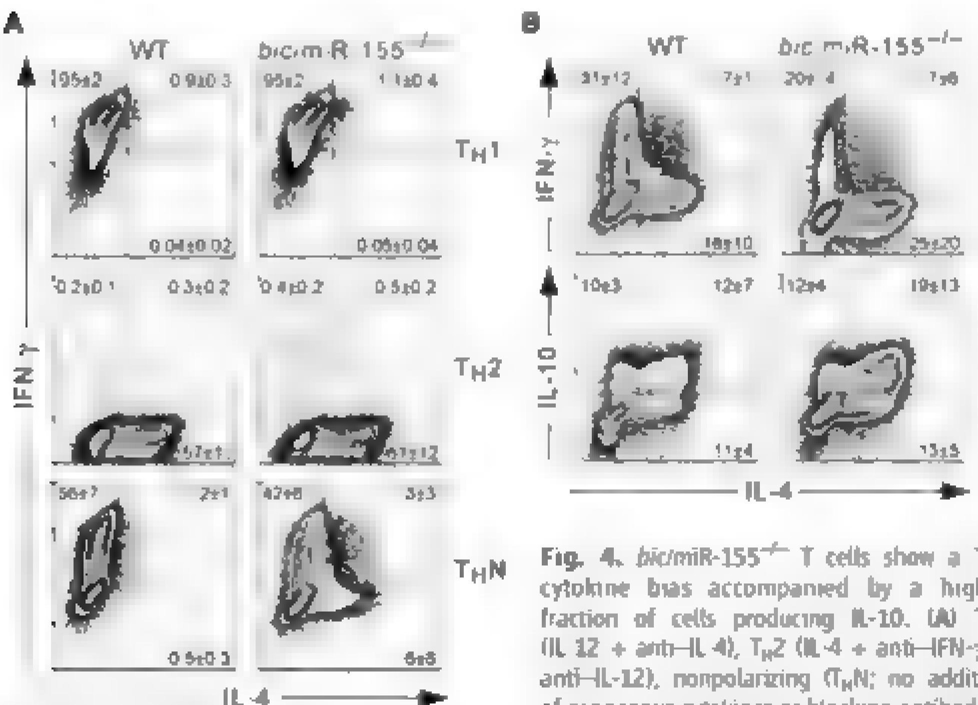

Fig. 4. *bic*/miR-155$^{-/-}$ T cells show a T_H2 cytokine bias accompanied by a higher fraction of cells producing IL-10. (**A**) T_H1 (IL-12 + anti–IL-4), T_H2 (IL-4 + anti–IFN-γ + anti–IL-12), nonpolarizing (T_HN; no addition of exogenous cytokines or blocking antibodies) conditions were used to study T cell differentiation with purified CD4$^+$ T cells from peripheral lymph nodes. On day 5, intracellular IL-4 and IFN-γ production was measured by FACS (mean ± SD, five knockout and four wild-type mice from three independent experiments). (**B**) Cells prepared as in (A) were differentiated under the influence of a limited quantity of IL-4 (12.5 U/ml) (mean ± SD, four knockout and three wild-type mice, from two independent experiments). Numbers in panels represent the percentage of cells.

References and Notes

1. B. E. Clurman, W. S. Hayward, *Mol. Cell. Biol.* **9**, 2657 (1989).
2. W. Tam, S. H. Hughes, W. S. Hayward, P. Besmer, *J. Virol.* **76**, 4275 (2002).
3. W. Tam, *Gene* **274**, 157 (2001).
4. W. Tam, D. Ben-Yehuda, W. S. Hayward, *Mol. Cell. Biol.* **17**, 1490 (1997).
5. P. S. Eis *et al.*, *Proc. Natl. Acad. Sci. U.S.A.* **102**, 3627 (2005).
6. M. Metzler, M. Wilda, K. Busch, S. Viehmann, A. Borkhardt, *Genes Chromosomes Cancer* **39**, 167 (2004).
7. A. van den Berg *et al.*, *Genes Chromosomes Cancer* **37**, 20 (2003).
8. S. Costinean *et al.*, *Proc. Natl. Acad. Sci. U.S.A.* **103**, 7024 (2006).
9. D. Haasch *et al.*, *Cell. Immunol.* **217**, 78 (2002).
10. K. D. Taganov, M. P. Boldin, K. J. Chang, D. Baltimore, *Proc. Natl. Acad. Sci. U.S.A.* **103**, 12481 (2006).
11. K. Rajewsky, *Nature* **381**, 751 (1996).
12. D. M. Valenzuela *et al.*, *Nat. Biotechnol.* **21**, 652 (2003).
13. Materials and methods are available as supporting material on *Science* Online.
14. Y. Sasaki *et al.*, *Immunity* **24**, 729 (2006).
15. M. Kraus, M. B. Alimzhanov, N. Rajewsky, K. Rajewsky, *Cell* **117**, 787 (2004).

16. M. Schmidt-Supprian *et al.*, *Mol. Cell* **5**, 981 (2000).
17. G. Esposito *et al.*, *Proc. Natl. Acad. Sci. U.S.A.* **97**, 1166 (2000).
18. R. Endres *et al.*, *J. Exp. Med.* **189**, 159 (1999).
19. Y. X. Fu *et al.*, *J. Exp. Med.* **185**, 2111 (1997).
20. Y. Wang, J. Wang, Y. Sun, Q. Wu, Y. X. Fu, *J. Immunol.* **166**, 330 (2001).
21. S. Vasudevan, J. A. Steitz, *Cell* **128**, 1105 (2007).
22. K. M. Ansel, I. Djuretic, B. Tanasa, A. Rao, *Annu. Rev. Immunol.* **24**, 607 (2006).
23. K. M. Murphy, S. L. Reiner, *Nat. Rev. Immunol.* **2**, 933 (2002).
24. R. Kuhn, J. Lohler, D. Rennick, K. Rajewsky, W. Muller, *Cell* **75**, 263 (1993).
25. A. Roers *et al.*, *J. Exp. Med.* **200**, 1289 (2004).

26. We thank D. Ghiza, C. Aristoff, M. Cumulte, and A. Monb for expert mouse generation, and the entire Rajewsky lab, particularly K. Otipoby for reading of the manuscript and C. Patterson for helpful suggestions. We also thank N. Bartenava for cell sorting and T. Curne for histology. This work was supported by NIH grant AI064345.

Supporting Online Material
www.sciencemag.org/cgi/content/full/316/5824/604/DC1
Materials and Methods
Figs. S1 to S9
References

13 February 2007; accepted 30 March 2007
10.1126/science.1141229

Requirement of *bic/microRNA-155* for Normal Immune Function

Antony Rodriguez,[1]* Elena Vigorito,[2]* Simon Clare,[1] Madhuri V. Warren,[1,3] Philippe Couttet,[1] Dalya R. Soond,[2] Stijn van Dongen,[1] Russell J. Grocock,[1] Partha P. Das,[4] Eric A. Miska,[4] David Vetrie,[1] Klaus Okkenhaug,[2] Anton J. Enright,[1] Gordon Dougan,[1] Martin Turner,[2]† Allan Bradley[1]†

MicroRNAs are a class of small RNAs that are increasingly being recognized as important regulators of gene expression. Although hundreds of microRNAs are present in the mammalian genome, genetic studies addressing their physiological roles are at an early stage. We have shown that mice deficient for *bic/microRNA-155* are immunodeficient and display increased lung airway remodeling. We demonstrate a requirement of *bic/microRNA-155* for the function of B and T lymphocytes and dendritic cells. Transcriptome analysis of *bic/microRNA-155*–deficient CD4+ T cells identified a wide spectrum of microRNA-155–regulated genes, including cytokines, chemokines, and transcription factors. Our work suggests that *bic/microRNA-155* plays a key role in the homeostasis and function of the immune system.

MicroRNAs (miRNAs) posttranscriptionally regulate gene expression by forming imperfect base pairing with sequences in the 3′ untranslated region (3′ UTR) of genes to prevent protein accumulation by repressing translation or by inducing mRNA degradation (*1, 2*). More than 500 miRNAs have been identified in mammals, although their functions are only now being elucidated (*3*). In the immune system, the enzyme responsible for regulatory RNA biogenesis, Dicer, is required for T cell function, which suggests regulatory roles for miRNAs in lymphocytes (*4, 5*). One miRNA, miR-155 (*6*), maps within, and is processed from, an exon of the noncoding RNA known as bic (*7, 8*), its primary miRNA precursor (*9*). *bic/miR-155* shows greatly increased expression in activated B and T cells (*9–11*), as well as in activated macrophages and dendritic cells (DCs) (*12, 13*). Overexpression of *bic/miR-155* has been reported in B cell lymphomas and solid tumors (*14*), and transgenic miR-155 mice have also been shown to develop B cell malignancies in vivo (*15*), indicating that the locus may also be linked to cancer.

To define the in vivo role of *bic/miR-155* (*bic*), we generated mutant alleles in embryonic stem cells (*16*) to obtain *bic*-deficient ($bic^{m1/m1}$ and $bic^{m2/m2}$) mice (fig. S1, A and B). *bic*-deficient mice were viable and fertile but developed lung pathology with age. At 320 to 350 days, 56% (5 out of 9) of $bic^{m1/m1}$ mice displayed significant remodeling of lung airways, with increased bronchiolar subepithelial collagen deposition and increased cell mass of sub-bronchiolar myofibroblasts (Fig. 1, B, D, and F), relative to age-matched control mice (*n* = 8) (Fig. 1, A, C, and E). A statistically significant increase in the ratio of collagen thickness/bronchiolar diameter and smooth muscle cell area/bronchiolar diameter could be measured in *bic*-deficient mice, compared with wild-type controls (Fig. 1, G and H). Increased airway remodeling in aged $bic^{m1/m1}$ mice was accompanied by a significant increase in the numbers of leukocytes in bronchoalveolar lavage fluids (BAL) (Fig. 1, I) but not the lung (data not shown). These changes are reminiscent of the lung fibrosis that often complicates systemic autoimmune processes with lung involvement (*17, 18*). We also noted that many $bic^{m1/m1}$ mice developed enteric inflammation, a trait we have not investigated further. Thus, the phenotype we observed suggested that *bic/miR-155* may participate or play a role in regulating the homeostasis of the immune system.

[1]The Wellcome Trust Sanger Institute, Wellcome Trust Genome Campus, Hinxton, Cambridge CB10 1SA, UK. [2]Laboratory of Lymphocyte Signalling and Development, The Babraham Institute, Cambridge, CB2 4AT, UK. [3]Department of Pathology, Addenbrooke's Hospital, University of Cambridge, Cambridge CB2 2QQ, UK. [4]Gurdon Institute and Department of Biochemistry, University of Cambridge, Cambridge, CB2 1QN, UK.

*These authors contributed equally to this work.
†To whom correspondence should be addressed. abradley@sanger.ac.uk (A.B.), martin.turner@bbsrc.ac.uk (M.T.)

The pathology observed in *bic*-deficient mice prompted us to examine the requirement of *bic/miR-155* in immunity. Although no gross defect in myeloid or lymphoid development in *bic*-deficient mice was observed (tables S1 and S2), protective immunity did appear to be impaired. Thus, after intravenous immunization with the live attenuated form of the enteric pathogen *Salmonella typhimurium* (*aroA* mutant strain), mice were assessed for their ability to resist oral challenge with virulent *S. typhimurium* bacteria (*19, 20*). Both unvaccinated $bic^{m2/m2}$ and wild-type control mice (5 out of 5, *n* = 5) died within 7 days after infection (Fig. 2A). However, unlike their wild-type counterparts, $bic^{m2/m2}$ mice were less readily protected by *aroA* vaccination, and the majority of mice (5 out of 6; *n* = 6) succumbed to challenge with the virulent strain by 33 days after infection (Fig. 2B). Thus, immunized *bic*-deficient mice, unlike wild-type mice, could not be protected by immunization to this pathogen.

Protective immunity requires the function of T and B lymphocytes. Therefore, we next examined the in vivo B and T cell responses of *bic*-deficient mice immunized with the T-dependent antigen, tetanus toxin fragment C protein (TetC). Immunized $bic^{m1/m1}$ mice produced significantly reduced amounts of immunoglobulin M (IgM) and switched antigen-specific antibodies (Fig. 2C), indicative of impaired B cell responses. For examination of T cell function, splenocytes from mice immunized with TetC were restimulated in vitro, and the levels of interleukin (IL)–2 and interferon (IFN)–γ cytokines were measured. As expected, splenocytes from wild-type mice immunized with TetC produced significantly increased levels of IL-2 and IFN-γ relative to naive mice (Fig. 2D). In contrast, $bic^{m1/m1}$ immunized mice failed to produce significant levels of these cytokines (Fig. 2D). Thus, B and T cell responses were diminished in *bic*-deficient mice, possibly contributing to their impaired enteric immunity.

To understand the nature of defective immune responses in vivo, we explored the possibility of an intrinsic requirement for *bic/miR-155* in B cells and T cells. Dendritic cell (DC) function was also tested, because these cells act as professional antigen-presenting cells (APCs) with the ability to influence T cell activation and differentiation. Production of IgG1 by lipopolysaccharide (LPS)– and IL-4–stimulated $bic^{m2/m2}$

B cells was significantly reduced (Fig. 2E), although this defect did not appear to correspond with abnormal proliferation (fig. S2). After encountering antigen, DCs increase their immunostimulatory capacity (27) through a process that is mimicked in vitro by stimulation with LPS. After treatment with LPS $bic^{m2/m2}$ bone marrow–derived DCs expressed levels of major histocompatibility complex II and costimulatory mol-

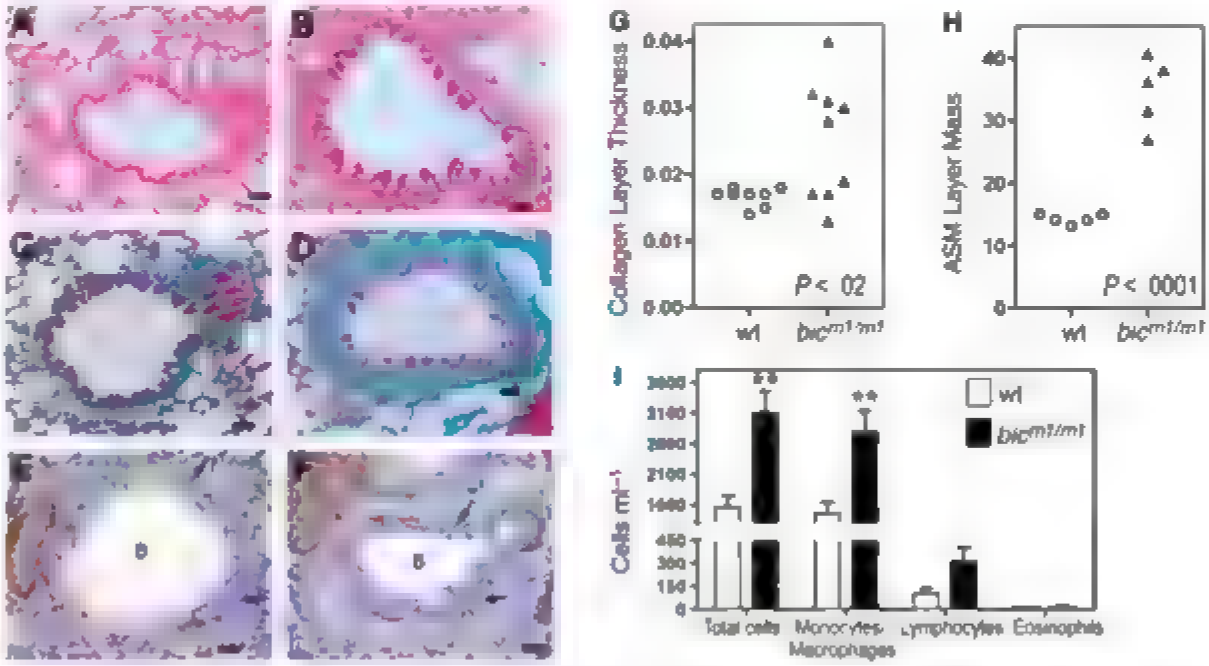

Fig. 1. Mice deficient for *bic/miR-155* show increased lung airway remodeling. (**A** to **F**) Histological examination of sections of lung bronchioles from control wild-type (A, C, and E) and $bic^{m1/m1}$ mice (B, D, and F). Scale bar, 100 μm. (A and B) Haematoxylin and eosin stain; (C and D) Masson Trichrome stain; (E and F) Immunohistochemical staining for smooth muscle actin. Collagen layer (white arrows), lung myofibroblasts (black arrows), bronchioles (B), and blood vessels (V) are indicated. (**G**) Quantitation of peribronchiolar collagen thickness or (**H**) airways smooth muscle cell (ASM) mass in $bic^{m1/m1}$ mice compared with that of wild-type mice. (G) $P < 0.02$ or (H) $P < 0.0001$, in comparison with wild-type group, Student's two-tailed t test. Open circles, control mice; filled triangles, $bic^{m1/m1}$ mice. Notably, $bic^{m1/m1}$ mice with increased collagen layer thickness also had increased ASM mass. (**I**) Total and differential cell counts in BAL from the indicated mice. Data are the mean + SE from seven *bic*-deficient mice and six control mice. $^{**}P < 0.01$ in comparison with wild-type group, Student's two-tailed t test.

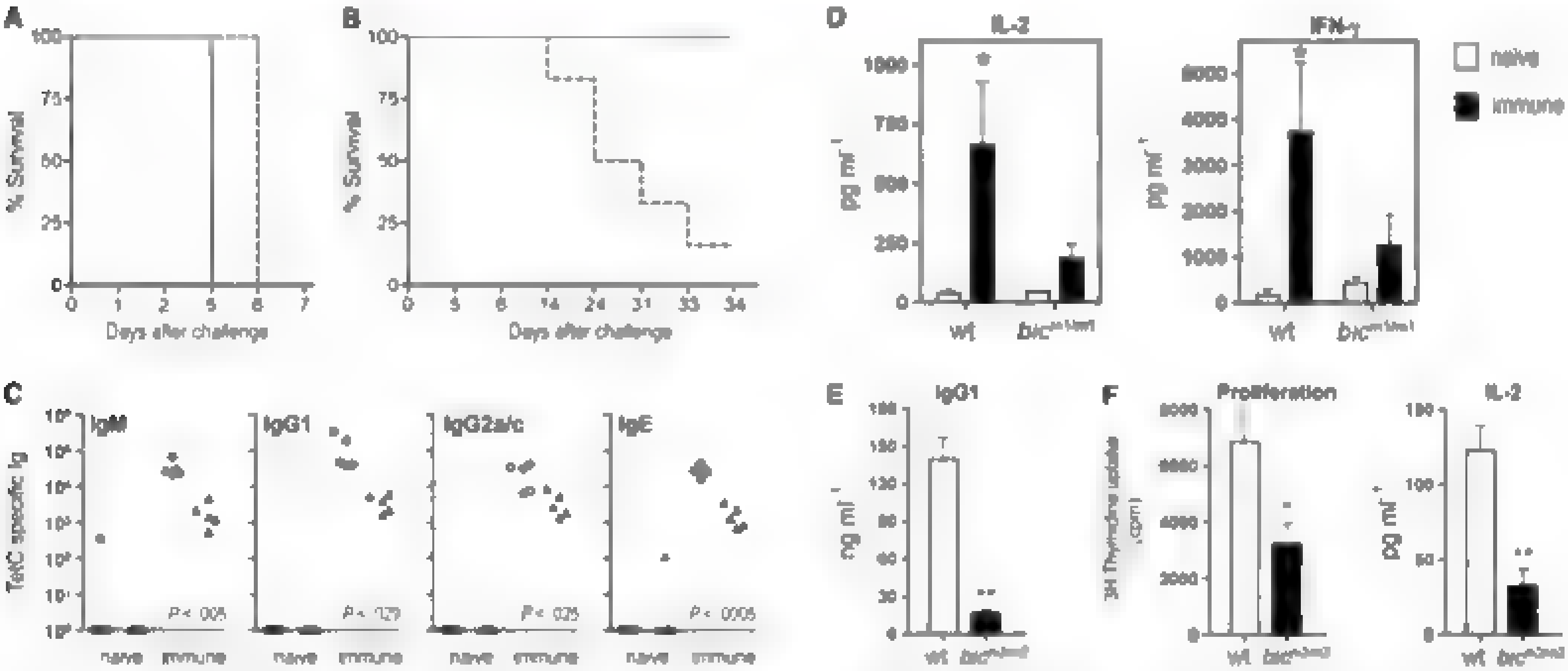

Fig. 2. Defective adaptive immunity by *bic*-deficient mice. (**A**) Survival curve for mice ($n = 5$ in each group) infected orally with 1×10^8 colony-forming units (CFU)—virulent *S. typhimurium* strain SL344. As expected for mice of this genetic background, all failed to survive challenge. (**B**) Survival of mice ($n = 6$ in each group) infected intravenously with 1×10^4 CFU of *S. typhimurium* aroA strain followed by oral challenge with *S. typhimurium* SL344 6 weeks after prime. In contrast with control mice, $bic^{m2/m2}$ mice demonstrate reduced survival after challenge. (A and B) Line, control C57BL/6J (wild-type) mice; dashed line, N5 C57BL/6J backcross $bic^{m2/m2}$ mice. (**C**) TetC-specific Ig levels from control mice (open circles) or *bic*-deficient mice (filled triangles) immunized with TetC at days 1 and 21 and analyzed 13 days after secondary immunization. P values denote significant differences; Student's two-tailed t test. (**D**) Production of IL-2 and IFN-γ by splenocytes isolated from wild-type or $bic^{m1/m1}$-naïve mice (open bars) or immunized with TetC as in (C) (closed bars) and cultured for 48 hours in the presence of TetC. Data are the mean ± SE from four mice. $^{*}P < 0.05$ versus naïve mice; Student's two-tailed t test. (**E**) Reduced IgG1 production by $bic^{m2/m2}$ B cells cultured in the presence of LPS and IL-4 for 4 days. Data are the mean + SE from 3 mice. $^{**}P < 0.01$ versus wild-type Student's two-tailed t test. (**F**) Significantly reduced proliferation and IL-2 production by ovalbumin T cell receptor transgenic (OT-II) cells cultured with LPS-matured, bone marrow–derived, *bic*-deficient DCs in the presence of cognate (2.5 μM) ovalbumin protein. Cell proliferation was determined by [^{3}H]-thymidine incorporation at 72 hours. IL-2 was measured from supernatants by enzyme-linked immunosorbent assay (ELISA) at 48 hours. Data are the mean + SE from five mice of each genotype. $^{*}P < 0.05$ versus wild-type; Student's two-tailed t test.

ecules similar to those seen on identically treated matured wild-type DCs (fig. S3, A and B), which indicates that *bic/miR-155* is not required for maturation. Nevertheless, *bic*$^{m2/m2}$ DCs failed to efficiently activate T cells, consistent with defective antigen presentation or costimulatory function (Fig. 2F). Collectively, these results suggest that the effects of *bic/miR-155* may operate in part on T cells through its influence on DC function.

To establish whether there is also an intrinsic requirement for *bic/miR-155* in T cell function, the response of receptor-stimulated naïve *bic*$^{m2/m2}$ CD4$^+$ T cells was tested. Despite normal proliferation, uncommitted *bic*$^{m2/m2}$ CD4$^+$ cells showed a significant reduction of the T helper (Th) 1 cytokine IFN-γ after stimulation with antibodies to CD3 and CD28 (fig. S4). A reduction by a factor of 5 in the number of IFN-γ producing cells was also observed after restimulation of *bic*$^{m2/m2}$ CD4$^+$ T cells cultured under conditions designed not to polarize Th responses (Fig. 3A); and was accompanied by a doubling in the number of IL-4 single-producing cells (Fig. 3A). In light of the expression of bic/miR-155 in both Th1 and Th2 cell lineages (fig. S5, A and B), we next examined the phenotype of *bic*$^{m2/m2}$ CD4$^+$ T cells after culture in conditions that promote Th1 or Th2 cell differentiation. The levels of IFN-γ, as well as the number of *bic*$^{m2/m2}$ Th1 cells secreting cytokine, were similar to controls, which indicates that *bic/miR-155* is not required for Th1 differentiation (Fig. 3, A and B). However, phenotypic alterations were observed as *bic*$^{m2/m2}$ Th1 cells produced elevated levels of CCL-5 (Fig. 3B and table S3). By contrast, increased commitment to the Th2 pathway was evident in *bic*$^{m2/m2}$ Th2 cell cultures as higher numbers of IL-4 producing cells were observed (Fig. 3A). In support of this result, enhanced levels of the Th2 cytokines IL-4, IL-5, and IL-10 were generated by *bic*$^{m2/m2}$ cells after culture in Th2 polarizing conditions (Fig. 3C). Taken together, these data demonstrate that *bic*-deficient CD4$^+$ T cells are intrinsically biased toward Th2 differentiation. Moreover, Th1 cells may have altered function despite normal production of IFN-γ.

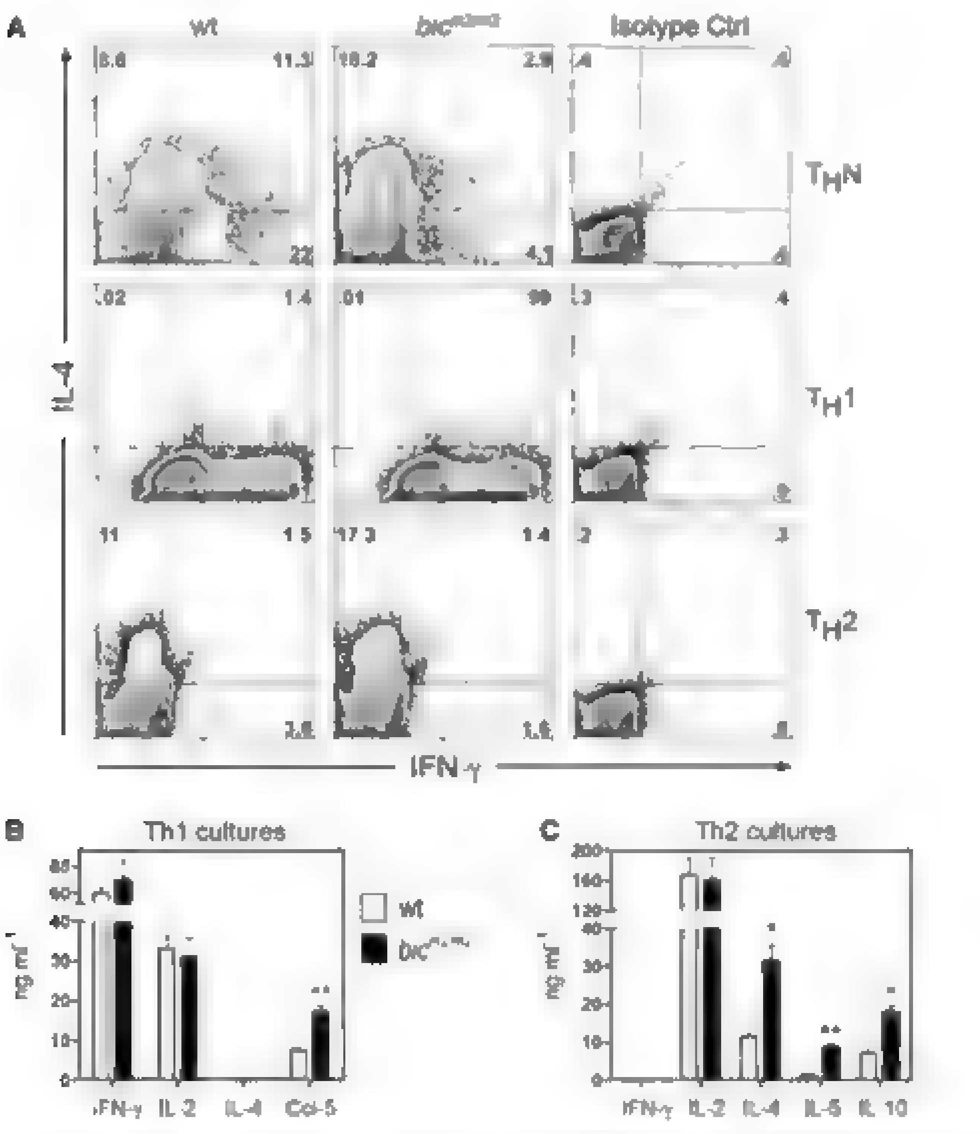

Fig. 3. Increased Th2 polarization and amplified Th2 cytokine production by *bic*-deficient CD4$^+$ T cells. CD4$^+$CD62L$^+$ cells of indicated genotypes were cultured under (**A**, middle panel, and **B**) Th1 conditions, (**A**, lower panel, and **C**) Th2 in vitro differentiation conditions, or (**A**, upper panel) nonpolarizing (ThN) conditions and restimulated with immobilized antibody to CD3 (10 μg/ml) and soluble 2 μg/ml antibody to CD28 on day 6. (**A**) Intracellular cytometric analysis for IFN-γ and IL-4 production (*16*). The panel shows a representative result of three mice of each genotype analyzed in the same experiment. Data are representative of two independent experiments (n = 3 per genotype). Numbers in each quadrant are percentages of cells of indicated phenotype. (**B** and **C**) Cytokine levels were assayed by ELISA 21 hours after restimulation of cells cultured under (B) Th1 or (C) Th2 polarizing conditions. Data are the mean + SE from three individual mice. *P < 0.05 or **P < 0.01 versus wild-type; Student's two-tailed t test.

To understand how *bic/miR-155* regulates Th2 commitment and to gain a more global insight into the extent of deregulation in T cells, we analyzed gene expression in *bic*$^{m2/m2}$ Th1 or Th2 cells using microarray analysis. In addition, because the 5′ region of miRNAs (referred to as the "seed" region) is believed to be crucial for target mRNA recognition (*1, 2*), we searched the 3′ UTRs of significantly up-regulated genes in microarrays for the presence of seed matches specific for miR-155. In *bic*-deficient Th1 cells, we identified 46 of 53 up-regulated transcripts as potential miR-155 targets (table S3 and fig. S6). In *bic*-deficient Th2 cells, 53 out of 99 up-regulated transcripts were predicted targets (table S4 and fig. S7). To confirm these genes as likely targets of miR-155, we then searched the 3′ UTRs for seed matches specific for all of the known mouse miRNAs in the miRbase public database (*3*). miR-155 seed sequences were significantly overrepresented over all other tested mouse miRNAs, indicating a significant probability that these genes are direct targets of miR-155 (Fig. 4, A and B). This computational data strongly suggests that miR-155 represses a wide assortment of genes in CD4$^+$ T cells and lends support for the hypothesis that miRNA targets are generally abundant in mammals (*22*).

A wide spectrum of miR-155 target genes with diverse molecular roles, such as T cell costimulation (e.g., *Tnfsf9*), chemotaxis (e.g., *Ccl-5*), and signaling (e.g., *Ikbke*), were identified. Among these, we noted that the transcription factor *c-Maf* contains phylogenetically conserved miR-155 seed matches in the 3′ UTR (fig. S8). c-Maf is a potent transactivator of the *IL-4* promoter, and ectopically expressed c-Maf is sufficient to cause increased IL-4, IL-5 and IL-10 production by Th2 cells (*23–25*). In concordance with the microarray results, a significant induction of *c-Maf* mRNA was detected in *bic*$^{m2/m2}$ Th2 cells, and the levels of c-Maf protein were correspondingly increased (Fig. 4, C and D). By contrast, levels of *Gata3* transcript, which does not contain a miR-155 seed, were not elevated (Fig. 4C). Increased

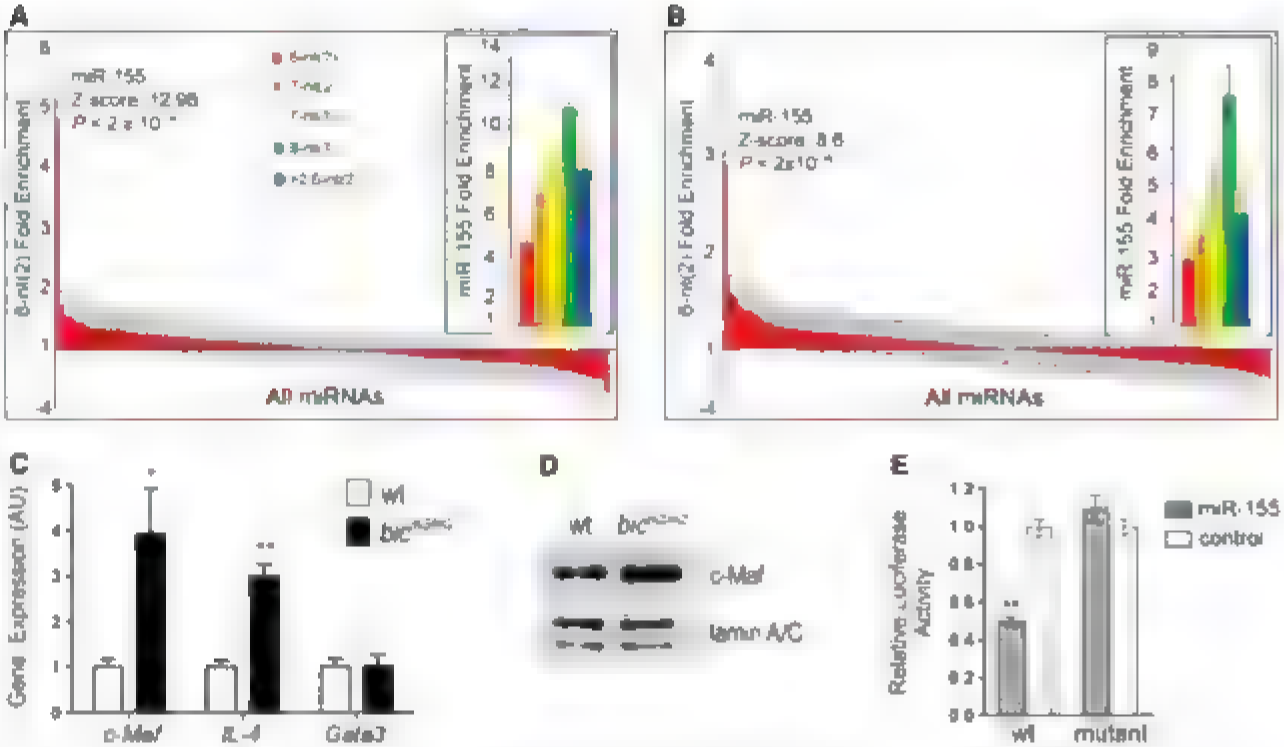

Fig. 4. miR-155 pattern sequences are enriched in the Th1 and Th2 cell up-regulated genes, and *c-Maf* is a bona fide target of miR-155. (**A** and **B**) Fold enrichment of 5′ miRNA pattern sequences of the indicated types contained in the 3′ UTRs of the (A) Th1 or (B) Th2 cDNA microarray significantly up-regulated gene sets. The standard deviation, *Z* score, and *P* value were calculated by sampling 1000 random sets of 53 (for Th1 set) or 99 (for Th2 set) genes from the mouse genome (*16*). Data are fold enrichment ± SD. (**C**) Quantitative PCR analysis for *Gata3*, *c-Maf*, and *IL-4* transcript levels from Th2 cells restimulated with antibodies to CD3 and CD28. Data are the mean + SE from three mice. *$P < 0.05$ versus wild-type; Student's two-tailed *t* test. (**D**) c-MAF protein levels were assessed by Western blot of nuclear extracts of Th2 cells isolated from the indicated genotypes. Expression of lamin A/C was used as loading control. (**E**) miR-155–dependent repression of *c-Maf* reporter in vitro. A luciferase (Rluc) reporter was used to validate *c-Maf* as a direct target of miR-155. Wild-type (wt) or mutant plasmids (mut) were cotransfected with the indicated duplex miRNA for miR-155 (open bars) or control Cel-miR-64 (filled bars) into HeLa S3 cells. Data are mean ± SE from three experiments. **$P < 0.0001$ in comparison with wild-type plasmid treated with nonspecific RNA duplex, Cel-miR-64. Student's two-tailed *t* test.

expression of *c-Maf* may thus contribute, at least in part, to the increased Th2 cytokine production phenotype observed in *bic*$^{m2/m2}$ Th2 cells. To further confirm whether *c-Maf* is a direct target of miR-155, we cloned its 3′ UTR into a luciferase reporter plasmid. The wild-type *c-Maf* reporter exhibited significant miR-155–dependent repression relative to the reporter with a mutant seed sequence, which indicates that this is a direct target for miR-155 (Fig. 4E). We conclude from these experiments that *bic/miR-155* modulates levels of *c-Maf* in CD4^{+} T cells and this is likely to contribute to the attenuation of Th2 cell responses in vivo.

Our data demonstrate that mice carrying a null mutation in the *bic/miR-155* gene display altered immune responses. Thus, along with an increase in airways remodeling suggestive of altered homeostasis, we observed that *bic/miR-155* regulates the function of both lymphocytes and DCs, leading to an overall diminution of immune responses. The identification of multiple novel potential targets of miR-155 supports the view that *bic/miR-155* is a core regulator of gene expression in multiple cell types, with a "targetome" optimized to modulate the immune response. Interestingly, *bic*-deficient mice share some of the cellular features observed in CD4-*Cre Dicer*^{FL} mice, including defects in CD4^{+} T cell cytokine production and immune homeostasis (*3*, *4*). It will now be important to define the pathophysiology of *bic*-deficient lymphocytes and further test the role of miR-155–dependent repression of *c-Maf* on immune responses in vivo. The strength of the *bic/miR-155* mutant phenotype more generally suggests critical roles for miRNAs in vivo, with potentially severe loss-of-function phenotypes directly relevant to human disease. In this regard, it is intriguing that the human *BIC/miR-155* gene maps to an asthma, pollen sensitivity, and atopic dermatitis susceptibility region on chromosome 21q21 (*26*–*28*). Given the severe phenotypes noted in these mice, BIC/miR-155 should be investigated as a potential immune disease locus in humans.

References and Notes

1. D. P. Bartel, *Cell* **116**, 281 (2004).
2. B. M. Engels, G. Hutvagner, *Oncogene* **25**, 6163 (2006).
3. S. Griffiths-Jones, R. J. Grocock, S. van Dongen, A. Bateman, A. J. Enright, *Nucleic Acids Res.* **34**, D140 (2006).
4. S. A. Muljo *et al.*, *J. Exp. Med.* **202**, 261 (2005).
5. B. S. Cobb *et al.*, *J. Exp. Med.* **203**, 2519 (2006).
6. M. Lagos-Quintana *et al.*, *Curr. Biol.* **12**, 735 (2002).
7. W. Tam, D. Ben-Yehuda, W. S. Hayward, *Mol. Cell. Biol.* **17**, 1490 (1997).
8. W. Tam, *Gene* **274**, 157 (2001).
9. P. S. Eis *et al.*, *Proc. Natl. Acad. Sci. U.S.A.* **102**, 3627 (2005).
10. D. Haasch *et al.*, *Cell. Immunol.* **217**, 78 (2002).
11. A. van den Berg *et al.*, *Genes Chrom. Cancer* **37**, 20 (2003).
12. K. D. Taganov, M. P. Boldin, K. J. Chang, D. Baltimore, *Proc. Natl. Acad. Sci. U.S.A.* **103**, 12481 (2006).
13. B. B. Stetson, R. Medzhitov, *Immunity* **24**, 93 (2006).
14. G. A. Calin, C. M. Croce, *Nat. Rev. Cancer* **6**, 857 (2006).
15. S. Costinean *et al.*, *Proc. Natl. Acad. Sci. U.S.A.* **103**, 7024 (2006).
16. Materials and methods are available as supporting material on *Science* Online.
17. C. K. Lai, W. D. Wallace, M. C. Fishbein, *Semin. Respir. Crit. Care Med.* **27**, 613 (2006).
18. S. K. Jindal, R. Agarwal, *Curr. Opin. Pulm. Med.* **11**, 438 (2005).
19. P. Mastroeni, J. A. Chabalgoity, S. J. Dunstan, D. J. Maskell, G. Dougan, *Vet. J.* **161**, 132 (2001).
20. S. Clare *et al.*, *Infect. Immun.* **71**, 5881 (2003).
21. J. Banchereau, R. M. Steinman, *Nature* **392**, 245 (1998).
22. L. P. Lim *et al.*, *Nature* **433**, 769 (2005).
23. I. C. Ho, D. Lo, L. H. Glimcher, *J. Exp. Med.* **188**, 1859 (1998).
24. I. C. Ho, M. R. Hodge, J. W. Rooney, L. H. Glimcher, *Cell* **85**, 973 (1996).
25. E. S. Hwang, J. A. White, I. C. Ho, *Proc. Natl. Acad. Sci. U.S.A.* **99**, 13026 (2002).
26. C. Ober *et al.*, *Hum. Mol. Genet.* **7**, 1393 (1998).
27. M. N. Blumenthal *et al.*, *J. Allergy Clin. Immunol.* **117**, 79 (2006).
28. L. M. Bu *et al.*, *Allergy* **61**, 617 (2006).
29. The authors acknowledge D. Corry, F. Colucci, and members of the Bradley laboratory for critical reading of the manuscript. We also thank Beverley Haynes for histology work. A.R. was supported by a Ruth Kirschstein Fellowship. E.V. was supported by a Babraham Institute Career Progression Fellowship. M.T. was supported by the Medical Research Council and Biotechnology and Biological Sciences Research Council. A.B., G.D., A.E. were supported by the Wellcome Trust and Sanger Institute grant number 79643.

Supporting Online Material

www.sciencemag.org/cgi/content/full/316/5824/608/DC1
Materials and Methods
Figs. S1 to S8
Tables S1 to S4
References

26 December 2006; accepted 30 March 2007
10.1126/science.1139253

Distinct Pathways of Antigen Uptake and Intracellular Routing in CD4 and CD8 T Cell Activation

Sven Burgdorf,* Andreas Kautz, Volker Böhnert, Percy A. Knolle, Christian Kurts*

The mechanisms that allow antigen-presenting cells (APCs) to selectively present extracellular antigen to CD8$^+$ effector T cells (cross-presentation) or to CD4$^+$ T helper cells are not fully resolved. We demonstrated that APCs use distinct endocytosis mechanisms to simultaneously introduce soluble antigen into separate intracellular compartments, which were dedicated to presentation to CD8$^+$ or CD4$^+$ T cells. Specifically, the mannose receptor supplied an early endosomal compartment distinct from lysosomes, which was committed to cross-presentation. These findings imply that antigen does not require intracellular diversion to access the cross-presentation pathway, because it can enter the pathway already during endocytosis.

Adaptive immunity requires activation of T lymphocytes by dendritic cells (DCs), which present antigen bound by major histocompatibility complex (MHC) molecules (*1*). Antigens that are synthesized intracellularly (for example, those of viral or tumor origin) are presented by MHC I molecules and activate cytotoxic CD8$^+$ T cells. In contrast, extracellular antigens are presented by MHC II molecules to activate CD4$^+$ T helper cells (*1*, *2*). A further mechanism termed cross-presentation permits some forms of extracellular antigen to also stimulate CD8$^+$ T cells via the MHC I pathway (*3*–*5*). This is required for immunity against viruses that do not infect APCs directly or against tumor antigens that are not endogenously expressed by DCs (*5*–*10*). The mechanisms that divert endocytosed antigen from the classical MHC II restricted presentation pathway to that facilitating cross-presentation are controversial (*10*–*16*). Before substantial experimental evidence for cross-presentation had become available, the assumption that extracellular antigen was presented exclusively to CD4$^+$ T cells had implied that the different mechanisms of endocytosis supplied only MHC II restricted antigen presentation. Thus, the possibility that a differential influence of these uptake mechanisms on antigen presentation might exist, in particular on cross-presentation, remained to be clarified.

We recently demonstrated that mannose receptor (MR)–mediated endocytosis of the model antigen soluble ovalbumin (OVA) enabled its cross-presentation to CD8$^+$ T cells (*17*). We therefore investigated whether this was specific for the class I pathway or whether the MR also targets extracellular antigen for MHC II restricted presentation. DCs from MR-deficient (*18*) and wild-type control mice were allowed to endocytose OVA (*19*), and the response of OVA-specific CD4$^+$ T cells (OT-II cells) was examined. This revealed a complete independence from the MR for all OVA concentrations tested (Fig. 1A). In contrast, the response of OVA-specific CD8$^+$ T cells (OT-I cells) was absolutely dependent on the MR, regardless of the antigen concentration (Fig. 1A). Intrinsic differences in DCs resulting from MR deficiency, such as altered costimulatory molecule expression or proportions of DC subtypes, were not observed (*17*). Thus, MR-mediated endocytosis was essential for cross-presentation but dispensable for MHC II restricted presentation of OVA.

To elucidate the pathway by which antigen was endocytosed for the activation of MHC II restricted OT-II cells, we studied the in vitro uptake of OVA labeled with the fluorochrome alexa$_{647}$ (OVA$_{647}$) by DCs. Although a distinct DC subset took up large amounts of OVA$_{647}$ via the MR, a smaller fluorescence shift of about four- to fivefold was noted, which was MR-independent and appeared to encompass all DCs (Fig. 1B). This shift could be blocked by dimethylamiloride (DMA), an inhibitor of pinocytosis that leaves receptor-mediated endocytosis intact (Fig. 1B). DMA treatment of DCs during OVA uptake abrogated the activation of OT-II cells in a dose-dependent and MR-independent manner (Fig. 1C), indicating that only pinocytosed, but not MR-endocytosed, OVA was used to activate CD4$^+$ T cells. The response of OT-I cells was unaffected by DMA (Fig. 1C), excluding toxic effects.

Pinocytosis was active both in MR$^+$ DCs that endocytosed a large dose of OVA and in MR$^-$ DCs that did not, because both DC subsets were able to take up lucifer yellow (LY) (Fig. 1D), a pinocytosis marker (*20*). Despite slightly smaller pinocytotic activity (Fig. 1D) and severely reduced total uptake of OVA (Fig. 1B), MR$^-$ DCs were superior at activating OT-II cells as compared to MR$^+$ DCs (Fig. 1E). This indicated that MR$^-$ DCs processed pinocytosed antigen more efficiently than MR$^+$ DCs, which is consistent with the recent finding that antigen processing for MHC II restricted presentation depended on intrinsic properties of particular DC subtypes (*21*). In summary, all DCs constitutively pinocytosed small amounts of OVA, which was used specifically for presentation to CD4$^+$ T cells, while MR$^+$ DCs could simultaneously internalize large amounts of OVA exclusively for cross-presentation.

Cross-presentation requires a high antigen dose (*7*). Thus, its dependency on the MR may simply be due to the large amount of antigen endocytosed by this receptor as compared to the small amount internalized by pinocytosis (Fig. 1B). This possibility was addressed with the use of another type of APC capable of cross-presentation: bone marrow–derived macrophages (MΦs) (*22*). As with DCs, cross-presentation of OVA by these APCs was entirely MR-dependent (Fig. 2A). In contrast to DCs, however, MΦs also internalized large amounts of OVA in the absence of the MR (Fig. 2B). This additional uptake could be blocked with polyinosinic acid (polyI) (Fig. 2B), a specific inhibitor of scavenger receptors (SRs) (*23*). The inability of MR-deficient MΦs to activate OT-I cells, despite having internalized large amounts of OVA via SRs, indicated that the mechanism of endocytosis, rather than levels of antigen, was a requisite for cross-presentation. Moreover, SR-mediated OVA uptake was not responsible for OT-I cell activation, because MR-mediated endocytosis was sufficient (Fig. 2C). In further experiments using polyI and DMA blockade, we demonstrated that MΦs used pinocytosed OVA, as well as SR-endocytosed OVA, only for presentation to OT-II cells (Fig. 2, A and C).

To investigate why pinocytosed, SR- and MR-endocytosed antigen were presented differently, we monitored their intracellular routing by fluorescence microscopy in immature APCs, which are active in endocytosis (Fig. 3 and fig. S1). Within DCs, endocytosed OVA$_{647}$ strictly colocalized with the MR (Fig. 3A), whereas the small quantities taken up by pinocytosis (Fig. 1B) were insufficient for microscopic visualization. Therefore, pinocytosed antigen was monitored with the use of the surrogate marker LY amplified by antibody staining. This approach revealed that LY and OVA did not colocalize (Fig. 3A and table S1), indicating that pinocytosis and the MR supplied distinct intracellular compartments. MR-endocytosed OVA was localized in organelles expressing the early endosomal marker Rab5 and the early endosomal antigen 1 (EEA1). Consistent with the previous finding that the cytoplasmic domain of the MR did not target antigen toward lysosomes (*24*), MR-endocytosed OVA was excluded from late endosomes or lysosomes revealed by Rab7 or lysosomal-associated membrane protein 1 (LAMP-1) staining or by the fluorescent dye lysotracker that accumulates in the acidic lysosomes (Fig. 3B and table S1). In contrast, pinocytosed antigen was transported exclusively toward lysosomes lacking the early endosomal markers (Fig. 3B). This

Institute of Molecular Medicine and Experimental Immunology, Friedrich-Wilhelms-Universität, Bonn, Germany.

*To whom correspondence should be addressed. E-mail: ckurts@web.de (C.K.), sven.burgdorf@ukb.uni-bonn.de (S.B.)

separation was stable because, even for 6 hours after antigen uptake, MR-endocytosed OVA remained confined to EEA1^{+} endosomes and was excluded from lysosomes, whereas the opposite was observed for pinocytosed material (fig. S2).

Subcellular antigen localization correlated with the selectivity of its presentation, because pinocytosed LY colocalized specifically with lysosomal MHC II, whereas MR-endocytosed OVA colocalized exclusively with MHC I (Fig. 3C). Only MR^{+} early endosomes, and not MHC II^{+} lysosomes, contained cross-presented OVA (Fig. 3D and table S1), which was visualized by means of the monoclonal antibody 25-D1.16 (19) that specifically recognizes the OVA peptide SIINFEKL (Ser-Ile-Ile-Asn-Phe-Glu-Lys-Leu) when bound to the MHC I molecule K^{b} (25) and that has been previously used for immunofluorescence microscopy (11, 26). Specificity of 25-D1.16 staining for cross-presented OVA was confirmed by the lack of such staining in the absence of antigen or of the MR and after blockade of the proteasome (fig. S3), which is required for cross-presentation (4, 7, 8, 10–12). The confinement of cross-presented OVA to a distinct class of endosomes and its exclusion from lysosomes were also observed in MΦs (Fig. 3E and table S1) and in ex vivo–isolated splenic DCs (Fig. 3F). This suggests that cross-presentation of OVA in these experiments depended on antigen location in an early endosomal compartment. This interpretation was tested with the use of SR-deficient MΦs to determine the subcellular location of SR-endocytosed OVA. Such OVA was not cross-presented (Fig. 2A and fig. S3), despite uptake at high amounts (Fig. 2B) that even sufficed for direct intracellular visualization (Fig. 3G). If antigen location in these early endosomes was required for cross-presentation, then such organelles should not contain SR-endocytosed OVA. Indeed, this appeared to be the case (Fig. 3G and table S1), because SR-endocytosed OVA did not colocalize with EEA1 (Fig. 3G) or MR-endocytosed antigen (Fig. 3H). Instead, it colocalized with pinocytosed LY in lysosomes over an extended period (Fig. 3G and figs. S4 and S5). These findings provide further evidence that high-dose antigen intended for MHC II–restricted presentation and for cross-presentation are routed through different organelles in MΦs. The ability of the MR to sequester OVA away from lysosomal degradation may also explain why bone marrow–derived MΦs were particularly efficient at cross-presentation in our experiments (Fig. 2), although their lysosomal compartment has been shown to degrade antigen far more efficiently than that of DCs (27).

The experiments examining T cell responses in Figs. 1 and 2 did not permit us to quantitatively and directly compare the capabilities of DCs and MΦs to cross-present. However, some comparisons could be made by directly examining cross-presented antigen on the APC surface. When viable DCs and MΦs were stained

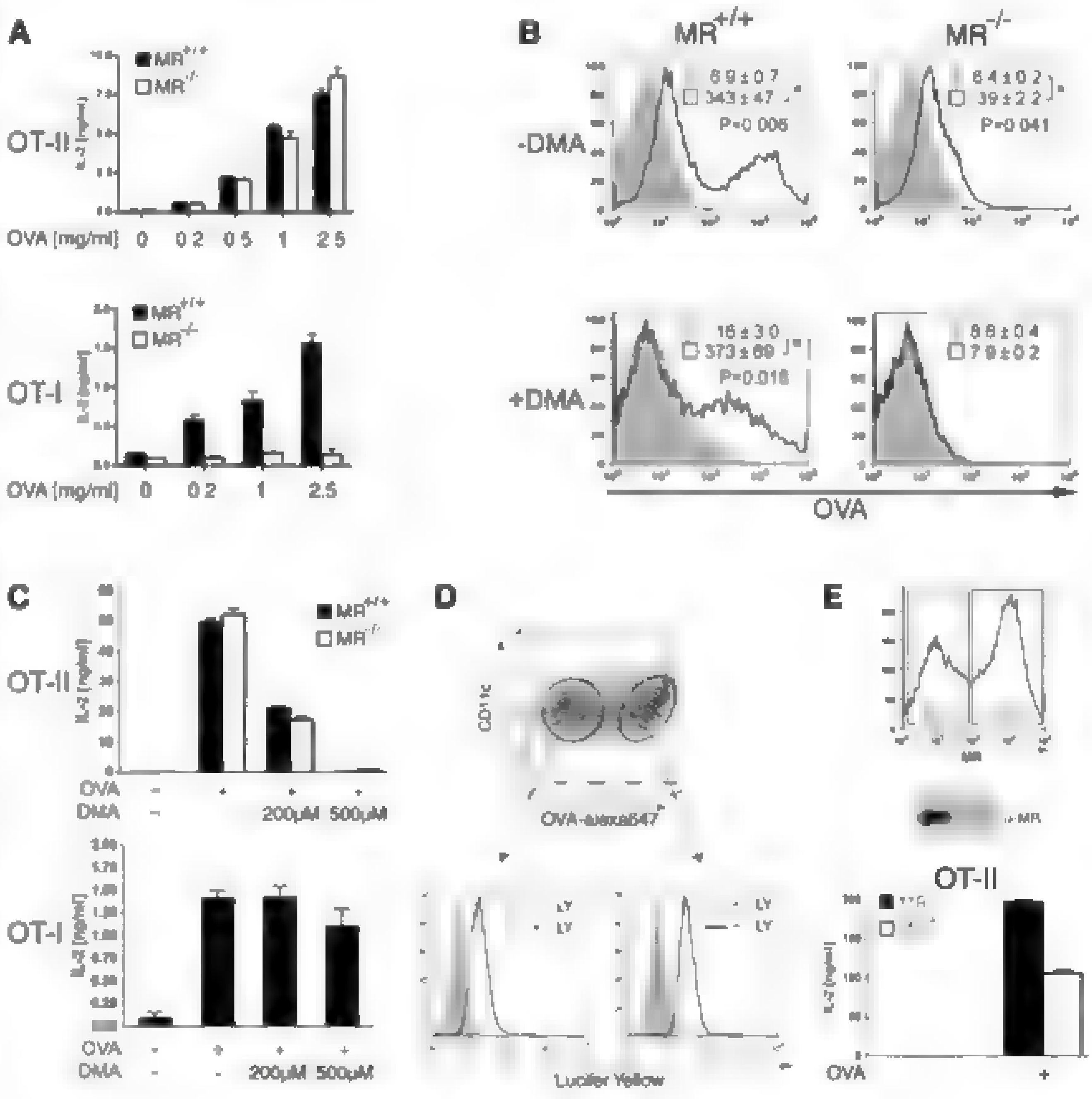

Fig. 1. DCs use only MR-mediated endocytosis to obtain antigen for CD8^{+} T cell activation and pinocytosis for CD4^{+} T cell activation. **(A)** MR-deficient DCs cannot cross-present OVA to OT-I cells, whereas OT-II cell activation is unaffected. IL-2, interleukin-2. **(B)** The MR mediates the uptake of large amounts of OVA by a subpopulation of DCs, resulting in an ~100-fold fluorescence increase. All DCs took up small amounts of OVA by DMA-inhibitable pinocytosis, causing a four- to sixfold fluorescence increase. Gray areas denote DCs cultured without antigen. Mean fluorescence intensity values ± SD are shown. Asterisks refer to given P values. **(C)** Blocking pinocytosis does not alter cross-presentation to OT-I cells, whereas OT-II cell activation is abolished. **(D)** Pinocytosis of LY is unaffected by MR-mediated OVA uptake. **(E)** MR^{-} DCs, obtained by cell sorting, present OVA to OT-II cells more efficiently than MR^{+} DCs. Error bars in (A), (C), and (E) indicate 1 SD.

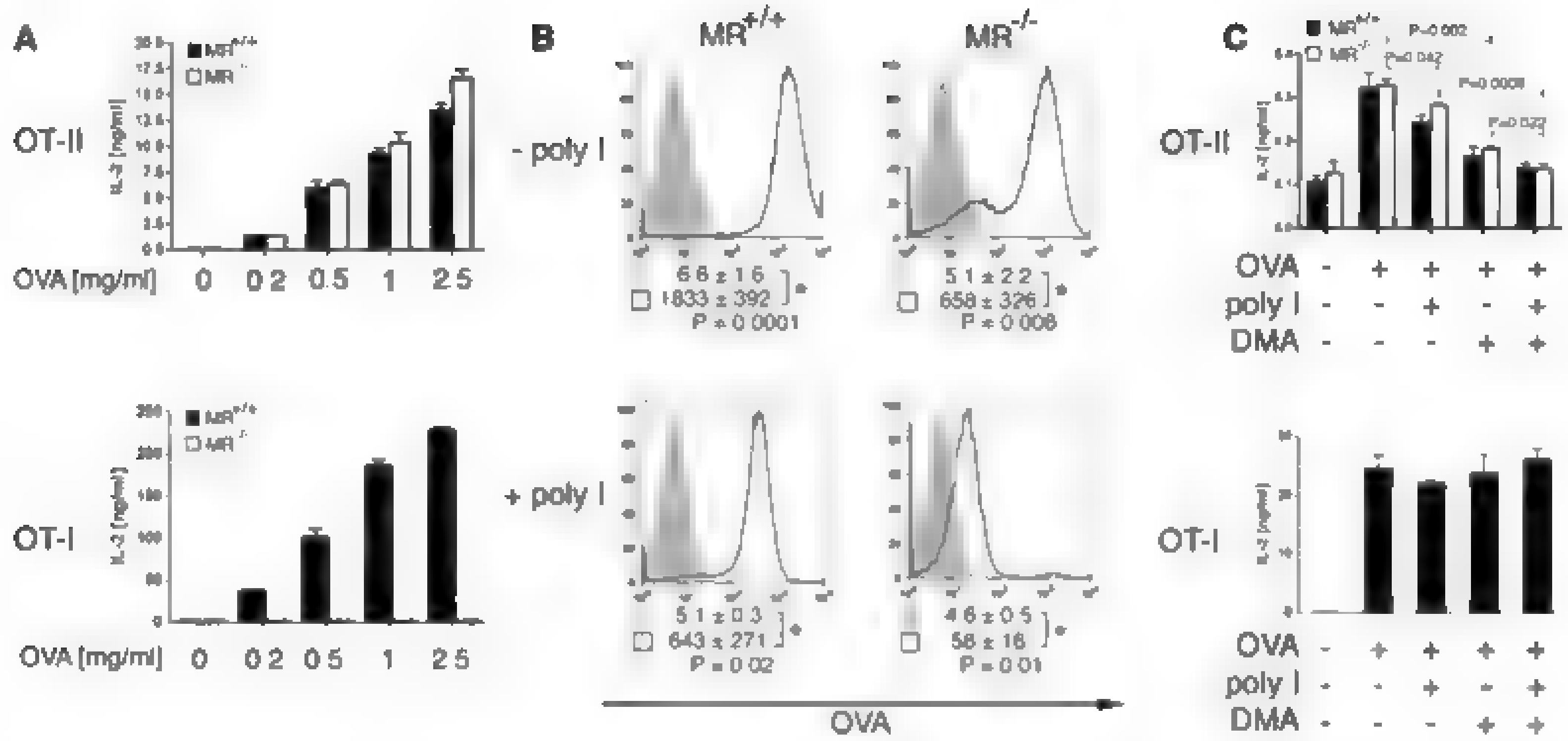

Fig. 2. MΦs use only MR-endocytosed antigen for CD8⁺ T cell activation, whereas pinocytosed and SR-endocytosed antigens were used only for CD4⁺ T cell activation. (**A**) MR-deficient MΦs cannot cross-present OVA to OT-I cells, whereas OT-II cell activation is unaffected. (**B**) Endocytosis via MR and polyI-inhibitable SR is responsible for high-dose OVA uptake by MΦs. Gray areas denote controls without antigen. Mean fluorescence intensity values ± SD are shown. Asterisks refer to given *P* values. (**C**) Simultaneous blockade of the SR with polyI and of pinocytosis with DMA abolishes OT-II cell activation, whereas cross-presentation to OT-I cells is unaffected. Error bars in (A) and (C) indicate 1 SD.

with the 25-D1.16 antibody, flow cytometry revealed a small fluorescence shift (fig. S6), which has been reported to indicate the presence of cross-presented OVA on the cell surface (8). This shift was confined to MR⁺ DCs and MR⁺ MΦs and was absent from APCs lacking the MR (fig. S6). Thus, only those APCs carrying cross-presented OVA in endosomes also displayed it on their cell surface, which is consistent with the observed restriction of OT-I cell activation to these APCs (Figs. 1A and 2A). Quantitative analysis showed that, on a per cell basis, MR⁺ DCs were superior to MΦs in displaying cross-presented OVA on the surface (fig. S6).

These results support a model of antigen presentation, in which the MR introduces OVA specifically into a stable early endosomal compartment for subsequent cross-presentation. Simultaneously, pinocytosis and, in MΦs, SR-mediated endocytosis conveyed OVA to lysosomes for MHC II restricted presentation (Fig. 3D). Our results indicate that mechanisms of antigen uptake can dictate the intracellular destination compartment and thus the presentation of antigen to CD4⁺ or CD8⁺ T cells.

Several possible implications arise from this model. First, receptor dependence of cross-presentation may allow APCs to restrict this pathway to stages of maturation that express suitable receptor(s) or to distinct classes of antigen. Second, receptor dependence may be a complementary mechanism to differences in intracellular processing pathways (27) that restrict cross-presentation to particular APC subpopulations. Consistent with previous reports showing that murine CD8α⁺ DCs had dedicated cross-presenting functions (9, 27, 28, 29), we observed that only CD8α⁺ DCs expressed the MR (fig. S7), suggesting that only these DCs could internalize OVA into endosomes dedicated to cross-presentation. DEC-205 may be a further receptor linked to such endosomes, because antigen targeted to this molecule on CD8α⁺ DCs by means of a specific antibody was cross-presented (27). However, DEC-205 differs from the MR by its ability to also target antigen toward MHC II restricted presentation (27, 24). Consistent with this capability, a major part of DEC-205 internalized antigen has been reported to be localized within lysosomes (24). Future studies may determine whether DEC-205 can target its cargo both to the lysosomal compartment and to the MR⁺ early endosomal compartment described here. Third, the constitutive activity of pinocytosis seen in all DC subsets may ensure that cross-presenting DCs can acquire antigen for induction of cognate CD4⁺ T cell help. Such help requires that the same DC stimulates both specific CD4⁺ and CD8⁺ T cells, which is essential for effective CD8⁺ T cell responses (30, 31). Constitutive pinocytosis avoids situations in which cross-presenting DCs cannot simultaneously stimulate specific CD4⁺ T cells because of a lack of receptors capable of targeting the MHC II presentation pathway. A fourth implication pertains to the cell biology of cross-presentation. Current mechanistic models assume that antigen must be rescued from lysosomal degradation by intracellular diversion toward less acidic compartments (4, 7, 12, 15, 32). Our finding that soluble antigen can already enter the cross-presentation pathway during endocytosis demonstrates that intracellular antigen "crossing" may not be necessary, but this of course does not rule out an additional role of intracellular antigen-sorting mechanisms. Fifth, the Rab5⁺ EEA1⁺ stable early endosomes that we identified as committed to cross-presentation resemble organelles recently described by Lakadamyali *et al.* (33), who proposed that endocytosed cargo was not indiscriminately delivered to a common endosomal pool. Instead, the cargo was introduced either into dynamic, fast-maturing endosomes carrying cargoes toward rapid lysosomal degradation or into Rab5⁺ EEA1⁺ "static" early endosomes, whose biological role in antigen presentation was not addressed in that study. Further studies that characterize the cell biology of a possible early endosomal compartment committed to cross-presentation are required to elucidate their relation to previously described static early endosomes (33). Finally, the lack of intracellular staining for cross-presented OVA after proteasome blockade suggested that antigen had to be exported to the cytoplasmic proteasome for peptide generation, reminiscent of the recently described export of cell-associated antigen from phagosomes and subsequent reimport of peptides for MHC I loading within phagosomes (8, 11, 12). It is possible that similar antigen-relocation mechanisms operate in

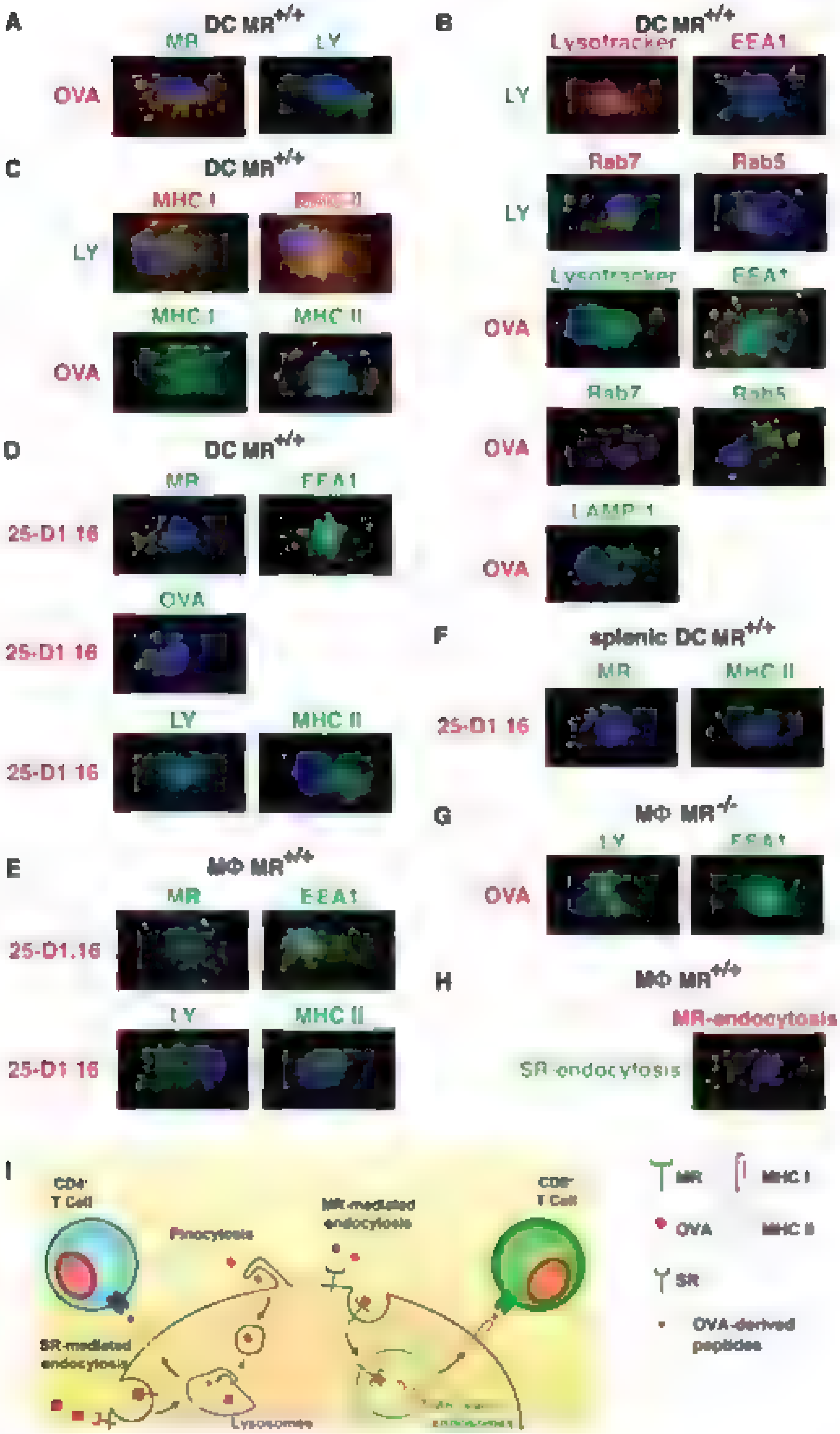

Fig. 3. MR-mediated endocytosis conveys antigen into an endosomal compartment distinct from that supplied by SRs and by pinocytosis. **(A)** Immature DCs were allowed to endocytose OVA_{647} and/or LY for 20 min, were chased for another 20 min, and were fixed and stained for intracellular MR expression or for pinocytosed LY (19). MR-endocytosed OVA is excluded from the organelles that received LY. **(B)** Pinocytosed LY is localized in lysosomes identified by lysotracker but not in organelles expressing EEA1, Rab5, or Rab7. MR-endocytosed OVA is located only in early endosomes containing Rab5 and EEA1 but not Rab7, LAMP 1, or lysotracker. **(C)** Pinocytosed LY colocalizes with MHC II but not with MHC I. MR-endocytosed OVA does not colocalize with MHC II but partially colocalizes with MHC I. **(D)** In DCs, cross-presented OVA, intracellularly revealed by the 25-D1.16 antibody, was located exclusively in MR^+ $EEA1^+$ endosomes but colocalized neither with MHC II nor with pinocytosed LY. Cross-presented OVA partially colocalized with unprocessed OVA. **(E)** In MΦs, cross-presented OVA was also found only in MR^+ $EEA1^+$ endosomes but not in MHC II^+ lysosomes. **(F)** Cross-presented OVA is confined to MR^+ endosomes also in $CD11c^+$ splenic DCs that had been isolated ex vivo. **(G)** MR-deficient MΦs internalized high-dose OVA, which was not delivered into $EEA1^+$ endosomes but instead colocalized with pinocytosed LY. **(H)** Visualization of simultaneous uptake of SR and MR-endocytosed antigen into separate compartments of the same MΦ (19). Cell nuclei were revealed with 4′,6-diamidino-2-phenylindole staining in blue. Lysotracker staining was performed with unfixed cells, and nuclei of unfixed cells were visualized with Hoechst 33342 dye. Separate channel images and controls are available in figs. S1 and S3. Statistical analysis is provided in table S1. **(I)** Proposed model of antigen uptake, routing, and presentation.

the stable early endosomes committed to cross-presentation of soluble antigen. It is to be emphasized, however, that cross-presentation of cell-associated antigen mechanistically differs from that of soluble antigen (8, 10, 12, 17). If this [illegible] uptake mechanism via stable early endosomes in classical cross-priming (3) remains to be shown. We suggest that targeting antigen to the MR may represent an effective [illegible] CDs [illegible] against viruses or tumors.

References and Notes

1. Mellman, R. M. Steinman, Cell 106, 255 (2001).
2. E. S. Trombetta, M. Ebersold, W. Garrett, M. Pypaert, I. Mellman, Science 299, 1400 (2003).
3. M. J. Bevan, J. Exp. Med. 143, 1283 (1976).
4. C. C. Norbury et al., Science 304, 1318 (2004).
5. C. Kurts et al., J. Exp. Med. 184, 923 (1996).
6. A. Y. Huang et al., Science 264, 961 (1994).
7. W. R. Heath, F. R. Carbone, Nat. Rev. Immunol. 1, 126 (2001).
8. A. L. Ackerman, A. Giodini, P. Cresswell, Immunity 25, 607 (2006).
9. J. M. den Haan, S. M. Lehar, M. J. Bevan, J. Exp. Med. 192, 1685 (2000).

Tissue Homogenizer

The benchtop Precellys 24 is dedicated to the grinding, lysis, and homogenization of biological samples. It can handle difficult samples such as microorganisms and bacteria spores, hard tissues such as teeth, bone, kidney, muscle, and hair, soil samples, plants, and more. It can load up to 24 tubes simultaneously. Protocols are flexible and easy to set. Buffer and samples are added in 2-ml tubes pre-filled with specific beads, either glass, ceramic, or metal. The single-use tubes prevent cross-contamination. The high speed and specific motion guarantee homogeneous and efficient grinding for reproducible, high-quality results.

Bertin Technologies For information +331 39 30 61 69 www.bertin.fr

Liquid Chromatography Literature

A new CD contains a large collection of liquid chromatography (LC) application notes in a concise template for ease of searching and reference. It includes more than 230 one-page application notes and alphabetically catalogs information regarding more than 500 compounds. The CD also includes the PerkinElmer consumables catalog.

PerkinElmer For information 412-456-0986 www.perkinelmer.com/LCseparations

High-Throughput Dynamic Light Scattering

The new High Throughput Dynamic Light Scattering (HTDLS) instrument combines the benefits of Viscotek's patented single mode fiber technology and an entirely new three-axis, automated platform. The HTDLS delivers high sensitivity, and features a wide range of temperature control and low sample volume. The HTDLS cuts measuring times to about a minute per sample.

Viscotek For information +44 1344 467 180 www.viscotek.com

Solid Phase Extraction System

The Microlute Solid Phase Extraction (SPE) system for analysis of pharmaceutical compounds in biological fluids can be used for analyzing compounds ranging in chemical nature from highly lipophilic steroids to water-soluble nucleoside analogues. The individual well capacity of the low-sorbent mass phases used in the Microlute are sufficient for robust and reproducible analysis of drug metabolites in the low ng/ml concentration region typically found in biological fluids. The instrument offers automated, high-throughput SPE sample preparation in a convenient microplate format capable of rapidly processing 96 samples. Constructed from a single piece of molded plastic, the Microlute will not bend or distort because individual SPE cartridges do not have to be repeatedly plugged in and out. Featuring a proprietary sorbent slurry loading technique, the instrument eliminates the channeling effects that often limit the performance of dry powder-loaded SPE columns. Each well on the Microlute has an individual drain spout, ensuring 100% sample transfer and no crossover contamination.

Porvair Sciences For information +44 1932 240255 www.porvair-sciences.com

MAPK Cell Signaling Antibodies

A number of antibodies are available to study the mitogen activated protein kinase (MAPK) cell signaling pathway. Anti-ACTIVE MAPK and Anti-ACTIVE JNK antibodies are designed specifically to detect the active, dually phosphorylated forms of MAPK (ERK1 and ERK2) and JNK, respectively. Anti-ERK1/2 pAb, Rabbit, is an antibody that recognizes both the phosphorylated and non-phosphorylated forms of ERK1 and ERK2. Anti-pT^{183} MAPK pAb recognizes phosphorylated ERK1/2 at the threonine residue in the TEY motif present in the catalytic core of ERK1 and ERK2.

Promega For information 800-356-9526 www.promega.com

Peroxidase Substrate

The ImmPACT DAB is based on a new formula for diaminobenzidine (DAB)-based peroxidase substrate. Its enhanced sensitivity generates a darker, crisper, brown precipitate than conventional DAB substrates. It is suitable for immunohistochemical staining and membrane-based blot detection with any horseradish peroxidase-based detection reagents. The ImmPACT DAB reaction product is resistant to ethanol and organic solvents, enabling dehydration and permanent mounting of stained preparations. The sharp color deposit on on tissue sections allows for excellent contrast with traditional counterstains like hematoxylin or in combination with other enzyme substrates for multiple antigen labeling.

Vector Laboratories For information 650-697-3600 www.vectorlabs.com

Cytochrome *c* Release Kit

The InnoCyte Flow Cytometric Cytochrome *c* Release Kit relies on selective permeabilization of the cellular membrane to release cytosolic components, while leaving the mitochondrial membrane intact. Cells are fixed and can be used for multi-parameter analysis of apoptotic cells or stored for future analysis. Cytochrome *c* is detected with a specific monoclonal antibody and a secondary antibody labeled with fluorescein isothiocyanate (FITC), either by flow cytometry or fluorescent microscopy. Other fluorescent-labeled antibodies can be substituted for the FITC-labeled secondary antibody, offering the flexibility of multi-parameter analysis. Viable cells stain cytochrome *c*, but cells committed to the apoptotic process release cytochrome *c* from the mitochondria to the cytosol and do not stain. Unlike traditional cellular fractionation protocols, this assay is amenable to high-throughput screening and useful for analysis of scarce samples.

EMD – Calbiochem For information 800-854-3417 www.calbiochem.com

Newly offered instrumentation, apparatus, and laboratory materials of interest to researchers in all disciplines in academic, industrial, and government organizations are featured in this space. Emphasis is given to purpose, chief characteristics, and availability of products and materials. Endorsement by Science or AAAS of any products or materials mentioned is not implied. Additional information may be obtained from the manufacturer or supplier.

POSITIONS OPEN

ASSISTANT CURATOR
The Field Museum, Department of Geology
Chicago, Illinois

The Field Museum's Department of Geology seeks a broadly interested, productive colleague with an innovative specimen-based research program in invertebrate paleontology. Special areas of interest include systematics, phylogenetics, morphology, evolution, biogeography, biostratigraphy and faunistics, and paleoecology. The successful candidate will have a Ph.D., a significant record of scientific achievement, and is expected to build a strong research program with a field component. The position entails the curation of a major fossil invertebrate collection. Curators participate in a wide range of public learning programs including exhibits, mentoring, and informal [illegible] and service activities. Participation in undergraduate and graduate education at area universities is also strongly encouraged.

The search is targeted at the Assistant Curator level, but candidates at a higher level may be considered. Please [illegible] statement of research objectives, and copies of relevant publications. Direct applications to, and arrange for three letters of reference to be sent to:

Search Committee, Department of Geology
The Field Museum
1400 South Lake Shore Drive
Chicago, IL 60605-2496

Please ensure that all of the listed items except copies of publications are also sent as e-mail attachments, such as PDFs or Word documents (the preferred application is Microsoft Word, although WordPerfect is also acceptable). E-mail address for this search is e-mail: klawson@fieldmuseum.org.

Deadline for applications is September 1, 2007. Consideration of applications will begin September 25, 2007.

MULTIPLE FACULTY POSITIONS IMMUNOLOGY, BACTERIAL, and VIRAL PATHOGENESIS
Indiana University School of Medicine
Department of Microbiology and Immunology
Website: http://www.iupui.edu/~micro/

The Department of Microbiology and Immunology is seeking outstanding candidates with a Ph.D. or M.D./Ph.D. degree for faculty positions in the areas of cellular and molecular mechanisms of immunology, and/or bacterial or viral pathogenesis. Academic credentials and experience will determine faculty rank.

NIH Research Project Grant Program or equivalent external peer-reviewed funding is required, as is peer-reviewed publications in high-ranking journals. The faculty member will be expected to pursue independent programs in original basic research, continue to secure external grant support, and participate in teaching graduate and medical students.

A competitive startup package is available including new laboratory space. The environment is highly interactive and productive with close ties on campus to other basic science and clinical departments, and research centers.

Interested candidates should send their curriculum vitae, description of research goals and names, addresses, phone, fax numbers, and e-mail addresses of at least three references to:

Hal E. Broxmeyer, Ph.D.
Chairman and Professor
Department of Microbiology and Immunology
Scientific Director, The Walther Oncology Center
Indiana University School of Medicine
635 North Barnhill Drive, Room 420
Indianapolis, IN 46202-5120 U.S.A.

Indiana University is an Affirmative Action, Equal Opportunity Employer. Minorities, females, persons with disabilities

POSITIONS OPEN

School of Pharmacy
TEMPLE UNIVERSITY

TEMPLE UNIVERSITY SCHOOL of PHARMACY
Assistant/Associate/Full Professor of Pharmaceutics

Temple University School of Pharmacy is seeking pharmaceutics specialists for tenure track faculty positions in the Department of Pharmaceutical Sciences. Qualified applicants (recent Ph.D., postdoctoral, or experienced academic or industrial pharmaceutics specialists), who could maintain an independent research [illegible] professional and graduate students, are encouraged to apply. Temple [illegible] research opportunities located in the heart of the pharmaceutical industry.

Applications will be reviewed immediately and continue until the positions are filled. Mail a letter of intent, curriculum vitae, and the contact information for three references by regular mail or e-mail to: Robert B. Raffa, Ph.D., Chair, Search Committee, Temple University School of Pharmacy, 3307 North Broad Street, Philadelphia, PA 19140. E-mail: robert.raffa@temple.edu.

Temple University is an Equal Opportunity, Affirmative Action, ADA Employer.

Board of Governors' Gene Therapeutics Research Institute, Cedars-Sinai Medical Center, and Department of Molecular and Medical Pharmacology, University of California at Los Angeles. A **POSTDOCTORAL POSITION** is available in the Gene Therapeutics Research Institute and the Department of Molecular and Medical Pharmacology, University of California at Los Angeles, to study the molecular and cellular mechanisms involved in brain immune responses and the formation and function of immunological synapses in vivo. (See *Journal of Experimental Medicine* 203: 2095-107, 2006, *Cancer Res.* 65: 7194-7204, 2005, *Nat. Biotechnol.* 19: 582-5, 2001, *Proc. Natl. Acad. Sci. USA* 97: 7482-7, 2000, *Nat. Med.* 5: 1256-63, 1999). A strong background in immunology, cell biology, virology, neuro[illegible] is essential. Please visit [illegible] information, websites: **http://www.cedars-sinai.edu/3255.html** or **http://www.uclaaccess.ucla.edu/UCLAACCESS/Web/Faculty.asp?id=10016**.

Our Institute is located at the Cedars-Sinai Medical Center campus and offers state-of-the-art facilities in an exciting environment for postdoctoral research. A strong background in molecular, cellular [illegible] required. Interested candidates should have a Ph.D. and/or an M.D. and have under five years of postdoctoral experience. Salary is dependent on education and research experience, with a range of $36,000 to $45,000. Please submit a cover letter, curriculum vitae including bibliography, and contact information for three references to: **Pedro R. Lowenstein, M.D., Ph.D., or Maria G. Castro, Ph.D., Cedars-Sinai Medical Center, 8700 Beverly Boulevard, Davis Building, Room: R5090, Los Angeles, CA 90048. E-mail: lowensteinp@cshs.org or e-mail: castromg@cshs.org.**

Two **POSTDOCTORAL POSITIONS** available immediately in the Department of Pharmacology, Toxicology, and Therapeutics under the direction of **Dr. B.T. Zhu, Professor (website: http://www.kumc.edu/pharmacology)**, to study DNA methylation and estrogen's actions. Hardworking, self-motivated applicants with experience in biochemistry, molecular biology, and/or immunology must apply online only at website: **http://jobs.kumc.edu** and search for positions J0084255 and J0084256. Applicants should provide curriculum vitae and the names of three references. *The University of Kansas Medical Center (KUMC) is proud to be an Equal Opportunity, Affirmative Action Employer. Paid for by KUMC.*

THE RIGHT FIT

For scientists considering careers in the life science industry, the choice between biotech and pharma has sometimes been a difficult one. However, as both industries change, the question may be moot. **By Gunjan Sinha**

To work in biotech or pharma? For newly minted Ph.D.s as well as postdocs considering jobs in industry, that frequently may be the question. The answer, however, may be that it does not matter. Pharmaceutical companies are increasingly acquiring biotech companies to broaden their portfolios, and some biotech companies have grown so diverse that they resemble pharmaceutical companies. "The line between biotech and pharma has been blurring for years," says **Thomas Boehm**, director of clinical development at Jerini, a biopharmaceutical company in Berlin, Germany.

As little as 15 years ago, the two industries were clearly distinct. Pharmaceutical companies generally focused on developing small molecule drugs. They were large, structured environments that supported the bulk of research and development via sales and private or public investment. By contrast, biotechnology companies focused on biological drugs—those made from human or animal proteins, or created recombinantly. They offered tight-knit and relatively unstructured work environments and supported their research through venture capital funding, government seed money, or private and/or public investment.

The disparate industries made for distinct work environments. Pharma promised predictability, stable incomes, and defined roles. Biotechnology companies offered volatility, unpredictability, and the opportunity or necessity, depending on one's point of view, to muddy one's hands with all aspects of the business.

But while the general distinction between the two industries still exists, a company's size and management style are better predictors of the type of work environment a scientist is likely to encounter as both industries continue to evolve, say experts. For Ph.D.s weighing a decision to work in one field over another, individual company qualities and personality are important characteristics to consider when deciding which job would provide the best fit.

Stories from the Industry

Jean Yves Bonnefoy certainly experienced a nonstereotypical environment during his decade working for Glaxo in Geneva during the '90s. Bonnefoy was hired as a research scientist in immunology. But he was always interested in other aspects of drug development. The company took notice and offered to send him to the London School of Business to attend a senior management program.

"I took the opportunity and it's been very useful," Bonnefoy says. "Not turning research into something that was useful for patients was unacceptable to me. To achieve that, you need to understand more than just basic research."

Today Bonnefoy is vice president of research and development at Transgene, a biotechnology company based in Strasbourg, France, that is focusing on immunotherapy to treat cancer and infectious disease. The company has four products in clinical development to treat small-cell lung cancer, cervical intraneoplasia, B-cell lymphoma, and hepatitis C.

His job is largely managerial, but that doesn't mean paper pushing. "It's a lot of management coordination to make the company as efficient as possible," Bonnefoy explains. "I really like the proximity between research and development, especially in this field [immunotherapy]. There are no marketed products yet, but there's a huge need."

Of his experience at Glaxo, Bonnefoy says he was lucky. At the time the company had acquired biotech company Biogen's Geneva-based facility. Glaxo's Geneva research center was small and the addition of Biogen employees contributed to a laid-back culture. The company not only trained him in business management, but also in project

“The line between biotech and pharma has been blurring for years.”

UPCOMING FEATURES

Focus on Diversity — May 11

Regional Focus: NC/Research Triangle — June 8

International Careers Report: UK and Ireland — June 22

Careers in Biotech and Pharma

"It's a lot of management coordination to make the company as efficient as possible."

—Jean Yves Bonnefoy

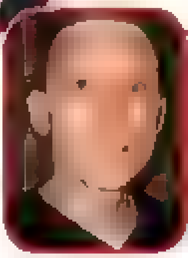

Andrew Garner

and staff management. In his role as researcher, he developed a potential drug to treat different types of immune diseases and was able to accompany the molecule through the next stages — something most scientists at pharmaceutical companies are not able to do. However, "Someone's experience at another pharma company might be completely different," he adds.

Indeed, **Andrew Garner's** experience in big pharma is closer to the norm. Garner has worked at AstraZeneca in Alderley Park, UK, for six years where he presently leads a team of eight people responsible for finding compounds that target cancer. After the team establishes that a compound is effective against a particular target, they pass the project on to other teams. But even though he is limited to early drug research, Garner is satisfied. "I like working on the early stages such as figuring out what a drug should look like," he says.

Pharma Changes Face

As the industry is changing, so too is the tendency to compartmentalize tasks. In recent years the flow of drugs hitting the market has slowed to a trickle and the pipeline of compounds in development has narrowed. In response, companies are restructuring their R&D. Pfizer, for example, recently announced plans to cut 10,000 jobs over two years, many in management and marketing.

Those moves represent a shift by Pfizer toward a more specialized approach to drug discovery and follow another trend in the industry: streamlining R&D by focusing on specific disease areas — a strategy biotechs already employ albeit on a smaller scale. Oncology, immunology, and neurodegenerative diseases top the list at most companies as these are areas in which very few effective drugs already exist. This has meant internal restructuring to place scientists with varied backgrounds into small groups to promote interdisciplinary collaboration and spur innovative ideas.

"The research is evolving in that direction," says **Ginger Gregory**, global head of human resources for Novartis Institutes for BioMedical Research. Diseases were not usually studied as related disorders. But as science has revealed the links between cancer and the immune system, for example, or heart disease and diabetes, industry has needed to respond. "Traditionally you would have silos of thinking," Gregory adds. "But those days are over."

Another force drawing the two industries closer is the growing number of pharmaceutical companies acquiring biotechs to broaden their portfolios to include biological drugs. In 2006, AstraZeneca bought Cambridge Antibody Technology Group. The move followed the company's acquisition of another biotech, KuDOS Pharmaceuticals, in 2005 and several agreements with small biotechs to co-develop drugs. The company expects that by 2010 up to a quarter of drug candidates will be biological therapeutic agents, said AstraZeneca's chief executive officer David Brennan in a statement. In 2006, Merck also bought two small biotech firms with which it had been partnering, GlycoFi of Lebanon, New Hampshire, and Abmaxis of Santa Clara, California.

Some companies are even restructuring to include internal research on biological drugs. Schering-Plough, for example, merged two of its California research facilities in 2005 to create a new unit in Palo Alto that focuses on monoclonal antibodies and other therapeutic proteins.

Biotechs Still More Dynamic

Despite pharma's revamp, biotech companies generally remain more dynamic work environments because of their relatively small size, says **Indu Parikh**, president of BioMarck Pharmaceuticals, a biotech in Durham, North Carolina.

Parikh, a 30-year veteran of the pharmaceutical industry, co-founded a biotech company in 1991 simply because he craved a change of pace. "It was a pioneer experience," Parikh says. "We started from the ground up and after five years had hired 450 people." It wasn't easy nor was it stress-free. He recalls days when he would don work overalls to mop and clean glassware and then later switch into a tie and suit to meet potential investors.

"In some respects, working in a small biotech is like climbing a steep ladder. It's difficult to climb and there are a lot of places you might fall down," Parikh says. "By contrast, in a large company environment that ladder wouldn't be so steep,... but you might prefer the excitement of climbing the steeper ladder."

But biotech doesn't necessarily offer the freewheeling environment that people assume. "Suppose a scientist at a biotech wants to study a drug's mechanism of action," Parikh explains. "The company may not allow him to do that because it isn't in line with their goals." By contrast, a pharmaceutical company with more funds and a bigger staff may allow it.

Boehm agrees. "People have the impression that biotechs only do cutting-edge research. But I'm not sure we can take more risks than pharma. If our late-stage clinical development fails, we are in trouble. If a pharma company drug fails in the clinic, it's one project out of many." So both industries tend to take a similarly cautious approach to risk.

People who work in biotech, however, do tend to be more adventurous by nature. That's because the continued »

Astrazeneca
www.astrazeneca.com

BioMarck
www.biomarck.com

Genentech
www.gene.com

Jerini AG
www.jerini.com

Merck
www.merck.com

Novartis
www.novartis.com

Transgene SA
www.transgene.fr

CREDITS (TOP TO BOTTOM): BENOIT HELLER; FIONA GRIGLER

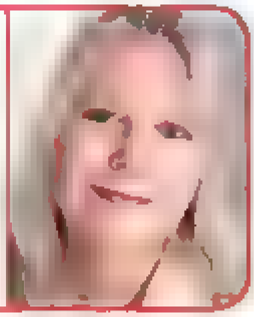

"Each scientist is part of a development team that follows the drug along the pathway."
– Holly Butler

[illegible] industry may self select for risk takers, says Boehm. A biotech's finances are precarious. Venture capital funding rarely extends beyond five years. Meanwhile, a drug takes 10 to 15 years to develop. Employees know that the company can quickly go bust. So a person who has a family and debts may be more likely to seek out a stable job.

That might explain Boehm's decision to stick to biotech over the past decade. The pace and the environment of biotechnology simply suited his personality, he says. "Pharma has many layers of management," he explains. "There's usually a long decision-making process and things can take too long to get done." By contrast, most biotechs are bare bones operations. "Here people just jump in and learn as they go along." That carries some disadvantages, he admits, because people make mistakes, which makes the process inefficient. Nevertheless, he prefers learning by doing.

Other Models

Still other companies have evolved a culture of their own. San Francisco-based Genentech, for example, started out as a small biotech in 1976. The company has since grown to 10,500 employees. Despite its size, "We still consider ourselves a biotech company," says **Holly Butler**, principal staffing consultant for research. That's because the company maintains a flat management style. Butler likens the work environment to academia. Scientists work in interdisciplinary teams and participate in drug research from start to finish.

"So if you imagine drug development as a biochemical pathway, each scientist is part of a development team that follows the drug along the pathway," she explains. A basic scientist is expected to participate in his or her drug's development from start to finish. Genentech also allows its scientists discretionary research time to pursue science that may not be related to the company's goals. Avastin, a drug to treat colorectal cancer, for example, grew out of a scientist's discretionary research that was only peripherally related to the main project.

Companies Are Hiring

Like other companies interviewed for this article, Genentech is hiring. But finding talent is easier said than done. "Baby boomers are retiring, the government has placed a cap on H1-B visas [for foreign researchers], and there has been a surge in biotechs. The demands have increased but the supply hasn't, so our pool of top talent is very limited," says **Chris Hong**, senior director of recruiting and staffing for Merck. And everyone is looking for similar characteristics.

Merck is, however, aggressively hiring, says Hong. Many of the new hires are to support research in areas on which the company has chosen to focus its R&D such as metabolic disorders and infectious disease. But the limited pool from which to choose has prompted some companies to shift their strategy. Instead of drawing people to them, some have opted to move nearer to the talent.

Novartis, the giant Swiss drug maker, made waves in the pharmaceutical industry three years ago when it relocated its global research headquarters to Cambridge, Massachusetts. Novartis's chief executive Daniel Vasella made the decision after company executives analyzed potential places to expand, and concluded "that the single most important factor was access to talent."

Novartis currently employs over 1,200 people in Cambridge and plans to continue expanding albeit only in specific areas such as biologic drugs like monoclonal antibodies and RNA interference molecules.

Last year both Amgen and Schering-Plough also announced plans to expand R&D operations in Cambridge. Amgen plans to increase its total staff of scientists to 400 and Schering-Plough expects to bump up scientific staff from 80 to about 200 people.

The pharmaceutical giant AstraZeneca, which already runs one of the largest drug company labs in Massachusetts, plans to expand its Waltham complex and add up to 100 jobs.

Genentech, on the other hand, has an easier time finding qualified people. This year, the company topped the charts of Fortune magazine's "100 best companies to work for." Genentech has also consistently ranked at the top in AAAS's annual survey of scientists. "We're lucky, people come to us," says Butler. The company does, however, actively recruit by attending conferences and other events where recruiters are likely to meet scientists. "We are looking for the best," she adds, "and the word 'settle' is just not in our vocabulary."

Other companies employ similar tactics but also advertise and use external recruiting agencies. But very often, potential employees are recommended by existing ones, say recruiters.

A search on company websites shows open positions for chemists, immunologists, oncologists — positions across a range of disciplines. One difficult niche to fill is people who have experience in animal research and who also have an M.D. Ph.D., says Hong. There is also considerable competition for experienced chemists, Novartis's Gregory adds.

Academic pedigree aside, companies also look for team players who have an ability to think innovatively and flexibly. AstraZeneca, in fact, puts candidates through exercises to judge their ability to work in a team. Integrity and self discipline are also important traits, says Butler.

"We really want people who want to make an impact," says Gregory. "We want basic researchers who also think about patients and curing disease. We don't want somebody who likes doing the same thing over and over again. We don't like complacency."

Biotech recruiters largely echoed those criteria. Consequently, a job in biotech or pharma may offer similar benefits and costs. And as Bonnefoy and Parikh demonstrate, anyone who is dissatisfied can always change jobs.

Gunjan Sinha is a freelance writer living in Berlin, Germany.

Innovation is in our genes.

you & i – your experience, Illumina's resources. Illumina develops high quality, easy-to-use tools for large scale analysis of genetic function that will lead to curing and ultimately preventing disease. We pursue this mission with a focused intensity that actively engages all stakeholders – employees, customers and the scientific community as well as physicians, investors and others who strive to improve human health. We call this diverse, driven team The Illumina Community.

Illuminating the possibilities.

Illumina's collaborative approach to developing next-generation genetic analysis solutions is an ever-evolving cycle of listening to all stakeholders, anticipating their needs, and then innovating accordingly. It's the essence of discovery through teamwork, of breakthroughs achieved through partnerships built across a broad spectrum of determined individuals.

We invite you to join The Illumina Community. As part of this extraordinary team, you'll enjoy highly challenging work that will have a truly global impact.

you & i. Let's find the answers together.

www.illumina.com/JoinUs

Ideas come naturally to us.

9885 TOWNE CENTRE DRIVE
SAN [illegible]
FAX 858 [illegible] 4895

illumina

COLUMBIA UNIVERSITY
RESEARCH SCIENTIST

The Center for Holistic [illegible] in the Department of [illegible] at Columbia University Medical Center is seeking a PhD Research Scientist to direct the basic scientific research efforts of the Center. The goal of the Center is to study herbal/natural product preparations for use as integrative therapies for urologic cancers and to [illegible] their molecular mechanisms of action. Promising agents are then tested for safety and efficacy through IRB approved patient based trials in conjunction with the Center's Director, Dr. Aaron Katz.

This research involves the use of both in vitro and animal model systems to study the ability of potential therapeutic agents to halt the growth and/or kill human cancer. Primary interests include the use of herbals/natural products as chemopreventive agents in high risk patients, in the prevention of tumor recurrence following surgery and in combination with standard [illegible] regimens to either reduce toxicity and/or increase efficacy of these therapies.

Additional responsibilities include writing grant proposals, generating project proposals for submission to [illegible] and giving presentations at conferences and meetings.

PhD in molecular biology or related field with 2-4 years of postdoctoral training experience preferred.

Interested applicants should send their complete curriculum vitae, brief summary of their research history and plans and the names of three references to:

Dr. Aaron Katz
Associate Professor
Columbia University Department of Urology
Herbert Irving Pavilion
161 Fort Washington Avenue, 11th floor
New York, NY 10032

We are an affirmative action/equal opportunity employer.

MGH 1811

Massachusetts General Hospital
Harvard Medical School

Faculty Position in Brain Tumor Research

The Massachusetts General Hospital and Harvard Medical School are seeking applications at the level of Assistant or Associate Professor to [illegible] research program in the biology of gliomas. [illegible] growth [illegible] will be considered. The appropriate candidate should have a Ph.D. or M.D. degree or both [illegible] Harvard Medical School [illegible]. The candidate should be [illegible] with demonstrated research excellence, publications [illegible] and peer-reviewed grant support. The [illegible] should be [illegible] a better understanding of the biology of gliomas and their therapy.

This opportunity includes generous start-up funds and laboratory space in the [illegible] Research Center [illegible]. The position features [illegible] Massachusetts General Hospital. [illegible] brain tumor program at Harvard Medical School supported by multiple NIH grants and the opportunity to supervise research fellows supported by an NCI-sponsored training grant in neuro-oncology. Applications from women and representatives of minority groups are encouraged. Interested candidates should forward a curriculum vitae, a brief statement of research interests and 3 letters of recommendation to: **Valerie J. Smith, Stephen E. and Catherine Pappas Center for Neuro-Oncology, Yawkey 9E, Massachusetts General Hospital, 55 Fruit Street, Boston, MA 02114-2696; vjsmith@partners.org**

The Massachusetts General Hospital is an Equal Opportunity Employer.

Tenure-Track Faculty Positions
University of Pittsburgh
School of Medicine
Structural Biology Department

The Department of Structural Biology at the University of Pittsburgh School of Medicine is conducting a search for creative individuals who [illegible]. We are [illegible] candidates [illegible] X-ray crystallography, [illegible] solid state NMR [illegible] techniques. Current [illegible] Department are **James Conway** [illegible], **Angela Gronenborn** [illegible] NMR), **Rieko Ishima** [illegible] and NMR [illegible], **Judith Klein-Seetharaman** [illegible], **Ron Wetzel** [illegible], **Joanne Yeh** [illegible] X-ray [illegible] and **Peijun Zhang** [illegible]. The Department of Structural Biology is housed in a new [illegible] outstanding equipment for NMR spectroscopy, X-ray crystallography, [illegible] and mass spectrometry.

The University of Pittsburgh is the seventh most highly ranked domestic [illegible] NIH [illegible] and offers a very wide spectrum of [illegible] opportunities. Applications [illegible] and highly competitive salaries and start-up packages will be offered. Applicants should hold PhD and/or MD or equivalent degrees and have demonstrable expertise and scholarly achievement in structural biology or biophysics. Applications [illegible] including the candidate's [illegible] a statement of research interests as well as names and contact information of three references and should be sent to: **Angela M. Gronenborn, Ph.D. c/o Janet Zambotti, Rosalind Franklin Professor and Chair, Department of Structural Biology, University of Pittsburgh School of Medicine, 3501 Fifth Avenue, 1051 BST3, Pittsburgh, PA 15260, or jobs@structbio.pitt.edu.**

The University of Pittsburgh is an Affirmative Action, Equal Opportunity Employer.

NIDDK Tenure-Track Position in Clinical Research in Diabetes and Kidney Disease

We seek an outstanding scientist to direct a rigorous, innovative clinical research program in the epidemiology, physiology, and treatment of type 2 diabetes, diabetic nephropathy, and related disorders. Applicants must be highly motivated and have a demonstrated track record through publications that address significant issues of causation, prevention, and treatment of these conditions. Applicants must also be licensed to practice medicine in [illegible] of the United States and have substantial experience in community relations, recruitment, and clinical research among U.S. minority groups. The successful candidate is expected to develop an independent, world-class research program complementary to current investigations within the Phoenix Epidemiology and Clinical Research Branch (PECRB). The position comes with generous start-up funds and ongoing support.

The PECRB, NIDDK, is located in Phoenix, Arizona. The Branch represents interests similar in range to those of an academic department. There are extensive interactions among the independent research groups and the provision of expansive, collaborative opportunities for multidisciplinary collaboration within NIDDK and throughout NIH. Applicants should submit a current curriculum vitae, bibliography, copies of three major publications, a summary of research accomplishments, a brief statement of future research goals, and arrange for three letters of reference to be sent to:

Dr. James Balow, Chair, Search Committee, c/o Glynnis Vance, NIDDK, 9000 Rockville Pike, Bldg. 10-CRC/Rm. 5-2551, National Institutes of Health, Bethesda, MD 20892

Application Deadline: June 8, 2007

This position is subject to a background investigation.

Principal Investigator
PET Radiochemistry Laboratory-NIBIB

The Intramural Research Program of the National Institute of Biomedical Imaging and Bioengineering (NIBIB) is seeking a tenured or tenure-track scientist to lead the Positron Emission Tomography (PET) Radiochemistry Laboratory located on the Bethesda campus of NIH. The laboratory currently consists of three experienced staff radiochemists as well as technicians and postdoctoral fellows. Dedicated space includes a fully equipped PET radiochemistry laboratory with direct access to three cyclotrons and a new PET/CT animal imaging facility as well as space for expansion of lab space. We seek an individual who will provide scientific leadership for cutting-edge, high-impact PET research programs with an emphasis on the chemistry. [illegible] radiosynthesis, microfluidics, PET instrumentation or image processing. A competitive research package and abundant collaborative opportunities exist throughout the NIH campus, including interactions with numerous investigators, unique animal models, and access to human and large animal PET imaging studies.

The applicant should hold a Ph.D., M.D., or equivalent degree. Interested individuals should submit their complete CV and cover letter along with a brief outline of potential research plans along with 3 letters of recommendation to **Ms. Patty Runyon, 6707 Democracy Boulevard, Suite 202, Bethesda, Maryland 20814**. The closing date for this position will be **June 30, 2007**.

Standards of Conduct/Financial Disclosure: All employees of the Federal Government are subject to conflict of interest and regulations, including the Standards of Ethical Conduct, that govern activities with outside organizations and reporting financial holdings. Before entering on duty you will be required to complete a confidential Financial Disclosure Report (OGE-450). You will need to provide this information annually. Applicants are encouraged to review the NIH Ethics Program website http://ethics.od.nih.gov.

NIH is an Equal Opportunity Employer. Selection for this position will be based solely on merit, without discrimination for non-merit reasons such as race, color, religion, sex, national origin, politics, marital status, sexual orientation, physical or mental disability, age, or membership or non-membership in an employee organization.

The National Institutes of Health inspires public confidence in our science by maintaining high ethical principles. NIH employees are subject to Federal government-wide regulations and statutes as well as agency-specific regulations described at http://ethics.od.nih.gov. We encourage you to review this information. This position is subject to a background investigation.

CHIEF, OFFICE OF EDUCATION

The Division of Cancer Epidemiology and Genetics (DCEG) of the National Cancer Institute (NCI) in Rockville, Maryland, is recruiting a Chief to lead its Office of Education (OE). The DCEG OE oversees the recruitment of high-caliber post-doctoral and pre-doctoral fellows, provides oversight of fellows' training and career progression, and develops and promotes graduate program partnerships with public health and medical schools in the U.S. and abroad. Currently, there are approximately 65 post-doctoral and pre-doctoral fellows in DCEG. The OE also coordinates the DCEG summer research program that offers fellowships to high school, college, and graduate students interested in exploring careers in cancer epidemiology and genetics. The Chief represents DCEG at NCI and National Institutes of Health (NIH) meetings relevant to the coordination of training, recruitment, and educational activities. The possibility of research resources and appointment is subject to negotiation.

The successful candidate must hold a medical or doctorate degree in epidemiology, biostatistics, or a related field or demonstrate the equivalent level of epidemiologic training. He or she must possess strong communication skills, both oral and written, and provide evidence of successful mentoring, along with other relevant administrative experience. Salary will be commensurate with qualifications and experience. Full Federal benefits including leave, health and life insurance, long-term care insurance, retirement, and savings plan (401k equivalent) will be provided.

Individuals should send a statement of interest, curriculum vitae and bibliography, and the names and addresses of three references to: **Ms. Sandy Rothschild, Division of Cancer Epidemiology and Genetics, National Cancer Institute, 6120 Executive Blvd., Room 8063, Bethesda, MD 20892, E-mail: rothschs@mail.nih.gov, http://dceg.cancer.gov. The search will continue indefinitely until a qualified applicant is found.**

This position is subject to a background investigation.

Postdoctoral Fellowship
Experimental Transplantation and Immunology

Post-doctoral positions are available in the Experimental Transplantation and Immunology section of the National Cancer Institute in the laboratory of Dr. Dennis Hickstein. The laboratory focuses on translational research in the genetic correction of hematopoietic stem cells in animal models of human genetic diseases. Experience in molecular genetic techniques is strongly recommended. The laboratory is located on the main campus in the new Clinical Research Center in close proximity to the clinical units facilitating the clinical application of basic investigation.

The NCI offers competitive Post-doctoral stipends along with an excellent work environment. The DHHS and NCI are Equal Opportunity Employers that value and foster diversity throughout the entire organization. Position is subject to a background investigation.

Interested applicants should send a CV, brief description of research interests and experience, and contact information for three references to **Dennis D. Hickstein, M.D., Senior Investigator, Experimental Transplantation and Immunology, Center for Cancer Research, National Cancer Institute, Bldg. 10 CRC, Room 3-3142, Bethesda, MD 20892, Email: hicksted@mail.nih.gov**

This position is subject to a background investigation.

Cochlear Genetics

The Section on Neurogenetics at the National Institute on Deafness and Other Communication Disorders seeks to fill a postdoctoral or research fellow position. The position is supported by a stipend/salary and generous research funds. Applicants interested in pursuing their research interests related to the genetics of the cochlea in the mouse are invited to submit a two-page proposal along with their CV, bibliography and names of three references. A Ph.D. and/or MD with less than five years of experience is required.

The intramural program has a synergistic assembly of state-of-the-art facilities and provides ample opportunities to perform innovative research. Please email material to **Konrad Noben-Trauth, Section on Neurogenetics, National Institute on Deafness and Other Communication Disorders, 5 Research Court, Rockville, MD 20850, USA, nobentk@nidcd.nih.gov.** This position is subject to a background investigation.

Postdoctoral, Research and Clinical Fellowships at the National Institutes of Health

www.training.nih.gov/pdopenings

www.training.nih.gov/clinopenings

Train at the bench, the bedside, or both

[illegible] ning and [illegible]ucation
[illegible] 2 [illegible] 0

NIDDK — Tenure-Track Position in Human Energy Metabolism

We seek an outstanding scientist to direct a vigorous, innovative research program in human energy metabolism and serve as Director of the newly established Metabolic Core Laboratory (MCL), Clinical Endocrinology Branch, NIDDK. The MCL performs a number of analyses including exercise testing, physical activity monitoring, body composition measurement, and 24-hour energy expenditure analysis in health and disease. Applicants must be highly motivated and have a demonstrated track record through publications that address significant contributions to the area of energy expenditure and physical activity as it relates to metabolism and weight regulation. The successful candidate is expected to develop an independent, world-class research program complementary to current investigations within the Branch and to successfully oversee the functioning of the MCL. The position comes with generous start up funds and on-going support.

The Clinical Endocrinology Branch, NIDDK is located on the main NIH campus in Bethesda, Maryland, a suburb of Washington DC. The Branch represents interests similar in range to those of an academic department. There are strong interactions among the independent research groups and the position offers unparalleled opportunities for interdisciplinary collaboration within NIDDK and throughout NIH. Applicants should submit a curriculum vitae, bibliography, copies of three major publications, a summary of research accomplishments, and a brief statement of future research goals, and arrange for three letters of reference to be sent to:

Dr. James Balow, Chair, Search Committee, c/o Glynnis Vance, NIDDK, 9000 Rockville Pike, Building 10-CRC, Room 5-2551, National Institutes of Health, Bethesda, MD 20892

Application Deadline: **June 8, 2007**

This position is subject to a background investigation.

NIDDK — Tenure-Track Position in Endocrinology and Metabolism and Human Obesity

We seek an outstanding scientist to direct a vigorous, innovative research program in the Clinical Endocrine Section of the Clinical Endocrinology Branch to advance knowledge in the area of obesity and weight regulation with particular emphasis on the neuroendocrine aspects of weight regulation and the role of sleep in obesity. Applicants must be highly motivated, and have a demonstrated track record through publications that address significant contributions to the field of endocrinology and metabolism. The successful candidate is expected to develop an independent, world-class research program complementary to current investigations within the Branch. The position comes with generous start up funds and on-going support.

The Clinical Endocrinology Branch, NIDDK is located on the main NIH campus in Bethesda, Maryland, a suburb of Washington DC. The Branch represents interests similar in range to those of an academic department. There are strong interactions among the independent research groups and the position offers unparalleled opportunities for interdisciplinary collaboration within NIDDK and throughout NIH. Applicants should submit a curriculum vitae, bibliography, copies of three major publications, a summary of research accomplishments, a brief statement of future research goals, and arrange for three letters of reference to be sent to:

Dr. James Balow, Chair, Search Committee, c/o Glynnis Vance, NIDDK, 9000 Rockville Pike, Building 10-CRC, Room 5-2551, National Institutes of Health, Bethesda, MD 20892

Application Deadline: **June 8, 2007**

This position is subject to a background investigation.

Newcastle. One of only six Science Cities.
One growing and prosperous region.
One great place to live and work.

School of Mechanical & Systems Engineering

Science City Chair in Bio-MEMS & Microfluidics

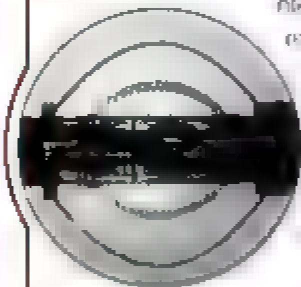

This is an exciting opportunity [illegible] ... Newcastle Science City. Central to the vision is the development of world class research [illegible]

Prospective [illegible] ... to discuss [illegible] Professor [illegible]

For further details and information on how to apply, please visit our web site at **www.ncl.ac.uk/sciencecity**

Closing date: 25/05/07

Newcastle Science City
TRANSFORMING TOMORROW

Newcastle University

BCM

Baylor College of Medicine

FACULTY POSITION

The Department of Molecular Physiology and Biophysics at Baylor College of Medicine is seeking scientists with outstanding records of research accomplishment for faculty positions at the Assistant (tenure track), Associate or Full Professor level. New candidates will develop a strong independent research program and be committed to excellence in graduate and medical student education. Our search will be broadly focused; however candidates employing advanced technologies or studying vertebrate models of human disease are particularly encouraged to apply. The department has a strong commitment to both basic and translational biomedical research and has state-of-the-art facilities for confocal and multiphoton imaging, mouse MRI, computed tomography and cores for the creation and phenotypic analyses of new mouse models. Baylor College of Medicine is a well-renowned research institution with strengths in many areas including human and mouse genetics, cardiovascular sciences and neuroscience. Ample opportunities exist for scientific interaction and collaborations within the department, throughout the College and within the Texas Medical Center. Located in the heart of the Texas Medical Center, Baylor College of Medicine is in close proximity to the MD Anderson Cancer Center, Rice University, the Texas A&M Institute of Bioscience and Technology, the University of Texas Medical School at Houston and the University of Houston.

Applications will be reviewed until the positions are filled. Please email your application materials to **molphys@bcm.edu** and include a curriculum vitae and a description of your current and future research program. Candidates for a junior position should have three references sent separately to the same email address or to:

Dr. Henri Bayle
Department of Molecular Physiology and Biophysics
Baylor College of Medicine
One Baylor Plaza, BCM335
Houston, TX 77030

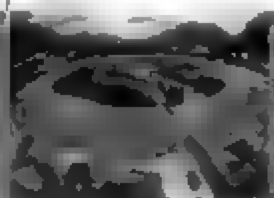

The ESRF is a multinational research institute employing [illegible] staff, located in Grenoble. The ESRF is financed by 18 countries and carries out fundamental and technological research with synchrotron radiation. We are currently seeking the post

Director General

You will be the chief executive of the ESRF and its legal representative. You will decide on the planning, co-ordination and execution of the tasks as laid down in the Statutes, and prepare and implement decisions of the ESRF Council.

You will implement the ESRF programme and the annual budget, set up the general directives for the development of the ESRF by the formulation of a medium term scientific programme, oversee the development of a long-term strategy.

Your profile: distinguished scientist with extensive experience of the application of synchrotron radiation (preferably in an international environment), leadership, well-developed management and communication skills.

For further information, please consult:
http://www.esrf.fr/jobs/Directorate/1001

To apply, send a letter and CV before 31/05/2007 to: rodrigue@esrf.fr or ESRF, Chairman of Council, c/o M. Rodriguez Castellano, BP 220, F-38043 Grenoble cedex 09

ESRF
The European Light Source

esrf.fr

The Health Sciences Research Division of PM USA is seeking **Leading Scientists** in several biomedical-related research areas.

The primary goal of the Health Sciences Research Division (HSR) is to conduct health science research to facilitate the development of new methods and technologies with the potential to reduce harm associated with our products.

In June 2007, PM USA research scientists will begin occupying the new 450,000 sq. ft., state-of-the-art Center for Research and Technology (CRT) facility. HSR scientists will work in collaboration with other PM USA scientists at the CRT to investigate and discover technologies for the reduction of harm associated with our products.

To view job descriptions and apply for the HSR positions, please visit **www.cantbeattheexperience.com** and select RD&E under Job Searches.

Health Sciences Research for Harm Reduction New Positions at Philip Morris USA

Cigarette Smoke-Related Disease Scientists

[illegible] cigarette [illegible]

- Cancer Scientists investigating [illegible] cancer with emphasis [illegible] cancer. Req. #[illegible]BR
- COPD Scientists investigating chronic obstructive pulmonary disease. Req. #[illegible]BR
- CVD Scientists investigating cardiovascular disease.

Experimental Pathologists

[illegible] to investigate the [illegible] cigarette smoke-related diseases. Req. #[illegible]BR

Oxidative Stress Scientists

[illegible] health processes [illegible] cigarette smoke-related diseases. Req. #[illegible]BR

Inflammation/Immune System Scientists

[illegible] processes in cigarette smoke-related diseases. Req. #[illegible]BR

Inhalation Toxicologist for Aerosol Dosimetry

[illegible] cigarette smoke to quantify airway smoke deposition [illegible] relevant exposure models. Req. #9228BR

Toxicologist for PK-PD Studies

[illegible] PK-PD [illegible] inhalation [illegible] models. Req. #92[illegible]BR

Epidemiologists (Molecular/Genetic and Chronic Disease)

[illegible] throughout [illegible] cigarette smoke-related diseases [illegible] COPD Cancer. Req. #8211BR

Biostatisticians

[illegible] cigarette smoke-related diseases (CVD, COPD, Cancer). Req. #[illegible]BR

Geneticists (Statistical and Population)

[illegible] throughput [illegible] studies of cigarette smoke-related diseases (CVD, COPD, Cancer). Req. #9[illegible]19BR

Complex Systems Analysts (Systems Biology)

[illegible] throughput [illegible] data of cigarette smoke-related diseases (CVD, COPD, Cancer). Req. #8219BR

Philip Morris USA is an equal opportunity, affirmative action employer, M/F/D/V. We support diversity in our workforce. Philip Morris USA is a drug free workplace.

CANTBEATTHEEXPERIENCE.COM PhilipMorrisUSA

Director
Washington State University Spokane Program in Basic Medical Education – WWAMI

Applications and/or nominations are sought for the Director of the new WWAMI (Washington, Wyoming, Alaska, Montana, Idaho) Medical Education Program at Washington State University (WSU) Spokane. This position is also appointed as Assistant Dean at the University of Washington School of Medicine (UWSOM).

The WWAMI Program is a five-state cooperative medical education program. First-year basic science medical classes are taught at existing state universities, the Seattle campus for the second year, and clinical sites across all five states for clinical education. The WSU Spokane WWAMI Program will be a new first-year site and will work in cooperation with the Regional Initiatives in Dental Education (RIDE) and WWAMI clinical education sites in Spokane (**http://www.uwmedicine.org/education/WWAMI**).

Responsibilities. The Director is responsible for administering a first-year medical curriculum at WSU Spokane, coordinating the curriculum with that of UWSOM [illegible] officers and public and private health care organizations in Washington.

Rank. The Director will report to the Vice Provost for Health Sciences at WSU Spokane [illegible] Assistant Dean at the UWSOM and will report to the Dean through the Vice Dean for Academic Affairs. The Director will have an affiliate academic appointment [illegible] UWSOM [illegible].

Minimum Qualifications. M.D. and/or Ph.D. in a science basic to medicine; demonstrated excellence in teaching medical students; demonstrated excellence in research [illegible] **Preferred Qualifications**. [illegible] risk families and children and translational research. Strong collaborative ties exist with the WSU Pullman campus.

Salary: DOE. **Beginning Date**: September 1, 2007. For further information see **www.hrs.wsu.edu**. For other information contact **Dr. Michael Laskowski (mlaskow@wsu.edu)**. Send letters of application, including a CV and e-mail addresses of three references to **Patti Petersen (petersen@wsu.edu)**. Review of applications will begin **June 1, 2007**.

EEO/AA

Stem Cell Network
North Rhine Westphalia

The State of North Rhine-Westphalia (NRW) welcomes applications for

Junior Groupleader Fellowships
within the Stem Cell Network NRW

Candidates with a genuine interest in stem cell research, a successful record of postdoctoral research and a competitive scientific concept are invited to apply.

Successful applicants will receive up to 1.25 Mio. Euro for a 5 year groupleader engagement at one of the North Rhine-Westphalian stem cell centers.

Deadline for application: July 1, 2007

For further details see www.stemcells.nrw.de

Become part of an innovative stem cell network comprising more than 35 scientific and medical institutions in one of the most vibrant academic settings in Germany.

Ministry of Innovation, Science, Research and Technology of the State of North Rhine-Westphalia

NRW.

University of Heidelberg

The **Faculty of Medicine Mannheim, University of Heidelberg** offers the following two positions

Full Professor (W3) of Neurosurgery

The Full Professorship will be a tenured position. The successful candidate should have a distinguished record of qualifications in all areas of neurosurgery. The current reputation of the department for vascular, oncological, and spinal neurosurgery should be preserved. An additional emphasis on functional neurosurgery is intended. The successful candidate should actively take part in established and developing research programs of the Faculty in the field of neural plasticity, molecular oncology, vascular medicine and medical technology. He/she should actively participate in restructuring the undergraduate curriculum at the faculty (MaReCUM).

The successful candidate should be a board certified neurosurgeon and should have high ranking, internationally acknowledged academic qualifications commensurate with the rank of a full professor with life-time tenure including extraordinary clinical and teaching skills, a distinguished record of original research, administrative experience and an understanding of departmental financing in universities.

The successful candidate will fulfil his/her clinical duties with the University Medical Centre Mannheim; to this end he/she will be appointed Chairperson of the Dept. of Neurosurgery at University Medical Centre Mannheim. In this respect, he/she will negotiate a separate contract with the University Medical Centre Mannheim. He/she will be responsible for the economical management of the department finances.

Full Professor (W3)/Chair of Internal Medicine – Hematology and Oncology

(succession to Prof. Dr. R. Hehlmann)

The Full Professorship will be a tenured position. The successful candidate should have a distinguished record of qualifications in all areas of hematology and oncology including patient care, teaching and research. He/she should secure highest level patient care in all clinical in- and outpatient areas of hemato-oncology, hematology and medical oncology with a special focus on hemato oncology including autologous and allogeneic bone marrow transplantation. In the area of medical oncology the candidate should contribute to the newly formed Interdisciplinary Tumor Center Mannheim. He/she is expected to make every effort to further develop the "Competence Net Acute and Chronic Leukemias" and the "European Leukemia Net". As an independent principle investigator, the candidate should actively take part in established and developing research programs of the Faculty in the field of clinical and molecular oncology with a focus on hemato-oncology including topics such as tumor resistance, targeted therapy, target identification and stem cells. He/she is furthermore expected to attract extramural funding by grant applications to non-university funding institutions.

The successful candidate should be board certified in internal medicine – hematology and oncology and should have high ranking, internationally acknowledged academic qualifications commensurate with the rank of a full professor with life time tenure including extraordinary clinical and teaching skills, a distinguished record of original research, administrative experience and an understanding of departmental financing in universities. The candidate should be a cooperative personality to actively master the integrative task of participating in developing and implementing the novel medical curriculum of the Faculty, MaReCuM.

The successful candidate will fulfill his/her clinical duties at the University Medical Center Mannheim. To this end he/she will be appointed Chairperson of the III. Dept. of Internal Medicine (Hematology and Oncology) at University Medical Center Mannheim. In this respect, he/she will negotiate a separate contract with the University Medical Center Mannheim.

Interested candidates should submit a full CV with copies of certificates, publication list and selected reprints within 4 weeks of publication of this advertisement to **Prof. Dr. Dr. h.c. K. van Ackern, Dean of the Medical Faculty Mannheim, University of Heidelberg, University Medical Center Mannheim, 68135 Mannheim, Germany.**

The positions are available unlimited. In case that the successful candidate has not been appointed to a professorship position before, State law regulation demands under chapter 50 of the university law to fill the position as a tenure track position for 3 years. Exceptions are possible for candidates from abroad or from non-university institutions if candidates cannot be attracted otherwise. When the position is tenured after the tenure track period, the formal application process need not be repeated.

The University of Heidelberg is an Equal Opportunity/Affirmative Action Employer.

WestVirginiaUniversity
ROBERT C. BYRD HEALTH SCIENCES CENTER

Hubert A. and Hazel L. Shaffer Chair of Human Genetics

The **Center for Neuroscience (www.hsc.wvu.edu/wvucn/)** and the **Department of Behavioral Medicine and Psychiatry (www.hsc.wvu.edu/som/bmed/)** at West Virginia University are seeking [illegible] Ph.D. or M.D. [illegible] **Hubert A. and Hazel L. Shaffer Chair of Human Genetics**. Candidates should [illegible] molecular genetics or pharmacogenetics related to depression [illegible]. The selected candidate will be appointed Associate or Full Professor in the Department of Behavioral Medicine & Psychiatry and lead his or her own research group and assume a lead role in the ongoing development of translational research in [illegible] **Health Sciences Center Strategic Research Plan** [illegible] Candidates should [illegible] and [illegible] mentoring junior faculty. The position offers a competitive salary and resources needed to establish a strong research program at the Health Sciences Center.

West Virginia University [illegible] with approximately 20,000 undergraduate and [illegible] students. The Health Sciences Center includes the Schools of Medicine, Pharmacy, Dentistry, and Nursing, each with health professions and graduate programs. Two new research buildings are under construction on the Health Sciences campus to accommodate our aggressive research growth agenda. Patient care [illegible] include a 400-bed University Hospital (Ruby Memorial) with a new 90-bed addition and [illegible] 70-bed psychiatric hospital (Chestnut Ridge). Morgantown is rated as [illegible] small cities in the U.S. with affordable housing, excellent schools, a picturesque countryside, and many outdoor activities (**www.morgantown.com**).

Review of applications will continue [illegible] **sfinnegan@hsc.wvu.edu** [illegible] **James M. O'Donnell, Ph.D., Search Committee Chair, c/o Sean Finnegan, Administrator, Center for Neuroscience, PO Box 9304, West Virginia University, Morgantown, WV 26506-9304. Inquiries may be directed to Dr. O'Donnell (304-293-2433, jodonnell@hsc.wvu.edu).**

West Virginia University is an Affirmative Action/Equal Opportunity Employer.

School of Medicine

Clinical Department of Medicine and Therapeutics

Research Fellow in Cell Signalling/Bone Biology

An exciting opportunity in the multidisciplinary Bone & Musculoskeletal Resear[illegible]

[illegible] new signalling pathways in osteoclasts and other bone cells and will be based in the [illegible]

You must ha[illegible]

appropriate level of expe[illegible]

Experience in molecular bi[illegible]

Sal[illegible]

for a period of up t[illegible]

Informal enquiries to Professor Mike Rogers (e-mail [illegible])

Online application forms and further particulars are available from www.abdn.ac.uk/jobs Alternatively telephone (01224) 272727 (24 hour answering service) quoting reference number YMT166RX for an application pack.

Closing date: 10 May 2007

Promoting Diversity and Equal Opportunities throughout the University

UNIVERSITY OF ABERDEEN

MINISTRY OF HEALTH
SINGAPORE

Singapore Invites Applications for the Singapore Translational Research ("STaR") Investigatorship Awards

Agency for Science Technology and Research
SINGAPORE

A unique and innovative opportunity for outstanding
Translational and Clinical Research Investigators

STaR INVESTIGATORSHIP

The **STaR Investigatorship Award** is a prestigious award jointly offered by the Singapore Ministry of Health's National Medical Research Council (NMRC) and the Agency for Science, Technology and Research (A*STAR) to recognise and support investigators with outstanding qualifications in translational and clinical research. This award is part of the Biomedical Sciences Phase II initiative to promote translational and clinical research in Singapore.

Tenable in Singapore, **STaR Investigators** can either be part of the team leading or contributing to the **Translational and Clinical Research (TCR) Flagship Programmes** (jointly supported by A*STAR and NMRC) or start a new research programme which can potentially advance Singapore's priorities in biomedical research and healthcare. STaR investigators may also spend up to 20% of their time engaging in direct patient care in Singapore.

In keeping with the international status of the **STaR Investigatorship Awards**, recipients will receive very competitive research support and remuneration or appointments at A*STAR's Singapore Institute for Clinical Sciences (SICS) as well as tenure-track appointments at the National University of Singapore's (NUS) Yong Loo Lin School of Medicine or Duke – NUS Graduate Medical School (GMS).

Three categories of the STaR Investigatorship are available:

i) Distinguished Senior Investigator (DSI)

ii) Senior Investigator (SI)

iii) Investigator (INV)

Successful candidates will receive 5-year support for DSI and SI and 3- to 5-year support for INV. The awards are renewable for further terms upon excellent external reviews.

Profile of a STaR Investigator:

- Medically qualified doctors, MDs, or PhDs active in translational and clinical research or who conduct research that involves integrating basic scientific discoveries with clinical applications.
- You may be a physician scientist, clinical investigator, population geneticist, epidemiologist, health services researcher or an investigator engaged in other kinds of population-based biomedical research.
- Applicants should have a strong track record of scientific achievement and impact in translational and clinical research.

A separate but related call for proposals for **TCR Flagship Programmes** is also open to local institutions in Singapore, in the following disease oriented areas: cancer, cardiovascular, metabolic disorders, neurosciences, infectious diseases and eye diseases. **TCR Flagship Programmes** should seek to integrate, coordinate and leverage on the full spectrum of research capabilities in Singapore from basic science to clinical research, and be highly competitive with the potential for the supported programme to be an international leader. It is not necessary for applicants to be part of the TCR Flagship team to apply to the STaR Investigatorship Award.

The STaR Selection Panel includes:

- Professor Tan Chorh Chuan (Deputy Chairman, A*STAR)
- Professor Edward Holmes (Executive Deputy Chairman, Clinical Translational Sciences, A*STAR Biomedical Research Council)
- Professor Sir David Lane (Executive Deputy Chairman, Biomedical Sciences & Technology, A*STAR Biomedical Research Council)
- Professor Edison Liu (Executive Director, Genome Institute of Singapore)
- Professor Judith Swain (Executive Director, Singapore Institute for Clinical Sciences)
- Professor John Wong (Dean, Yong Loo Lin School of Medicine, National University of Singapore)
- Professor Sanders Williams (Dean, Duke – NUS Graduate Medical School)
- Professor K Satkunanatham (Director of Medical Services, Ministry of Health)
- Professor Malcolm Paterson (Scientific Director, Office of Research, Singhealth)

Short-listed applicants will be invited to Singapore for a 3- to 5-day visit for in-depth interaction with the scientific community, including lead investigators from short-listed Translational and Clinical Research Flagship programme proposals, to better understand the local research support and environment, and to meet with the STaR Selection Panel.

Interested applicants, please complete your application using the prescribed STaR Application Form available for download on NMRC website and send it to the following address before **02 July 2007** 5pm Singapore time (+0800 UTC/GMT):

Singapore Translational Research (STaR) Investigatorship Awards
National Medical Research Council
11 Biopolis Way #09-10/11 Helios Singapore 138667
Email: MOH_NMRC@moh.gov.sg
You may refer to the website for more details at: **http://www.nmrc.gov.sg/**


Does your next career step need direction?
Have a great new research idea
Where can I find more grant options?
For a career in science
turn to Science
ScienceCa
We know science
You know ScienceCareers.org
is part of the non profit AAAS
That means they're putting
something back in to science

I got the offer I've been dreaming of.
With thousands of job postings, it's a lot easier to track down a career that suits me.
Now what?
reers.org
AAAS
I want a career, not just a job.
There's only one place to go for career advice if you value the expertise of Science and the long experience of AAAS in supporting career advancement — ScienceCareers.org. The pages of Science and our website ScienceCareers.org offer:
• Thousands of job postings
• Career advice articles and tools
• Funding information
• Networking opportunities
www.sciencecareers.org
Science

POSITIONS OPEN

ASSISTANT PROFESSOR (VISITING)
Endocrinology

The Biology Department of St. Lawrence University invites applications for a one-year visiting position at the Assistant Professor level beginning fall 2007. A Ph.D. (including all-but-dissertation) in endocrinology or a related field with a major emphasis at the cellular or physiology level is required.

The successful candidate will be expected to teach an endocrinology course in the fall along with a course in human anatomy (or a related physiology based course).

Two spring semester courses are expected. Preferred courses include reproductive physiology, cell biology/systems level biology, neurophysiology, histology, or other related courses. There is a possibility that this position will be searched in the fall as a tenure-track appointment. This plus the opening of new facilities and the opportunity to gain teaching experience at a quality liberal arts and science university is inviting. We encourage applications from candidates who bring diverse cultural, ethnic, and national perspectives to their scholarship and teaching.

The successful candidate may have the option to participate in the continued development of our introductory biology courses towards a more investigational, inquiry-based, collaborative, and personalized learning environment.

A demonstrated expertise in the use of computers and instructional technologies is preferred.

Interested candidates should submit a letter of application, curriculum vitae, and a statement of teaching experience and philosophy that reflects innovative and progressive pedagogies, and have three letters of recommendation forwarded to: **Dr. T. Budd, Biology Department, St. Lawrence University, Romoda Drive, Canton, NY 13617.** Applications will be reviewed until the position is filled.

St. Lawrence University, chartered in 1856, is the oldest coeducational university in New York State. Please see the University **website: http://www.stlawu.edu** and the biology homepage at **website: http://it.stlawu.edu/~biology** for more information.

St. Lawrence University is an Affirmative Action/Equal Employment Opportunity Employer. Women, minorities, veterans, and persons with disabilities are encouraged to apply.

SUPERVISORY RESEARCH FISHERY BIOLOGIST, ZP-0482-05
Department of Commerce
Job Announcement Number: NMFS-SEFSC-2007-0013

This position is the **CHIEF of SUSTAINABLE FISHERIES DIVISION,** Southeast Fisheries Science Center, National Marine Fisheries Service, National Oceanic and Atmospheric Administration, located in Miami, Florida.

The incumbent, in addition to having supervisory responsibilities, guides the development of scientific advice in direct support of fishery management plans and the sustainable use and conservation of marine resources; coordinates scientific interactions with fishery management councils, international organizations, state, territorial and federal agencies and other constituent groups; and promotes the wide application of scientific results through publications, presentations, authoritative reports, and analyses.

Marina N. Derksema
Telephone: 206-526-6517
Fax: 301-562-8968
E-mail: marina.derksema@noaa.gov

POSTDOCTORAL FELLOW/RESEARCH ASSOCIATE with experience in virology to join group which prepares "seed" viruses for the annual influenza vaccine. Focus will be on development of high yield/growth type B influenza viruses. Send resume to: **Dr. Doris Bucher, New York Medical College, Department of Microbiology and Immunology, Valhalla, NY 10595,** or **e-mail: doris_bucher@nymc.edu.**

POSITIONS OPEN

FACULTY POSITION, Molecular Pathology. The Department of Pathology at the University of California, San Diego (UCSD), **website: //http://medicine.ucsd.edu/Pathology,** seeks a **PATHOLOGIST** (M.D. or M.D.-Ph.D.) to lead a translational anatomic pathology research program. The selected individual will assume primary responsibility for establishing a first-rate, tissue-banking enterprise and research procedures for state-of-the art molecular and morphologic analysis of human tissue. Training in anatomic pathology is necessary. Appointment is available at the **ASSISTANT, ASSOCIATE, or FULL PROFESSOR** level. Clinical responsibilities will be assigned depending on experience and qualifications. Candidates should possess or be eligible to obtain a state of California medical license, have strong area-specific publications, an understanding of the use of gene expression profiling and proteomics technologies in the analysis of human tissue, strong communication skills, the ability to collaborate, and commitment to an academic career. Rank will be commensurate with experience. Salary will be consistent with established UCSD pay scales. Please forward application letters addressed to **Search Committee Chair, Dr. Noel Weidner,** together with curriculum vitae and names/addresses of at least three references, care of: **Ms. Catherine Schumacher, Search Coordinator, Department of Pathology 0717, University of California San Diego School of Medicine, 9500 Gilman Drive, La Jolla, CA 92093-0717.** Applications by e-mail are acceptable to **e-mail: cdschumacher@ucsd.edu.** Review of applications will begin June 22, 2007, and will continue until filled. *UCSD is an Affirmative Action/Equal Opportunity Employer with a strong institutional commitment to excellence through diversity.*

FACULTY POSITION
Pulmonary Center, Boston University

We are soliciting applications for a position at the **ASSOCIATE or ASSISTANT PROFESSOR** level to join our Stem Cell and Lung Development Program. We are a highly collaborative/interactive group seeking to expand its research scope. Applicants must have a Ph.D., M.D., V.M.D./D.V.M. or equivalent degree, and be interested in basic questions relating to: cell biology, gene regulation, signaling, genetics in mammalian and other model organisms, or an area that can be integrated into our multidisciplinary program. Generous support packages are available.

Candidates should submit a PDF file with curriculum vitae, description of research interests, and arrange for electronic submission of three reference letters to: **Alan Fine, M.D., e-mail: afine@bu.edu** or **Wellington Cardoso, M.D., Ph.D., e-mail: wcardoso@bu.edu. Pulmonary Center, Boston University, 715 Albany Street R304, Boston, MA 02118.**

POSTDOCTORAL POSITION available at the Department of Anatomy and Physiology, Kansas State University, to study N-methyl-D-aspartate receptor regulation. Ph.D. in neuroscience/pharmacology or a related field is required. Experience with molecular biology techniques and mammalian cell culture is essential. Screening of applications will begin April 30, 2007, and continue until position is filled. Submit letter of interest and curriculum vitae, along with names and addresses of three references, electronically to **Dr. Antje Anji (e-mail: aanji@vet.ksu.edu).**

ANATOMY/CELL BIOLOGY
FACULTY POSITION

The Edward Via Virginia College of Osteopathic Medicine (VCOM) invites applications for a tenure-track, open-rank faculty position in the discipline of anatomy and physiology. VCOM is a post-baccalaureate professional medical college located in Blacksburg, Virginia. For more information on this position, please visit our **website: http://www.vcom.vt.edu.**

POSITIONS OPEN

POSTDOCTORAL POSITION
in Neurodegenerative Disorders
Canadian Institutes of Health Research-Funded

We are a dynamic, energetic, and well-funded laboratory focused on mechanisms of neuron death and neuron-glial communication in stroke and other degenerative disorders of the brain. While specific opportunities are available in mouse models of stroke and multiple sclerosis, candidates will have access to a wide variety of technical capabilities to facilitate multidisciplinary approaches. Candidates will enjoy an environment that encourages interaction and full participation in intellectual development of research projects. Multiple collaborative avenues are available toward this end. St. Boniface Hospital Research Center is a research institute and part of the University of Manitoba located in Winnipeg, Canada, constructed in 2000 with state-of-the-art resources for molecular/cellular biology, single photon and 2-photon imaging, and small and large animal surgery. Applicants must have demonstrated scientific productivity, and are expected to work both independently and in a team setting. An M.D. or Ph.D. in neurobiology or a related field is required. Salary will be commensurate with experience and publications. Please send curriculum vitae and contact information for at least two references to **Dr. Chris Anderson** by **e-mail: canderson@sbrc.ca.**

POSTDOCTORAL POSITION
University of California, San Francisco

Position in the Laboratory of Molecular Endocrinology at University of California, San Francisco, requires skills in protein chemistry and computational modeling; studies concern factors involved in steroidogenesis (see **website: http://ucsf.edu/wlmlab).** Send letter, curriculum vitae, and address/telephone/e-mail of at least three references to: **Professor Walter L. Miller, HSE 1401, University of California, San Francisco, CA 94143-0978.**

MARKETPLACE


What if staying up to date with the latest technology published in journals and patents were as easy as pushing a button?